TURBULENCE STRUCTURE IN STRAIGHT GRAVEL-BED CHANNELS

Alistair David Kirkbride

A Thesis presented
for the degree of
Doctor of Philosophy

Department of Geography
University of Sheffield

Submitted: September 1993
Accepted: January 1994

Abstract

It is clear when looking at a gravel-bed river that the flow turbulence is not random: eddies and boils can be seen at the surface. Understanding the behaviour of gravel-bed rivers is limited until the flow structures are described and their origins explained. This work uses a combination of point monitoring of velocity and visualisation of flows over gravel beds in both the field and flume to describe and explain the structure of the boundary layer and the generation mechanisms of flow structures within it.

The boundary layer over fluvial gravel beds can be split into two main flow zones. The inner zone consists of eddies developing and shedding off relatively large obstacles clasts and more confused eddying in the inter-obstacle wake zone. There is some evidence to suggest that flow directly above the inner zone is characterised by the domination of negative Reynolds stress associated with the upwards ejection of eddies at higher than average streamwise velocity. The visualisations show that the eddy shedding becomes more confused as the flow rate is increased, and is best described as intermittent.

Above the obstacle crests is the outer flow zone in which there are larger flow structures. Visualisations of the vertical streamwise plane and simultaneous logging of velocity at three points suggest that the larger structures consist of inverted wedges of high-speed fluid which move at more than the mean streamwise velocity as "sweep-like" structures. Low-speed fluid is ejected away from the bed after a high-speed front has passed. These structures become increasingly dominant as the flow rate is increased. The high-speed zones appear to be associated with the passage of the front slopes of water surface waves, although this cannot explain some of those monitored in the field.

The flow structures are observed to exhibit a crudely intermittent behaviour in the visualisations. Attempts to quantify the intermittency both from the visualisations and by time series analysis of both velocity and stress does not produce the clear quasi-periodic velocity signatures that some other workers have found. There is some agreement between the periods of dominant peaks in the spectra of Reynolds stress and calculated burst periods. This is interpreted as meaning that a similar bursting process occurs over mixed gravel beds as that reported over the smooth and uniformly rough surfaces. There is no evidence that eddy shedding produces a periodic signature in either the velocity or stress series.

A mechanistic model is proposed which involves the coupling of eddy shedding with the outer flow wedges. In conditions of high relative roughness (or low flow), eddy shedding is predominantly responsible for the generation of turbulent structures in the boundary layer, whereas at low relative roughness (or high flow conditions), the outer zone wedges dominate. This allows the interpretation of flow structure in gravel bed rivers to be made with respect to that observed in sand bed rivers and in tidal flows over gravels.

Observations of gravel entrainment in the visualisation experiments suggest that there are two modes of entrainment. At marginal transport conditions, fines are entrained from the wake zones of the larger obstacle clasts by vertical velocity fluctuations. At higher flow

conditions, the high speed "sweep-like" structures are responsible for entraining the larger clasts, although the timescale of entrainment is greater that that of an individual flow structure.

Contents

List of Figures

List of Tables

Notation

d	Flow depth
D_n	nth percentile of a particle size distribution
k_n	nth percentile of the bed height distribution
T_b	Burst period
S	Strouhal number
y	Distance above boundary
y^+	Dimensionless distance above boundary ($y^+ = y.U^*/\nu$)
Qn	nth quadrant
u	Streamwise velocity at a point
$\langle u \rangle$	Time-average streamwise velocity at a point
u'	Streamwise velocity fluctuation ($u' = u - \langle u \rangle$)
$\langle U \rangle$	Profile mean velocity
U^*	Shear velocity ($U^* = \sqrt{(\tau_0/\nu)}$
U_∞	Free stream velocity
Re	Reynolds number
Fr	Froude number
δ_{sub}	Sublayer thickness
κ	Von Karman constant
λ	Spanwise streak spacing
ν	Kinematic viscosity
ρ	Density
σ	Standard deviation
τ	Shear stress
	τ_0 Bed shear stress
	τ_R Reynolds stress
	τ_u Instantaneous shear stress
	$\langle \tau \rangle$ Arithmetic time average of stress
	Geo(τ) Geometric time average of stress (G_τ in tables)

Acknowledgements

It is difficult to split the people who have actively helped in this thesis from those who have contributed to other aspects of life in four years at Sheffield; the following people fall into the former category (with a few exceptions).

Judith Maizels, Shiona Park and Malcolm MacIntyre gave the initial impetus to apply for this PhD through the cozy, lengthy discussions on anything fluvial, often on a cold day on the banks of The Quoich. I hold them directly responsible for defining my life's direction.

The technical staff at the Geography Department at Sheffield University deserve awards for patience and perseverence for building and mending obscure bits of equipment, and developing several miles of film. In particular, I would like to thank Chris Turner, Paul Bently and John Owen. I am grateful to the NERC for funding this PhD, and for their efficiency in processing claims for fieldwork.

Valuable discussions about watery things were had with Rob Ferguson, Jim Best, Phil Ashworth, Andre Roy, Jack Hardisty and various people during the Arolla and Sunwapta fieldwork in 1992. Andre Roy and Jack Hardisty were brave enough to lend me equipment, for which I am very grateful.

The "few exceptions" mentioned above either fed me or who provided escape from thinking of water. These include Steve Trudgill (who could fill several wheelbarrows with the food he's supplied me with), Ellie Dilks for being mad as trousers, Mollie Chappell for so effectively using a cooker to recombine ingredients to satisfy my voracious appetite, Nick Spedding, Pete Nienow, Mark Skidmore and Stuart Lane for introducing me to the concept of hatstands, Jill Ulmanis for allowing me to moan, Gill Foster for putting up with me for so long (and the green cake), Greg for the inner-tube Morris Dancing sessions, Nash for his contagious at*a*x*a*ph$_o$*bi*a, Andrew-bear for "time series expertise" and CD collection, Mick Whelan for his Emails..... oh, all sorts of people too numerous to mention here. They know who they are, and I'm glad that I met and know them.

Although they have already been mentioned, I am particularly grateful to Rob Ferguson and Jim Best for being constantly supportive, efficient and tactful idea filters, and for their efficiency in comprehensively reading thesis drafts, often at weekends when I'm sure there were dozens of other activities they would have preferred to have been doing!

Chapter 1 Introduction

1.1 Gravel-bed Rivers in the Environment

Rivers transport water and sediment, and in doing so act as agents in both the hydrological cycle and in the denudation of landmasses. Gravel-bed rivers are important features of the landscape in upland environments in many climatic zones from semi-arid through temperate to alpine.

Upland rivers in temperate environments are perceived as a resource and a hazard. There are many examples of gravel-bed rivers as a resource. Many are spawning grounds for fish such as salmon and trout. Although this gives them importance at the local rural scale, their significance extends across national boundaries due to the thousands of miles associated with fish migration. Traditionally, they have been sources of washed building materials, and rights to this resource are still exercised in several parts of Britain. They are being increasingly perceived as a recreational resource. The increase in the past two decades of outdoor leisure has meant that more walkers and canoeists are joining the anglers in their appreciation of the balance of power and tranquillity that a gravel-bed river provides.

As a hazard, they are dynamic features being prone to flooding, high rates of coarse sediment transport and, if unrestrained, channel change. This means that human activity in the riparian zone must take into account the effects of such hazards.

The desire to understand the processes responsible for the dynamism of gravel bed rivers has been the driving force behind many studies. Section 1.2 aims to outline the subject of this thesis, and to set this work into various different contexts.

1.2 Scope and Approach

Newton unwittingly provided the answer to the question of *why* rivers flow downhill: the force of gravity acts on a mass of water resulting in its movement towards the centre of the earth; if it is restrained it forms a lake, if it is free, then it is a river.

This thesis is concerned with *how* water flows downhill over the rough surface of a gravel bed. Different approaches have been adopted to this end by workers in different disciplines.

1.2.1 Geomorphic Context

Figure 1.1 depicts the geomorphic setting of rivers. It shows that the channel form, sediment and fluid flow interact, hence the explanation of one cannot be made fully without the understanding of the other two. This can be illustrated by two examples. Firstly, avulsions leading to channel changes in braided rivers (form) have been attributed to large flood events (flow) and changes in in-channel rates of erosion and deposition (sediment) (Ferguson & Werritty, 1983). Secondly, the explanation of the size-sorting and packing structure of the sediments on point bars can only be explained with reference to secondary flow cells (flow) (Ashworth *et al*, 1992) which themselves are the result of flow forcing around the bend (form).

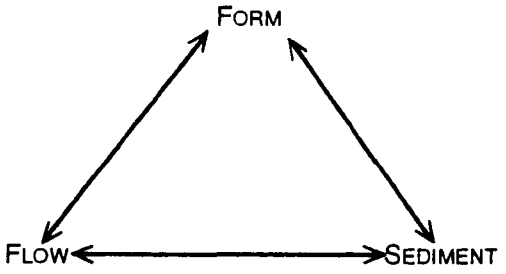

Figure 1.1 The interaction between river channel form, fluid flow and sediments.

This thesis concentrates on understanding and explaining the subsystem relating to flow. The influence of channel form is minimised by considering flow in straight channels without lateral slope. The reason for doing this is to isolate the effects of the roughness of the sediment surface on the flow field.

Consideration of the flow is made in the framework of its influence on the entrainment of gravel. There is an ever expanding body of evidence that suggests that turbulence in natural fluid flows is not random, but contains organised flow structures. These have been monitored in tidal flows over coastal gravels (e.g. Williams *et al*, 1989), in sand-bed rivers (e.g. Lapointe, 1992) and in gravel-bed rivers. In addition, visual observation of sediment movement in gravel-bed rivers has shown that it is intermittent (Drake *et al*, 1988).

The presence of flow structures and the intermittency of sediment movement in gravel-bed rivers raise 3 questions.

1. What are the characteristics of the flow structures?
2. How are they generated?
3. Are they responsible for intermittent sediment transport, and if so, how?

In relation to Figure 1.1, investigation into these questions should allow a clearer understanding of part of the system which explains the activity of rivers.

1.2.2 Fluid Dynamical Context

The problem of *how* water flows downhill is the focus of a major part of fluid dynamics, and has attracted attention for centuries. The approach is different from that of the geomorphologist as it concentrates on the mechanics of flow rather than on the application to the explanation of form.

Many fluvial features such as a river's concave long profile or different plan form patterns can be explained in terms of adjustments to attain optimum rates of energy dissipation. In this context, the scale that is relevant to this work involves the interaction of the flow with the bed. This approximates to the depth of flow.

In fluid dynamics, fluid flows from many different environments exhibit similar features. For example, the velocity of wind, water and ice increase in a similar manner as distance from the desert surface, river or glacier bed increase, the main differences being the density and

viscosity of the "fluid"; weeds in a river bed are seen to move in response to turbulence in the same way that trees are buffeted by the wind.

A fluid dynamic approach to the explanation of flow in rivers, therefore, would consider firstly the nature of the imposed boundary conditions, e.g. a rough bed and limited depth, and then determine how these would influence the flow field. In this context, there is much to be learnt from other similar environments where observations are more easily made and more aspects of the system are known or can be controlled.

1.2.3 Scientific Context

In order to explain a phenomenon, it is necessary to understand the problem. This thesis aims to explain the intermittency of flow and sediment transport in gravel-bed rivers, and so it is necessary to understand the mechanisms which generate the structures which lead to the intermittency.

At the onset of this work, there were no published reports of turbulence measurements in gravel-bed rivers, although this has subsequently been at least partly redressed by the valuable work of two sets of groups (Clifford & French, 1992; Robert *et al*, 1993). This means that it is difficult to identify exactly what we are trying to understand. This necessitates two approaches to the problem.

The first is largely investigative and aims to describe what we are looking to explain. The second is a reductionist approach. The rationale behind this is that any apparently random phenomenon can be explained if the relevant elements which influence the phenomenon can be identified and their interaction understood (Nagel, 1961). This is illustrated in Figure 1.2 in relation to an avulsion.

For the problem of this thesis, a purely deductive approach would rely solely on reductionism. This is, however, impossible to achieve due to not being able to fully describe the initial problem. The mixed approach overcomes this problem by allowing a clearer definition of the flow phenomena to be made before attempting to explain them.

1.3 Overview of Thesis Structure

This thesis is presented as four main chapters. Chapter 2 attempts to determine, from the literature, the nature and possible origins of flow structures over gravel beds. This is done largely in reference to measurements and observations made in non-gravel-bed environments. It aims to provide the basis for a more rational interpretation to be made of the measurements and observations discussed in subsequent chapters. At the end of the chapter, the specific aims of the thesis are outlined.

Chapter 3 outlines the methodology for data collection and the criteria for designing the sampling strategy. It then describes the techniques adopted and the procedures used for checking the data. Finally, the field sites are described.

Chapter 4 provides a qualitative description of direct and indirect observations of flow structure at a scale approximating to the flow depth. It refers to flume experiments of visualised

flow over mixed gravel beds, and to flow monitored simultaneously at three points in the field. This allows a qualitative description to be made of the structure of the turbulent flow field over a gravel bed.

Chapter 5 aims to describe quantitatively the turbulence characteristics relative to proximity to the bed, mean hydraulics and roughness. The temporal characteristics of flow at a point are also investigated.

Chapter 6 synthesises the findings of chapters 4 and 5 in order to propose a model which describes the turbulence structure over a mixed gravel bed. It interprets and explains the mechanisms which generate the flow structures with respect to those outlined in Chapter 2.

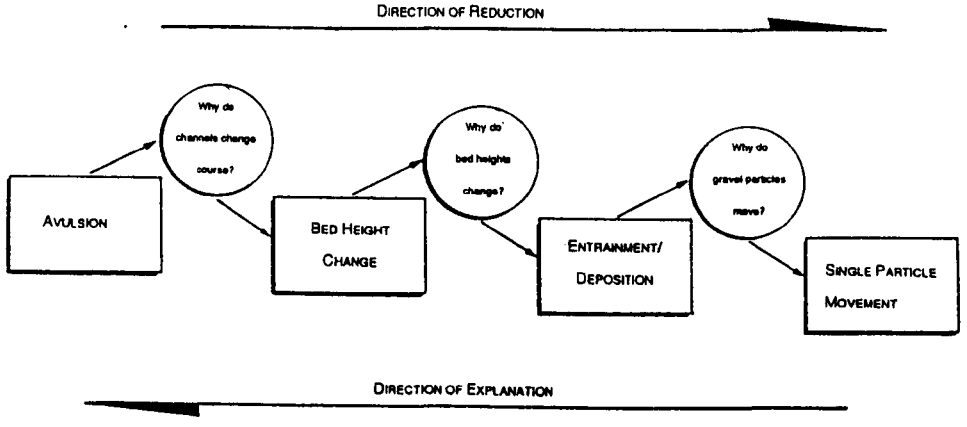

Figure 1.2 An example of the role of reductionism in the explanation of an apparently random phenomenon, in this case, river channel change due to an avulsion.

Chapter 2 Turbulent flow structure over fluvial gravels

2.1 Introduction

The major challenges of this work are to determine the relationships and feedback between gravel beds and turbulent flow. This chapter briefly reviews the mechanisms by which gravel is entrained and provides a context for subsequent arguments relating to turbulence. Additionally, it will attempt to document the nature of the turbulent flow field which exists over fluvial gravel beds as given from the existing literature, and identify the mechanisms involved and the parameters which influence the turbulence.

The turbulent phenomena introduced and explained in this chapter provide a strategy for the collection and analysis of data outlined in Chapters 3, 4 and 5. They also serve as a basis for the interpretation of the results in Chapter 6.

2.1.1 The entrainment of fluvial gravels: the force-balance model

Entrainment, when referring to fluvial gravels, is a condition of incipient motion bounded by stability and transport. The extent of departure from stability and to which the condition progresses before transport is a subject which has attracted attention in the literature with regard to the definition of entrainment (e.g. Lyles & Woodruff, 1972; Carling *et al*, 1992). The definition adopted for this work is as follows: if a particle is acted on by a force which causes it to move, then it is said to have been entrained only if it does not relax back into its original position when the force has been removed.

The basic mechanistic model to be used is the force-balance model of a single particle (White, 1940; Paintal, 1971; Naden, 1987; Wiberg & Smith, 1987a; Andrews & Smith, 1992). It will be outlined first in order to provide a focus for the subsequent discussions of fluvial turbulence and bed structure.

Consider the vertical streamwise plane through a particle on the surface of a bed of gravel in a turbulent flow with a mean bed shear stress of τ_0 (Figure 2.1). In order for the particle to become entrained, the fluid forces acting on it must overcome those which keep it in its quasi-stable position.

There are two forces acting on the particle as a result of the mean flow. In the streamwise direction, there is a *drag force*, F_D, which may be given by

$$F_D = 0.5.\rho_w.C_D.\langle u^2(z)\rangle.A_p \qquad (2.1)$$

where A_p is the elevation area of the particle encountered by the approaching flow, $\langle u^2(z)\rangle$ is the velocity averaged over this area. C_D is the drag coefficient which is a result of skin friction and the reaction on the particle of its disturbance on the flow. In addition to drag, there is a *lift force*, F_L, which is due to the Bernoulli effect of a vertical gradient of streamwise velocity resulting in lower pressure on the particle's upper compared to its lower surface. F_L is given by

$$F_L = 0.5.\rho_w.C_L(u_T^2-u_B^2)A_p \qquad (2.2)$$

where u_T and u_B are the velocities at the top and bottom of the particle. C_L is the lift coefficient and is usually empirically derived.

The total resisting force, F_R, against which the drag must act is the resolved component of the submerged particle weight and lift force

$$F_R = [((\rho_s-\rho_w)g.v.\cos ß) - F_L] \tan ø_0 \quad (2.3)$$

where ß is the slope of the bed and $ø_0$ is the friction angle (the angle up which the particle must move to be successfully entrained). At the moment of entrainment, $F_D \geq F_R$

$$0.5.\rho_w.C_D.\langle u^2(z)\rangle.A_p \geq [((\rho_s-\rho_w)g.v.\cos ß) - (0.5.\rho_w.C_L(u_T^2-u_B^2)A_p)] \tan ø_0 \quad (2.4)$$

The above approach was used successfully by Wiberg & Smith (1987) and Andrews & Smith (1992) as the basis of numerical models explaining the entrainment of non-embedded grains from the surface of a gravel bed. The general application of the model to field situations has not been entirely successful due to assumptions made concerning the approaching velocity field, the exposure or embeddedness of the particle and turbulent flow fluctuations.

As will be discussed later, the flow field over fluvial gravels is turbulent. This means that the velocity will fluctuate both in magnitude and direction. This complicates the velocity terms in Equations 2.1, 2.2 & 2.3 by introducing continually varying velocity and making the velocity vector three dimensional. The latter causes problems in the otherwise convenient splitting of the forces on the particle into the lift and drag components. In order to assess the nature of the approaching velocity field, it is therefore necessary to investigate the generative mechanisms and properties of turbulence over gravel beds. The following sections will present arguments from the literature and from basic physical reasoning which help to determine the nature of the turbulent field.

2.2 Homogeneous turbulence

When considered in the time-average sense, flow over rough gravel beds appears to be unidirectional. It is this apparent property of the flow which is intrinsic in the force-balance entrainment model, although in reality flow reversals and eddying are superimposed on the mean streamwise flow field.

In considering turbulence at a point, it is useful to make use of a 3-D velocity vector to define the instantaneous magnitude and direction of velocity. The frame of descriptive reference adopted is shown in Figure 2.2 where u, v and w relate to velocities in the x (streamwise), y (vertical) and z (spanwise, cross-stream) directions. The Reynolds decomposition resolves the vector into three Cartesian components as

Streamwise, x direction: $u = \langle u\rangle + u'$

Vertical, y direction: $v = \langle v\rangle + v'$

Spanwise, z direction: $w = \langle w\rangle + w'$

where u, v, w are the instantaneous velocities, <u>, <v>, <w> are the time-average velocities onto which are superimposed u', v', w', the instantaneous fluctuations from the mean. Positive fluctuations in u', v' and w' are in the downstream, upwards and true left directions respectively.

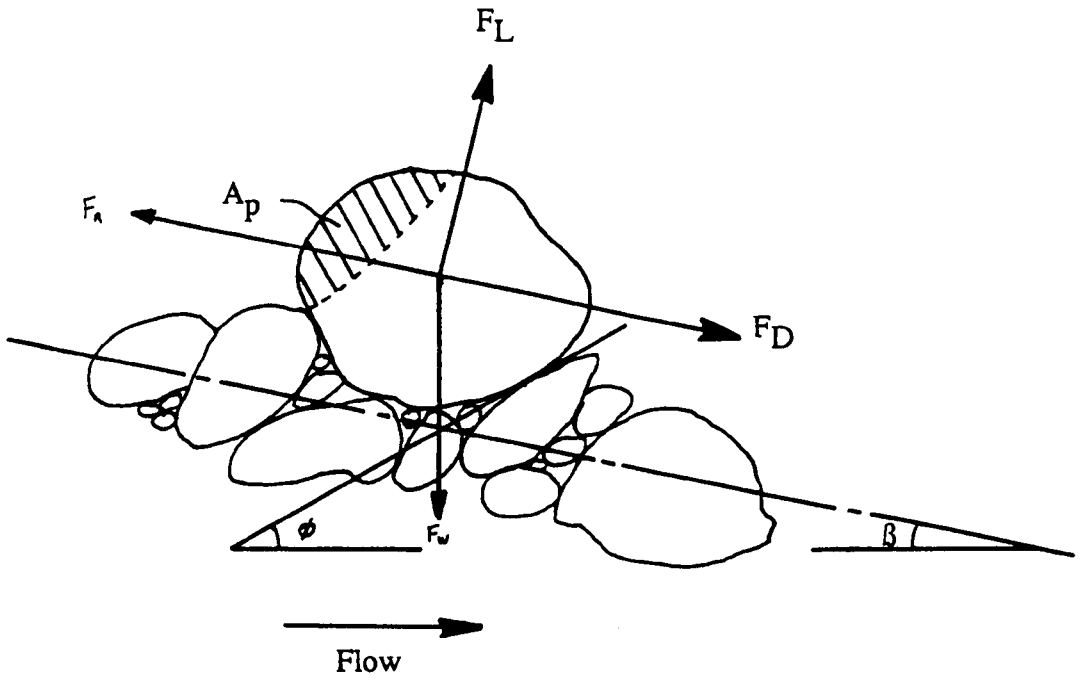

Figure 2.1 The forces acting on a particle in unidirectional flow; lift force, F_L, drag force, F_D, area facing approaching flow, A_p, weight, F_W and resistance, F_R.

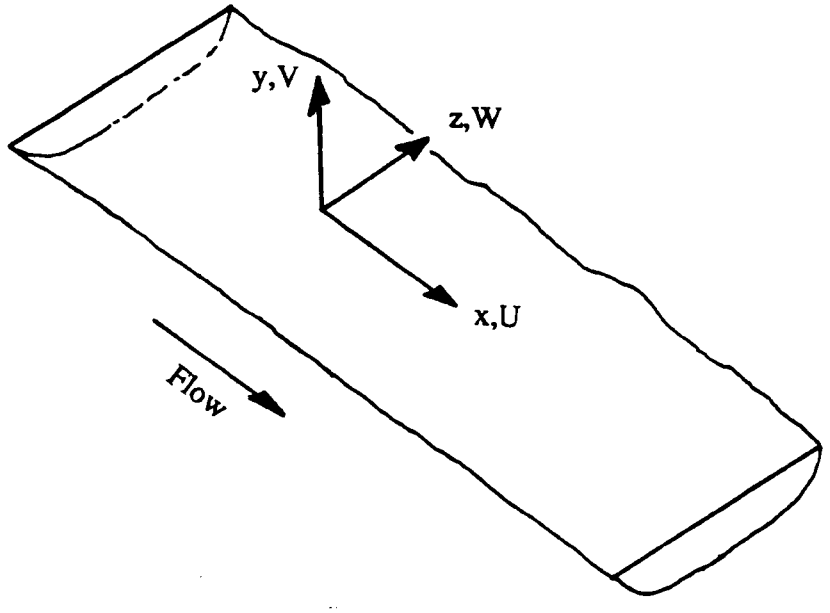

Figure 2.2 The Cartesian components of direction (x, y & z) and velocity (U, V & W).

Flow over fluvial gravel beds is turbulent. This means that during the observed time, the magnitude and direction of the 3-D velocity vector can vary considerably. This has important consequences for the drag and lift forces of Equations 2.1, 2.2 & 2.4.

Turbulence is generated by the spatial rate of change of velocity, d_u/d_y (shear) being too great to be accommodated by the viscosity, ν, resulting in distortion and ultimate collapse and mixing of the otherwise parallel streamlines. The degree of turbulence depends on the ratio between the fluid's inertial and viscous forces, as expressed in the Reynolds number

$$Re = UR / \nu \qquad (2.5)$$

where ν is the kinematic viscosity, R is the hydraulic radius and U is the mean velocity..

If $Re < 500$ then laminar flow exists, $500 < Re < 2000$ then the flow is 'transitional' whilst if $Re > 2000$ then the flow is turbulent. For water flowing over gravel beds, typical values of Re are > 5000 at low flow conditions, and can be over 10^5 at conditions resulting in gravel transport. It is these latter conditions that are of interest to this work.

Turbulent boundary layer flows can be split into three zones: the viscous sublayer, the log or 'buffer' zone and the free stream (Figure 2.3).

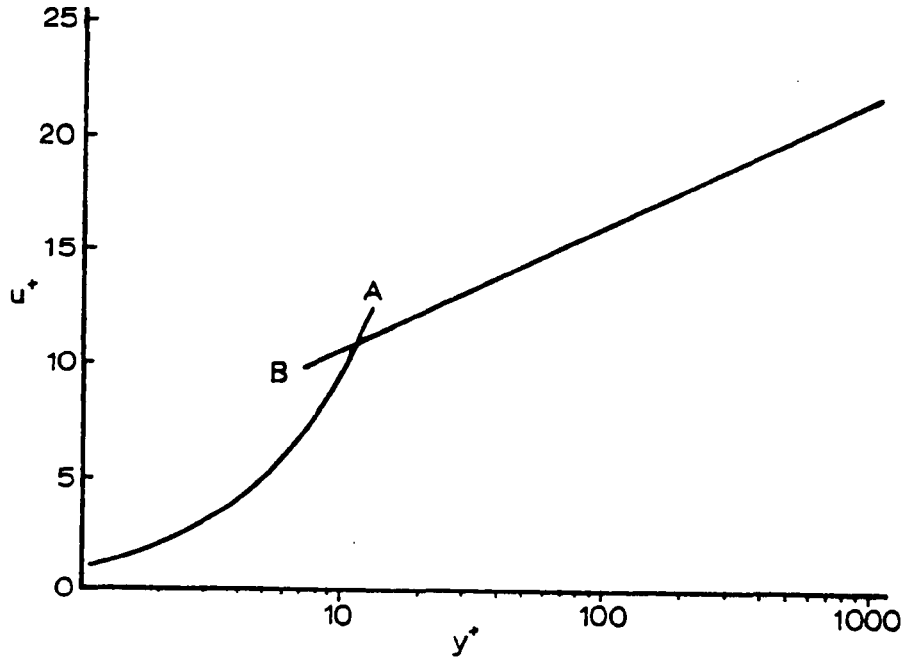

Figure 2.3 The wall-normal profile of dimensionless streamwise velocity. Sublayer exists from $0 < y^+ < 10$, free stream not shown (after Smith & Metzler, 1983) ($y^+ = y.U^*/\nu$, $u^+ = u.U^*/\nu$).

Although du/dy may be very high near to the boundary, the absolute velocity is low which makes it possible for a viscous 'sublayer', δ_{sub}, to exist beneath otherwise turbulent flow. Keulegan (1938) gave the thickness of the sublayer as

$$\delta_{sub} = 11.6.\nu / \sqrt{(\tau_0.\rho_w)} \qquad (2.6)$$

Nikuradse (1933) showed that as Re increases, then the thickness of the sublayer decreases. Therefore, with increasing flow Re, the relative roughness of the 'wall', k_s/d (where k_s is a characteristic roughness height, d is depth), increases relative to the viscous sublayer thickness. It is also the case that as the absolute roughness of the boundary increases, the greater the disturbance to the sublayer.

Outside the sublayer is the buffer zone. The vertical profile of mean streamwise velocity in this zone shows a characteristic increase as ln(y) away from the wall (Figure 2.3). The Karman-Prandtl law of the wall expresses this as

$$u_y/u_* = 1/\kappa \, . \, \ln(y/y_0) \qquad (2.7)$$

where u_y is the velocity at height y above the wall, κ is the empirically derived Von Karman constant κ 0.4 and y_0 is a roughness height. Full derivations of this relation can be found in various texts (e.g. Chang, 1988). There is some debate regarding the universality of κ = 0.4 (Kuhnle, 1992), and it is believed that high suspended sediment concentration can reduce the value of κ by as much as 50% (Coleman, 1981). This relationship is poorly understood (Kuhnle, 1992), but the error can be minimised by measuring u in the lower 20% of flow depth. κ = 0.4 was adopted in this work, and it is accepted that there may be some error.

The shear strain within the profile results in a shear stress, τ, and the mean shear stress acting on the bed is τ_0. This represents the force per unit area of the flow on the bed. U_* is the shear velocity, and is given by $\sqrt{(\tau_0/\rho_w)}$.

The rate of change in velocity with distance from the wall decreases until it becomes negligible. This region is known as the free stream and represents the flow field which is largely independent of the drag influence of the wall. The mean velocity of this zone is the free stream velocity, U_∞. A non-fluvial example of this is geostrophic wind which exists above the atmospheric boundary layer. The shear and velocity characteristics of these winds are completely independent of the ground conditions beneath.

In gravel-bed rivers, the definition of these zones is complicated for several reasons.

A boundary is said to be 'hydraulically rough' when the roughness elements protrude through the viscous sublayer and into the buffer zone, strictly $k_s > 5\delta_{sub}$. In gravel bed rivers, characteristic values of viscosity, ν and water density, ρ_w, are of the order of $\nu = 1.31 \times 10^{-6} m^2 s^{-1}$ and $\rho_w = 1000 kgm^{-3}$, respectively. Shear stress, τ_0, will typically range from 5 to $100 Nm^{-2}$, and through Equation 2.6 this gives a thickness of δ_{sub} to be between 2×10^{-7} to $5 \times 10^{-8} m$. The lower size limit in the Wentworth scale for gravel is $2 \times 10^{-3} m$, and if viewed as an approximation to the length scale of the roughness, it is four orders of magnitude greater than the hypothetical thickness of the sublayer that would exist for these hydraulic conditions in the absence of roughness. This means that in gravel bed rivers, a spatially coherent viscous sublayer does not exist. This becomes significant later when the generation mechanisms of coherent structures in the turbulent boundary layers are being considered (Section 2.3.1).

The majority of the boundary layer depth over fluvial gravel beds can be considered as being a buffer zone. Velocity profiles taken over gravel beds usually approximate to a

logarithmic form, and it is from this that boundary shear stresses are calculated (e.g. Wilkinson, 1984; Ashworth & Ferguson, 1989, Wiberg & Smith, 1991). If the regression of u on ln(y) yields the equation, $u = a + b(\ln(y))$, then it can be shown that $\tau_0 = \rho_w.b^2.\kappa^2$ (Wilkinson, 1984). Over gravel beds, y_0 represents a hypothetical surface within the gravel framework at which the velocity profile goes to zero.

In fluvial flows over gravel beds, the upper parts of the buffer zone often appear to become confused. This is why, when calculating shear stress from the velocity profile, it is recommended to use the lower parts of the profile (Wilkinson, 1984). However, the velocity still tends to increase, and so it cannot be considered to be the free stream. Generally, due to the limited flow depths over gravel beds, the free stream does not exist.

The flow within the buffer zone is turbulent. Homogeneous turbulence is defined as u', v' and w' being distributed as $N(0, \sigma^2)$ and not mutually correlated. In addition, there is no temporal structure to the flow. This can be formalised in various ways by reference to time series analysis techniques, but let us for now be satisfied with the qualitative definition. This definition will be used as the basis from which to compare the evidence of flow non-homogeneity that emerges from both the literature and the data analysis.

2.3 Coherent turbulent structures.

There is an expanding base of evidence supporting the existence of flow structures in geophysical turbulent boundary layers (e.g. Bowden & Fairburn, 1956; Kline *et al*, 1967; Williams et al, 1989; Clifford 1990; Lapointe, 1992, Robert *et al*, 1993). It is in the context of the debate concerning the nature and generative mechanisms of flow structures in gravel bed rivers that this thesis is set.

A coherent structure may be defined as "... a large scale turbulent fluid mass with a phase-correlated vorticity over its spatial extent" (Hussain, 1983). This means that the direction and magnitude of any two velocity vectors within the structure will show a degree of transient correlation over a timescale similar to the lifetime of the structure. Coherent flow structures are often vortices within the flow field.

The generation of vortical structures in a boundary layer involves some form of hydraulic instability across a shear layer in the fluid. The vortical structure can be considered as a type of mixing. Shear layers develop in turbulent flows as a result of or resulting in (or both) the existence of vortical structures.

Let us consider the mechanism by which shear can result in the formation of vortical structures. Consider one parcel of fluid passing another as two parcels of fluid of different momentum separated by a shear layer. Due to the Bernoulli effect, the velocity gradient across the shear layer results in a pressure gradient being set up across it. This forces fluid from the side of lower momentum to that of higher momentum producing a turning moment and the onset of vortex development.

In many cases, a series of counter-rotating vortices form along a shear layer, the reasons for which are similar but more complex than that given above, and are outlined in many texts (e.g. Massey, 1979; Chadwick & Morfett, 1986). This is known as a Kelvin-Helmholz instability.

In relating the mechanism of vortical structure generation to its possible application to flows in gravel bed rivers, two pertinent questions need to be addressed: where and how do the shear layers form, and how do the resulting structures contribute to the macro-turbulence of the whole flow field? As a general principle, let us assume that if a shear layer can exist, there is the potential for a vortical structure to form. In flows involving a fluid of single density, shear layers can exist for three reasons - due to the frictional drag of a wall, the separation of flow at a step in the wall, or free shear between initially independent fluid parcels.

Several explanatory and descriptive models of coherent structure generation exist. They are the result of various approaches and involve observations made in several geophysical environments. Their interpretation will be made in the context of shear layer instability as the common mechanism. They will now be considered in terms of whether they can be applied to flows over fluvial gravel beds.

There are basically two categories of model. The first assumes that the gravel bed is a surface (e.g. Offen & Kline, 1975). The second ultimately treats the gravel bed as an array of individual elements. It will be referred to as the 'vortex shedding' model (e.g. Clifford *et al*, 1992), and asserts that the dominant generation mechanism is a function of the boundary roughness.

2.3.1 The sublayer-buffer layer roll-up model.

The original version of this model resulted from experimental flume work over hydraulically smooth beds. Invariably, flow visualisation is employed, and from observations of filmed plan and side elevations qualitative and quantitative descriptions of the observed structures are made. The first complete description of the model was made by Kline *et al*, (1967), and this, along with the reviews of its development by Kline & Robinson (1990), Grass *et al* (1991) and Best (1993), will be used as the basis for this section.

Broadly, the mechanism of the model can be summarised as follows. A unidirectional turbulent flow over a smooth bed has a viscous sublayer of finite thickness, δ_{sl}, at the wall. Within this layer there exist sub-parallel streamwise 'streaks' in the region $0 < y^+ < 10$ where y^+ is an inner wall distance variable and given by

$$y^+ = y.U^*/\nu \qquad (2.8)$$

where y is the perpendicular distance from the wall (Theodorsen, 1952; Smith & Metzler, 1983).

The streaks are filaments of low speed fluid with a sub-parallel streamwise axis and counter-rotational vorticity (Figure 2.4) (Lighthill, 1963; Blackwelder & Eckelmann, 1979; Levi, 1983b). Several of these streaks intermittently undergo distortion resulting in concave-upwards flexing, and are uplifted to experience the slightly higher velocities away from the wall. The reasons for this distortion are poorly understood (Kline & Robinson, 1990), but it may be

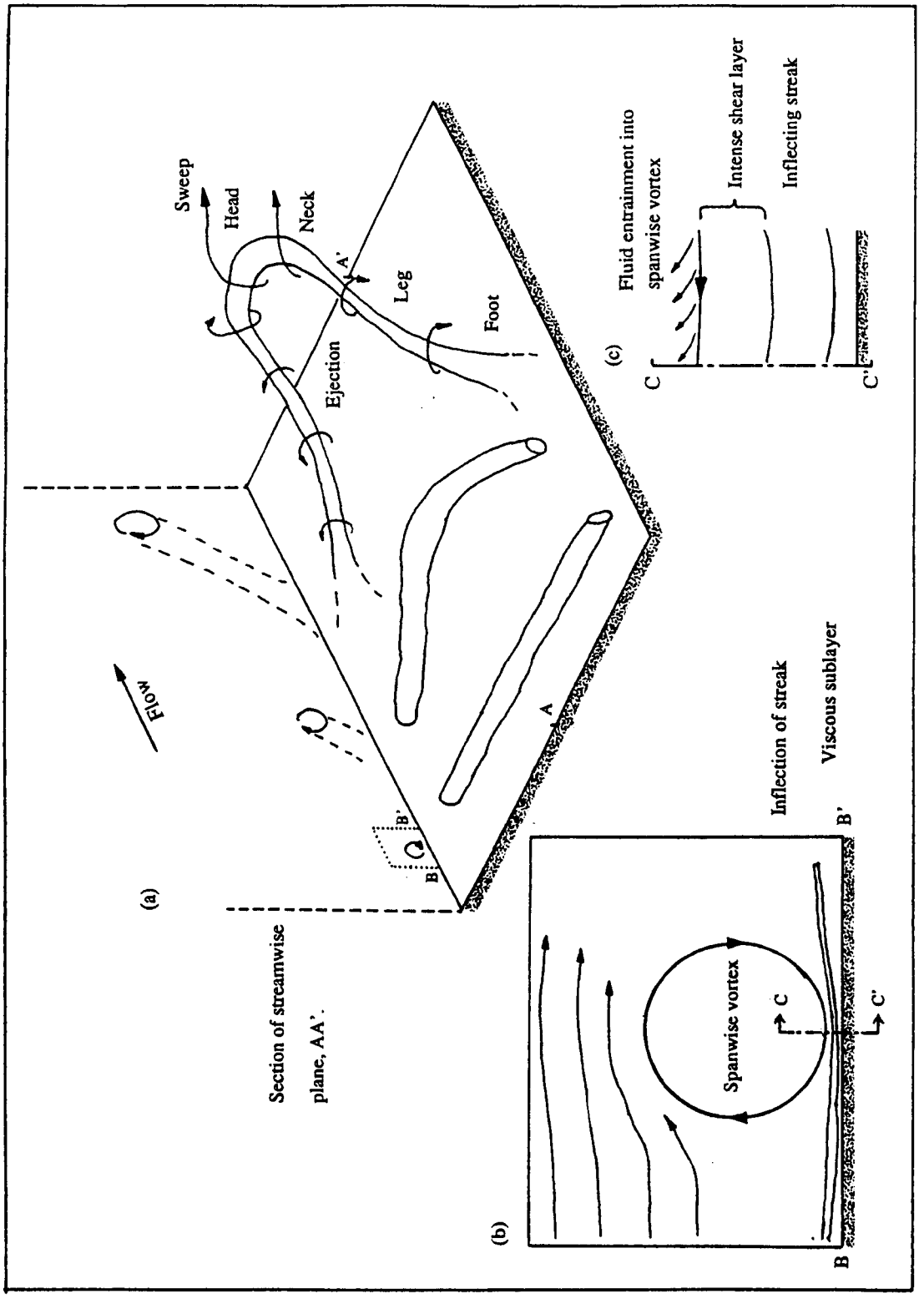

Figure 2.4 The generation of a hairpin vortex over a smooth bed. (a) General schematic illustration of hairpin stretching. (b) Section BB': inflection of sublayer streaks, spanwise vortex generation, upwards fluid motion. (c) Detail of wall shear zone.

caused by the impact of an outer-zone macro-turbulent structure with the near-wall region (Kline & Robinson, 1990; Levi, 1983b).

The uplift of the streaks from the wall generates intense rates of shear between the low-momentum near-wall region and the higher-momentum outer zone fluid (Robinson, 1990). This results in roll-up and the formation of a vortex with a spanwise axis of rotation. This vortex experiences shear at the outer edge of the viscous sub-layer (y^+ » 8-12) due to intermittent pressure gradients set up from the outer flow region. This produces an oscillation of the vortex which becomes increasingly violent and of increasing amplitude ($10 < y^+ < 30$).

The oscillation of the vortex is due to its rapid absorption of energy from the outer flow (Grass *et al*, 1991; Levi, 1991) and instability set up due to the rapid rate of shear across the interface of the high and low momentum fluid layers. From numerical simulations of the inception of the spanwise vortex, it has been suggested that this rapid energy absorption can help to explain the sudden ejection of fluid from the near wall region (Walker & Herzog, 1988; Smith *et al*, 1991; Walker, 1990). The vortex is progressively 'stretched' into a 'hairpin' shaped vortex loop (e.g. Kline *et al*, 1967; Wallace *et al*, 1972; Hinze, 1975; Smith, 1978; Best, 1992) and lifted away from the wall by the shear in the main-stream (Kim *et al*, 1971). This violent lifting of low-momentum fluid from the wall zone is referred to as an ejection, and is characterised by -u' and +v' fluid components.

Grass *et al* (1991) have visualised several loops and show them to be irregular three-dimensional features which crudely exhibit an anatomy of two **legs** pinned by their **feet** to the near-wall zone, and linked via the **neck** to the **head** of the loop (Figure 2.4). Elevations of the loops in the x-y plane show the vortex is stretched at an orientation of $\underline{c}.45^{\circ}$ to the wall (Head & Bandyopadhyay, 1981). Perry *et al* (1987) and Head & Bandyopadhyay (1981) both suggest that the trailing legs of stretched vortices are in fact the same as the near-wall streaks.

Associated with the direction of the vorticity are local zones of fluid transfer. Between the limbs of the 'hairpin' is a zone of upwardly mobile low-momentum fluid. Such ejections are characterised by positive vertical velocity (+v') and a streamwise velocity of less than the local mean velocity ($u \approx 0.8\langle u \rangle$) (Kline *et al*, 1967). The ejections represent an important mechanism of momentum transfer of low-speed fluid from the near-wall zone to the outer regions of the boundary layer.

Figure 2.4 shows that the head of the hairpin vortex is responsible for directing high-momentum outer-zone fluid downwards and forwards towards the wall region. These are referred to as 'sweeps' and are characterised by +u' and -v' velocity components. Muller & Gyr (1986) observed that the plan shape of the impact of the high-velocity fluid with the bed is indeed similar to that of the horseshoe of the vortex. Observations suggest that these 'sweeps' slow down on impact with the inner zone fluid, are at least partly responsible for the generation of the next generation of streaks, and may be responsible for the kinking of the near-wall streaks which instigates the structure. This implies that the structures are temporally linked, and can be viewed as cyclical in their generation.

The two dominant structures of the above model have led to it being called the 'burst-sweep' model. There is some debate regarding whether the period of bursting, T_b, scales with wall variables or outer zone flow variables. This has important implications regarding whether the system is driven by the sublayer or the outer zone.

It has been shown from flume experiments over smooth beds, from sand bed rivers and from tidal flows that T_b scales with outer zone variables as

$$<T_b> \approx 5.d / U_\infty \qquad (2.9)$$

(Rao *et al* ,1971; Jackson, 1976; Gordon, 1975). All of these data relate to flow Reynolds numbers of order 10^3-10^5 which represent the types of values likely to be encountered over gravel beds. As Rao's work concerned small-scale bursting in a flume, whereas Jackson's related to the larger scale of rivers, the similarities of the independently derived burst periods is even more remarkable (Levi, 1991). This relation (Equation 2.9) will be used as an indicator of the presence of these structures in the more complex fluvial gravel-bed environment.

One of the main assumptions in this model is the existence of a spatially coherent boundary layer undisturbed by the protrusion of roughness elements. The same structures have been observed over hydraulically rough beds (Grass, 1971; Perry *et al*, 1987; Grass *et al*, 1991). In all of these cases, the beds were of uniform roughness size and spacing. In terms of roughness element density as explained by Nowell & Church (1979), the bead beds used by Grass (1971, 1991) and 'grid' beds of Perry *et al* (1987) would produce 'skimming flow' which is effectively blind to the presence of the roughness. This appears to have allowed a form of organised sub-layer to have developed. The process by which this occurs is discussed further in Chapter 6.

Over mixed gravel beds, however, the roughness exhibits less consistency in the roughness element spacing and a greater amplitude in protrusion. The effect of this would be deflection of flow in the spanwise and vertical directions leading to the generation and interaction of eddies around clasts. This more open roughness would not allow any spatially coherent sub-layer to develop over the bed surface. Indeed, section 2.2 showed that characteristic gravel bed roughness heights are typically four orders of magnitude greater than the hypothetical sublayer thickness. Therefore, the interaction of wall streaks cannot be the reason for the development of coherent structures over natural gravel beds.

The stoss, roof and side surfaces of the gravel particles themselves are effectively walls from which a local boundary layer may develop. This raises the question as to whether these surfaces are sufficiently extensive to allow the generation of wall streaks and the subsequent development of hairpin vortices.

Let us consider the spanwise direction first. Kline *et al* (1967) suggest that the average dimensionless spanwise spacing of streaks in a viscous sub-layer is given by $\lambda^+ \approx 100$ (where $\lambda^+=\lambda.U^*/\nu$, λ is the observed streak spacing). Assuming shear stresses of 1-10 Nm^{-2} on the particle face, this gives a characteristic spacing of $\underline{c}$. 0.4 - 1mm. For gravel particles, their

exposed surfaces would be 2 - 64mm wide, suggesting that enough width exists to accommodate streaks.

In the streamwise direction, there are two aspects that need to be considered. Firstly, from the upstream end of the particle facet, the local boundary layer would develop over some distance downstream before becoming quasi-stable into a sublayer and buffer zone. Secondly, a hairpin vortex which develops as a result of streak deformation is fed by the low-speed sublayer fluid until it is shed. This means that for the successful and complete development of hairpins over the facets of particles, the developed boundary layer must be of sufficient streamwise length to accommodate the hairpin from inception to shedding. Due to the absence of quantitative information regarding the spatial scale of hairpin development, it is impossible to suggest whether they would form. However, the published visualisations of vortex sections in the streamwise wall-normal plane (e.g. Grass, 1982) suggest that they are of a similar order of magnitude to the size of a gravel particle.

On the basis of the limited information available, it may be possible for hairpin vortices to form over the surfaces of individual particles of a gravel bed. However, it is no better than conjecture, and any better understanding of their characteristics would require extensive experimental work to be undertaken.

To summarise, the non-uniform high relative roughness of gravel beds obviates the development of a spatially coherent viscous sublayer. Assuming that a major requirement for the development of the burst-sweep structures is the interaction of an outer, turbulent layer with the viscous sublayer, the absence of a sublayer means that such a development cannot take place. This is significant as either the structures observed over fluvial gravel beds are not genetically the same as those observed over smooth walls, or the presently hypothesised mechanisms of sub-layer - outer zone interaction to explain their formation and development are not entirely correct.

2.3.2 Vortex shedding from obstacles.

Two recent studies have shown that changes in roughness in gravel-bed rivers lead to significant differences in turbulence characteristics (Clifford & French, 1993, Robert *et al*, 1993). This suggests that the macro-turbulent component of the flow field is at least partly determined by the nature of the roughness. This necessitates investigation into how the roughness influences the turbulence.

The underlying axiom of the vortex shedding model is that it considers the individual roughness elements of a gravel bed as obstacles locally deflecting flow in three dimensions. Visualisations of the flow separation in the lee of hemispherical obstacles have revealed the existence of intermittently shedding vortices over a wide range of flow Reynolds numbers (Acarlar & Smith, 1987; Kawanisi *et al*, 1993).

Consider flow over a hemispherical obstruction (Figure 2.5). Stagnation of the flow occurs on the stoss side of the obstruction producing a standing vortex, the limbs of which

extend to the lee of the obstruction. In the range of Acarlar & Smiths' experiments (30 < Re < 3200), the stoss standing vortex is spatially stable. It does not form, however, if the stoss side of the hemisphere is streamlined towards a tear-drop shape.

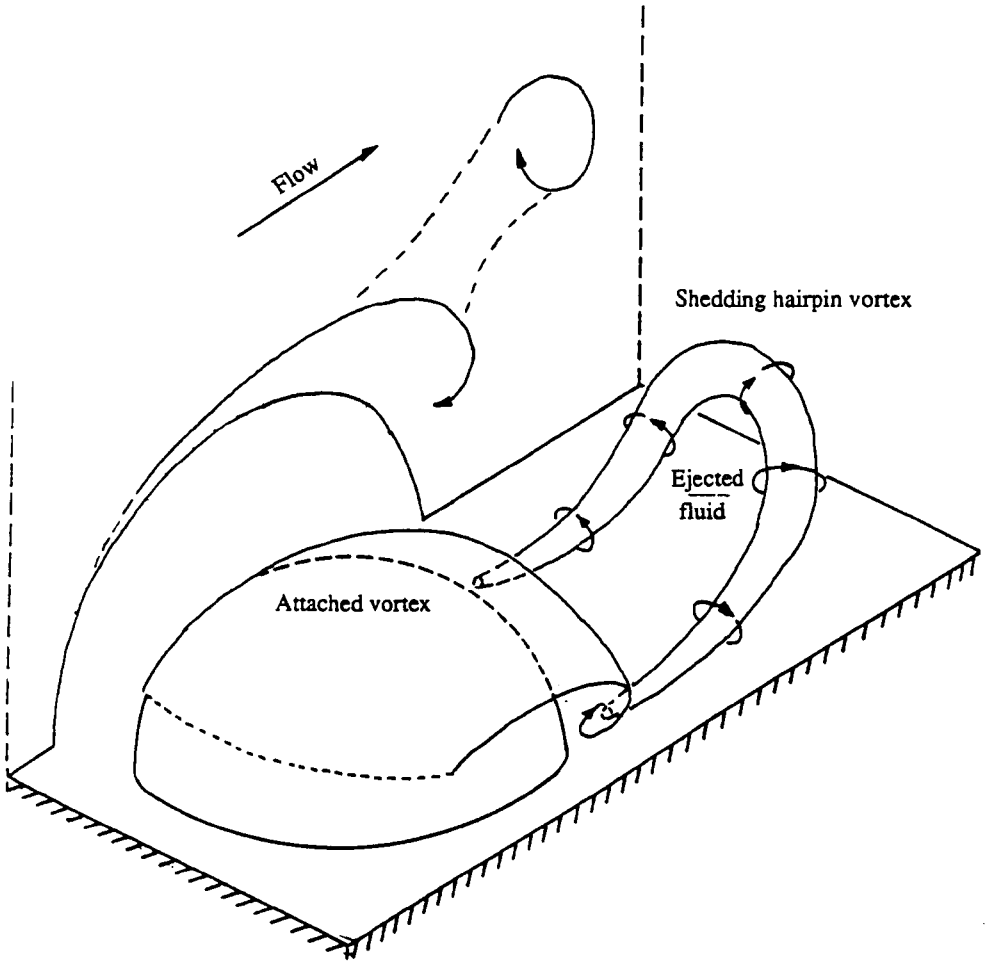

Figure 2.5 Oblique and streamwise elevation of the shedding of the lee vortex from a hemi-spherical obstruction.

In the lee of the obstacle, separation of the flow occurs at Re > 30 (Massey, 1979), and a hemi-annular vortex is generated (Figure 2.5). At Re > 120, the vortex is shed from the obstacle, the mechanisms of which are illustrated in Figure 2.5. The vortex extracts energy from the outer flow zone which adds to its vorticity. This in turn causes it to expand and become less stable. As the rate of energy interchange is related to the velocity gradient across the separation layer, it is the roof of the vortex that leads the process. Once the vortex tip impinges on the main velocity field, it is 'sucked' out of the obstacle wake and progressively stretched, causing the evolution to a 'hairpin' shaped structure. In the vertical streamwise plane, this structure lies at $\underline{c}$. 45° to the horizontal. The stretching of the limbs and the fluid convection between them forces them to move together. This ultimately weakens the vorticity of the limbs until they snap, releasing the tip to be advected by the free stream.

A vortex re-forms in the lee of the obstacle, and the cycle is repeated causing periodic shedding. For the shedding of vortices from the lee of cylinders in free flow, a vortex "street"

develops downstream of the cylinder (Tritton, 1977) comprising a tail of advecting shed vortices. The temporal shedding frequency, *f*, is related to the cylinder diameter, D, and the free stream velocity, U_∞, and is related to the empirically derived Strouhal number, *S*

$$S = f.D / U_\infty = 0.198 [1-(19.7/Re)] \quad (2.10)$$

(Strouhal, 1878).

Levi (1983) suggests that the Strouhal number is largely independent of Reynolds number and shows that for a variety of shedding conditions involving shedding in both 2 and 3 dimensions, a general form can be expressed as

$$S = f.D / U_\infty = 0.16 \quad (2.11)$$

However Chang & Chern (1991) suggests that for shedding from cylinders, the periodicity of shedding is regular only for $250 < Re < 10^4$. This is not the case for the shedding from a hemisphere. Figure 2.6 shows how the Strouhal number is related to Re for hemispheres. It suggests that at Re < 1600, the relation is linear with a discontinuity at ç. Re = 500 (Acarlar & Smith, 1987).

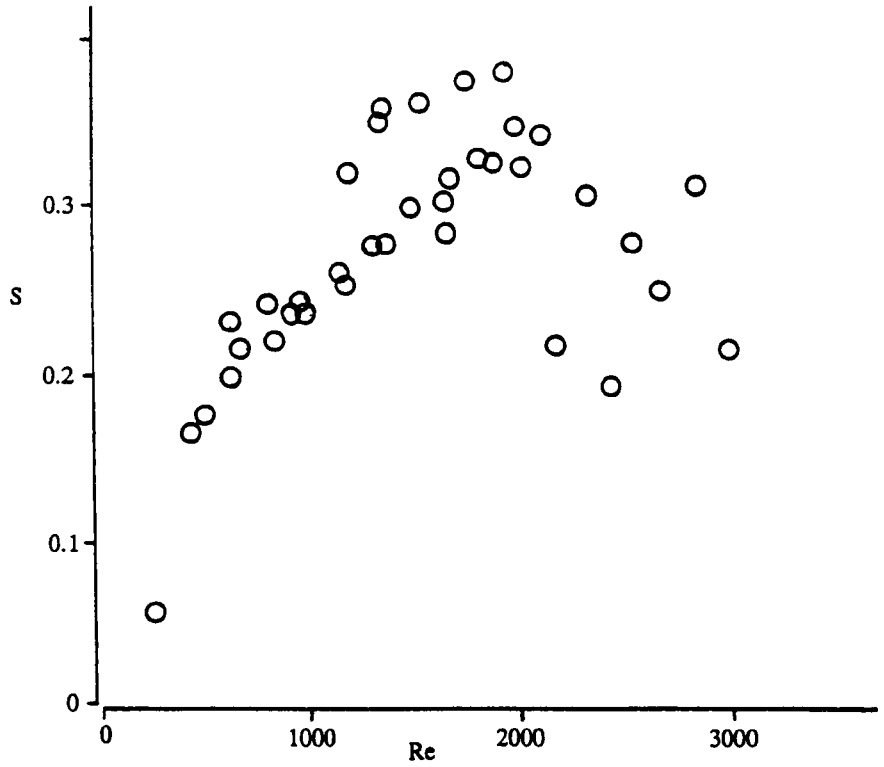

Figure 2.6 The relation of Strouhal number, S, against Reynolds number, Re, for the shedding of vortices from isolated hemispheres (After Acarlar & Smith, 1987).

At Re > 1600, the linear relation appears to break down yet it is these conditions that are of primary interest to the problem of gravel-bed turbulence. At higher Re, the shedding is better described as intermittent rather than periodic. Moller (1938) suggests that there are two modes of shedding mechanism, and Acarlar & Smith interpret these as supplementing the radius and velocity in the Strouhal relation.

In a simplistic sense, it would seem sensible to accredit the breakdown to a turbulent approaching velocity field. Through the Strouhal relation, this would be represented by a fluctuating velocity term. U_∞ determines the spatial geometry and the rate of shear on the boundaries of the detached eddy zone, and subsequently influences the developing vorticity and stability of the shear-layer instabilities which are responsible for the shedding. A fluctuating U_∞ would feed through the Strouhal relation producing intermittent shedding of decreasing regularity. At a timescale appropriate to the shedding mechanisms, U_∞ cannot be assumed to be constant in turbulent flow. Even if a fluctuation in U_∞ exists for a short time relative to a shedding timescale, it would cause a perturbation in the processes leading to shedding. In order to incorporate a fluctuating U_∞, it would be necessary to describe probabilistically the approaching velocity field.

For a river bed composed of a mixed gravel, there is a distribution of obstacle sizes which is related, but not identical, to that of the bed particle size distribution. The presence of an array of obstacles would have two effects on the macro-turbulence. Firstly, vortices would be shed at different frequencies and would be of different sizes, and secondly the presence of adjacent obstacles would affect the approaching flow field.

Through the Strouhal relation (Equations 2.10 & 2.11), it would be expected that for similar turbulence fields, the shedding would be less frequent from larger obstructions than from small. In addition, the larger obstacles would shed larger vortices, and hence their persistence in the free flow once detached would be greater. The coalescence of the shed vortices would therefore be complicated by the hierarchy of vortex sizes and frequencies. This is discussed further in section 2.5.1.

Investigations have been made into the mutual interference of neighbouring cylinders on vortex shedding characteristics, but not of adjacent hemispherical obstructions. Cylinders closely spaced in the spanwise direction act as single obstructions (Spivack, 1946), but as they are separated in the cross-stream direction, a critical spacing exists at which the cylinders begin to act individually. For two adjacent cylinders, Kim & Durbin (1988) identified two states where the position of the streets were quasi-stable. In each state, the street of one cylinder dominated that of the other, but occasionally dominance would switch to the other. The 'flopping' between the two states was seen to generate a further periodicity $\underset{\sim}{<}.10^{-3}$ times the vortex shedding frequency. At L/d > 4.2 (where L is the centre-to-centre spacing), the shedding is independent but the frequency of shedding from the adjacent cylinders is in phase (Thomas & Kraus, 1964).

If the cylinders are separated in the streamwise direction, there is a point, at L/d = 3.2, where the periodic shedding is suppressed altogether (Thomas & Kraus, 1964; Strykowski & Sreeivasan, 1990). At spacings greater than this, different complex patterns of constructive interference develop.

Arrays of more than two cylinders produce more complex patterns of vortex street development, the frequencies and development of which are being continually modified by further interactions (e.g. Lam & Cheung, 1988).

Over gravel beds, the obstacle array is very complex both in terms of spacings and sizes. This would affect the shedding characteristics by generating fluctuating approach velocities which would result in varying shedding frequencies and very complex interactions between neighbouring obstacles. The end result of this would be an extremely complex suite of vortices being shed into the main flow. The post-shedding interaction of the vortices is inevitable, and vortex coalescence is discussed in section 2.5.1.

The 'attached vortex' hypothesis of Townsend (1976) relates the size of vortices in a boundary layer to the distance from the wall. In the light of Head & Bandyopadhyay's visualisations, Perry & Chong (1982) interpret such an increase in terms of a hierarchy of scale of grouped hairpins with the increase in spatial scale between hierarchical levels being related to the square of the distance from the wall (Perry & Chong, 1982). The boundary layer thickness therefore provides a limit to the size of the largest vortex which could be accommodated. Although the mechanism of connection between the scales is as yet vague (Grass *et al*, 1991), it supports the conjecture of Robinson (1990) that vorticity is 'pumped' from the near-wall to the outer regions of the boundary layer.

2.4 The application to gravel-bed rivers of coherent structure models

The two macro-turbulent structure models are not only based on different generative mechanisms, but produce different outcomes when applied to real flows. In a simplistic sense, the layer roll-up model generates coherent structures which are characterised by a mean periodicity, $<T_b>$. Conversely, the vortex shedding model generates a suite of similar structures, the dimensions and associated frequencies of which scale with the range of obstacles present in the flow and the mean approach velocities at each. Let us now compare these for the conditions of a typical gravel bedded channel.

Consider a flow field in a fluvial channel where d = 0.5m, the velocity profile is given by $u = 1.5 + 0.163\ln(y)$ (giving $<U> = 0.93\ ms^{-1}$, Re = 496,000, $\tau_0 = 4Nm^{-2}$). The bed is composed of a mixed gravel producing a size distribution of obstacles (OSD), f(O), where $<O> = 19mm$, $\sigma_O = 5mm$, and f(O), can be represented by

$$f(O) = e^{-1/2[(O-<O>)/\sigma]2} / \sqrt{2\pi} \qquad (2.12)$$

This distribution is truncated at 2mm and 40mm.

If the generation of macro-turbulence is caused by the stretched vortex model, then from Equation 2.9, the mean burst periodicity, T_b, is given as 2.7 s.

It is possible to calculate the range of frequencies generated due to vortex shedding by using Equation 2.10. Firstly, the shedding frequency for each size of obstacle present in the OSD is calculated, using u_y instead of U_∞ where u_y is the velocity at the top of each obstacle

size given by the velocity profile. This assumes that the troughs in between obstacles are co-planar. Secondly, for unit time, the frequency distribution of the frequencies themselves is derived by weighting each frequency, f_i, by the relative proportion of obstacle size, O_i, in the OSD.

Figure 2.7 shows the components of these calculations for the conditions stated above. The distribution of frequencies tends to be positively skewed relative to the OSD. The dominant frequency shed by the assemblage of obstacles ≈ 9.1 Hz (≡ a period of 0.11 s.) which relates to those shed by a particle slightly finer than the mean. The range of shed frequencies for the assemblage covers an order of magnitude from 4.8 to 48 Hz. (≡ periods of 0.21 to .021 s.).

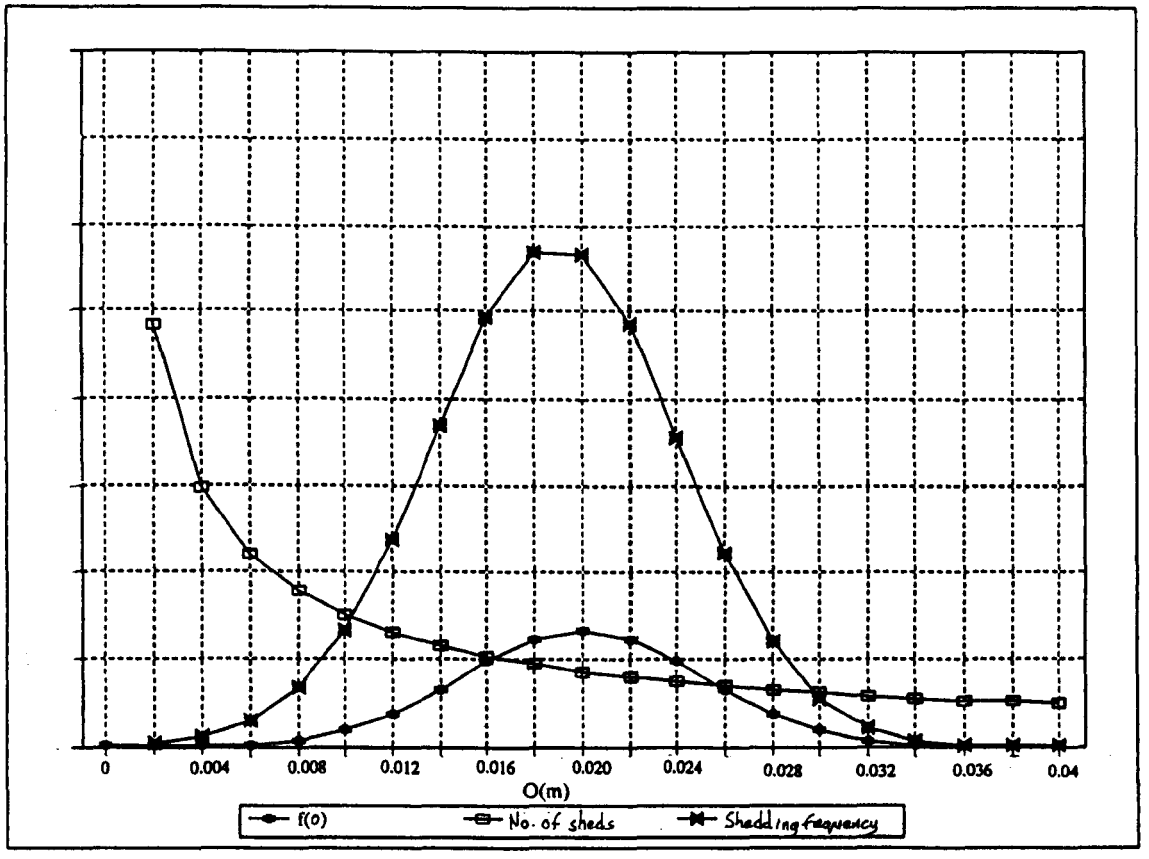

Figure 2.7 The distribution of shedding frequencies from a distribution of obstacles, f(O).

In order to compare the effects of the two models on intermittency characteristics, the burst period, T_b, given by Equation 2.9 can be compared to the period of shedding, given by 1/f in Equation 2.11. The above calculation shows a large discrepancy between the temporal character of the structures to which they relate. This is useful in helping to determine the type of feature present over gravel beds, and is utilised in the discussion of the results in Chapter 6.

2.5 Larger vortical structures

Larger vortical structures than those described above have been observed and monitored in geophysical flows (e.g. Fiedler & Head, 1966; Laufer, 1975; Willmarth, 1975; Grass, 1982).

The structure of these vortical features is less well documented that for the smaller features described above. Their formational mechanisms are less well understood than those of the hairpins (Grass, 1982), but generally there are two general hypotheses; either they are the agglomeration or coalescence of smaller vortices (e.g. Head & Bandyopadhyay, 1981) or are separate structures altogether (e.g. Fiedler & Head, 1966; Brown & Thomas, 1977).

2.5.1 Vortex coalescence

The general idea behind coalescence is that when a vortex is being advected it is possible that it will coalesce with one or more other vortices to generate a larger single vortex which is more resilient to destruction by the shear in the boundary layer. Several mechanisms of coalescence have been proposed.

Due to the paucity of information in the literature regarding coalescence of 3-D vortices, it is again useful to consider the 2-D case of a cylinder in a unidirectional flow. In the lee of a cylinder, a 'vortex street' forms (Berger & Wille, 1972) which gradually loses coherence downstream (Cimbala *et al*, 1981). There have been several reported observations of coherent structures with larger spatial and temporal scales compared to those of the vortex street (e.g. Grant, 1958; Taneda, 1959; Gerrard, 1966; Zdravkovich, 1968; Williamson, 1985). Associated with the decay is a characteristic shift to lower frequency and an increase in the range of frequencies of the intermittency of streamwise velocity (Nagib & Desruelle, 1982).

From the single cylinder case, there is evidence of the coalescence of vortices distant from the cylinder. Townsend (1979) observed a subtly different structure at 180 cylinder widths downstream for a flow of Re = 8000. He describes groups of 3-5 vortices passing downstream, the groups being separated by more random fluctuations. These could represent either a stage in the decay of the vortex street before the re-emergence of the larger structures, or as proposed by Matsui & Okude (1981) could be evidence for the pairing and grouping of vortices. Both of these processes would have the effect of decreasing the apparent frequency of the shedding as observed at a position distant from the cylinder.

For hemispherical elements, a clearly defined vortex street or vortex train does not develop, yet the relics of the shed vortices are intermittently incorporated into the flow. In a similar manner to the spreading of the components of the vortex street, the shed vortices may also increase their spatial and temporal scales as they decay.

Head & Bandyopadhyay (1981) observed the coalescence of hairpin vortices over smooth beds. The legs of the vortices, having opposite vorticity, tended to cancel each other and decay. The heads of the vortex loops were observed to be more resilient than the legs in the outer flow once the legs had decayed. Having like-signed vorticity (rotating with sub parallel axes in the same direction), the heads often tended to coalesce into vortex 'clumps' as they

were advected downstream. Indeed, these authors stated that there is no mechanism whereby the tips of hairpin vortices can mutually cancel, implying that coalescence is inevitable on interaction. Associated with this coalescence was an increase in spatial and temporal scales of the structures, although there are no reported quantitative data to support this.

Although the modes of vortex agglomeration described above do not refer to the gravel bed environment, it is reasonable to infer that broadly similar process occur due to the similarity of the mechanisms of vortex advection in the different environments regardless of their origins. Generally, it may be expected that the high frequency of vortex shedding from obstacles will be reduced downstream and with distance from the bed due to post-shedding coalescence. It remains as speculation at present as to what determines the degree of the coalescence and associated frequency shift in such a complex environment.

2.5.2 Instability across a free shear layer

Kim & Moin (1986) suggest a mechanism for the formation of hairpin vortices without the presence of a viscous sub-layer. They observed from the Head & Bandyopadhyay visualisations that roll-up in the outer zone due to shear generates a vortex with a spanwise axis. This is then stretched by the strain field into a hairpin shape. This has been subsequently supported by numerical simulations (e.g. Lee *et al*, 1990).

Winant & Browand (1974) showed using flow visualisation that a shear layer generated by the near-parallel confluence of two streams of fluid of different velocity develops into a train of vortices which tend to pair up as they are advected downstream. The mechanism for their formation involves the Kelvin-Helmholz type instabilities outlined in section 2.3. They observed that downstream from the confluence, the paired vortices coalesced into larger vortices in a similar manner to the "clumping" of vortices downstream from cylinders observed by Matsui & Okude (1981).

The conditions necessary for the formation of such structures would indeed exist in flows over fluvial gravel beds. As the position and size of shear layers in flows over gravel beds can only be speculated on, it is impossible to make any conclusions regarding the generation, frequency or size of any resulting vortices. However, the mechanism of vortical structure development due to free shear can be seen as potentially contributing vortical material to the advecting vortical assemblage.

2.5.3 Advecting high/low momentum zones

Three studies of the boundary layer over smooth beds, two involving flow visualisation (Nychas *et al*, 1973; Falco, 1977) and the other involving correlations between a fixed and a mobile hot wire probe (Nakagawa & Nezu, 1981), suggest a structure of successive regions of high and low momentum fluid being advected in the buffer zone of the boundary layer. Their generative mechanisms are not understood (Yalin, 1992), but the structures are significant and also can explain the generation of spanwise vortical structures, bursting and sweeps.

Consider Figure 2.8 (after Nakagawa & Nezu, 1981). To a static observer, the interface between high momentum fluid being advected into low momentum fluid is more distinct than that between the low-high momentum regions. The existence of adjacent high and low momentum regions means that shear exists at the interfacial margins. Nychas *et al* (1973) show images from the visualisations suggesting that the shear does indeed lead to Kelvin-Helmholz-like instabilities across the interface resulting in roll-up into vortices with a span-wise axis, which is confirmed by the eddy correlations of Nakagawa & Nezu (Figure 2.8).

The visualisation experiments by Falco (1977) were made at higher Reynolds numbers than those of the other two workers. They show that vortical generation at the high-low momentum interface is more complex than in the lower Re conditions. Yalin (1992) proposes a sequence of events in the development of the high/low momentum interface, and how eddies are generated and interact with the structures (Figure 2.9). Initially a single vortex, e_1, is generated as in the lower Re conditions. The trajectory of the vortex means that fluid mass is removed from the low-momentum region, and so a second vortex, e_2, is generated to replace the fluid (Figure 2.9(ii)). Together, these force an ejection of fluid from the near-wall region inducing a further eddy, e_3. The eddies are by this time causing a significant obstruction to the advection of the high momentum fluid, which together with their upward motion results in the high momentum fluid breaking through the near-wall region, separating the eddies from the bed and causing a "sweep" of high momentum fluid towards the bed (Figure 2.9(iii)).

The initial eddy is still growing as the sweeping takes place, and increases in size to approximately the flow depth before disintegrating chaotically. This is believed to represent the end of the sequence of the structures.

One of the problems with the above model is in the explanation of the initial existence of the high and low momentum regions. The only suggestion about their origin is made by Levi (1983) who proposes that over hydraulically smooth beds, waves occupying the depth of the boundary layer are advected at $\underline{c}$. $0.7U_\infty$. Under the crests of the waves is the low momentum fluid, the high momentum fluid being under the troughs (Figure 2.10). The distortion of these columns of fluid occurs due to shearing within the boundary layer, such that they are manifested as advecting wedges of alternately high and low momentum fluid. The justification for such a structure is discussed further in Chapter 6.

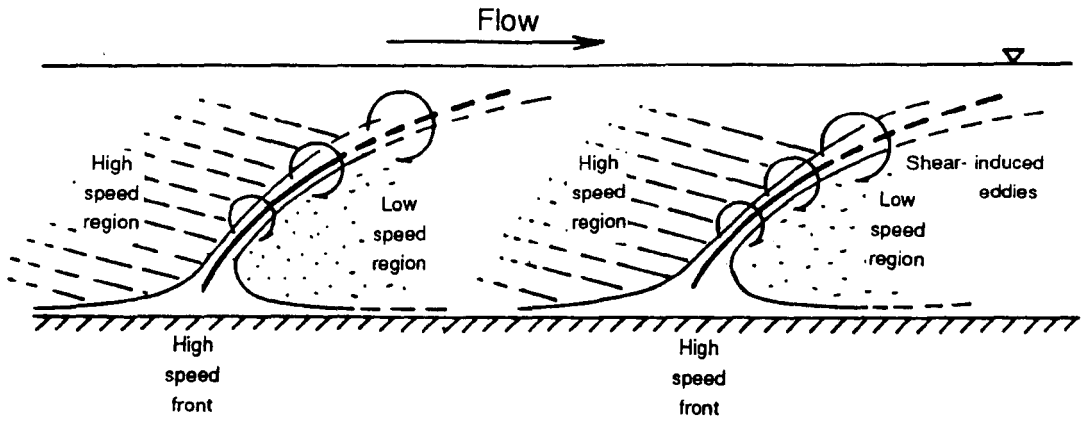

Figure 2.8 A succession of high speed and low speed fluid regions in a boundary layer (after Nakagawa & Nezu 1981).

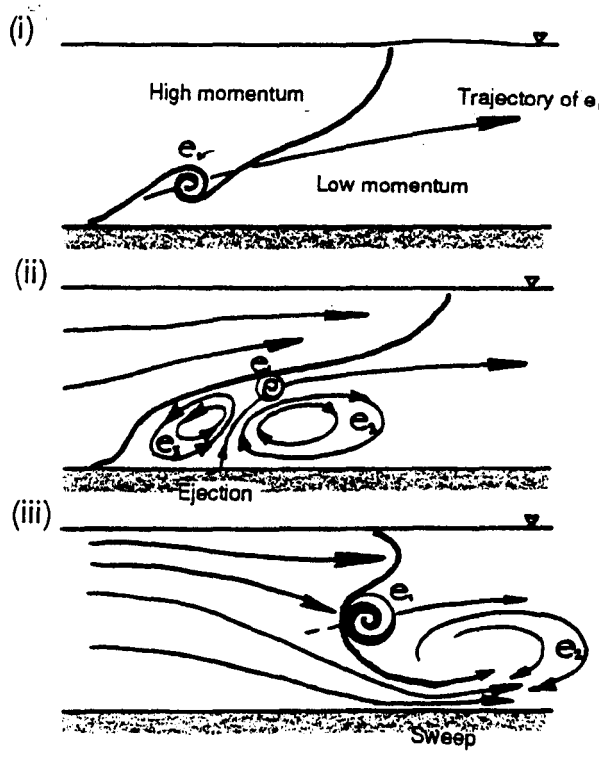

Figure 2.9 The interaction of high speed and low speed zones with a shear induced eddy (after Yalin 1992). See text for full explanation.

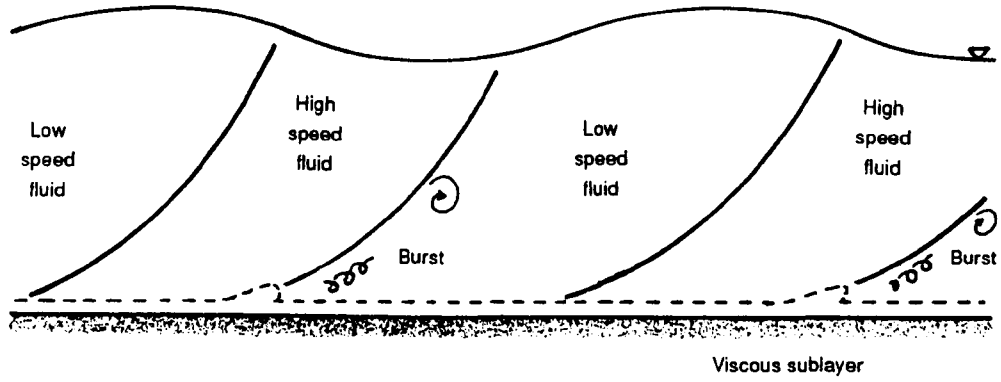

Figure 2.10 "How basic travelling waves can produce turbulent flow alternation of high speed and low speed fluid regions and excite bursts" (after Levi, 1983b).

There are no quantitative descriptions of intermittency characteristics of the system. This means that testing for its existence from single point velocity time series cannot be made.

Unlike the layer roll-up model, this one does not appear to require the existence of a viscous sublayer. This means that it is more likely to be relevant to the gravel bed environment. It must also be considered how eddy shedding from bed particles would interact with this model of vortex generation. This will be returned to in Chapter 6.

2.6 Evidence of coherent flow structures in gravel-bed rivers

There are various reports of coherent structures with timescales of several seconds in sand-bed rivers (e.g. Jackson, 1976; Barrage & Dracos, 1976; Lapointe, 1992) and in deep flows over coastal gravels (e.g. Bowden & Fairburn, 1952; Williams *et al*, 1989). There are, however, only two sets of workers who have attempted to interpret quantitative turbulence data relating specifically to gravel bed rivers (Clifford & French, 1993; Robert *et al*, 1993). In addition, Drake *et al* (1988) provide a qualitative description of intermittent gravel entrainment from which inferences are made concerning flow structure.

The basic quality of gravel bed rivers that differentiates them from either sand bed rivers or coastal flows is the high relative roughness. The implication of this is that the roughness would have a much greater influence on the flow field than in the relatively smoother environments, and hence the mechanisms of coherent structure generation are likely to be different.

Robert *et al* (1993) show that a change in roughness of a gravel bed results in a change in the timescale of the eddies within the boundary layer; larger timescales are associated with coarser roughnesses. This initially supports the role of eddy shedding in explaining the generation of coherent structures. However, timescales associated with the turbulence are too large to be the result of simple eddy shedding. Clifford *et al* (1991) use the

Strouhal relation to show that the timescales from the velocity data relate to obstacles of over $3.7D_{84}$. They interpret this by suggesting that the eddies are being shed from particle groupings rather than from single particles. This explanation must be questioned as particle clusters are streamlined (Brayshaw *et al*, 1983) and hence the flow separation will be minimal, and so it is unlikely that a large eddy would form.

It has also been demonstrated that the timescale of coherent structures in (deeper) pools is greater than in (shallower) riffles (Clifford, 1990; Clifford *et al*, 1993). However, it has not been shown that this is attributed solely to either change in roughness (which would advocate eddy shedding as the generative mechanism), or change in depth (which would have supported bursting). This therefore suggests that either the generative mechanisms require modification, co-exist but interact, or that a further mechanism that has not been identified exists.

The concept of eddy interaction has been approached as a mechanism of eddy size amplification, although no quantitative attempts have been made to justify it further. Indeed, Robert *et al* (1993) show that as distance from the bed increases, the dominant frequency decreases suggesting that eddy size is increasing.

Several authors have attempted to calculate the size of the vortices relating to the dominant temporal scales by the product of their return period and the mean velocity (Clifford, 1990; Lapointe, 1992). This results in apparent structures of up to 2 orders of magnitude greater than the flow depth which clearly cannot exist. This suggests that the monitored structures are not of a simple vortical form, or that the justification behind the procedure is flawed. If the passage of the structures is intermittent, it is reasonable to assume that they are separated by periods of inactivity; this is implicit in the assumption of coherent structures being superimposed on a random flow field (Jackson, 1976). Hence, calculation of a spatial scale from a return period is inappropriate as the actual timescale of a structure relates to its persistence rather than its recurrence.

The interpretation of the gravel entrainment "flurries" in Duck Creek, a small irrigation channel with a mixed sand and gravel bed made by Drake *et al* (1988) are the only direct observational evidence of coherent flow structure in gravel bed rivers. Although the interpretation of flow structure is only made by inference, it provides some useful insights about the nature of flow structure.

Drake *et al* describe intermittent "sweep transport events" of gravel which accounted for 70% of the total transport in 9% of the time (depth ≈ 35cm, D_{50} = 4mm). These events were characteristically 10-20cm wide, their active "footprint" is roughly circular, and they are randomly distributed over the bed. They last for up to 1s, and over that time propagate 20-50cm downstream at speeds of 1.5-1.8 times the mean flow velocity. This description suggests that they are not spatially related to individual gravel particles, and are larger structures than would be expected from either a simple eddy shedding model or a layer interaction model.

2.7 Summary

In attempting to determine the nature and generative mechanisms of fluid turbulence over fluvial gravel beds, it has emerged that macro-scale turbulent structures may be important features of the flow. The paucity of quantitative turbulence data from natural, fluvial environments means that the determination of the structures' properties and generative mechanisms is, as yet, speculative and open to debate and confusion.

There are several scales, both temporal and spatial, of macro-scale structure which have been observed in other similar environments which may possibly exist over gravel beds. The hairpin vortex emerges as a common feature of many of these, its generative mechanisms being determined by bed roughness. The common form of the vortical structures generated by different mechanisms makes conclusions about their generative mechanisms difficult solely from flow monitoring.

In terms of its application to the rough gravel-bed environment, the sublayer-buffer zone roll-up model with the often quoted terminology of 'bursts' and 'sweeps' has been rejected here in its present form due to the non-existence of a spatially coherent viscous sub-layer on which it relies. It is possible, however, that it may cause the generation of hairpin vortices from the surfaces of individual particles.

Vortical structures can be generated independently of the boundary roughness condition due to free shear in the flow. The details of the processes leading to this are not well understood and consequently the nature and form of the resulting structures are vague. However, vortex generation from free shear represents an additional source of vortical material into the boundary layer.

Inverted "wedges" of consecutively high and low momentum fluid have been observed in turbulent boundary layers. Instability at the shear between these generates vortical structures with spanwise axes, which can help to explain toward-bed rushes of high momentum fluid, and ejections of low momentum fluid from the bed. The basic problem with this model is the lack of explanation of the initial existence of the high and low momentum regions of the flow.

From basic physical reasoning and from the limited evidence from the literature, it is the 'vortex shedding' model which presents itself as the most viable proposition as the basis for macro-turbulence generation in the hydraulically rough, depth-limited fluvial gravel-bed environment. It has been shown, however, that the temporal and spatial scale of the individual shed eddies does not match that of the features observed in rivers.

Post-shedding vortex interaction and coalescence are inevitable processes over gravel beds, the nature of which is inherently probabilistic over the irregular obstacle field of a gravel bed. The outcome of coalescence is the formation of larger turbulent structures in the boundary layer. In terms of the high frequencies associated with the shed vortices, this represents a mechanism for generating structures which have a timescale more similar to that observed in fluvial environments.

Due to the limited information available regarding macro-turbulence, and the complexity of the arrangement of natural fluvial gravel beds, it is impossible to tie down precisely the flow processes that *do* occur from the literature alone.

2.8 Thesis objectives

The debate emerging from the above review and discussions yields the five basic aims of this thesis:

1. To identify the generative mechanisms of coherent flow structures in gravel-bed rivers.
2. To describe the morphology of the structures.
3. To characterise the fluctuating velocities and stresses associated with the structures.
4. To investigate the intermittency of the structures.
5. To link intermittency of flow with that of gravel entrainment.

These form the umbrella under which the strategy of data collection and analysis which forms the basis of the next three chapters lies. The inter-relationships between the objectives mean that they cannot be approached individually, and hence the organisation of the data analysis in Chapters 4 and 5 does not relate specifically to the objectives. The aim of Chapter 6 is to interpret the findings of Chapters 4 and 5 with regard to the five objectives.

Chapter 3: Methodology and techniques

This work requires the measurement of fluid flow and gravel surface form. The objectives of this chapter are to outline the methodology adopted for this work, explain the criteria for the collection of different types of data, describe the techniques used in obtaining these measurements and assess their reliability as a representation of that which was being measured.

The data were collected in a flume and at three field sites, the pro-glacial river of the Upper Arolla glacier, Switzerland; the Allt Dubhaig, Scotland; and Beauty Creek, Canada. Measurements were also made in the pro-glacial river of Solheimarjokull, Iceland, and the tidal inlet to Pagham harbour, Dorset. However, equipment failure meant that the Iceland data were not used, and the Pagham data are not included as it not a truly fluvial environment. Full descriptions of the field sites are given in section 3.9.

The initial methodological scheme comprised a series of controlled flume experiments followed by field data collection. The purpose of the flume experiments was to characterise the turbulent flow field over smooth beds (from time series of u and v), and then over increasingly complex beds at a variety of hydraulic conditions. This would have allowed an explanatory model of coherent structure generation to be proposed, against which the data from the field sites could be interpreted. However, this scheme failed due to problems with the early version of the laser Doppler flow monitoring system resulting in incomplete data sets, meaning that the explanatory model could not be made.

The data collection strategy was changed to using the flume for flow visualisation and the field for the collection of velocity time series. This meant that the rationale for the thesis changed to developing a qualitative model of flow structure from the flume which was quantified using time series data from the field.

This brief explanation of methodology will be elaborated upon at subsequent points within Chapters 4 and 5. The rest of this chapter is concerned with the description of the techniques and field sites used in this study.

Section A: Measurement of flow

The two main reasons for measuring fluid flow are to obtain mean parameters of the flow field and time series of velocity from which to characterise the turbulence. Three types of equipment were available - an Ott propeller current meter, a 2-component electromagnetic current meter (ECM) and a 2-component laser-doppler anemometer (LDA).

3.1 Flow monitoring with an electromagnetic current meter (ECM)

Electromagnetic current meters allow the monitoring of velocity in two perpendicular directions in the field. For this work, the ECM was used to measure the streamwise (u) and vertical (v) components. The model used was a Marsh McBirney 511.

3.1.1 Principles of ECM operation

The electromagnetic current meter relies on the Faraday principle for operation. The spherical probe of the meter generates an electromagnetic field in the water. As water is a conductor, its movement through the field induces a current which is monitored by sensing probes on the sphere. It is the fluctuations in this field that are converted to represent fluctuations in velocity. The orientation of the probes determines the direction in which the fluctuating velocity is monitored.

Two properties of the water can influence its conductive properties and hence the calibration of induced current to velocity: temperature and solute concentration. However, the ranges of these experienced in the flows monitored result in negligible variations in calibration.

3.1.2 Technical details of the Marsh McBirney 511

The Marsh McBirney 511 consists of two main components: the sensor head and the main electronics unit (Figure 3.1). Most of the following details are taken from the Marsh McBirney manual.

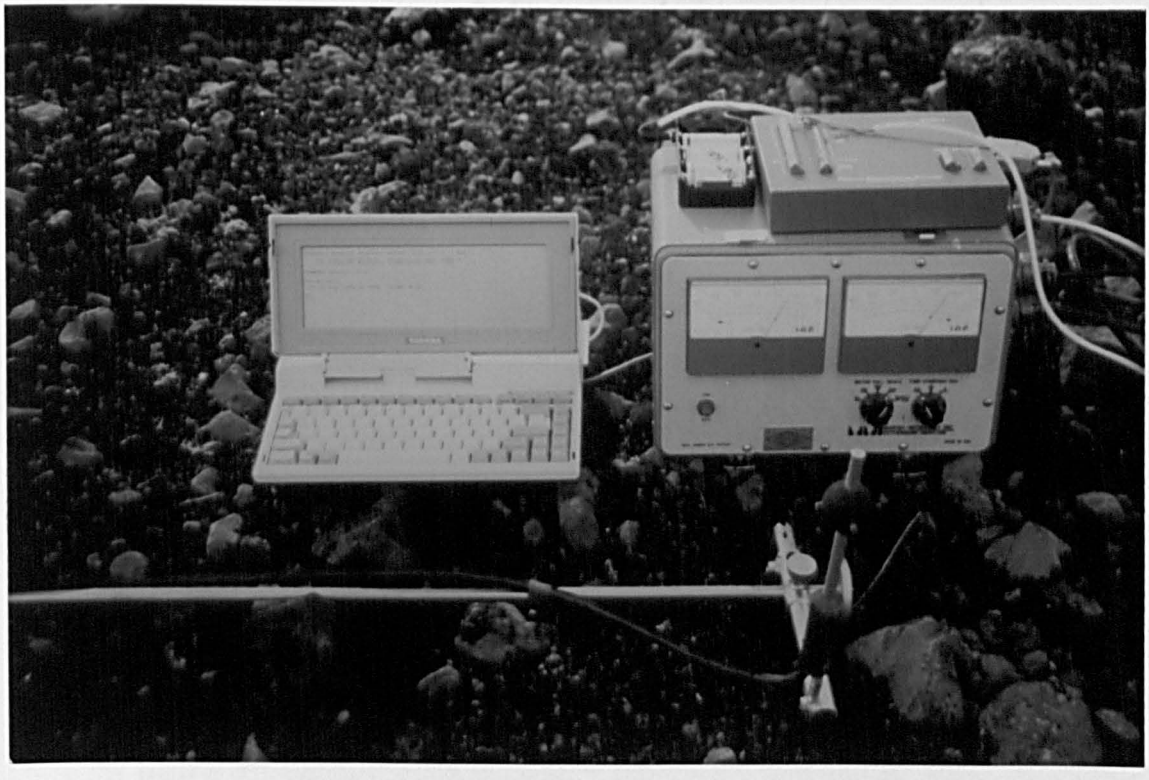

Figure 3.1 The ECM monitoring rig: portable PC, ECM electronics box with A/D converter on top, wading rod & ECM probe in foreground.

The 1.5" spherical sensor head generates an AC electromagnetic field driven at 30Hz. The two sets of perpendicular sensing electrodes operate on a carrier frequency of 30Hz, the amplitudes of the signals generated being linearly proportional to the velocity component. It has been suggested that the accuracy of response to velocity fluctuations of a spherical-headed current meter becomes less reliable as Reynolds number increases (Aubrey & Trowbridge, 1985; Guza, 1987). Although flow separation and intense eddying occur in the wake of the

sensing probe at higher velocities (Lane & Warburton, 1993), the effect of this on the calibration was not tested. The Marsh McBirney calibration accepts that at higher velocities the linearity of response is less good than at lower, but is still within ± 2% of the calibration.

The induced signals are amplified, synchronously detected and filtered of electronic noise to yield two analogue voltages that linearly relate to velocity.

No information was available concerning the size of the sensing volume of the probe, except a recommendation to keep it "...away from the side.." of containers. The use of steel as the probe shaft suggests that metal can be brought within 10cm of the head. Simple tests in still water involving slowly moving an iron rod of 2.5cm diameter near the probe suggest that conducting materials cause no detectable deflection from zero up to 7cm from the sensor head.

The current meter is factory calibrated and adjusted to $\pm 1V \equiv \pm 3ms^{-1}$ at the output socket. This calibration was testable using an on-board calibration check. This was further checked three times against a propeller current meter in a concrete spillway near Sheffield. The comparisons extending over half of the full velocity range of the ECM never yielded a discrepancy of over 6%, and never any appreciable systematic difference. Comparison of the mean velocity values taken in the field with the propeller current meter usually resulted in larger discrepancies, but these never suggested any systematic under or over-estimation of velocity.

Due to electronic noise being generated at the amplification stage, and to remove the carrier frequency (30Hz), low-pass filtering of the output signal is incorporated with switch-selectable time constants (0.2s, 1s and 5s). In all of the logging undertaken, this was set to 0.2s. The precision of the time response to a step change in the velocity is given in Table 3.1 (modified from the Marsh McBirney manual)

Table 3.1 Response time of the voltage output to a step change in velocity

Time after velocity step change		Percentage of change
1s constant:	0.2s constant:	at output socket:
1s	0.2s	63%
2s	0.4s	86%
3s	0.6s	95%
4s	0.8s	98%
5s	1.0s	99%

This shows that, at the 0.2s setting, a degree of smoothing takes place up to c. 1s, but that the output response to a step change in velocity is almost complete after 0.5s.

3.1.3 Deployment

The output from the two channels is an analogue voltage, and was logged via a Remote Measurement Systems ADC-1 12 bit analogue-to-digital converter into a Toshiba T1000 portable computer (Figure 3.1). A programme was written in MS QuickBasic to convert

the output voltages to velocities using the calibration provided by the supplier, and to log the velocities to a two-column ASCII file on the computer's extended RAM. Occasionally, these were downloaded to floppy disk.

The files were logged at 4Hz for either 100 or 120s. Apart from the limits on the logging frequency brought about by the time constant on the current meter, the sampling rate was also limited by the clock speed of the 8086 processor of the PC. Practically, this meant that the fastest sampling rate achievable for two channels was 4Hz.

There is a problem regarding the sampling rate relative to the time constant known as aliasing (Hardisty, *pers comm*; Lane & Warburton, 1993). This involves the sampling of frequencies higher than the sampling frequency resulting in an apparent waveform of lower frequency. The highest frequency detectable when the signal is smoothed with a 0.2s time constant has a wavelength of 0.4s. Figure 3.2 shows that sampling this signal at an interval of 0.25s would result in an alias waveform of L = 0.67s. Generally, aliasing would result in an artificial shift to the lower frequencies of power in the spectrum of the series. With the constraints of the system used, aliasing is an unresolvable problem.

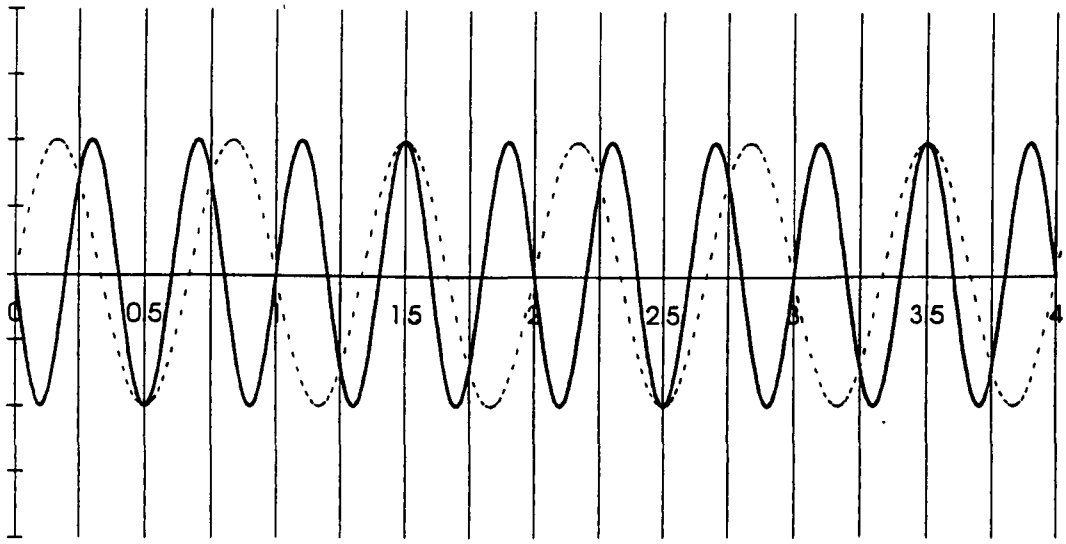

Figure 3.2 The problem of aliasing: a signal with a true wavelength of 0.4s when sampled at 0.25s gives an apparent wavelength of 0.67s.

A wading rod was built in the Geography Department on which to mount the probe of the current meter (Figure 3.1). This was designed to ensure that the vertical component of the probe head was parallel to the wading rod, and held securely. The dimensions of the rod meant that the probe head was held 17cm from the steel bulk of the wading rod i.e. sufficiently far to prevent either disturbance of the flow field by the rod or for the steel to interfere with the electromagnetic sensing field.

In the majority of cases, the probe head was not taken within 10cm of the river bed. This is due to the distortion of the sensing volume that the bed would have made, and to prevent the probe itself causing "jetting" of the water in the constriction between the probe and

the bed. A series of experiments was conducted in the flume at Sheffield to compare the mean velocity derived from the series of the streamwise component of the ECM with those from the propeller current meter. Figure 3.3 shows that there is only an appreciable difference between these when $y \leq 5$cm. As a general guide-line, this points to a 10cm gap being a very safe limit to adopt.

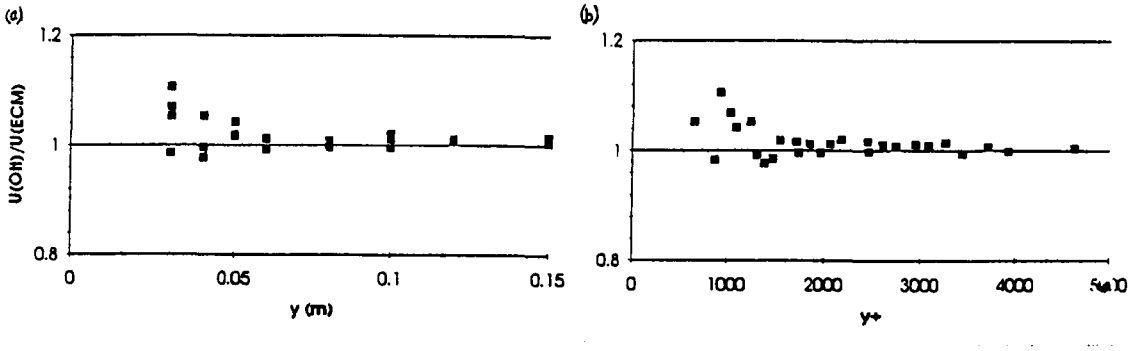

Figure 3.3 Comparison of velocities monitored by the ECM and an Ott propeller current meter. (a) $\langle u \rangle_{ECM}/\langle u \rangle_{Ott}$ against y, (b) $\langle u \rangle_{ECM}/\langle u \rangle_{Ott}$ against y^+.

Zero checks were regularly made in the field by positioning the probe in still water and logging the series. In the vast majority of cases, the mean and variance of the series were negligibly small. The only times that the zero test did not produce a zero reading was when the batteries of the ECM were low, and before the socket re-wiring explained in Section 3.3.2g.

3.2 Flow monitoring with a laser-Doppler anemometer (LDA)

The laboratory in which all of the flume experiments were conducted is in the Department of Earth Sciences at Leeds University. It contained an Armfield flume, and Dantec 2-component laser-Doppler anemometer system (LDA), and a high-resolution video system.

The flume used for all of these experiments is a 10m x 0.3m x 0.3m Armfield tilting flume. It has glass walls, a polished stainless steel floor and the slope can be adjusted between -0.005 and 0.025. It is possible to recirculate gravels of up to 6mm diameter, although this was never attempted

The LDA is a completely non-intrusive method of measuring velocity fluctuations in a fluid.

3.2.1 Principles and technical details

The velocities in the flume were monitored using a 2-component Ar-ion fibre-optic LDA manufactured by Dantec (Figure 3.4). This technique employs the Doppler principle whereby

when there is relative motion between a source of a waveform and an observer, the frequency observed is lower or higher than the real frequency depending whether the two are moving away from or towards each other. In the context of the LDA, beams of known wavelength are focused at a small area in the flow (in this case, 0.071mm^2). The beam is reflected off neutrally buoyant tracers in the flow, and the frequency shift of the back-scattered beam relative to the incident beam is converted to a fluid velocity.

Figure 3.4 The LDA monitoring equipment. Flume is on the right, LDA probe head on tripod, control unit and laser on left.

The system was controlled using a Compaq 386 PC initially running Dantec atTRACKtion control software, and later the superior FLOWare. This controlled the sampling rate, length of sample, processing of sample to velocities and output of file to ASCII format. The analysis and presentation modules of the software were not used as analysis techniques common to both the field and flume data were required.

The FLOWare software sampled whenever it sensed a particle within its sensing volume and hence did not generate a uniform sampling interval. This meant that spectral analysis could not be performed on the series in their raw form. In an attempt to overcome this problem, the raw series were re-sampled by generating a sub-series of points which were closest to a defined sampling interval. However, calculation of the standard deviations of the actual sampling interval relative to that defined produced discrepancies of up to 180%. These sub-series were therefore used for all analyses apart from those requiring a constant sampling interval.

3.2.2 Deployment

For all the files used in the analysis, the LDA head was mounted on a servo-motor controlled carriage. This allowed movement to be made to a resolution of less than 1mm. The measurements were made as close to the centreline of the flume as possible to minimise the drag effects of the walls. All of the measurements were made between 4 and 7 m from the upstream end of the flume in order to minimise the upstream input effects and down-draw or backwater from the downstream end. This was checked by measuring water surface profiles, and keeping within the uniform central zone.

At the beginning of each set of experiments, the orientation of the head was checked relative to the flume bed. The head was swivelled and tilted until the streamwise beams just passed over the steel flume bed.

Although the LDA head could be rotated in order to focus into the pockets of the bed, this was never done. The rate of convergence of the beams meant that two components of velocity could be measured at the centre line over 5mm above the bed. By sacrificing the vertical component, the horizontal could be measured to within 1mm of the bed.

All of the series were monitored for 100 seconds, and resampled to a rate of c. 10Hz.

3.3 Velocity time series checking

3.3.1 Strategy for checking time series

The procedures outlined above for logging velocity should theoretically have produced directly usable time series. This, however, was frequently not the case due to various sources of sampling pollution.

One of the problems encountered in identifying dubious data files is ignorance as to what a good file should look like and what its statistical characteristics should be; is a transient high velocity section in a series the passage of a flow structure or the sadistic humour of the ECM's electronics?

This necessitated a three stage strategy for file checking. Firstly, the files were corrected for known irregularities, e.g. the probe head being upside-down. Secondly, the files were checked for common identifiable problems which are outlined in the next section. Depending on the nature and seriousness of the problem, some files were modified and accepted, others rejected. It was at this stage that the files were used for analysis. Finally, if a file produced consistently dubious results during the analyses outlined in Chapters 4 and 5, it was re-inspected for faults.

3.3.2 Common problems with velocity time series

(a) Probe orientation

The ability to check the orientation of the LDA probe head meant that no further checking of the data was necessary. However, although as much care as possible was taken to ensure that the ECM sensing probe was oriented with the u component exactly horizontal and

the v vertical, it is inevitable that this was not always successful. A strategy therefore had to be developed to correct this error afterwards.

As the minimum distance above the bed of the ECM probe was several times the size of the largest obstacles, an assumption was adopted that the flow was not being deflected significantly by the bed obstacles. This allowed a further assumption to be made that the mean of the v component would be zero. A procedure was adopted to adjust the series of the u and v components to produce <v> = 0 (which also maximises <u>).

Consider Figure 3.5. OA represents the mean velocity vector which can be resolved into the x and y components of OB and OD respectively. OD is the discrepancy from zero of the mean vertical velocity. The associated discrepancy in the horizontal component is BC. If

by Pythagoras $OA = \sqrt{(OD^2+OB^2)}$

and $BC = OC - OB$

and $OC = OA$

then $BC = \sqrt{(OD^2+OB^2)} - OB$

As OB and OD are the means of the raw u and v components respectively (<x> and <y>), the adjusted series values, y^ and x^ become

$y^ = y - \langle y \rangle$

$x^ = x + \sqrt{(\langle y \rangle^2+\langle x \rangle^2)} - \langle x \rangle$

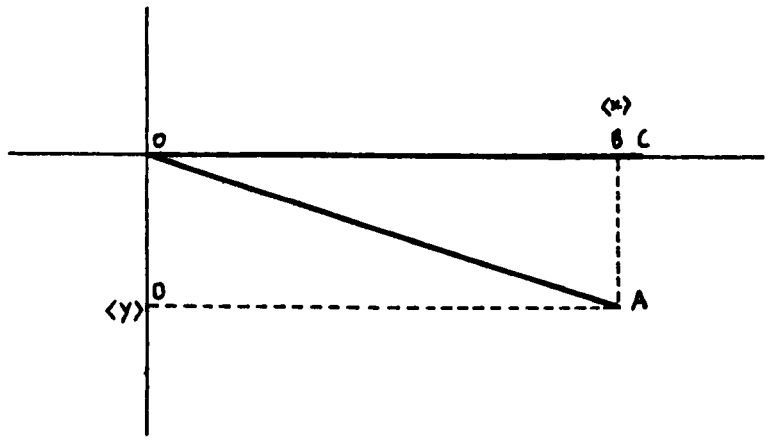

Figure 3.5 Explanatory Figure for velocity correction due to a mis-aligned probe. See text for explanation.

A QuickBasic programme was written to make these adjustments and routinely applied to the ECM data. A check was incorporated to calculate the angle of deviation from the horizontal of the raw velocity vector; if this angle was greater than 10°, then the file was rejected. This never happened on any files which were not also rejected by one or more of the other file checking criteria outlined below.

(b) Spikes, flat patches

The presence of spikes was a common problem with series from both the LDA and ECM. The reason for their existence is still not understood, but are presumed to be error. Figure 3.6 shows a spiky series from the field to illustrate the problem.

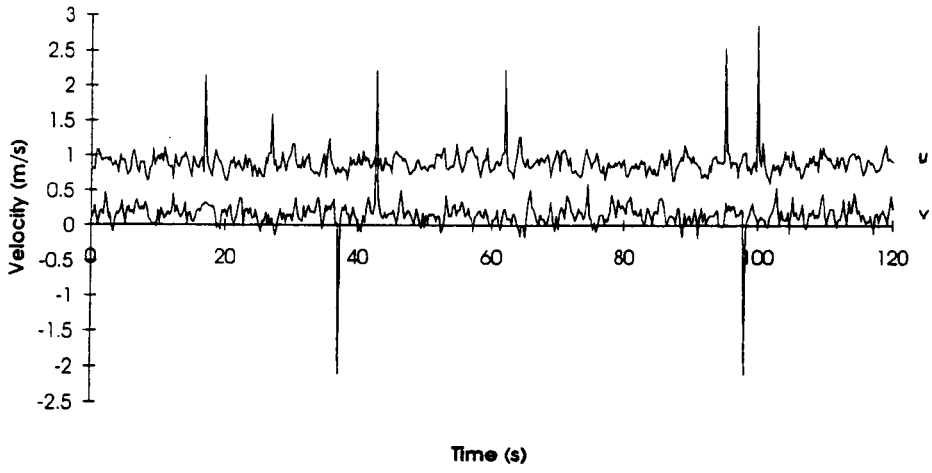

Figure 3.6 Spikes within a velocity time series.

Their identification was made subjectively by viewing the time series. The potential problem of confusing a spike with a transient high fluctuation did not emerge as they usually lasted for only one or two sampling points, and were considerably greater than the magnitude of the background fluctuations.

If a file contained spikes for less than 1% of the duration of the series, then they were removed by averaging the adjacent points to produce a synthetic replacement point. If more than 1% of the points were spikes, then usually the file was rejected.

Flat patches in the series was a problem exclusive to LDA derived series using the aTRACKtion logging software. It results from the lack of a back-scattered beam being sensed in the sampling time, or the back-scattered beam being re-scattered by other particles in the flow.

The design of the early flume experiments involved controlled variation in hydraulic and roughness conditions. As the problem of flat patches resulted in $\underline{c}$. 60% of the files being rejected, the experiments were meaningless with the amount of good data left. Therefore none of the data logged with the aTRACKtion software has been used in this work.

(c) Drift

Two types of drift were encountered in some of the ECM files. One involved a constant change in the mean velocity during logging. This only occurred in two files due to local intense scouring, and the files were rejected.

The other type of drift affected the first few seconds of a file, and was traced to cold conditions or low A/D converter batteries. When identified as a problem, the files were logged for an extra 20s then trimmed back to the required time. This only affected eight of the files which were finally included in the analysis.

(d) Steps

Steps in some of the ECM time series were the result of either local bed re-arrangement during logging or movement of the wading rod. If the problem was identified in the field, the files were re-taken; if it was identified afterwards, then the files were rejected.

(e) Noise

Noisy files were the largest problem encountered, and the one most difficult to identify and rectify. Some of the affected files were rejected directly after viewing the time series on the assumption that repeated acceleration and deceleration between ± 3ms^{-1} over 0.25s intervals was unlikely. Other less intense occurrences were less easy to initially identify.

Section 5.1.3 considers turbulence intensity - the ratio between the standard deviation of a series and its mean. It was during this analysis that many of the noisy files were identified as they plotted as definite outliers. Figures 5.6 and 5.7 include one of the velocity profiles which were rejected to illustrate this. Although in scientific investigations it is often the outliers which are of interest and require explanation, the ones rejected as noisy were often taken at a time when other files had been rejected for being more obviously noisy.

The causes of noise are not fully understood, but can be split into physical and electronic. Of the physical reasons, two were definitely identified as being air entrained in the lee of the probe head and rattling of the cable connecting the submerged probe to the electronics box.

Air entrainment was usually only a problem in very turbulent flows when the head was within 10cm of the water surface. Usually it was possible to make a note if an air bubble had developed behind the probe.

The problem of cable rattle was identified when an accidental kick of the cable during a still-water bucket test resulted in a large deflection of the needles on the electronics box. It was a more serious problem than air entrainment, and one difficult to isolate. One of the problems is that in more turbulent flow when the variance of the signal is expected to be higher, there is more potential for the cable to be rattled.

A series of tests were carried out in Beauty Creek, Canada, to assess the scale of the cable rattle problem. These involved repeatedly logging velocities at the same point in the river with various precautions against cable rattle taken. These involved encasing the probe head in still water using plastic bottle.

With the head shielded, the series produced should have a mean of near to zero (the bottle did not accommodate the whole sensing volume), but more importantly, there should be negligible fluctuation. Figure 3.7a shows the velocities logged with the probe shielded by the bottle in the flow, and with the cables held completely clear of the flow. It shows that the bottle is efficient at shielding the probe from the flow velocity, and so we can be confident that the following effects are of cable rattle alone.

Figure 3.7b is as 3.7a, but with the cable shaken every 15s; this shows that the ECM *does* pick up vibration in the cable. Figure 3.7c is as 3.7a, but with the cable held clear of the water. This is the technique usually used and is effectively free from the effects of cable rattle. Figures 3.7 d & e both involved the cable dragging in the flow, the latter with it taped to the wading rod after it emerges from the probe. Both of these generate significant fluctuations in apparent velocity due to what can only be a vibrating cable.

Two recommendations emerge from the cable-rattle tests. Firstly, it is best to hold the cable loosely out of the water, as this minimises "buzzing" of the cable under tension. Secondly, precautions should be taken not to kick or move the cable at any point during monitoring.

(f) Beats

An obvious underlying periodicity in the velocity series is the fluid dynamicist's Nirvana. This occurred twice when using the ECM, and depressingly was found out to be a sign that the ECM batteries were getting low.

Although in both of these cases its occurrence was obvious, it is possible that it occurred less obviously at other times. To check this, the spectra of the files taken before battery recharges were inspected in a more critical manner than the others. There did not appear to be any systematic difference between these spectra and those considered as safe.

(g) Other miscellaneous problems

Some of the series were rejected for no reason except being unbelievable. Four files, each taken directly before or after acceptable files, passed all of the above tests, but gave mean values of the u and v components of over $2ms^{-1}$. The reason for this is not known.

Occasionally files contained breaks in the middle of them. It is assumed that this is due to loose connections or short circuits. These series were rejected.

At the beginning of the Arolla field work, the plug connecting the probe to the main unit needed re-wiring in the field. This meant that although a zero check could be made, it was difficult to make an accurate calibration. Rough calibrations against the Ott current meter were made in the field, and as a result the standard calibration was used. Further flume calibrations were made on return to the UK which suggested that the standard calibration was indeed still valid.

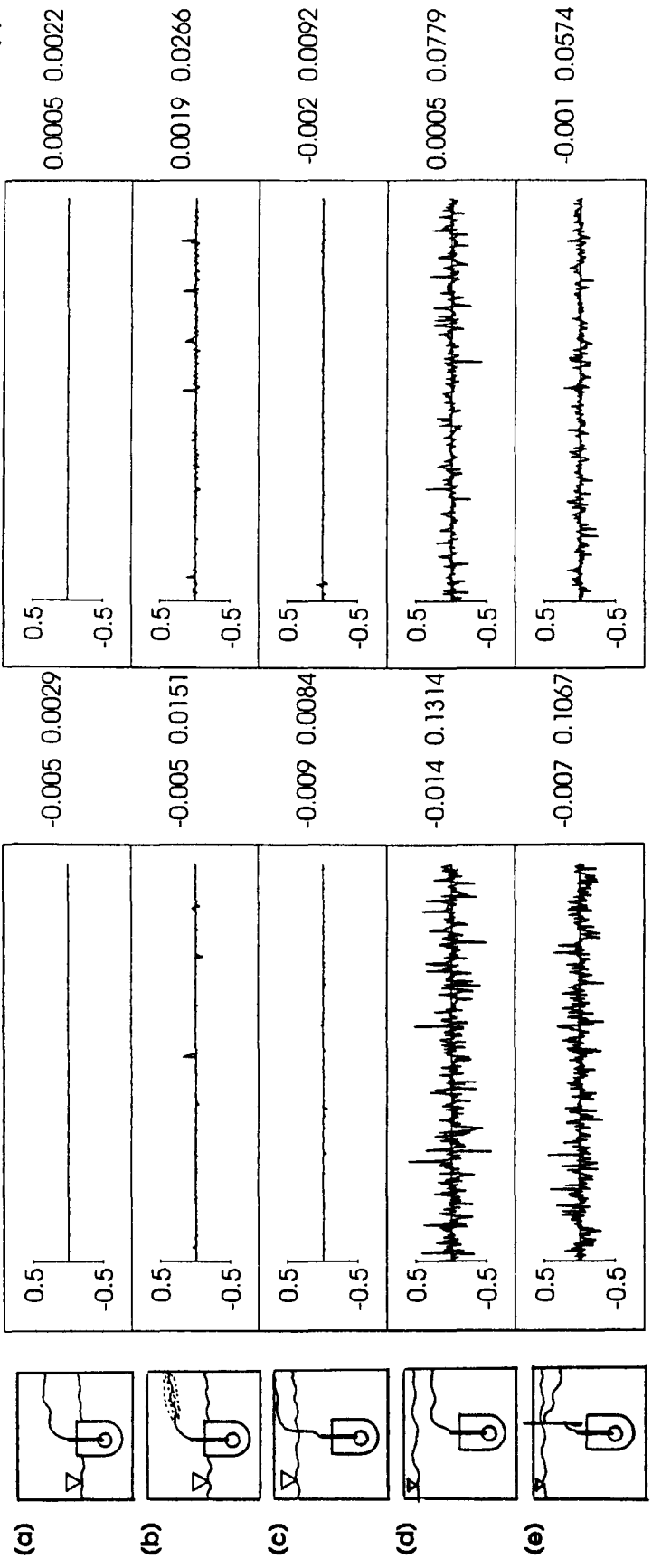

Figure 3.7 Velocity time series of cable rattle tests. Figures on left describe the position of the cable relative to the water surface.

3.3.3 Equivalence of LDA and ECM data

All of the ECM and all of the LDA data sets can be considered to be of equivalent precision. However, the ECM data is of poorer spatial and temporal resolution to that of the LDA due to the larger size of the sensing volume and the use of low pass filters.

The effect of this would be that the higher frequency fluctuations would be under-represented in the data taken using the ECM. The extent of this difference could be investigated further, but the results of Chapter 5 show that the important frequencies are smaller than those affected by these phenomena. In this respect it is accepted that the problem exists, but is generally ignored until it may explain otherwise inexplicable differences in some of the analyses.

Section B: Measurement of the gravel bed roughness surface

Gravel beds are considered here as having two properties; they are a store of potentially entrainable particles and a roughness surface. By making this distinction, it demands that the characterisation of the beds may require different techniques and methods. The main thrust of the following discussion is, however, towards the determination of a roughness parameter.

Until recently in the fluvial literature, the quantification of gravel beds has been restricted to deriving descriptive parameters from the size distribution of the gravel particles. Perhaps due to the increasingly reductionist approach regarding flow-sediment interaction, attention has been turning to consideration of the constructed bed as a surface, and various attempts have been made to derive parameters to describe its roughness characteristics. These two fundamentally different approaches necessitate further examination in order to determine the most appropriate descriptive parameters for the different purposes. A comprehensive review of approaches to this problem is provided by Robert (1988).

In a mechanistic sense, the two demands on a roughness parameter are that it should allow a quantitative description of the elements of the bed which are dominant influences on the turbulence structure, and should be usable in the explanation of energy dissipation by the bed. Schlichting (1979, p.615) states that the systematic description of rough surfaces is ".. frustrated by the fundamental difficulty that the number of parameters describing roughness is extraordinarily large owing to the great diversity of geometric forms".

One of the main conclusions of Chapter 2 was that the mechanisms of turbulence generation over mixed gravel beds were still not fully understood. This poses a problem regarding the specific requirements of the roughness parameter. The approach to be taken is to investigate the parameters that have been discussed in the literature, and to assess firstly whether they are relevant to this work, and secondly, whether they are measurable with the equipment available and therefore represent realistic options.

Several approaches exist which attempt to define a roughness parameter based on the empirical determination of a coefficient from the energy losses of the flowing fluid. These

include the Chezy coefficient, C (Chezy, 1775), Manning's roughness coefficient, n (Manning, 1891) and the Darcy-Weisbach friction factor, f_f (Richards, 1982).

There are two reasons why these are not employed in this work. Firstly, they are inherently empirical. The Manning coefficient is derived either on the estimation of roughness by sight or is back-calculated from <u>, slope and hydraulic radius. Estimation by sight would result in all of the rivers or flume beds used in this study falling into the same category. Secondly, and most importantly, it is the mechanism of how the roughness affects the flow that is of primary interest here; to use a measure of energy loss to determine roughness would result at best in an unresolvable circular argument developing, but also a problem concerning the direction of causality.

Several alternative methods of quantification of roughness are shown in Table 3.2.

Table 3.2 A summary of different roughness parameters

Parameter	Description	Literature	Data type	Comments
D_{50}, D_{84}	Percentiles of the bed PSD	Leopold *et al*, 1964 Bathurst, 1982 Naden, 1987	Bed material PSD	Easily measured, widely used parameters. Does not directly refer to roughness, and ignores bed structure.
y_0	Roughness length		Velocity profile	Easily and commonly measured. An indirect measure of effect of roughness on velocity profile. Sensitive to errors in measurement. Point specific.
k_{50}, k_{84}	Percentiles of the roughness space series	Kirchner *et al*, 1990	Digitised bed micro-profile	Represents the actual roughness. Not a widely used measure, very little data.
σ_k	Descriptive statistics of the roughness space series	Hutchings, 1991 Arnell *et al*, 1991	Digitised bed micro-profile	Widely used in the tribology literature.
S	Roughness length from ACF	Richards, 1976 Furbish, 1987 Robert, 1988	Digitised bed micro-profile	Incorporates spatial structure of roughness series. Does not refer to roughness height, requires long series.
D	Fractal Dimension	Andrle & Abrahams, 1989; Furbish, 1987 Robert, 1988	Digitised bed micro-profile	Not sufficiently sensitive to subtly different roughnesses, requires long series.

3.4 Quantification of the gravel surface particle size distribution

A characteristic of fluvial gravel beds is their poor sorting. Attempts at deriving a roughness parameter from the bed material size distribution have been made by many workers (e.g. Leopold *et al*, 1964; Limerinos, 1970; Burkham & Dawdy, 1976; Bray, 1979; Hey, 1979; Bathurst, 1982). It is the consensus that it is the larger particles that have a greater influence on flow resistance than the smaller ones. D_{90} and D_{84} have often been quoted as roughness parameters (where D_n is the size of the median axis for which n% are finer) (Hey, 1979; Bathurst, 1982; Aguirre-pe & Fuentes, 1990), although the choice of the specific percentile value is quite arbitrary. It has been shown in both the laboratory and the field that there is

negligible difference between D_{84} or D_{90} in the explanation of resistance to flow over mixed gravel beds (Ferro & Giordano, 1991; Bray, 1982).

As the reliability of percentile values decreases rapidly as higher value percentiles increase (Church *et al*, 1987; Ferguson, *pers comm.*), D_{84} will be used as the roughness parameter derived from the bed particle size distribution in preference to D_{90}.

The particle size distributions were taken in different ways in the field and the flume. In the field, either pebble counts by Wolman sampling were taken on a sample size of 100 or the bed was removed by scooping the surface into a Helley-Smith bedload sampler. The latter was only done if bedload transport was low or non-existent, as the transported material would have polluted the sample. The scooped sample was dried and weighed in the field. All bed sampling was done at the end of flow monitoring as it is inherently destructive.

In the flume, the bed surface was carefully removed at the end of flow monitoring. In order to ensure that only the surface layer was removed, a hair dryer was directed at the surface directly after the pump had been turned off. This made it easier to identify the surface particles due to their dry upper facets. The sample was restricted to the central 10cm of the flume as wall drag affected the margins, and the area removed was usually c. 1m long. The sample was dried and weighed to derive the surface PSD.

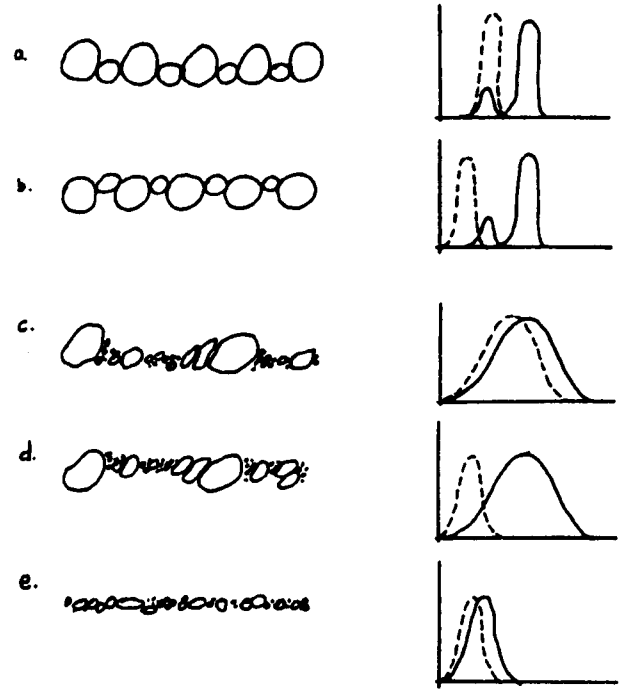

Figure 3.8 Similar particle size distributions (——) giving different roughnesses (- - -) (a & b, c & d); different particle size distributions giving similar roughnesses (d & e).

3.5 Gravel surface micro-profiling

Water worked mixed gravel beds are structured to a greater or lesser extent (Richards & Clifford, 1991) which means that the roughness characteristics also include particle shape,

orientation and spacing as well as particle size (Robert, 1988). This means that a PSD can be expressed in several different surface roughness forms, or conversely similar roughness surfaces can be composed of different PSDs (Furbish, 1987) (Figure 3.8). Although there are limits to such variations, the case still remains that a parameter derived from a PSD may be too crude to describe all of the important properties of the roughness surface.

Micro-profiling involves measuring the heights of the roughness elements *in situ*. In all cases in the literature where this has been carried out, a 2-dimensional space series has been taken using some form of pin gauge (e.g. Furbish, 1987; Robert, 1988; Robert *et al* 1992; Warburton *pers comm.*).

3.5.1 Deployment

The gauge used in this work was 44cm long containing 220 pins, each 2mm wide (Figure 3.9). This was built from two 25cm gauges bought from a hardware store, and modified to provide a locking nut to allow the pins to be fairly loose when applying the gauge to the bed, then locked to remove the gauge and record the profile.

The length of profile taken is defined by two factors. Firstly, the selection of sites was usually made in order to provide a homogeneous roughness surface. The length of the profile was therefore limited by a subjective assessment in the field of the area of homogeneously rough bed.

Secondly, the series needed to be long enough to include sufficient larger obstacles to accurately represent the roughness surface. If the first factor could be satisfied, then a rule of thumb was adopted whereby the profile was taken as 100 times the height of a "large" obstacle, a value which was itself estimated on site. This rule was not always adhered to due to the discomfort of taking the profiles (especially in meltwater channels!).

Usually, about $^2/_3$ of the profile was taken upstream of the flow sampling point, and $^1/_3$ downstream. This ensured that the local upstream topography was recorded, and that the flow sampling point was not just upstream of a roughness transition which could have affected the monitored flow.

All of the profiles were taken in the streamwise direction, which was easy to achieve by using the profiler itself as a directional vane when offering it to the bed.

Starting from the downstream end, a profile was taken by gently pressing the pins in groups of up to ten down into the gravel matrix. When in place, the distances from the upstream and downstream ends of the profiler to the water surface, d_1 and d_2, were measured. As the roughness was homogeneous over the sampling area, it is a reasonable assumption that the water surface slope would be constant also. This means that these depths of the profiler ends could be used later to correct the profiles for yawing of the profiler (Figure 3.9).

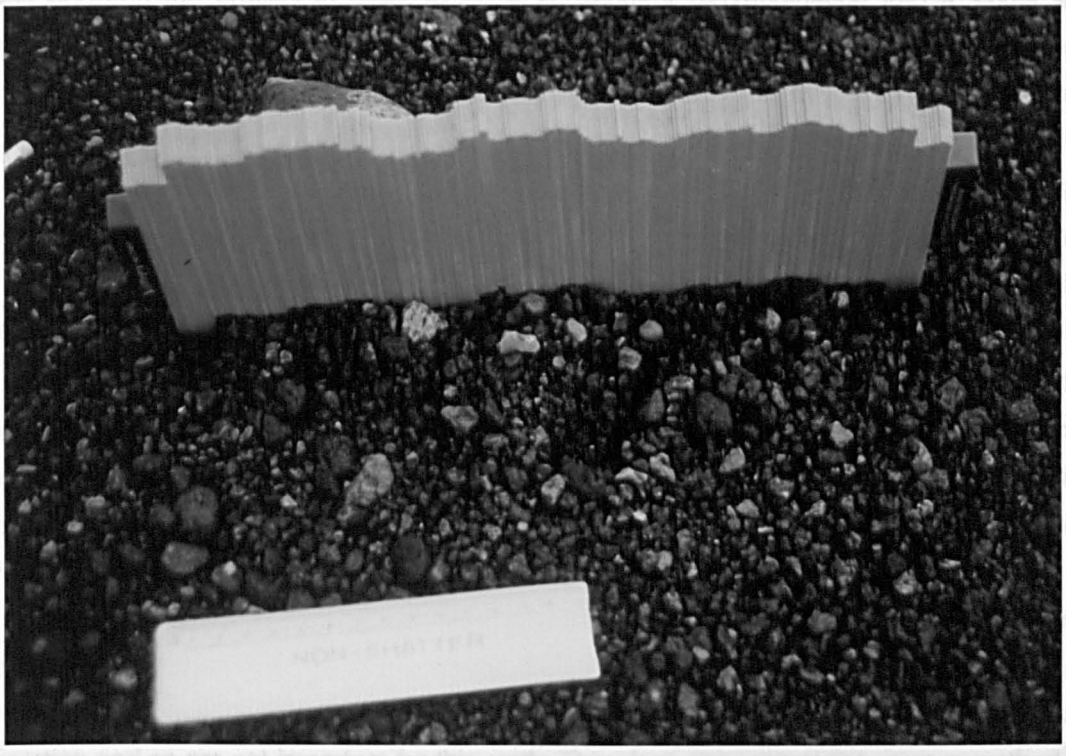

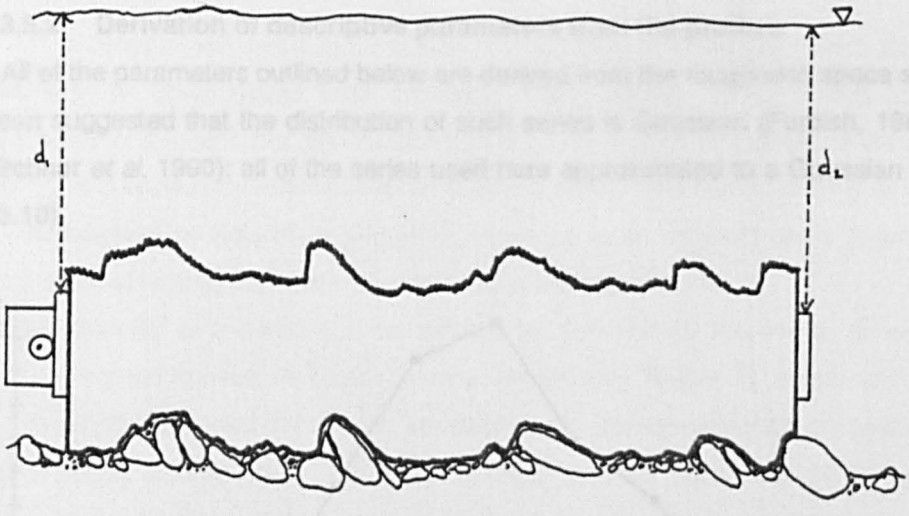

Figure 3.9 The bed profiling gauge. d_1 and d_2 are the depths to the water surface at the upstream and downstream end of the gauge.

When the bed could be seen (the flume, the Dubhaig and Beauty Creek), the upstream end of an individual profile was marked as a starting point for the next profile. An overlap was made between the profiles in order to allow subsequent re-combination into a single long profile. The profiles taken at Arolla were taken blind due to the high suspended sediment concentration of the river. This mean that the profiles could not be subsequently combined into a long profile.

Each profile was traced onto paper in the field, the way up and streamwise direction being marked. The profiles were digitised relative to a baseline which was parallel to the water surface slope. Digitisation was done manually using a ruler and set-square, the values being stored in a spreadsheet. The overlapping sections of the individual profiles in a long profile were identified initially, and the streamwise increments adjusted for the long profile. The series values of the individual profiles were then adjusted so that the overlapping sections corresponded with each other as closely as possible. The redundant parts of the overlapping areas were then deleted from the spreadsheet. Finally, the lowest point in the series was defined as the zero datum and the whole series was adjusted relative to it.

As the Arolla profiles could not be combined, it meant that the largest form that could be discerned in the profiles had a wavelength similar to the length of the profiler (i.e. 44cm). In terms of turbulence generation, forms of this size or larger are not likely to cause flow separation and so are not important for this work. Therefore, the long series were smoothed by subtracting a 22cm running average from the series.

3.5.2 Derivation of descriptive parameters from the profiles

All of the parameters outlined below are derived from the roughness space series, k(x). It has been suggested that the distribution of such series is Gaussian (Furbish, 1987; Robert, 1988; Kirchner *et al*, 1990); all of the series used here approximated to a Gaussian distribution (Figure 3.10).

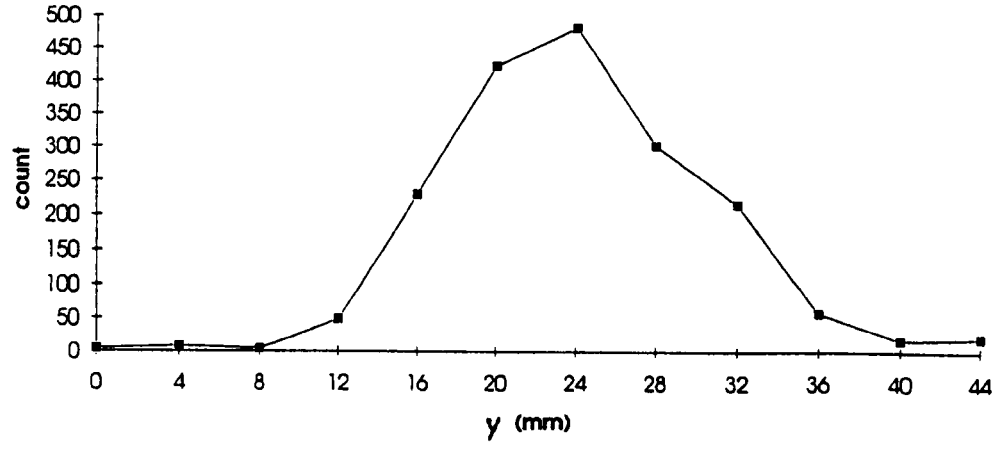

Figure 3.10 Frequency distribution of the heights of the de-trended Beauty Creek bed profile series.

(a) Descriptive statistics of the space series

Tribology is "the science and technology of interacting surfaces in relative motion" (Arnell *et al*, 1991). Standards exist regarding the smoothness of machine-finished metal surfaces, and one of the ways that these are defined is by using the mean and standard deviation of the 2-dimensional space series (Hutchings, 1991).

The standard deviation of the series, σ_k, can be interpreted as a measure of roughness height as it represents the internal spread of the roughness series. σ_k will be one of the values employed as a roughness parameter.

It is accepted that there are two potential flaws in the use of σ_k as a roughness parameter. Firstly, it does not differentiate between the sizes of the individual roughness elements, and secondly, it does not take into account the spacing of the obstacles. Its qualities must therefore not be artificially extended beyond it being a measure of the variance of the space series.

(b) Percentiles of the space series distribution

Higher percentiles of the PSD are used to describe the roughness because it is the coarser particles which are thought to produce the greatest resistance. The same argument can be applied to the distribution of k. k_{84}, the roughness series height value for which 84% is lower, will therefore be used as a roughness parameter.

(c) Fractal dimension

The concept of self-similarity introduced by Mandelbrot (1983) has been applied in the characterisation of fluvial gravel beds (Furbish, 1987; Robert, 1988). When applied to a roughness surface, it means that the surface can be described as self-similar if the only way of distinguishing the scale is by reference to an absolute scale. This can be extended to compare different roughnesses by determining whether reference to an absolute scale means that they are similar, or whether they are different in spite of scale adjustments.

Self similarity of a series can be defined by determining the fractal dimension. This involves counting the number of steps, N, of a certain step length, G, which are required to cover the length of the series. By varying the step length and repeating the procedure, a plot is produced of log(N) against log(G). If this plot is linear then the series can be considered self-similar, and the fractal dimension, D, is given by the slope of log(N) on log (G).

Several roughness series were selected on the basis of contrasting appearance, and their fractal dimension determined.

Robert (1988) showed that the plots of log(N) against log(G) were kinked, and interpreted this as representing two scales of self-similar roughnesses of the gravel beds, one relating to particle roughness, the other to form roughness. Such kinks did not emerge from the series tested here due to the de-trending of the series.

The similarity of the fractal dimensions of the beds means that this technique does not resolve the subtleties in the roughness differences between the beds concerned. As a result, fractal dimension was not chosen as a roughness parameter.

(d) Series analysis of the bed profiles

It has been shown that bed profile series exhibit the properties of a first order autoregressive model (e.g. Furbish, 1987). This has been used in two ways to quantify the roughness. Firstly, Robert (1988) has used the autocorrelation properties to derive fractal dimensions of the series. Secondly, Furbish (1987) derived a horizontal dimension, S, based on the autocorrelation function of the series. Furbish defines the aspect ratio of a series as S/σ_k. As this combines a characteristic length scale, S, with a vertical scale, σ_k, it is a useful roughness parameter. The problem with using an aspect ratio here is that an absolute scale is required.

The size of the individual obstacles relative to (short) length of the Arolla profiles means that the application of series analysis is not justified. The importance of the Arolla data due to the higher shear stress conditions and the transport of sediment mean that they should be incorporated into any analyses done. This means that series analysis was not carried out on any of the data, even though it is accepted that it provides the best potential for the quantification of roughness.

3.6 Relation between roughness parameters derived from the PSD and from the roughness profile

Section 3.5 showed that similar PSDs can be expressed as different roughness fields, and that similar roughness fields can be composed of different PSDs (Figure 3.8). If this was not the case, then the parameters which have been chosen to quantify roughness should be systematically related.

Figure 3.11a shows k_{84} plotted against σ_k for all of the data. As would be expected, it suggests that as k_{84} increases, so does σ_k. Figure 3.11b suggests a positive correlation between D_{84} and k_{84}, although it is not a 1:1 relation. It shows that the D_{84} overestimates the size of the roughness relative to the equivalent percentile derived from the roughness distribution. Although there are only a few points on the plot, the relation between the two descriptors does not appear to be strong, supporting the notion that similar PSDs can be expressed as different roughnesses and vice versa.

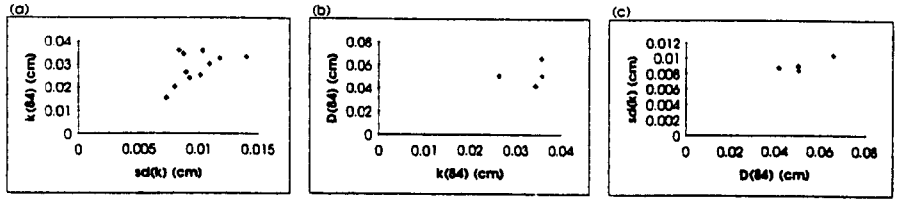

Figure 3.11 Comparison of roughness parameters of the field and flume data. (a) k_{84} against σ_k, (b) D_{84} against k_{84}, (c) σ_k against D_{84}.

Figure 3.11c suggests that σ_k is not sensitive to variation in D_{84}. If it is assumed that σ_k is a better representation of roughness than D_{84}, this supports the idea that different PSDs can be expressed as similar effective roughnesses.

Bed profiles exist for all of the turbulence data which were finally used, but there is not a complete set of corresponding PSDs of the bed material. The relative roughness values quoted in section 3.9 are depth/σ_k rather than the more conventional depth/D_n. This is to allow comparison between all of the data.

Section C: Measurement of bedload transport

The monitoring of bedload transport is notoriously difficult. All monitoring techniques involve the disturbance of that which is being measured which produces difficulties in the calibration of the samplers. The reason for measuring transport for this work was to obtain a continuous record of the fluctuating transport to compare against the turbulence data. To achieve this, the plan was to adopt the acoustic technique which monitors the self generated noise (SGN) of inter-particulate collisions.

3.7 Acoustic bedload monitoring

3.7.1 Principles of acoustic bedload monitoring

The monitoring of SGN is a technique first developed in the 1960s (Bedeus & Invicsics, 1963; Johnson & Muir, 1969), but has been applied in both coastal and fluvial environments to monitor gravel transport (e.g. Tywoniuk & Warnock, 1973; Richards & Milne, 1979; Heathershaw & Thorne, 1985; Thorne *et al*, 1989).

It relies on the simple principle that when particles collide, some of the energy of the collision is emitted as sound. Sound intensity increases with increasing transport rate, and the sound frequency is inversely related to the size of the colliding particles (Hardisty, 1990). The requirements of the monitoring here mean that derivation of particle sizes and absolute rates of transport are not required. This simplifies the theory down to presence or absence of transport.

The hydrophone that monitors the SGN also monitors the water noise. The frequency of the noise generated by colliding gravels is higher than that of water noise. The majority of the water noise can be filtered out of the total noise signal to leave the SGN (Hardisty, 1990).

3.7.2 Deployment of acoustic rig

The rig used for this work had to be cheap, easy to maintain in the field, and completely portable. Figure 3.12a shows a schematic diagram of the set-up used.

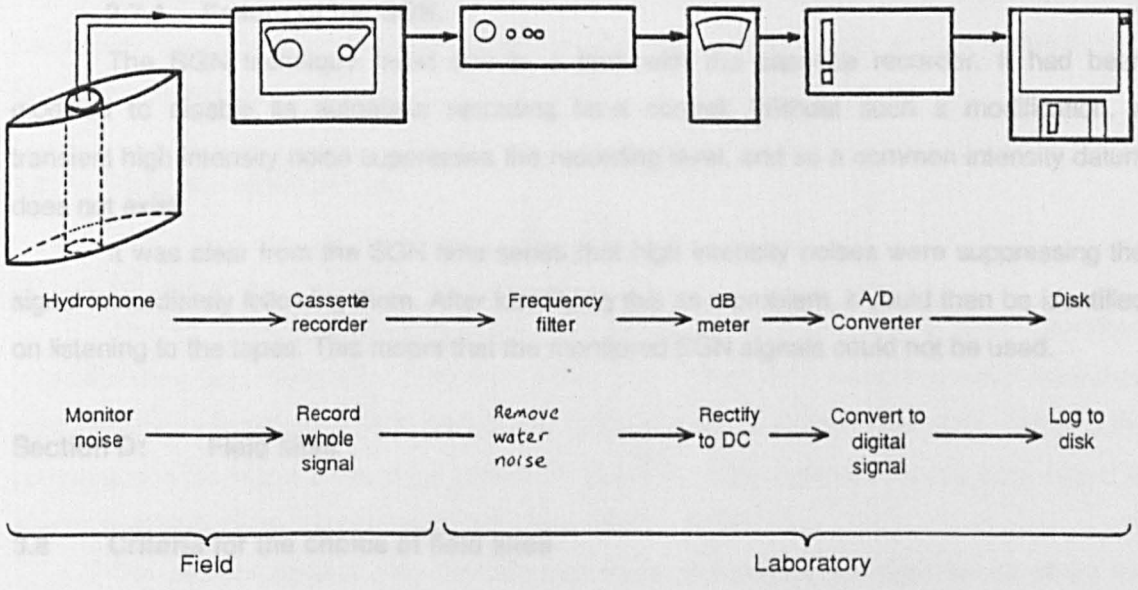

Figure 3.12 Monitoring gravel SGN: (a) The components of the monitoring set-up. (b) The hydrophone in position.

The "hydrophones" consisted of small microphones glued onto the end of perspex tubes. The microphones, made by Maplins electronics, had a frequency response of 50Hz to 16 kHz, which adequately covered the range of the gravel impact frequencies. They were made waterproof by sealing them inside light gauge condoms. These were chosen after testing various materials for acoustic transparency.

The microphone was mounted in a streamlined housing to cut down on excess water noise. This was attached, using various improvised mounts, onto the wading rod, downstream of the ECM probe (Figure 3.12b). In most cases it was positioned 10cm above the bed.

In the field, the total signal from the hydrophone was recorded directly into a cassette recorder. This reduced the amount of equipment required in the field, and simplified the deployment.

3.7.3 Digitisation of the acoustic signal

In the laboratory, the recorded signal was filtered and logged onto a PC.

A Barr & Stroud EF3 band pass frequency filter was used to chop the lower frequencies which are of water noise. To the ear, water noise is clearly distinct from gravel noise, and so the low pass filter was set manually to remove the water noise. The output signal was an AC voltage, and had to be rectified to DC before it could be logged. This was done using a modified decibel meter. The fluctuating DC voltage was logged via the same A/D converter used in logging the ECM. The signal was sampled at 16Hz in order to obtain as much resolution about the sediment transport as possible. This value represents the fastest response time of the A/D converter. The digitised signal was stored in a spreadsheet.

3.7.4 Failure of the SGN.

The SGN technique failed due to a fault with the cassette recorder. It had been modified to disable its automatic recording level control. Without such a modification, a transient high intensity noise suppresses the recording level, and so a common intensity datum does not exist.

It was clear from the SGN time series that high intensity noises were suppressing the signal immediately following them. After identifying this as a problem, it could then be identified on listening to the tapes. This meant that the monitored SGN signals could not be used.

Section D: Field sites

3.8 Criteria for the choice of field sites

(a) Geomorphic/hydraulic considerations

Any potential site had to satisfy criteria relating to channel and sediment size. It was necessary to be able to wade the channel, with easy access from the banks. The part of the channel that was to be used for monitoring had to be within $\underline{c}$. 6m of a stable, level part of the

bank, as the ECM cable was only 10m long and the electronic parts of the equipment had to be protected from the risk of getting wet.

The bed sediment ideally needed to be within the gravel size range. At the site, there should be a range of different roughnesses within the gravel size limits to allow the hydraulics over contrasting roughness conditions to be monitored. Differentiating gravel-bed from sand-bed channels was easy, but separating gravel from cobble channels was sometimes less straightforward. The aims of this work are to consider the flow over *gravel* beds and although the processes of interaction between the flow and cobble sized obstacles are probably similar to those of gravel, the larger scale makes the issue more complex.

Ideally, the site should allow the monitoring of a wide range of hydraulic conditions over the same bed. This involves monitoring during flood events. As most floods in the UK are either due to or associated with rainfall events, and as electronics and rain do not mix, a UK field site was not chosen. High humidity due to continuous rain was at least partly to blame for the equipment failures of the Iceland fieldwork.

Pro-glacial rivers are ideal outdoor laboratories. Floods are generated by the melting of glacial ice or snow, and hence tend to occur in dry sunny conditions. The timing of the floods is predictable and the dry conditions tends to encourage reliability in the monitoring equipment.

(b) Logistical considerations

The basic logistical consideration for field site choice regarded accessibility. As the computer and the current meter both relied on electrical re-charging from the mains, there had to be easy access to a power point. As the ECM itself weighs nearly 20kg and is slightly larger than a rucksack, it was advantageous that walking distance was cut to a minimum. More importantly, the PC's batteries needed charging after every day's logging, and so frequent visits to a power socket were required.

3.9 Field site descriptions

(a) Allt Dubhaig

The Allt Dubhaig drains part of the Central Scottish Highlands and is amply described in the literature (e.g. Ashworth & Ferguson, 1989). It is a single thread channel which meanders over most of its length, and fines from $D_{50} \approx 115$mm to $D_{50} \approx 0.4$mm over 4km. Towards the bottom end, a transition takes place where the D_{50} of the bed material reduces from 16mm to 0.4mm over only 200m (Sambrook-Smith, *pers. comm.*, 1993).

The reaches chosen were the inflection points in between meander bends where the channel was fairly straight and there was minimal lateral slope of the bed. The flow depths at the points chosen ranged between 23-30cm. The D_{50} of the bed material ranged between 25mm and 42mm, and σ_k ranged between 8.3mm to 10.3mm. This provided relative roughnesses, depth/σ_k, of between 22.3 and 35.4. Mean bed shear stresses, determined from

the velocity profile of u, ranged from 0.9 to 8.0 Nm^{-2}. A summary of the hydraulic and sediment details is given in Appendix 1.

Monitoring was undertaken during May 1992. During this period, the river was at low stage, and no sediment transport was taking place.

(b) Arolla

The "Arolla data" refers to data collected in July and August 1991 in the pro-glacial river of the Upper Arolla glacier in the Pennine Alps, Switzerland. Two rivers emerge from the snout of the glacier which join c. 200m downstream (Figure 3.13); the one to the true right was the one chosen for study.

The section of river was actively braiding during the study period, and extensive channel change took place over six weeks (Figure 3.14). Reaches were selected within the braids according to the criteria outlined above. Depths ranged from 16cm to 33cm. Size distributions of the bed sediment were not measured for the files finally selected for analysis. However, D_{50} values measured at other reaches at the site ranged between 6-10mm. Relative roughness values for the files used (defined here as depth/σ_k) ranged from 17.0 to 35.8.

The mean bed shear stresses (from the velocity profile) ranged from 0.4 to 100.6 Nm^{-2}. This meant that there were often significant rates of bedload transport, the events discrete and defined by the diurnal flood regime. The rates ranged from 0 to 0.55 $kgm^{-1}s^{-1}$ measured using a Helley-Smith bedload sampler.

(c) Beauty Creek

Beauty Creek is a clear water snowmelt-fed tributary of the Sunwapta river in the Canadian Rockies. Measurements were made in July 1992. The reach chosen was the part of the river that meandered across the Sunwapta floodplain before joining the Sunwapta. The reach was on a wide right-hand bend, but the length of section chosen was effectively straight (Figure 3.15).

Flow depths at the sampling points were between 41cm and 43cm, the D_{50} being 29mm and σ_k was 8.7mm. This yielded a relative roughness, depth/σ_k, of 47 to 49. The mean bed shear stresses were between 2.2 and 3.2 Nm^{-2}, and there was no bedload transport.

Figure 3.13 General view of the Arolla field site, July, 1991. Flow is left to right. Reach used is the upper third of the channel at the bottom of the photograph.

Figure 3.14 Channel change in the Arolla reach. 19/7/91 (a) 10:15, (b) 16:45, (c) 21/7/91, 12:00. Photographs taken from glacier snout (see Figure 3.13). Various sites within the braids were used. (b) and (c) are on next page.

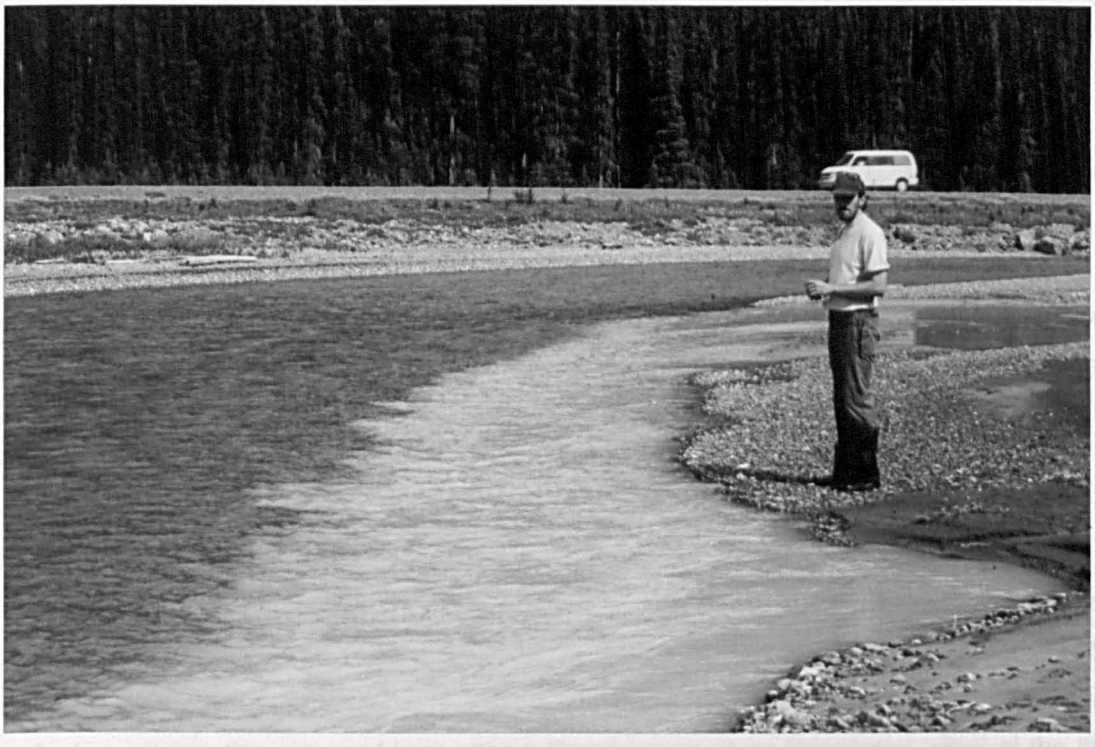

Figure 3.15 The Beauty Creek field site, flow is top right to bottom left. Measurements were made c. 5m from the near bank. The muddy tributary did not exist during monitoring.

Chapter 4 The Description of Turbulence Structure Over Fluvial Gravel Beds

4.0 Introduction

Chapter 2 outlined the possible mechanisms which could generate coherent structures in the boundary layer over fluvial gravel beds. This is the first of two results chapters that aim to provide evidence which helps to determine the nature of the structures. This chapter aims to describe qualitatively the basic spatial structure of the flow field over mixed fluvial gravels so that the quantitative results of Chapter 5 can be interpreted in relation to it. In doing this, it approaches the first two of the thesis objectives, namely to identify the structures present and to describe their morphology.

Two techniques are adopted in this chapter - flow visualisation, and analysis of simultaneously monitored time series at three points in the velocity profile. Flow visualisation allows the direct observation of the flow structure whereas multi-probe monitoring introduces a new way of visualising and describing the flow field. Both techniques allow the description of the flow to be made over an appreciable proportion of the boundary layer thickness.

4.1 Flow Visualisation

Flow visualisation refers to any method which assists in the observation of flow patterns. Unlike point measurements of velocity, it gives a broad spatial picture of how the activity at one point simultaneously relates to that at another. Of the types of visualisation methods available, the one used here uses a filmed image of an illuminated 'slice' of the flow field, similar to that used in the experiments reported by Head & Bandyopadhyay (1981).

These systematic visualisation experiments of the flow over water-worked naturally mixed fluvial gravels are thought to be the first to have been attempted. The purpose of these experiments is to provide a qualitative picture of the nature of the turbulence over a mixed gravel bed. The intention is to describe systematically the properties of the turbulent structures observed, and to attempt to define their mode of generation. The structures will be interpreted with regard to those described in Chapter 2, and a model of boundary layer structure resulting from this will be briefly outlined.

4.1.1 Experimental Set-up

The flume and equipment used for these experiments are those of the Department of Earth Sciences, University of Leeds. The bed of the 10m x 0.3m x 0.3m glass-sided Armfield flume was covered with a bar-surface gravel sample from the River Wharfe to $\underline{c}$. 20 mm depth (D_{84} = 22.1mm, D_{50} = 9.8 mm) (Figure 4.1).

As it is the intention to consider flow over a naturally structured bed, it was necessary to water-work the gravels in preparation for the main experiments. The hydraulic conditions were therefore arbitrarily set to generate moderate sediment transport; the slope was 0.002 and the water depth 20cm. After 6 hours, the transport rate was negligible, and the bed had the

appearance of a naturally structured gravel bed, showing clear imbrication and the presence of cluster bedforms.

Figure 4.1 The water worked flume bed used for the visualisation experiments.

The visualisation used a non-intrusive laser light sheet (made by Dantec Electronics Inc.) to illuminate 2mm thick 'slices' of the flow. It was positioned in the vertical-streamwise (U-V) plane, and its streamwise range extended to c. $5D_{84}$ (Figure 4.2). The water had been seeded with titanium coated mica flake dust to enhance the visualisation effect. A video record was made of the visualised plane through the side-wall of the flume at a resolution of 50 frames per second, and a shutter speed of 0.01s. The video was recorded and analysed on a Panasonic AG 6730E time lapse VTR.

A 65cm ($\approx 30D_{84}$) streamwise section of the bed along the flume centreline was selected for the experiments. This represents six connecting lightsheet spans. At the midpoint of the flume length, water surface profiles during the experiments showed that it was completely unaffected by input or downdraw effects of the ends of the flume. Figure 4.3 shows the bed profile of the section.

At each of the six positions of the light sheet, 2 minute video records were taken of the visualised plane for five arbitrarily chosen discharge settings at a constant slope of 0.002. This provides direct comparison of the effects of changing discharge on the turbulence activity over exactly the same section of the bed. The associated depths ranged from c.20mm to 200mm, giving an order of magnitude difference in relative roughness. A summary of the hydraulic parameters for each setting is given in Table 4.1. At the highest discharge setting, a slight amount of rattling of some of the particles was observed, although these were not in the video section.

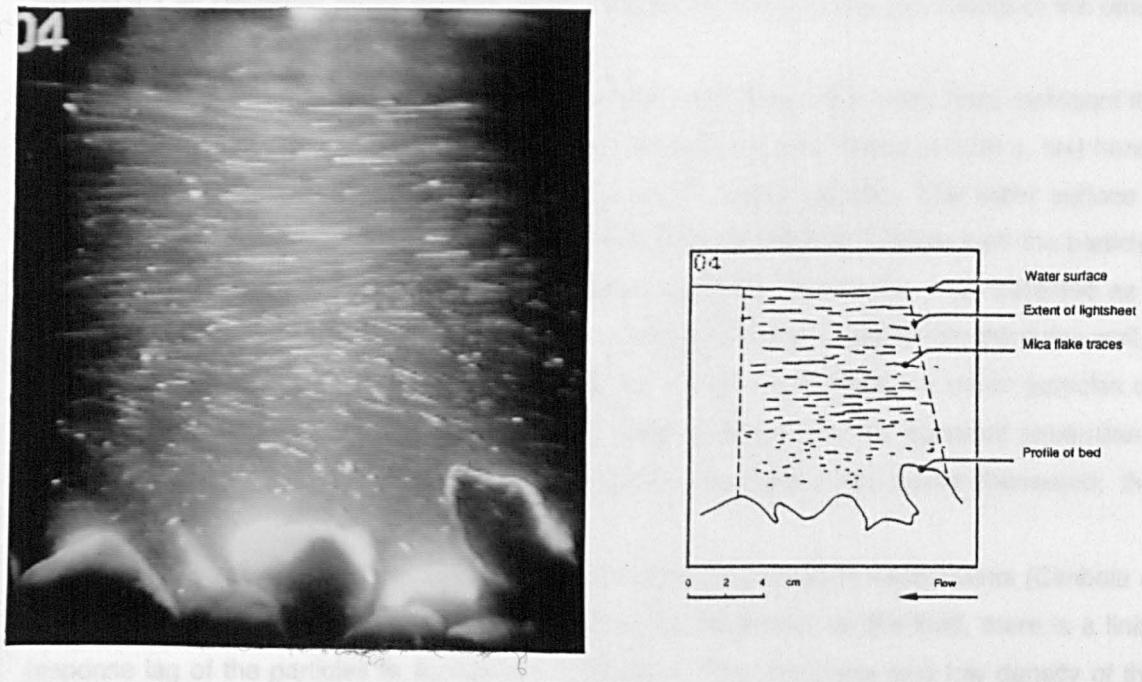

Figure 4.2 A typical visualised image.

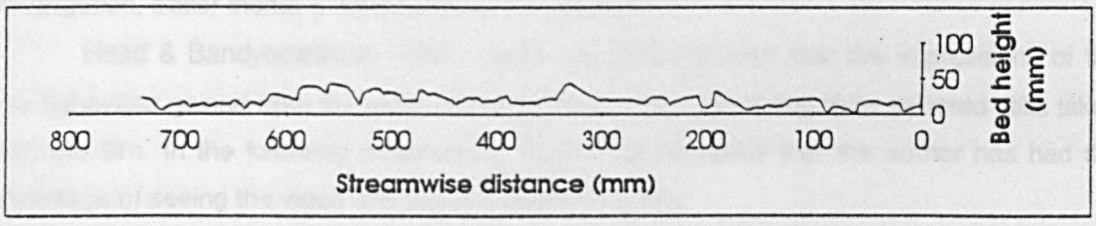

Figure 4.3 Bed profile of the visualised section. The streamwise axis is reversed to correspond to the photographs.

Table 4.1 Summary details of shear stresses (in Nm^{-2}) for the flume flow visualisation runs a to g.

	Shear stress at flow condition:							Means:
	a	b	c	d	e	f	g	
Section								
1	2.17	4.43	7.17	10.28	9.04	9.06	9.81	7.42
2	3.12	6.38	8.74	9.47	10.34	9.17	12.2	8.49
3	5.68	6.69	9.72	10.06	10.25	11.77	12.46	9.52
4	4.92	6.48	8.29	12.54	10.76	12.64	-	9.27
5	6.96	6.79	9.25	10.84	8.72	10.92	13.16	9.52
6	5.82	5.69	9.11	12.72	10.46	11.34	11.83	9.57
Means:	4.78	6.08	8.71	10.99	9.93	10.82	11.89	

At the end of these experiments, the discharge was set to maximum, and the slope increased until gravel entrainment began. Although measurements of velocity, slope and bedload transport rates were not taken, video recordings of the visualised plane were made.

Section 4.1.4c describes these, but the majority of the following discussion relates to the other, lower flow experiments.

Figure 4.2 shows a typical image of the visualised plane. The white lines represent the streamlines revealed by the illumination of the passage of the mica flakes in 1/50 s, and hence their length and direction can be interpreted as the U-V velocity vectors. The water surface is always obvious, but the bed profile section is occasionally troubled by reflection off the particles causing bright patches and problems with camera exposure. When this was identified as a problem, the reflections were masked from the camera by painting them out on the flume wall.

In the analysis of the images, it is assumed that for each frame the tracer particles do not leave the sheet slice. This would have the effect of shortening the apparent streamlines, hence suggesting lower velocities. As absolute velocities were not being measured, this problem was accepted but ignored.

Tracer inertia has been identified as a problem in visualisation experiments (Cimbala *et al*, 1988). As the tracer particles are not exactly the same density as the fluid, there is a finite response lag of the particles to fluctuations in the flow. The small size and low density of the mica flakes means that their associated inertial problems are not as great as those of the larger hydrogen bubbles as discussed by Cimbala *et al* (1988). At the level of detail of this investigation, tracer inertia is considered to be negligible.

Head & Bandyopadhyay (1981) made the pertinent point that the impressions of the flow behaviour gained from the video are very much more convincing than selected stills taken from the film. In the following descriptions, it must be accepted that the author has had the advantage of seeing the video whereas the reader has not.

4.1.2 Observed Flow Structure

Figure 4.4 is a schematic diagram representing the general flow pattern (cf. Figure 4.2). In the first instance, the boundary layer can be split into two main flow zones:

An **outer zone** of mean unidirectional flow

An **inner zone** dominated by an assemblage of vortices, some of which are attached to particles while others are free after being shed.

It will not be assumed at present that these directly represent a buffer zone and viscous sub-layer, but the similarities between these will be discussed later (Section 4.1.4b). The interface between the two zones is marked by a well-defined **separation layer** which is pinned to the crests of the larger obstacles, and tends to decline downstream from a crest. The point at which it re-connects with the bed is determined by the geometry of the obstacle field and the mean velocity. An increase in velocity or obstacle height tends to increase the streamwise length of the wake zones of the obstacles. Generally, its re-connection point is in the proximity of the next large obstacle downstream. The significance of this is discussed further in Chapter 6.

The separation layer is perpetually oscillating in the vertical plane. Levi (1991) attributed similar oscillations of shear layers between high speed fluid jets and low speed fluid

to pressure oscillations (Section 2.3), the oscillation frequency being defined by the local application of the universal Strouhal law (Equation 2.11).

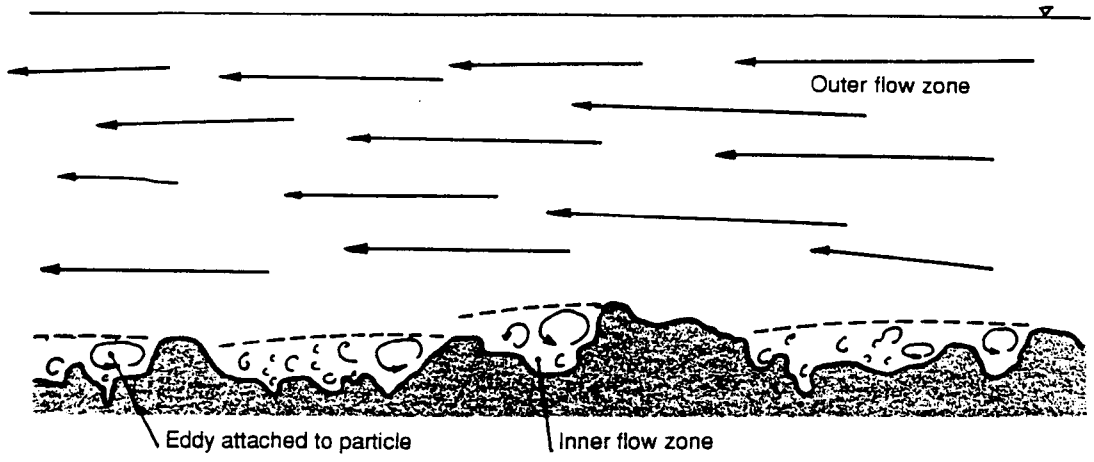

Figure 4.4 A schematic representation of the observed flow structure (compare with Figure 4.2).

Occasionally, an upwards flick in the shear layer causes its complete collapse, and associated with this is the ejection of fluid from the inner zone ($u < \langle u \rangle$; $v > \langle v \rangle$). In many cases, greater-than-average streamwise rushes of outer flow fluid ($u > \langle u \rangle$) directly precede or follow the intermittent ejections. In these experiments at high relative roughness, the effect of the more violent ejections extends right to the surface of the flow. The ejections and return rushes themselves last up to one second, and the separation between events is characteristically 1-10s.

There are three distinct types of ejection, two associated with coarse particles.

1. A momentary sustained declination in the oscillation of the upstream-pinned separation layer allows high-velocity outer zone fluid to impact on the stoss side of an obstacle. This convects high-speed fluid over the obstacle roof resulting in a low pressure zone to its lee in a similar manner to that observed in the lee of cylinders (Gerrard, 1966) (Figure 4.5a). The attached vortex expands into this zone and ultimately results in its detachment and the ejection of low-momentum fluid into the outer zone (Figure 4.5b). This appears to cause a blocking of the higher-momentum outer zone flow as shown by both a shortening of the 'frozen' streamlines directly upstream of the ejection, and superelevation of the water surface. The vortex becomes fully detached from its host obstacle, and is entrained by the outer flow. The blocked flow is then released and rushes with a higher-than-average streamwise velocity ($u > \langle u \rangle$; $v < \langle v \rangle$), and tends to consume the weakening vortex. A new vortex re-forms in the lee of the obstacle clast.

2. The vorticity of a vortex attached to the lee of an obstacle increases as it evolves (Figure 4.6 a-b). There is a concomitant increase in size until it either decays chaotically due to the passage of a high-momentum outer flow structure, or exploits a slackening of outer flow velocity and rises out of the sub-zone (Figure 4.6b). In the latter case, once the vortex begins to rise from behind the obstacle, it blocks the outer flow until the vortex is shed. The blocked

flow is again released as a higher-than-average velocity streamwise rush (U > <u>)(Figure 4.6c).

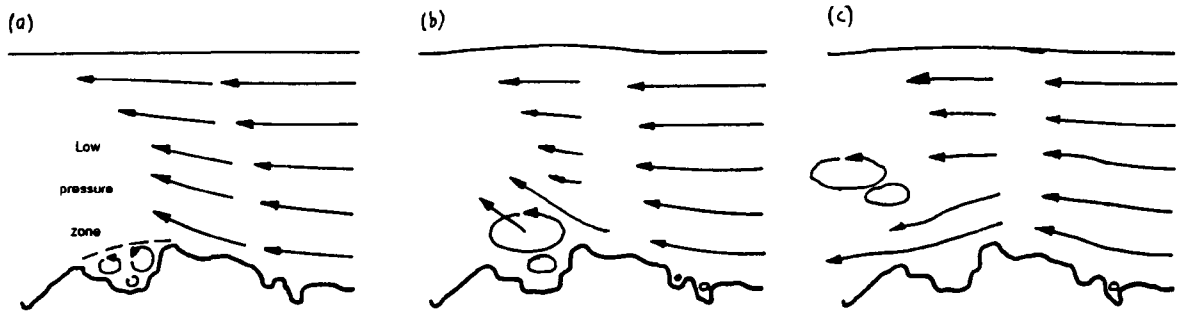

Figure 4.5 A sequence of events leading to eddy shedding: (a) forced convection of outer flow, (b) escape of lee vortices into low pressure zone, (c) Detachment of lee vortices and in-rush of outer flow fluid.

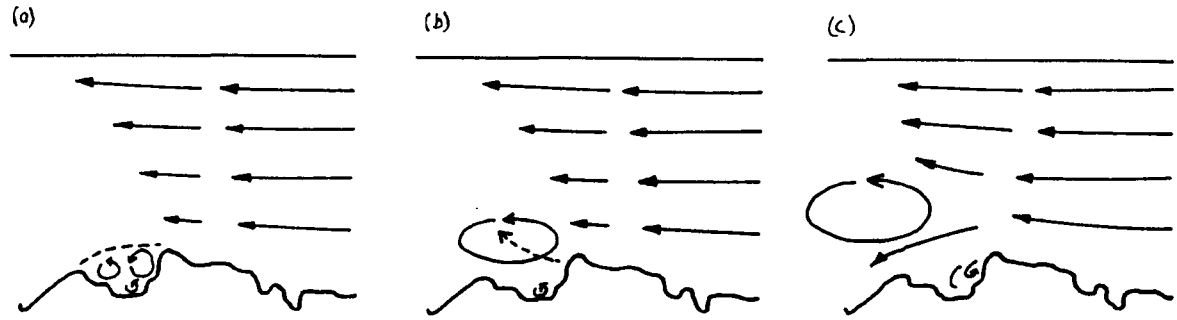

Figure 4.6 Another sequence of events leading to eddy shedding: (a) lull in outer zone flow, (b) expansion of attached vortex, (c) detachment of vortex and down-rushing of outer zone fluid.

3. Over those areas of the bed in the region of the re-connection of the separation layer, coherent ejections of fluid from several smaller obstacles take place. They occur just after the passing of a rush of outer fluid when there is a lull in the outer zone in a mechanism similar to that described in (2). Unlike (1) and (2), there is no obvious obstacle from which the vortices detach and eject, and they do not generate a persistent vortical structure.

Figure 4.7 incorporates the three modes of ejection into a general schema of the ejection - return structures. The individual events of ejections and returns cannot be considered in isolation from each other, nor can a description of the system be made by referring to an initial perturbation from isotropic turbulence. In order to explain the observations described, they will be interpreted in terms of the structure generation mechanisms discussed in Chapter 2.

4.1.3 Identification of Vortex Shedding Features

Vortices are clearly seen in the visualisations in the lee of the larger obstacles which tend to be the ones to which the separation layer is pinned (Figure 4.8). The direction of vortical rotation confirms that the vortex is generated and maintained by the separation of flow as it

traverses the negative step of the obstacle roof. The hemi-annular shape of the vortex, although crude, is confirmed by the existence of crude vorticity in the sections marginal to the obstacle roof. Generally, attached crudely hemi-annular vortices are commonly seen to exist in the visualisations in a form equivalent to those in Figure 2.5.

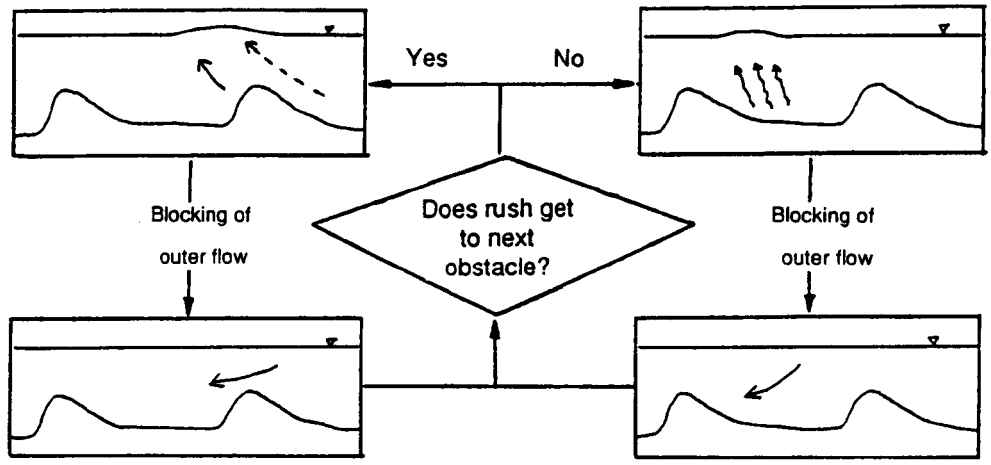

Figure 4.7 Schema of ejection rush structure.

The previous section described several modes of detachment and the intermittent shedding of the lee vortices. The 2-dimensional nature of the visualisation technique means that simultaneous observations of the shedding of the tip of the vortex and the development and stretching of the legs of the hairpin as shown in Figure 2.5 cannot be gained. However, most of the trajectories of the shedding heads tend to be at the characteristic 40-45° to the bed plane suggested by Head & Bandyopadhyay (1981). It is therefore reasonable to assume that this must represent hairpin stretching.

The persistence of the vortex form once shed from the host obstacle is a function of the nature of shedding. During the onset of detachment, the vortices are either advected by the outer flow or 'smeared' along the inner zone; it is those in the outer zone which tend to retain coherence the longest, and represent the majority of the cases observed. The nature of the outer zone flow field at the time of shedding determines whether the shedding vortices are advected or smeared. Often, the limit to the streamwise length of the light sheet means that the vortices still retain coherence as they are advected or smeared out of the field of view.

Within the inner zone i.e. the zone generally beneath the pinned separation layer, the roughness elements are not exposed to the dominantly unidirectional flow field of the outer zone like the larger obstacles. The flow field tends to be intensely turbulent, and composed of a confused assemblage of small eddies. This means that the opportunity rarely exists for an attached vortex to develop to the point of shedding. The eddies which exist in the inner zone are probably either the immature relicts of vortices which have been torn off roughness elements by other eddies, or are generated by small-scale shearing within the inner zone.

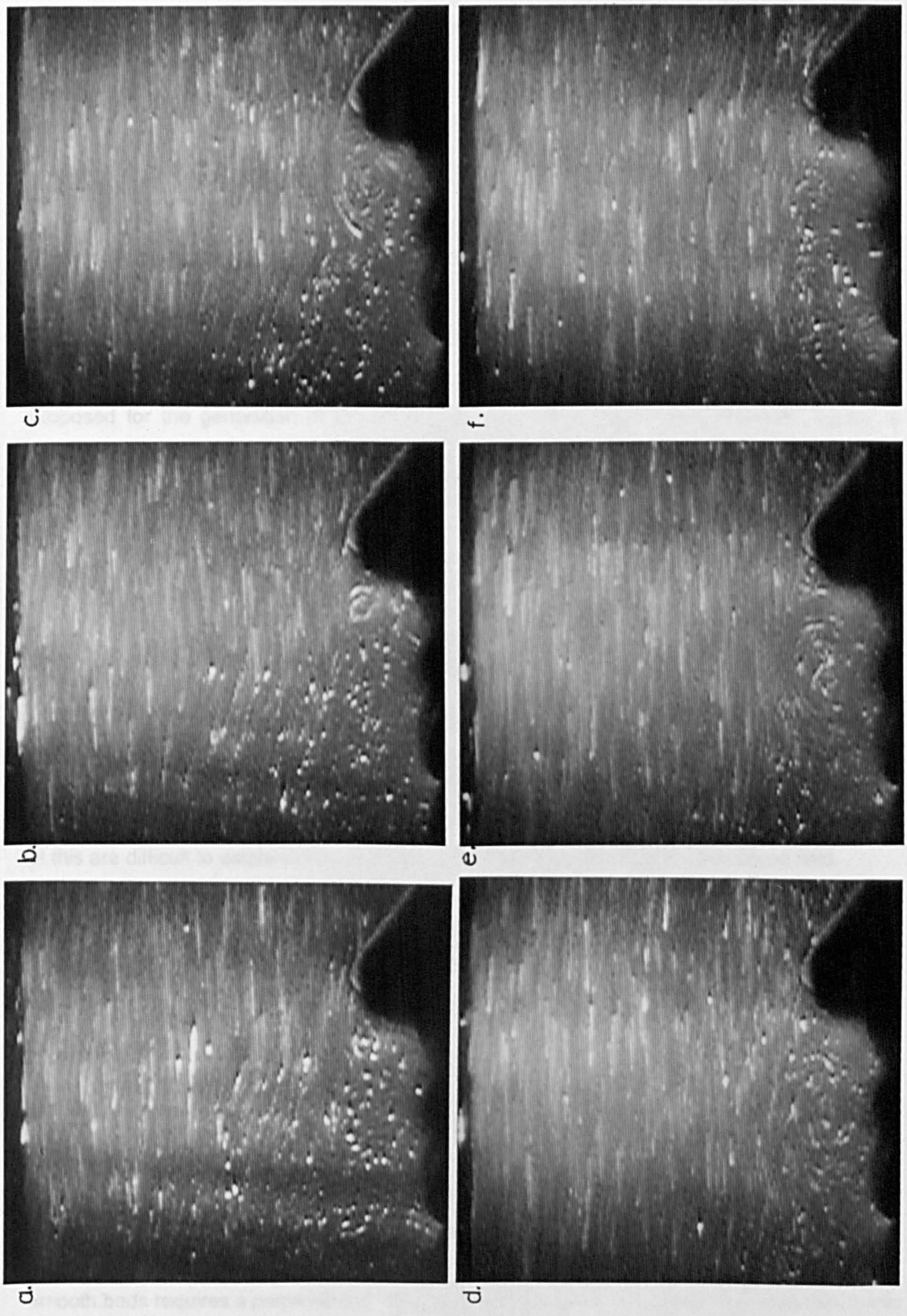

Figure 4.8 Visualisations of eddy shedding. Time separation between plates = 1/25th second, flow is right to left, depth = 15cm.

There is no evidence whatsoever of any streaks existing in the inner zone, even on the facets of particles.

4.1.4 Outer Flow Structures

The actual initiation of the shedding of vortices is caused by a perturbation in the direction or magnitude of the flow in the outer zone. The nature of the outer flow structures is determined by the relative depth of the flow.

In the shallower flows, the outer zone is dominated by larger turbulent structures which are advected into and out of the field of view at velocities greater than the mean flow velocity. These sometimes exhibit a crude vortical structure. Often the perturbation required to initiate further shedding is provided by the over-passing of these structures. Two hypotheses are proposed for the generation of the structures. They either represent a structural legacy of several vortex-shedding structures from upstream, or are a separate form of turbulence structure perhaps being related to the sublayer-buffer layer interaction of the burst-sweep model.

a. Post-Shedding Behaviour of Vortices

The vortices, once shed from the host obstacle, are advected by the outer flow. Section 2.5.1 explained how coalescence of the shed vortices could take place, and what effect it would have on the properties of the structure. As most of the shed vortices were 'lost' from view due to the limited width of the light sheet, it is not possible to comment on the mechanisms of coalescence specifically. However, it was occasionally observed that as an eddy is ejected it is consumed by a large over-passing structure in the outer zone. The details of this are difficult to establish due to the limited streamwise length of the visualised field.

b. Outer-Inner Zone Interaction

The inner/outer zone structure of the flow field over the gravels (Figure 4.4) can be viewed as being conceptually similar to the viscous sub-layer / buffer layer structure of the burst-sweep model, the fundamental difference being in the content and structure of the inner zone. Although the inner zone consists of the vortices attached to the larger obstacles and the more confused eddying, the inner zone vorticity would be concentrated in the tips of the obstacle-derived vortices, as these extract energy from the outer flow field. The *dominant* sense of vorticity in the inner zone is therefore perpendicular to that of the streaks in the viscous sublayer (spanwise compared to streamwise axes).

An incursion of high-momentum fluid from the buffer layer into the sub-layer over smooth beds requires a perpendicular realignment of the sense of vorticity to enable roll-up into the spanwise-axial vortex to produce an ejection (Figure 2.4). The perpendicular sense of inner zone vorticity compared to that of the viscous sub-layer would mean that an incursion from the outer zone into the inner zone over a gravel bed should generate roll-up and ejections more readily.

The activity of the obstacle-derived vortices significantly complicates the interface between the inner and outer flow zones. Intuitively, vortical structures derived from layer interaction would only exist when the conditions for their formation were able to dominate the boundary layer. In order to define such conditions, specific application of the eddy hierarchy hypothesis will be made, and the outcome interpreted with respect to co-existent vortex shedding conditions.

c. Outer Zone Structures at High Flow

As the flow was gradually increased throughout these experiments, changes in the turbulent structure were difficult to determine. However, when the discharge and slope were increased to cause entrainment, two points were immediately apparent: the outer zone structures never showed any vortical characteristics, and vertical ejections from no apparent source in the near bed region occurred.

Figure 4.9 shows a sequence of frames from the video which show typical activity. They show water surface waves propagating downstream, below the wave front being a zone of relatively fast streamwise fluid. The fast fluid exists as an inverted wedge with a "front" which is moderately well defined in the upper parts of the flow, but is less coherent towards the bed. Upstream of the front, the streamlines become shorter suggesting that the flow is slowing down.

After a front has passed, fluid is ejected from the near-bed region. The ejection does not appear to be associated with eddy shedding from a discrete obstacle, its source being apparently entirely independent of the local bed features. The ejections rarely reached the water surface due to being over-ridden by the next high-momentum front.

Over other parts of the bed, eddy shedding *was* observed, but it was considerably more chaotic than at lower flow conditions. Shedding took place after the passage of a high momentum front, and hence the shedding period was defined by the period of the succession of the high-speed wedges. The vortices generated were rather incoherent compared to those generated at lower flow, and any rotation soon disappeared.

4.1.5 Application of Vortex Scale Hierarchy Theory

The vortex scale hierarchy hypothesis is a conceptual model of vortex coalescence (Perry & Chong, 1982). It proposes that with increasing distance from the wall, a pairing of vortices takes place with a corresponding increase in vortex size. Figure 4.10 shows a symbolic representation of the hierarchy.

Over a smooth bed, the size of the smallest vortex in the hierarchy is defined by the Reynolds number of the flow; as Reynolds number increases, the size of the smallest vortex decreases, as does the spacing of the vortices in the vortex 'forest', λ_k, (Kline *et al.*, 1967) as given by

$$\lambda_k = 100\nu / U_\infty \qquad (4.1)$$

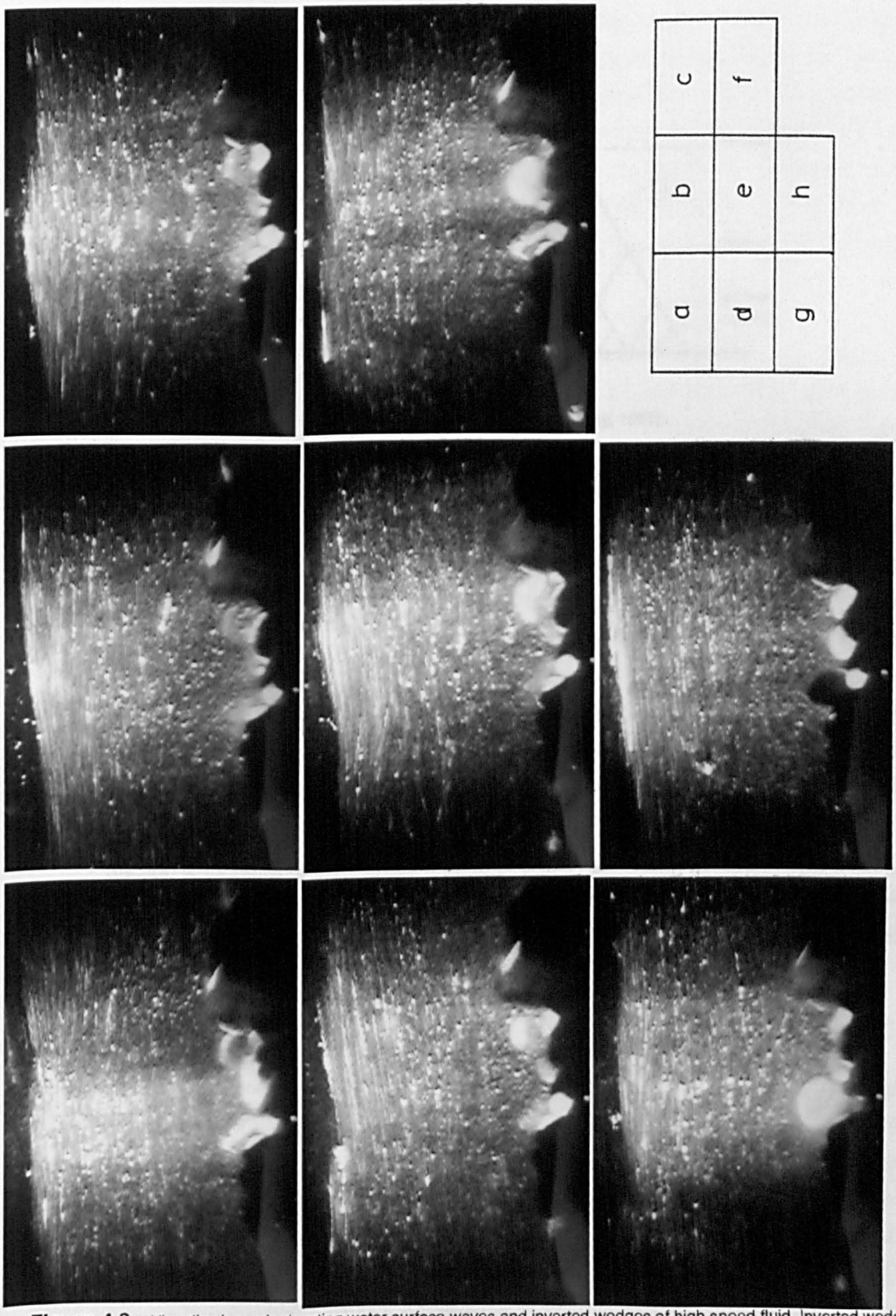

Figure 4.9 Visualisations of advecting water surface waves and inverted wedges of high speed fluid. Inverted wedge of high-speed fluid can be seen below the wave front in (b) and (d). Entrainment of obstacle clast is referred to in Chapter 6. Time separation of frames is 1/12th second, flow right to left, depth = 15cm.

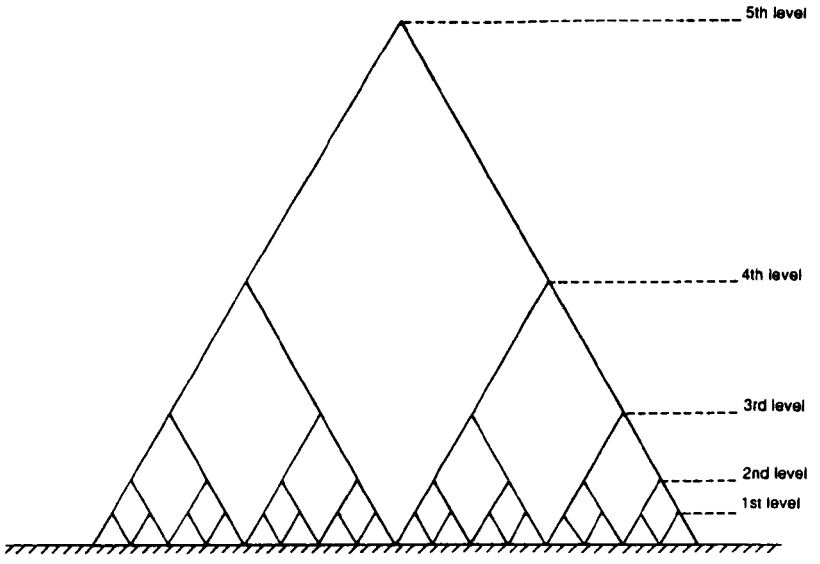

Figure 4.10 Schematic illustration of a vortex hierarchy (after Perry & Chong, 1982).

Figure 4.10 implies that between levels in the hierarchy, the pairing of vortices is a discrete process. Due to the probabilistic nature of vortex pairing, Perry & Chong suggest that the pairing is better represented by a continuous rather than discrete process. An implicit consequence of this is that for a specific set of boundary layer conditions, there is an upper size limit of the largest vortex which can be accommodated which approximates to the thickness of the boundary layer.

Over mixed gravel beds, as the depth of the boundary layer increases (assuming for now that there is no change in Re), the outer zone will thicken whereas the inner zone thickness will stay roughly constant. This will allow the scale of the vortices which could be accommodated to increase accordingly.

Section 4.1.4 explained that there are two possible methods of generation of vortices in the outer zone; they are derived either from the shedding of vortices from obstacles or the interaction of the inner and outer zones. Each of these would react differently to vortex hierarchy considerations.

a. Vortex Shedding Structures

The root vortices in the hierarchy are those attached to the obstacles. The size and spacing of the vortices in the root vortex 'forest' are therefore imposed by those of the obstacles. Generally, a characteristic obstacle spacing, λ_O, would be considerably greater than the root vortex spacing, λ_k (Equation 4.1). As λ_k derives from empirical investigations of streak spacings over smooth beds, it is not a value specific to the hierarchy pairing process. In this respect, it is an imposed root scale in the same way as obstacle spacings. Non-similarity of the two therefore does not preclude vortex pairing over an obstacle field.

The like-sensed vorticity of the hairpin tips would actually encourage vortex pairing. Indeed, Head & Bandyopadhyay (1981) closed their paper by stating that there is no

mechanism by which hairpin tips can cancel during interaction. This implies that if two hairpin tips meet in the boundary layer they would agglomerate into a larger vortical structure.

As the size of the largest vortical structure (the highest level in the hierarchy) is related to the boundary layer thickness, it is essentially independent of the spacing of the obstacle field. However, a decrease in obstacle spacing at the root level would have the effect of increasing the number of hierarchical levels and hence lengthening the time to generate a large structure. This implies that, for similar Re, the timescales associated with vortical structures over coarse roughness surfaces are less than those over smooth ones. However, as the visualisation experiments were carried out over a single roughness, this is not testable here. This point is returned to in Chapter 6.

b. Outer-Inner Zone Interaction Structures

Unlike obstacle-derived vortex shedding, there is no specific vortex size from which to base the hierarchy when considering zone interaction. The spatial scale of the hairpin generated by the interaction of the sub-layer and buffer layer over smooth beds is defined by the streak spacing and the impact area of the impinging sweep (e.g. Best 1992). Following the arguments of section 4.1.4b, the spacing of the 'dominant' obstacles would define the relevant attached vortex spacing. As an approximation, this will be taken as the equivalent to the streak spacing. This means that the root vortex sizes in the hierarchy will be equivalent to those of the vortex shedding discussions in the previous section, and hence the size of the resulting vortical structure would be the same.

The impact area of the initiating outer zone 'sweep' will be defined by the spatial scale of the outer zone vortical structure. This means that the 'sweep' area will always be larger than the size of the root vortex host obstacles.

4.1.6 A hypothesised turbulence structure from the flow visualisation experiments.

In flows where the roughness occupies an appreciable proportion of the flow depth, i.e. where relative roughness is high, and where sediment transport is not taking place, the turbulence structure in the outer zone of flow is dominated by individual vortices which have been shed from obstacles on the bed and other large vortices. The vortices which are attached to the obstacles are shed as a result of the passage of either a vortex shed from an obstacle in the local upstream vicinity or of another outer zone structure. This inner/outer zone coupling of vortical activity is self-perpetuating in an irregularly cyclical manner.

In deep flows, the vortices are shed from the bed particles and enter into a hierarchy of increasing vortex scale. The size is limited by the flow depth, at which point the large vortical structure is advected in the outer zone until it collapses. During its advection, it impinges on the inner zone, causing roll-up and the generation of a further vortical structure of comparable spatial scale. The latter structure will itself have the potential to interact with the inner zone to generate subsequent generations of structures.

The dichotomy in the generative process of the outer zone vortical structures as defined by relative roughness suggests that at intermediate relative roughnesses, both vortex shedding and layer interaction co-exist. The relative dominance of the two mechanisms will be defined by the relative roughness itself and the Reynolds number.

At higher flow conditions where sediment transport is taking place, a succession of advecting high speed wedges seem to dominate the boundary layer. The passage of a high speed front is followed by the ejection of near-bed fluid. Eddy shedding is confused, and the period seems to be determined by that of the high speed wedges. Explanation of these phenomena and their relation to those of lower flow conditions will be made in Chapter 6.

4.2 The Fluctuating Velocity Profile

Flow visualisation clearly is useful in determining the spatio-temporal structure of the boundary layer. Unfortunately, the set-up described above cannot be used in the field, and so the results are limited to the conditions governed by the dimensions of the flume. This presents a large conceptual gap between the spatial scale of the visualisations and the point measurements of velocity described in the literature and in Chapter 5.

The opportunity became available to monitor simultaneously three points in the flow in the field using three Marsh McBirney ECM probes. Simultaneous logging is rarely carried out due to the high cost of the required equipment. This section approaches the investigation of turbulence structure by analysing fluctuations in the velocity profile.

The main value of considering fluctuations in the velocity profile is that it will allow insight to be gained into how the coherent turbulent structures are expressed in different parts of the velocity profile at the same time. Difficulties in the spatial interpretation of flow structure from non-simultaneously monitored velocity signals has partly been the cause of the debate regarding the nature of such structures.

Analysis of the fluctuating velocity profile should help to bridge the gap between flow visualisation studies (e.g. Acarlar & Smith, 1987; Kawanisi *et al*, 1993; Section 4.1) and the point monitoring of velocities (e.g. Clifford, 1990; Clifford & French, 1993; Chapter 5).

There are 3 main purposes of analysing the fluctuating velocity profile which involve both the development of an approach and discussion of its findings. These can be broadly summarised as:

1. The definition of distinctive velocity profile states,
2. The determination of the persistence of these states,
3. The characterisation of sequences of state changes.

4.2.1 Experimental Set-up

The ECM rig was the same as that used by Robert *et al* (1993). It comprises three Marsh-McBirney ECM probes mounted on a single wading rod and orientated to log velocities in the vertical-streamwise plane (Figure 4.11). The lower two probes were of 1.3 cm diameter, and the upper one was the standard 3.8 cm probe. The probes are synchronised resulting in

exact simultaneity of the signals (Roy, *pers. comm.*). The output from the meters was logged at 10Hz into a Campbell CR10 data logger.

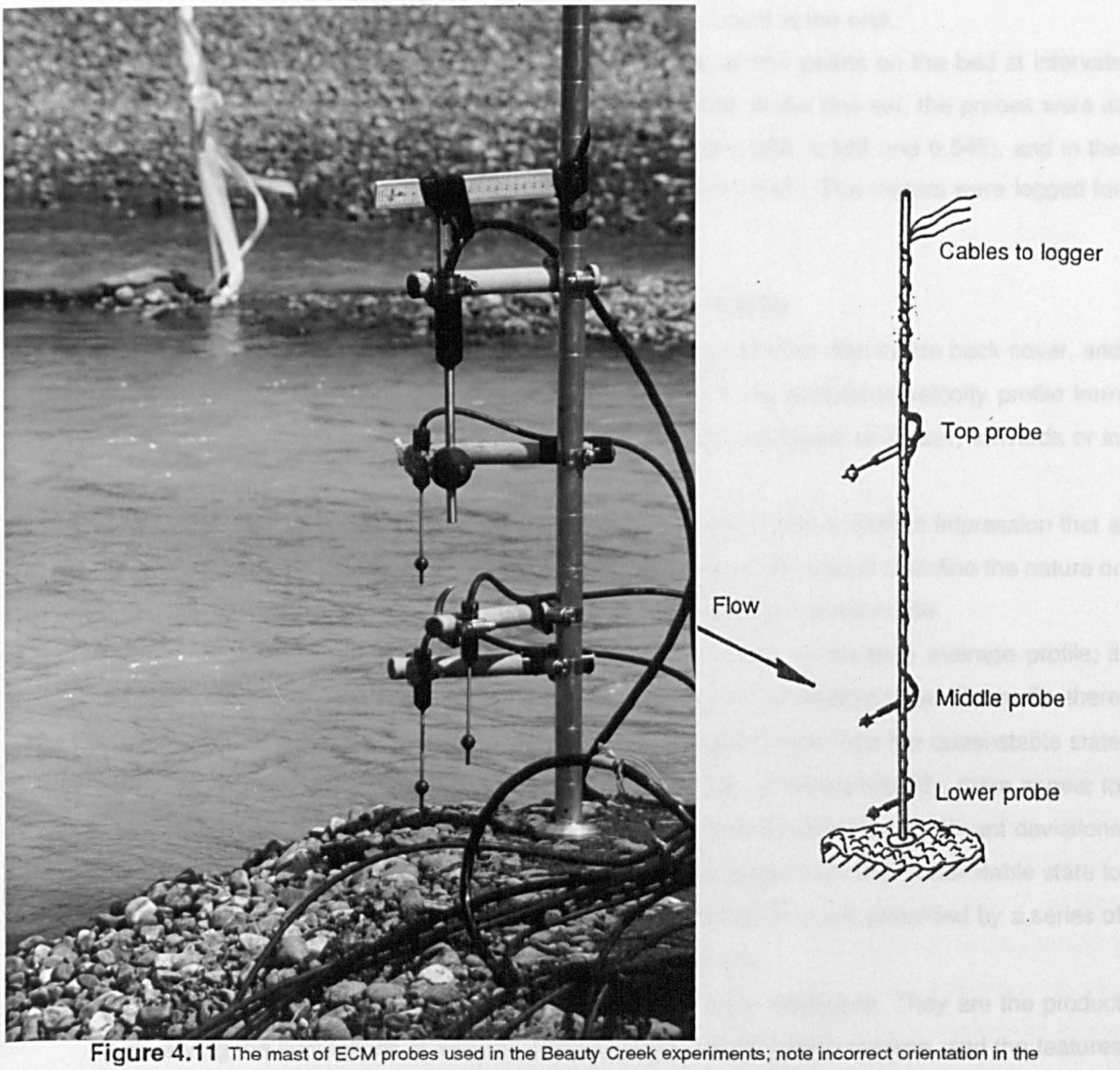

Figure 4.11 The mast of ECM probes used in the Beauty Creek experiments; note incorrect orientation in the photograph.

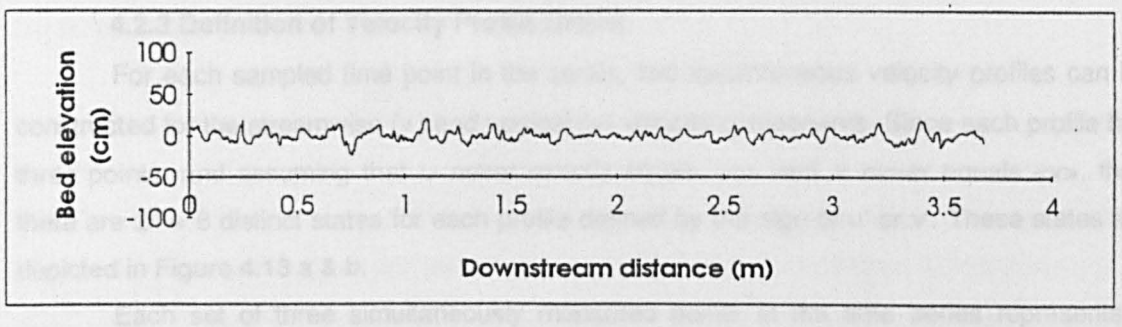

Figure 4.12 Streamwise bed profile of the Beauty Creek section, detrended by subtracting a running average over 440mm.

Measurements were made in Beauty Creek (Section 3.9). A 6m streamwise profile of the bed was taken at the beginning of the experiments (Figure 4.12), and a grainsize distribution of the bed surface material taken by a pebble count at the end.

Two sets of replicate velocity profiles were taken at four points on the bed at intervals of 0.5m upstream of the downstream end of the bed profile. In the first set, the probes were at 3cm, 10cm and 30cm above the bed (equivalent to y/d of 0.055, 0.182 and 0.545), and in the second, 14cm, 20cm and 30cm (≡ y/d of 0.255, 0.364 and 0.545). The meters were logged for two minutes at 10Hz.

4.2.2 Visualisation of the Fluctuating Velocity Profile

A BASIC programme, VELPROF, was written (enclosed on disc inside back cover, and listed in Appendix 2) which reconstructs a visual image of the fluctuating velocity profile from the time series. It also allows the profile run to be paused, run faster or slower, forwards or in reverse.

Observations of the fluctuating profile leave the viewer with a distinct impression that a degree of structure exists within the flow. Although it is extremely difficult to define the nature or patterns of the fluctuations, three subjective observational points can be made.

Firstly, the profile rarely exists in a form close to that of the time average profile; it appears to be quasi-stable in either a high-momentum or low-momentum state. Secondly, there are occasional profile "wobbles" involving relatively small deviations from the quasi-stable state which then revert to the same quasi-stable state. Thirdly, and most importantly, there appear to be transient periods of profile instability which are characterised either by significant deviations from the mean profile or by a gradual change in the profile shape from one quasi-stable state to the other. These events can last for more than 2s. Sometimes they are preceded by a series of profile "wobbles", but at other times they occur spontaneously.

It must be stressed that these observations are quite subjective. They are the product of observing the fluctuations at several speeds, both forwards and in reverse, and the features described rarely exist as tidy entities. The purpose of describing them is to provide a background to aid in the objective quantification presented below.

4.2.3 Definition of Velocity Profile States

For each sampled time point in the series, two instantaneous velocity profiles can be constructed for the streamwise (u) and vertical (v) velocity components. Since each profile has three points, and assuming that u never exactly equals $\langle u \rangle$ and v never equals $\langle v \rangle$, then there are $2^3 = 8$ distinct states for each profile defined by the sign of u' or v'. These states are depicted in Figure 4.13 a & b.

Each set of three simultaneously monitored points in the time series represents a profile state. A time series was generated of velocity profile states, and took the form of a string of the nominal state descriptors, 1-8. This will be referred to as the "state series", and for each time series, state series were generated for both u and v components.

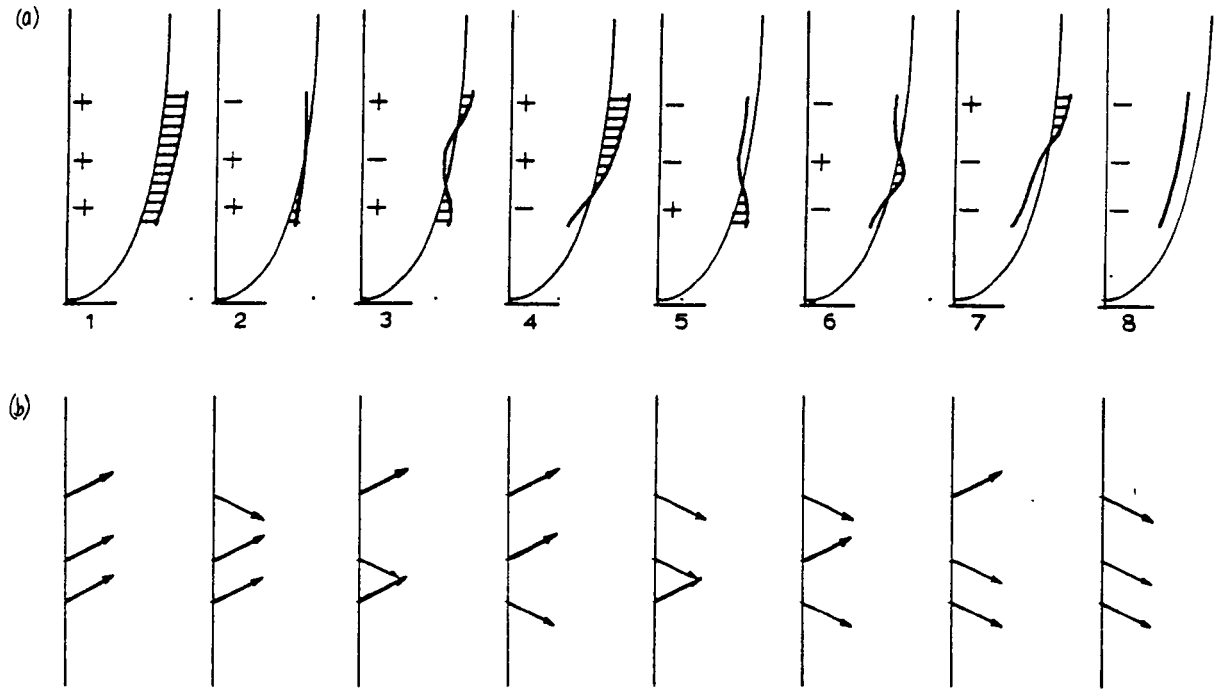

Figure 4.13 Velocity profile state definitions defined by combinations of (a) u <> <u> (b) v <> <v> at the three probes.

4.2.4 Velocity Profile Persistence and Transience

The persistence of a state of the profile which is dissimilar to the mean profile implies the existence of a coherent flow structure. Simplistically, a u profile state which has a higher-than-average bulge in the lower half (i.e. states 2 and 5) implies the presence of a "sweep-like" event, whereas one with a lower-than-average lull in the lower half (i.e. states 4 and 7) implies the presence of a "burst-like" event. This issue is raised again in section 4.2.5 when specific u profile states are linked to the corresponding v profile states. The use of these terms in no way suggests that they have any genetic similarity to the sweeps and bursts mentioned in the literature, but is solely to describe the spatio-temporal character of the flow features.

For each of the eight profile states, frequency distributions of their duration were generated for each state series. The first and last states in each series were ignored as it could not be assumed their full lengths were represented.

The computer visualisations of the fluctuating profile of streamwise velocity suggested that "fast" and "slow" profiles appeared to be more common, and to persist for longer, than other u' states. This is supported by the relative proportion of time occupied in each state (Figure 4.14a), and the mean and maximum durations of each state (Figure 4.14 b & c).

The most common states are 1 and 8 i.e. those in which the velocity deviation has the same sign at each height. For the u profiles these correspond to faster-than-average flow at each height, or slower-than-average flow at each height; for the v profiles they relate to entirely upwards or entirely downwards flow. There is a slight but systematic tendency for the state 1 of

the u component to be more common than state 8, and to a lesser extent, state 8 of the v component to be more common than state 1. The dominance of these two states is greater for the u series than the v, and for the B heights than the A; in the uB data the profile was in either the "fast" or the "slow" state for 55% of the time. These are interpreted as being quasi-stable states, and are strong evidence for coherent flow structures.

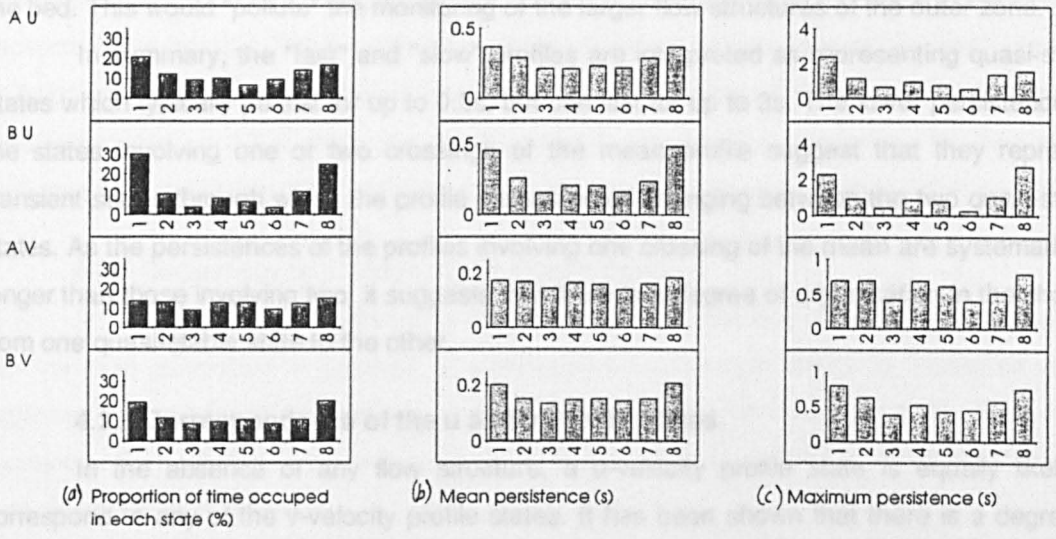

Figure 4.14 (a) The proportion of total time spent in each profile state (b) The mean duration of each profile state (c) The maximum duration of each profile state.

The least common states were generally those with two changes of sign along the profile of the velocity deviation, i.e. the states 3 and 6. Neither of these was occupied for more than 12% of the time in any of the four data sets, in the uB series their frequency was only 4% each, and only in the uA data was another state (5) even less frequent.

States involving one change of sign of u' or v' (2, 4, 5 & 7) have intermediate frequencies, in the range 7 to 14%.

The mean and maximum durations of each state show a similar pattern to the relative proportion of time occupied in each state. The U profile states persist for roughly twice as long as the V, suggesting that the U profiles are more stable than the V. This is reasonable as change in a U profile involves wholescale streamwise acceleration or deceleration, whereas change in the V requires only a slight re-direction of the velocity vector.

The "fast" and "slow" profiles persist for the longest, mean durations being 0.3s to 0.5s for the U component, and 0.18s to 0.2s for the V. Figure 4.14c shows that these profiles can last for over 2s. This supports the proposition that they represent coherent flow structures.

The difference between the mean durations of the fast or slow states compared to those involving one or two crossings of the mean profile is greater for the U component than the V, and for the B files than the A. This suggests that the quasi-stability of the fast or slow states is more marked in the streamwise rather than the vertical profile. It also suggests that multiple crossing profile states last longer for the B than the A files.

There are two possible explanations for why the persistences of the quasi-stable states are longer for the B than the A files. It might mean that the temporal scale of the flow structures is greater higher in the profile than near to the bed. However, after observing the presence of an inner and outer zone in the visualisations, it is more likely that the bottom probe of the A files was in the near-bed zone, the turbulence regime of which is dominated by ejections from the bed. This would "pollute" the monitoring of the larger flow structures of the outer zone.

In summary, the "fast" and "slow" profiles are interpreted as representing quasi-stable states which typically persist for up to 0.5s, but can last for up to 3s. The lower persistences of the states involving one or two crossings of the mean profile suggest that they represent transient states through which the profile passes when changing between the two quasi-stable states. As the persistences of the profiles involving one crossing of the mean are systematically longer than those involving two, it suggests that there is a degree of organisation in the change from one quasi-stable state to the other.

4.2.5 Correspondence of the u and v Profile States

In the absence of any flow structure, a u-velocity profile state is equally likely to correspond to any of the v-velocity profile states. It has been shown that there is a degree of persistence in the fluctuating velocity profile, and so it is reasonable to assume that there would be a corresponding element of structure in the v-velocity profile.

An implicit property of the velocity profile is that it gives a measure of the momentum of the fluid in the streamwise direction; fluid lower in the profile has less momentum than that further from the wall. This means that a streamwise lull in velocity in a section of the profile should correspond to the input of lower momentum fluid, and hence an upwards-directed U-V vector. Conversely, a bulge in the profile should have a corresponding downwards-directed vector, relating to the transfer of higher-momentum fluid from the upper to lower part of the profile.

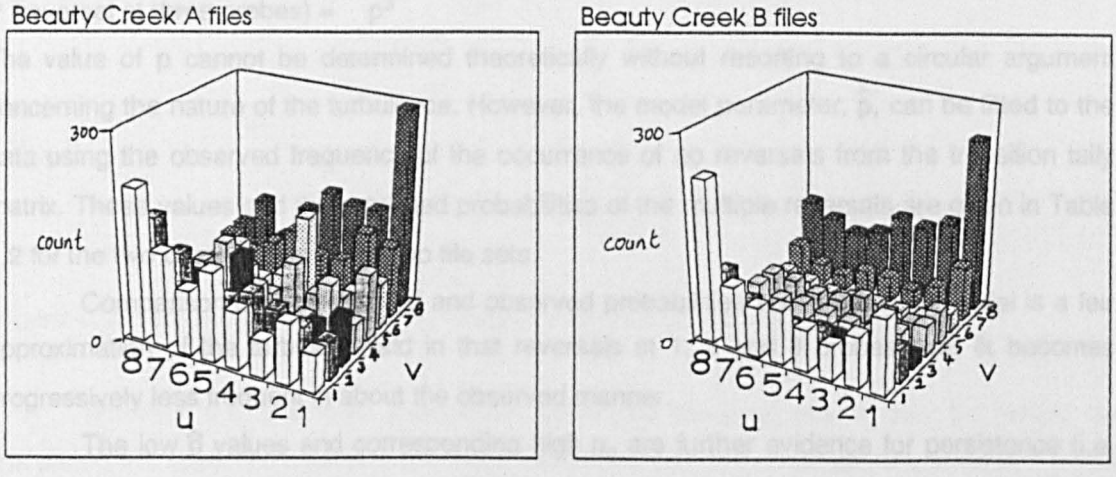

Figure 4.15 The correspondence of the profile states of the u and v components.

Figure 4.15 shows how profile states of the U component correspond to those of the V. A chi-square test on the contingency table from which the Figure was created reveals that the values are not randomly distributed at $p < 0.001$. This suggests that there is indeed some preferential correspondence between specific velocity and vector profile states.

If the Figure is interpreted with respect to the state definition diagram (Figure 4.13), it shows that although the expected correspondence pairs show high values, they are not necessarily the highest. There is maximum correspondence between the states which emerged as being quasi-stable in the previous section (1 and 8). In contrast, the less persistent states as identified in section 4.2.4 show low correspondence values. This reinforces the idea of the existence of quasi-stable "fast" or "slow" states, the change between which is rather confused.

4.2.6 Sequences of Change of the Profile States

At a profile where simultaneous measurements are taken, it is reasonable to assume that the local generation or passage of a coherent flow structure would be monitored as an organised sequence of fluctuations in the velocity profile. In order to differentiate such sequences from random ones, it is necessary to determine those which would be generated from structureless turbulence.

The previous sections showed that a degree of persistence exists in the profile states between sampling points. It can be inferred from this, at the sampling rate used, that between consecutive sampling points, change is least likely to take place at three probes, and most likely to take place at 1 or 0 probes depending on which files were being considered.

A simple binomial model can be used to describe these changes. Let us assume that velocity at each probe behaves independently of the others. Suppose the probability of the reversal over time δt of the sign of u' (or v') at each of the three probes is p, then

P (no reversal at any probe) = $(1-p)^3$

P (reversal at one probe) = $3p(1-p)^2$

P (reversal at two probes) = $3p^2(1-p)$

P (reversal at three probes) = p^3

The value of p cannot be determined theoretically without resorting to a circular argument concerning the nature of the turbulence. However, the model parameter, $\hat{p}$, can be fitted to the data using the observed frequency of the occurrence of no reversals from the transition tally matrix. These values and the predicted probabilities of the multiple reversals are given in Table 4.2 for the two components of the two file sets.

Comparison of the predicted and observed probabilities shows that the model is a fair approximation of the turbulent field in that reversals at 1, 2 and 3 probes over δt becomes progressively less frequent in about the observed manner.

The low $\hat{p}$ values and corresponding high p_0 are further evidence for persistence (i.e. no change) within the sequences of velocity profiles supporting the findings of section 4.2.4. These values are similar for each component of the A and B files (i.e. $\hat{p}(u_A) \approx \hat{p}(u_B)$, $\hat{p}(v_A) \approx \hat{p}(v_B)$), but these values are greater for the v than the u components. This is possibly due to the

greater change in momentum required to change a u profile than a v; a change in the v profile requires a redirection of flow whereas change in u requires acceleration or deceleration.

Table 4.2 The predicted probabilities of reversals at different numbers of probes. Observed probabilities in brackets.

Series	$\hat{p}$	p_0	p_1	p_2	p_3
u' (A)	0.140	0.637	0.310 (0.295)	0.050 (0.060)	0.003 (0.008)
u' (B)	0.125	0.671	0.287 (0.274)	0.041 (0.051)	0.002 (0.004)
v' (A)	0.266	0.395	0.430 (0.418)	0.156 (0.164)	0.019 (0.023)
v' (B)	0.267	0.394	0.430 (0.415)	0.157 (0.169)	0.019 (0.022)

The persistence analysis suggested that there are three levels of state quasi-stability defined by the number of crossings of the mean velocity profile. The binomial model would suggest that there is an equal level of quasi-stability regardless of state. This necessitates closer consideration of the probabilities for the individual states.

The binomial model defines that if a change does take place between states in the state series, it is most likely to occur with a sign change at a single probe. In this simple binomial model, the three transfers with single sign changes are equally likely. This would result in no tendency for preferential transfers or sequences of state changes to exist. This is depicted in the state change diagram of Figure 4.16.

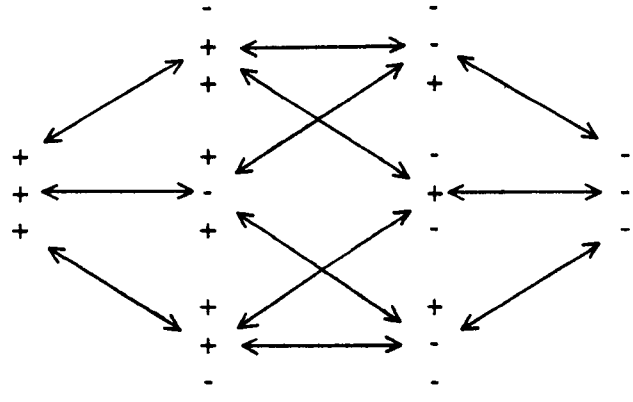

Figure 4.16 State changes involving a change in sign of u' (or v') at one probe only.

Whether the observed sequences follow the binomial model can be tested by comparing the observed counts of the three transitions from any given starting state with those expected if equiprobable by using a one sample chi-square test with 2 degrees of freedom. At the 5% significance level, of the transitions from the eight states, six of those from the u'(A)

files show a significant difference, all eight from the u'(B), six from the v'(A), and five from the v'(B). These results show a strong departure from the random model.

A clear pattern of preferred transitions also emerges from the bulked transition matrices of the uA, uB, vA and vB files as shown in Table 4.3.

Table 4.3 Preferred state transitions

Origin state:	Destination state:	Alternative states:	Files and components:			
1	2	3, 4	uA	uB		vB
2	1	5, 6	uA	uB	vA	vB
3	1	5, 7		uB	vA	vB
4	1	6, 7	uA	uB	vA	vB
5	8	2, 3	uA	uB	vA	vB
6	8	2, 4		uB	vA	vB
7	8	3, 4	uA	uB	vA	vB
8	7	5, 6	uA	uB	vA	vB

Table 4.3 suggests that there is a tendency for most of the states to head towards either states 1 or 8. Those that do not are states 1 and 8 as this would require a simultaneous sign change at three probes.

These results suggest that there are preferential transitions towards the high or low momentum states (1 and 8). It therefore seems reasonable to investigate further whether there is any tendency for preferential sequences of states to exist. Of particular interest are the sequences by which the profile changes from one end-member state to the other.

Two methods were adopted to generate sequences, both using the state transition probability matrices (TPM) of the U and V components of each file. The first uses a Markov chain approach; from each of the end-member states, a sequence of links is built up by progressing from each state to the next state of maximum transition probability (ignoring the no-change condition). A condition is stipulated whereby a direct return to the previous state is not allowed; such a return would result in a closed loop between two states, and would not generate a sequence. This is repeated until the other end member is reached. The second method of identifying preferred sequences calculates the product of the one-step probabilities of all possible link combinations between the end members i.e. the product of the transfer probabilities of all routes from state 1 to 8 (or 8 to 1) in the state change diagram (Figure 4.16). The route of maximum probability is taken as the preferential sequence.

The sequences from the Markov chain technique are shown in Figure 4.17, and from the maximum probability technique in Figure 4.18.

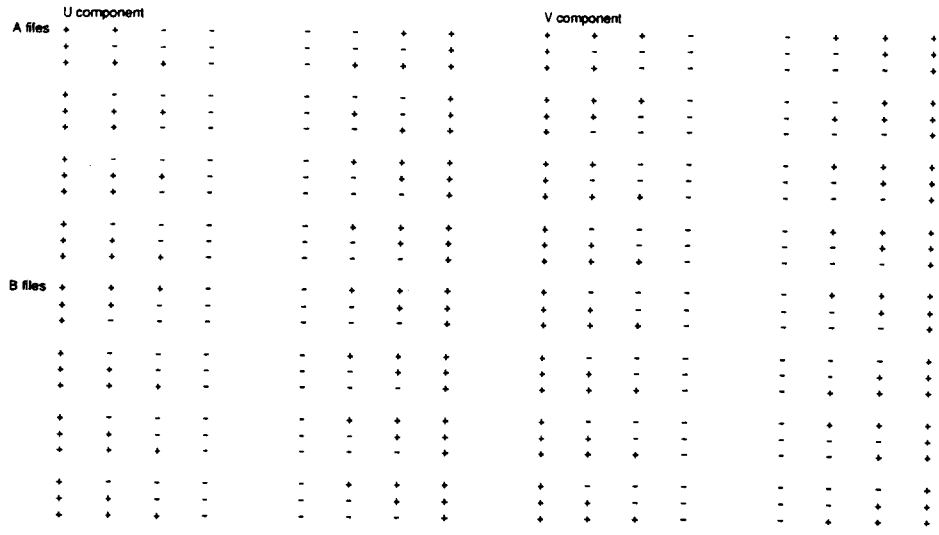

Figure 4.17 Sequences of states generated using the Markov chain method. Sequence direction is left to right.

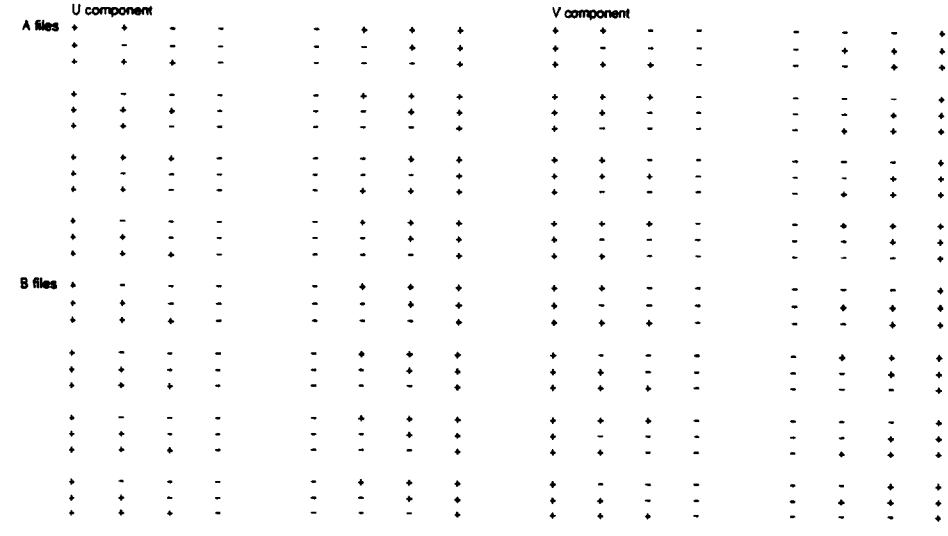

Figure 4.18 Sequences of states generated using the maximum probability method. Sequence direction is left to right.

4.2.7 Interpretation of Profile Sequences

The two methods for generating sequences produce generally similar results. The sequences are better defined for u than v and for the B-series than the A-series measurement heights. The two general points to note are that the preferred sequences tend to involve changes that migrate progressively up or down the profile, and that states involving multiple crossings of the mean profile are under-represented in comparison with those involving a single crossing. Tallies of the files which speed up or slow down without involving multiple crossing states are shown in Table 4.4.

Table 4.4 Preferred sequences between quasi-stable velocity profile states

Sequence and generation method:	u' series		v' series	
	Slow to fast	Fast to slow	Up to down	Down to up
Top down, (Markov chain)	A3, A4,A4 B1, B2, B3, B4	A4 B2, B3, B4	A1,A3 B1, B2, B3, B4	
Top down (Chain probabilities)	A1, A2, A4 B1, B2, B4	A4 B1, B2, B3, B4	B2, B4	A4 B2
Bottom up (Markov chain)		B1	A2	A4 B2, B4
Bottom up (Chain probabilities)			A2	A2, A3 B3
Other (Markov chain)	A1, A2	A1, A2, A3	A1, A3	A2 B1, B3
Other (Chain probabilities)	A3 B3	A1, A2, A3	A1, A3, A4 B1, B3	A1 B1, B4

The uB data reveal a clearly defined "slow" to "fast" sequence in both the u and v profiles. The changes develop from the top downwards, suggesting the incursion of fluid from higher in the profile. The acceleration at progressively lower points in the flow suggests that this is a sweep-like structure, though it should be recalled that the lowest probe in the B-series measurements was 14 cm above the bed.

The A files, in which measurements were made closer to the bed, do not produce such clear "slow" to "fast" sequences. The sequences often include profile states which cross the mean at least once. This suggests that although there is evidence of consistency in the acceleration of flow near to the bed with that higher in the flow, the relation is not clear. Like the lower persistences of the quasi-stable states in the A files compared to the B (section 4.2.4), this may be due to the bottom probe being in the near-bed flow zone, whereas the middle and top probes are in the outer zone.

Slowing down from the "fast" to "slow" states also appears to take place from the top down, but this is not quite as clear as the speeding up sequences. It occurs preferentially for the uB files and the vA of the Markov chain, and for the uB files of the maximum probability method. Clearly this is a consistent turbulent structure, but is the opposite of that which would be expected for a burst or ejection event. Such an event would involve the flow

decelerating at the bed first and the low-momentum fluid migrating upwards, yet this only occurs in a minority of the monitored cases.

If changes in the u profiles tend to occur progressively from the top downwards then it would be expected that changes in the v profiles would behave similarly. The results in Table 4.4 supports this in general, but there are some specific differences between the A and B files, and between the "up" to "down" and "down" to "up" sequences.

The clearest pattern is for the vB data in the up to down direction, where the 1-2-5-8 sequence emerges as preferred in all four replicate series by the one-step method and two of the four by the chain-probability method. This shows the flow turning downwards progressively from the top towards the bed, in a way which matches the sweep-like preferred slow to fast uB sequence discussed above. Like the uA data, measurements nearer the bed showed a less clearly defined fast to slow pattern so the vA data show no consistent preference for an up to down pattern.

In the down to up direction, two of the four vB series from the one-step method and two of the four uA series from the maximum probability method suggest that the vectors change from down to up progressively from the bed upwards. This disagrees with the results of the u component, and at first sight is evidence for the classic burst structure involving low momentum fluid moving upwards from the bed. However, in agreement with the u component, the vA data from the one-step method suggests a top-down down-to-up sequence. This suggests that although there is some evidence for conventional burst-like structures, the down-to-up sequences are by no means clear.

The sequences as represented so far relate to temporal changes at a static profile. Let us now consider the spatial arrangement of the flow structure which produces the profile changes at the static monitoring mast. The clearest structure to emerge from the above analysis is the incursion of fluid of high streamwise momentum from the top downwards, with an associated progressive declination of the velocity vector. Figure 4.19 shows how this could be represented as an inverted wedge of high momentum fluid being advected downstream. This structure is strikingly similar to the inverted wedges mentioned in the literature (e.g. Levi, 1987; Yalin, 1992, Figures 2.8 & 2.9), and which were seen in the visualisations described in section 4.1.4c. A broader interpretation of this structure in relation to both the visualisations and the structures mentioned in the literature is made in Chapter 6.

In summary, there appears to be a convincing structure represented by the incursion of high momentum fluid initially into the upper parts of the profile, but progressing towards the bed. The progressive bedwards declination of the velocity vectors confirms that this is due to the downwards direction of higher momentum fluid from the upper parts of the profile towards the bed. This is interpreted as the advection of a front of relatively fast fluid, the subsequent deceleration from which is not as organised. This is remarkably similar to the proposals made

in the literature of a succession of high momentum fronts propagating downstream, and there is some evidence from the visualisations to support this.

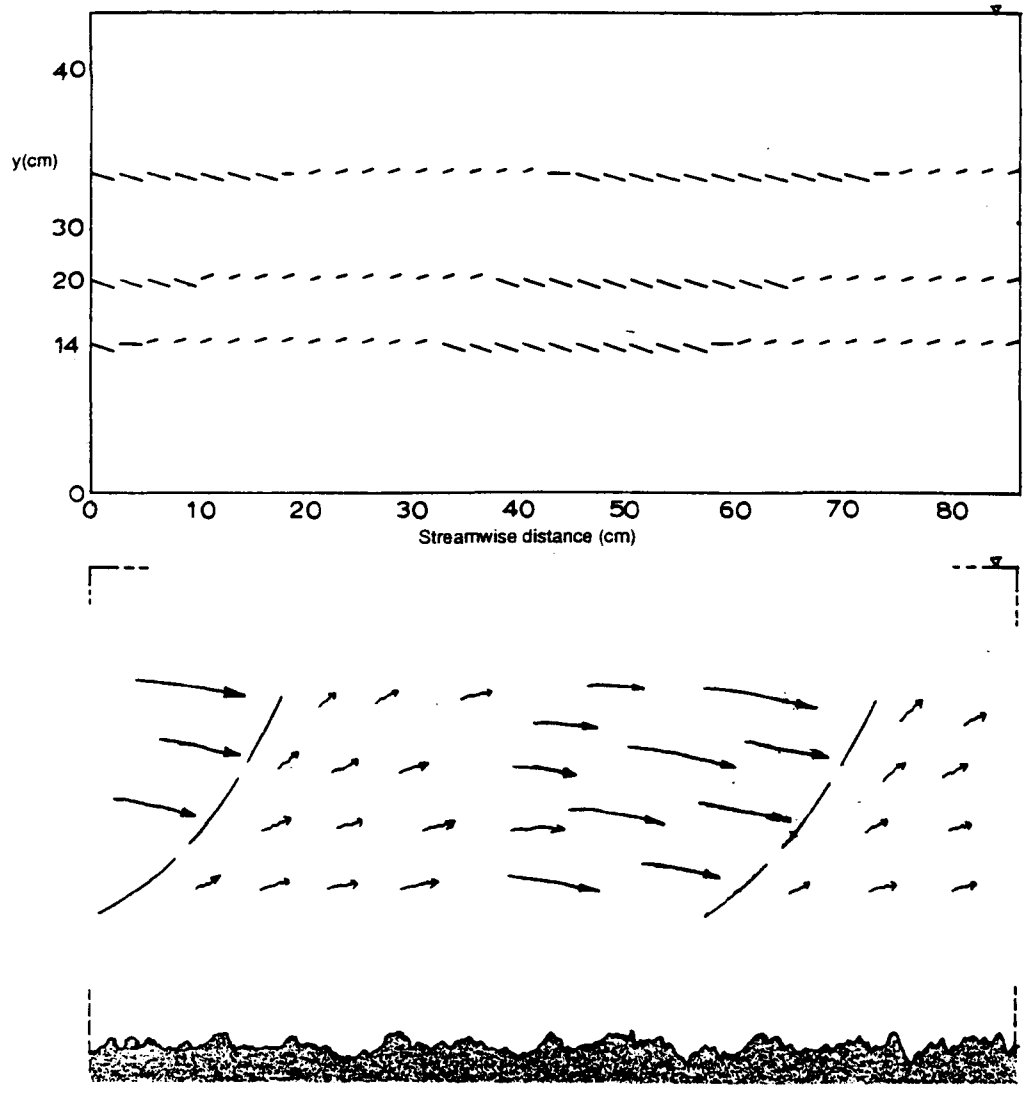

Figure 4.19 An interpretation of the spatial arrangement of the structures produced from analysis of the fluctuating velocity profile using the B file sequences. (a) Vectors are long if u' > <u>, inclined if v' > <v>, declined if v' > <v>. Reconstruction is made using mean state persistences, the streamwise spacing assumes that <U> = 0.6ms^{-1}. (b) An interpretation of (a) showing the high speed "fronts" and changes in vector magnitude and direction.

The poor resolution of the A files compared to the B suggest that these are outer zone structures, and that the near bed zone is dominated by a different turbulence regime. Evidence from the visualisations suggests that this is dominated by eddies of low momentum fluid being ejected from the near-bed zone.

4.3 Summary

Two fundamentally different approaches have been taken to investigate the spatio-temporal structure of the boundary layer over poorly sorted fluvial gravels, and provide mutual support for the structure of the boundary layer.

Basically, a combination of the two lines of evidence suggest that the near-bed region is dominated by ejecting vortices whereas further from the bed, advecting "wedges" of fluid dominate the flow field. The nature of the interaction of these is not clear, but a re-interpretation of the visualisations and a synthesis of the findings made here forms the basis for the model of turbulence structure made in Chapter 6.

Chapter 5 The quantification of turbulence structure

There is now a sufficient amount of evidence, from both the literature and the experiments described in the previous chapter, to state that flows over fluvial gravel beds *do* exhibit a degree of temporal and spatial structure. The previous chapter proposed a model to explain how the turbulence structure is generated in differing conditions of bed roughness and mean hydraulics. The purposes of this chapter are to:

1. Determine the statistical properties of the magnitude and intermittency of certain parameters associated with the velocity fluctuations.
2. Interpret these properties with respect to the velocity signatures that may be expected from coherent flow structures.
3. Identify and test the scaling parameters which influence the fluctuating velocity properties.

This chapter is split into two halves. Sections 5.1 and 5.2 are concerned with analysis of velocity, and Sections 5.3 to 5.8 relate to analysis of shear stress. Throughout these sections, the emphasis of the analyses will relate either directly or indirectly towards the problem of gravel entrainment. Chapter 6 synthesises the findings of Chapters 4 and 5 to outline a model of turbulent boundary layer structure over fluvial gravel beds so that in Chapter 7 it can be applied to the explanation of intermittent gravel movement.

Section A: Velocity

5.1 Introduction to velocity

This section focuses on the spatial and temporal variations in velocity over rough gravel beds. Its three objectives are:

1. To examine the shape of the time-averaged velocity profile, particularly in the near-bed region.
2. To characterise the distributions of the fluctuating velocity components with regard to position in the profile, mean hydraulic conditions, and boundary roughness conditions.
3. To determine the temporal structure of the fluctuating velocities, and attempt to relate this to mean hydraulic and boundary roughness conditions.

5.1.1 Vertical gradient of mean streamwise velocity.

Section 2.2 outlined the principles of the law of the wall. It states that for boundary layer flows, the time-averaged streamwise velocity will increase linearly with the logarithm of distance from the boundary, and this can be expressed by Equation 2.7.

An assessment was made of the goodness of fit of all of the monitored profiles to the logarithmic form by calculating the r^2 of the regression of u on ln(y). In the cases of profiles taken with the ECM or LDA, u was taken as the arithmetic mean of the series of u. A BASIC

routine was written and adopted which optimised the r^2 by adjusting the zero plane displacement (Ashworth, 1987; Ferguson & Ashworth, 1992).

Two conditions were stipulated in the acceptance of the profiles as logarithmic: firstly, the necessary adjustment of y had to be less than the D_{50} value of the bed material. Beyond this arbitrarily chosen range, the justification of the error due to displacement of the wading rod baseplate by the bed obstacles becomes difficult to support. Secondly, a arbitrary minimum value of the optimised r^2 of 0.95 was adopted (Ashworth, 1987; Wilkinson, 1984).

The majority of the velocity profiles were accepted within the above limits. Those which were not accepted immediately were inspected for two characteristics. Firstly, some contained 'rogue' points within them, which when excluded resulted in the acceptance of the residual profile. The rogue points were usually the result of short sampling times (usually 30s) using a propeller current meter, or were those taken in highly turbulent conditions in the field with the ECM, where cable rattle was found to pollute the monitoring (section 3.3.2e). This was used as a further procedure to eliminate unreliable data files.

Secondly, some profiles were taken using the LDA at least partly in the 'inner zone' defined as below the crests of the largest obstacles (Section 4.1.2). As profiles are rarely, if ever, taken so close to the bed in the field, this problem is considered to be restricted to the flume experiments with rough beds.

The failure of the logarithmic profile near to the bed prompted a series of flume experiments specifically to inspect the u-velocity profiles in the inner zone. Using the mixed gravel bed described in section 4.1.1, five LDA velocity profiles were taken in a streamwise line over a coarse obstacle clast which occupied 25-50% of the depth. In relation to the space series resulting from the profile of the bed material, its height represented the 85th percentile. The streamwise section is shown in Figure 5.1. The five profiles were repeated at three discharge settings.

The purpose of making measurements over a single large clast is that it represents an important element of the assemblage which constitutes a roughness surface. It therefore provides a controlled way of illustrating the reasons behind the deviation from the logarithmic profile shape.

Figure 5.1 shows the shapes of the measured profiles. Upstream of the crest, all of the profiles are approximately logarithmic in form down to 1mm from the wall, the closest that the LDA could be focused.

At the crest and to its lee, where the pressure gradient becomes adverse (Massey, 1979), the profile picks out the separation zone which was observed in the visualisation experiments (Section 4.1.2). Above the separation layer, the profiles *do* fit the logarithmic law, but the associated r^2 values are lower than those upstream of the crest, though still greater than 0.95. The profile through the separation layer itself is rather confused, but this is to be expected due to its oscillation as described in section 4.1.2. It is better, therefore, to describe the separation layer as a zone rather than a layer. Below the zone of the oscillating separation

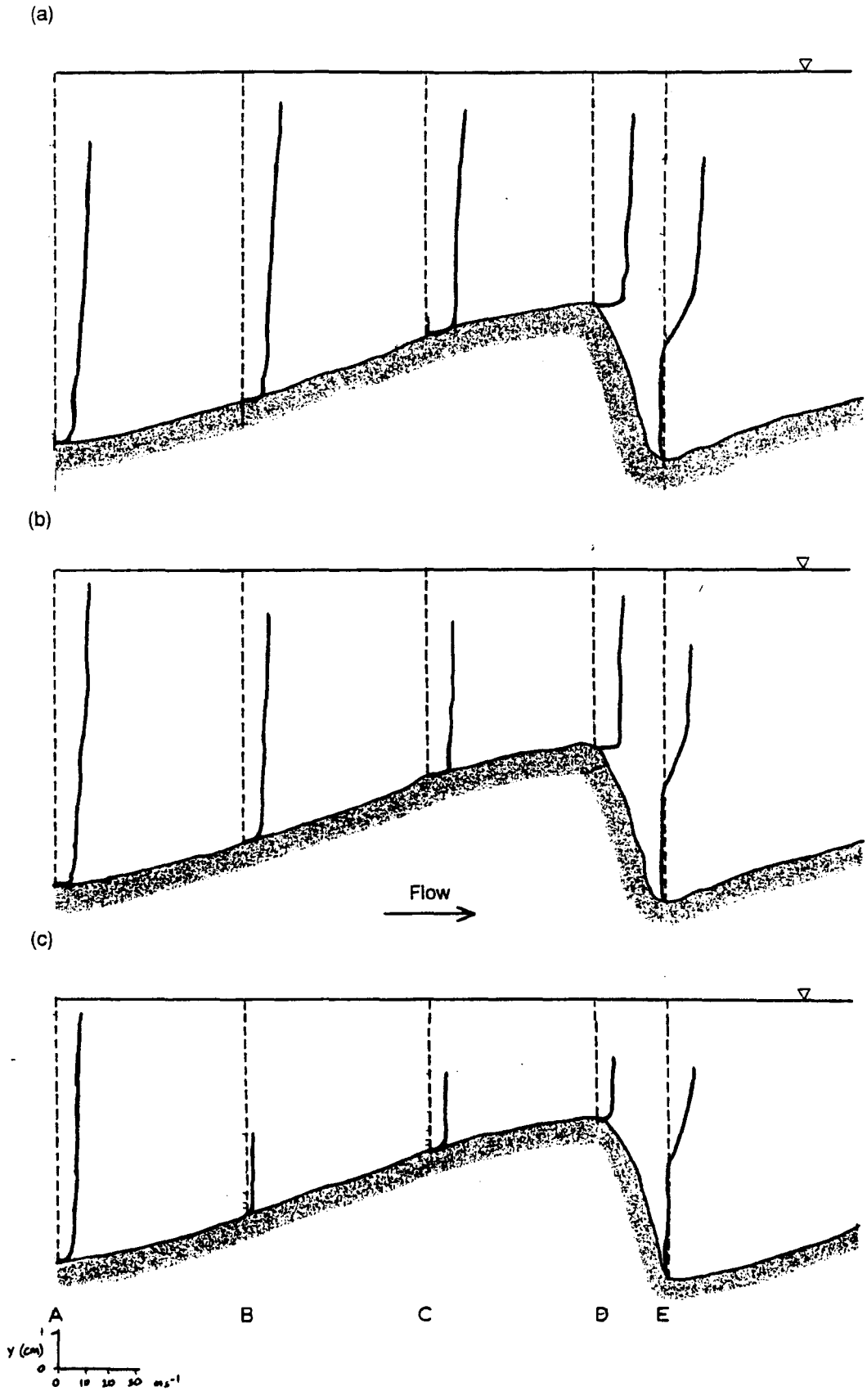

Figure 5.1 Velocity profiles at three discharge settings over a single obstacle of the bed shown in Figure 4.1 and featuring in Figure 4.8.

layer the vortex-induced reverse flows observed in the visualisations are shown by the slightly negative time-average velocities.

The important point that emerges from these measurements is that there can be considerable local variation in the shape of the velocity profile over mixed gravel beds. This has significant implications not only for the calculation of shear stress, but also in the interpretation of what the shear stress derived from velocity profiles actually represents. These points are discussed again in relation to shear stress in section 5.3.

Two main points emerge from considering the shape of the streamwise velocity profile. Firstly, most velocity profiles which are not in the 'inner zone' are close to logarithmic regardless of the boundary roughness condition. Secondly, within the 'inner zone' of a rough bed, mean velocity values are close to zero resulting in a meaningless velocity profile. Section 4.1.2 showed that velocity *fluctuations* dominate the fluid motion in the inner zone, and this is addressed in the following sections.

5.1.2 Frequency distributions of velocity fluctuations.

Turbulence in the flow results in fluctuations in both the magnitude and direction of the velocity vector. In a time-average sense, the characteristics of velocity at a point can be described by mutually perpendicular frequency distributions of u', v' and w' (Figure 5.2). The points to be addressed in this section concern the shapes of the distributions, and whether they change over space.

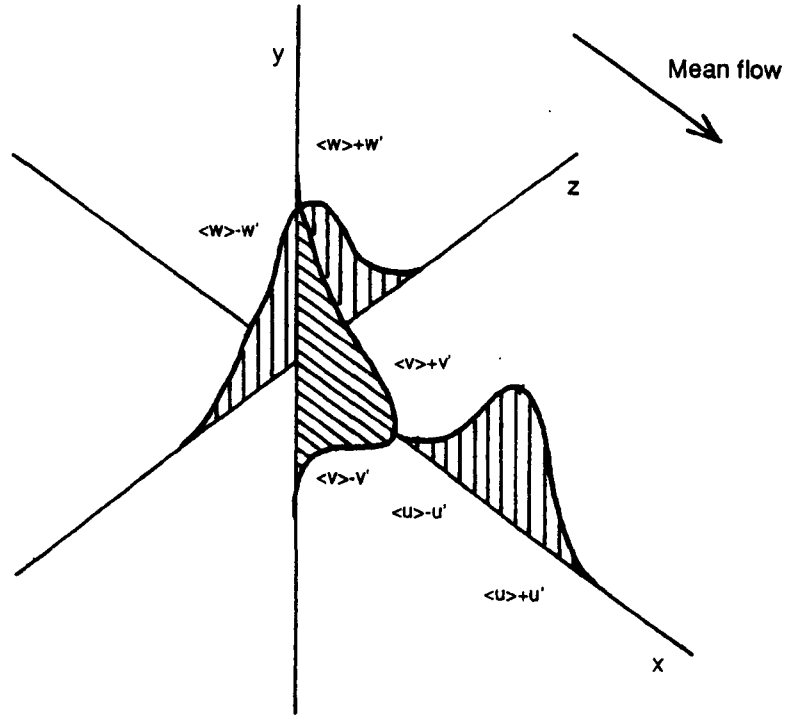

Figure 5.2 Mutually perpendicular frequency distributions of u', v' and w'.

The definition of homogeneous turbulent flow is that the fluctuating velocity components, u', v' and w' are normally distributed, and $\sigma_u \approx \sigma_v \approx \sigma_w$ (Schlichting, 1979). Naden

(1987) explicitly states that it is an unproven axiom that over rough beds u' *is* normally distributed. Two implications would arise from the non-normality of the distributions. Firstly, closer consideration would have to be given to which measure of central tendency is actually being represented by propeller current meters, and whether this relates to a mean calculated from a velocity time series. Secondly, skewing of the distributions would require investigation into the reasons for inhomogeneity.

Figure 5.3 shows several different frequency distributions of u' and v'. They are derived from various points in the flow, at a wide range of hydraulic and roughness conditions. Their purpose is to illustrate their basic symmetry. None of those shown nor any other set of points shows any systematic pattern of skewing.

In order to investigate the changes in the nature of the fluctuations away from the wall, it is more usual and useful to consider the range of the fluctuations relative to the means rather than in isolation. Such a parameter is termed **turbulence intensity**.

5.1.3 Magnitude of fluctuation of u: turbulence intensity, Ti

Turbulence intensity, Ti, is a measure of the temporal variability of velocity at a point. It is defined as the coefficient of variation of the temporally fluctuating velocity component. For the u component, this is given by:

$$Ti_{<u>} = \sqrt{[(\Sigma(u-<u>)^2)/n]} / <u> \qquad (5.1)$$

Being one-dimensional, for any point in the flow there are three values of Ti relating to the three co-ordinates, $Ti_{<u>}$, $Ti_{<v>}$ and $Ti_{<w>}$. The parameter is dimensionless, and hence comparison between points irrespective of the mean is possible. It is also time-averaged and hence does not provide any information regarding the temporal structure of the fluctuations. Firstly, the general pattern of $Ti_{<u>}$ in the boundary layer will be considered, then the effects of hydraulic and roughness parameters on its wall-normal profile will be addressed.

Within a boundary layer, $Ti_{<u>}$ decreases away from the wall suggesting that σ_u varies less than <u>. This can be interpreted by imagining observing a passive tracer at various points in the flow. Near to the bed, its motion would be more chaotic due to it being defined more by the fluctuations rather than by the mean advection velocity. As y increases, the mean velocity component would increase in its domination over the fluctuations, and the tracer's path would become more uni-directional. This effect can be seen in the visualisation images of Figures 4.8 and 4.9.

Before considering turbulence intensity over rough beds, let us firstly attempt to explain its relation to depth over a smooth boundary. Assuming that streamwise velocity obeys the log law

$$<u> = a + b.\ln(y)$$

and let us assume that

$$\sigma_u = c + d<u>$$

then

$$\sigma_u = c + d(a + b.\ln(y))$$

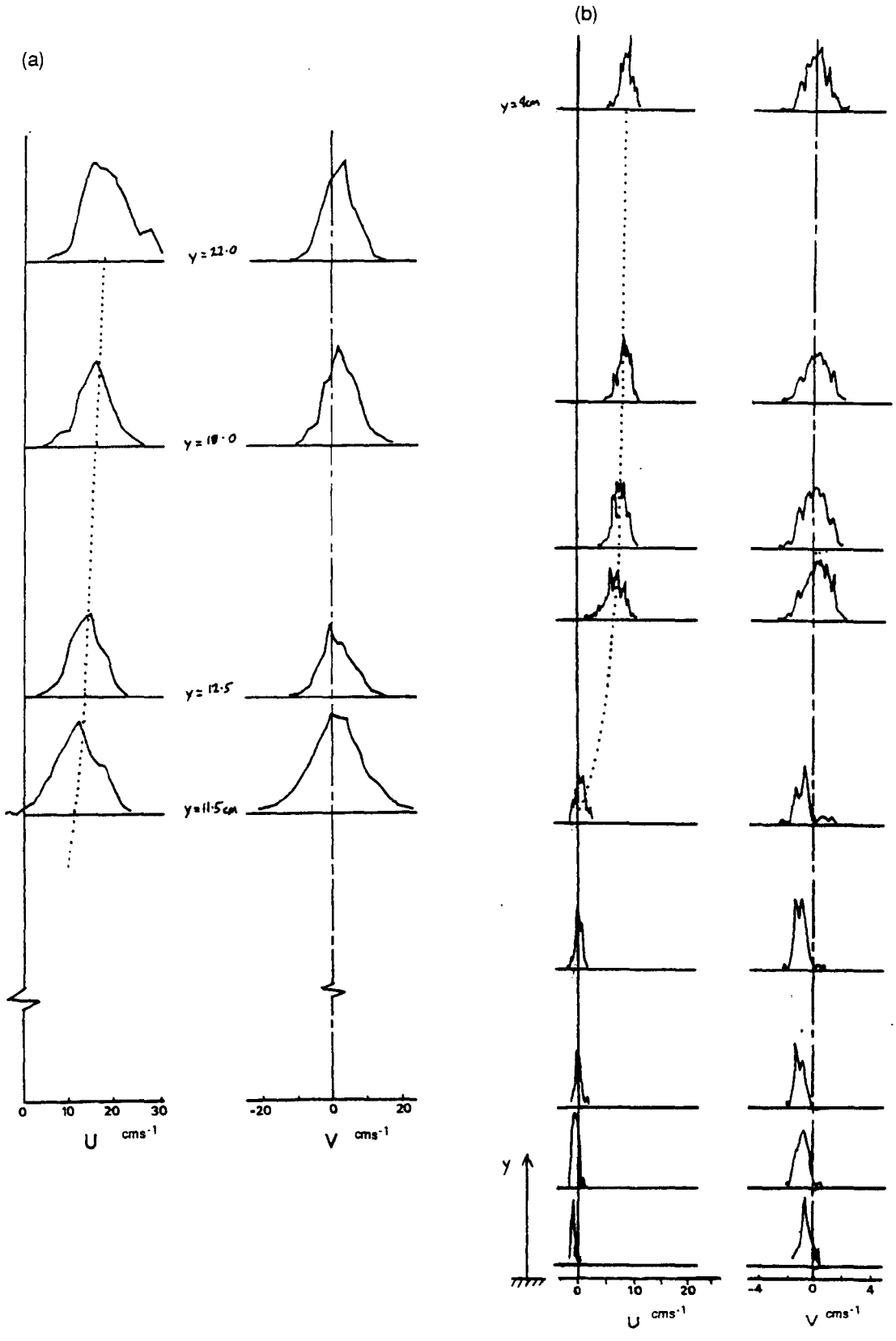

Figure 5.3 Frequency distributions of u' and v' for (a) one of the Aroila profiles and (b) Flume profile E at high flow (see Figure 5.1).

for which σ_u is linear with ln(y).

But

$$Ti_{<u>} = \sigma_u/<u> = (c + d(a + b.\ln(y))/(a + b.\ln(y))$$

which can be rearranged as

$$Ti_{<u>} = d + c/(a + b.\ln(y)) \qquad (5.2)$$

The function $Ti_{<u>}$ plotted against ln(y) is shown in Figure 5.4a.

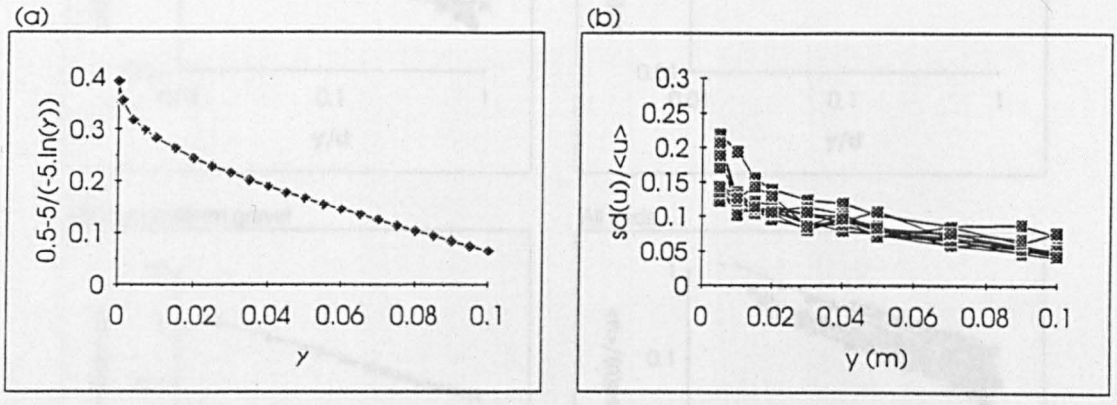

Figure 5.4 $Ti_{<u>}$ against ln(y) (a) given by Equation 5.2, (b) for smooth bed flume data.

Figure 5.4b shows how $Ti_{<u>}$ is distributed against ln(y) for smooth bed flume data representing a range of τ_0 from 0.008 to 0.04 Nm^{-2}. It is broadly similar to the theoretical plot of 5.4a and supports the rationale for the explanation of how $Ti_{<u>}$ varies with ln(y).

Let us consider the effects of roughening the wall of a boundary layer flow of constant discharge and bed slope. Firstly, an increase in flow drag over the rough wall due to a higher friction coefficient would increase the shear in the near-wall boundary layer. This would have the consequent effect of increasing the mixing and hence $Ti_{<u>}$ in the lower regions of the boundary layer. Secondly, eddies generated due to flow separation in the wake of discrete obstacles would add to those generated by shear-induced mixing alone. This would further increase $Ti_{<u>}$ close to the wall.

Using the data of McQuivey (1973), Naden (1987) shows that for flows over a hydraulically rough wall composed of uniformly sized lead shot, there is negative linear relation between the logarithms of $Ti_{<u>}$ and distance from the wall. Figures 5.5 a-c use McQuivey's data to show similar relations for profiles taken over beds composed of uniform 4.4mm lead shot, and uniform gravel of 19.1mm and 38.1mm diameters. The linearity of the relation of the logarithms of $Ti_{<u>}$ and y/d suggests that the influence of roughness on turbulence is distributed throughout the boundary layer.

Unlike the $Ti_{<u>}$ profiles taken over the smooth beds, those over rough beds do not collapse to co-linearity simply by non-dimensionalising σ_u by <u> and y by d (Figure 5.5d). This suggests that the roughness itself is influencing the whole profile of $Ti_{<u>}$. Naden (1987) incorporates roughness into the plots by dividing y by the diameter of the lead shot which constitutes the roughness instead of depth. This successfully collapses the profiles where the roughness is composed solely of uniform sized 'sediment'. It also raises the question of what

should be taken as an equivalent roughness parameter for not only mixed sized sediment, but the surface of a structured mixed gravel bed.

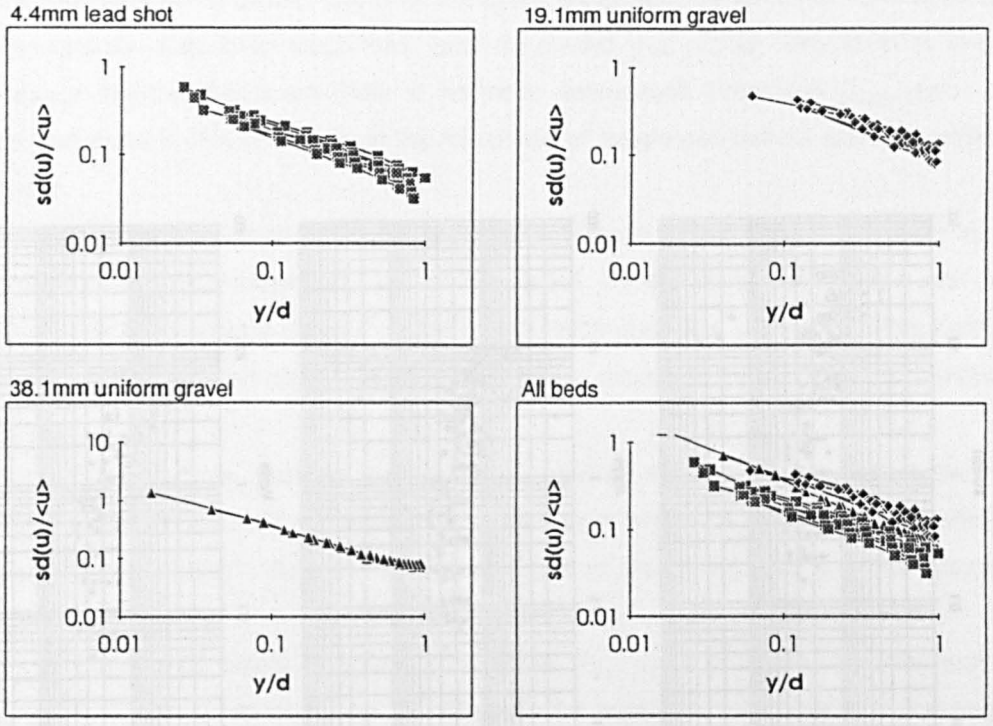

Figure 5.5 $Ti_{<u>}$ against y/d for flow over (a) uniform 4.4mm lead shot, (b) uniform 19.1mm gravel and (c) uniform 38.1mm gravel. (d) All data plotted together.

Chapter 3 (section B) discussed various methods of quantifying the roughness of a gravel bed. From these discussions, five roughness parameters will be tested here: D_{50}, D_{84}, k_{50}, k_{84}, σ_k. Figures 5.6 a-e show plots of $Ti_{<u>}$ against the various roughness parameters for the Arolla, Dubhaig, Beauty Creek and rough bed flume data. Note that not all of the Arolla data contain D_{50} and D_{84} values.

The different plots share a common general trend; unlike the simple log-linearity of the $Ti_{<u>}$-y/d plots, those non-dimensionalised by roughness parameters can be considered to be two intersecting lines. In the upper parts of the profile (higher values of y/roughness), there is a similar linear decrease in $Ti_{<u>}$ against y/roughness to those plots over smooth or uniformly rough beds. In the lower parts of the profile, however, the rate of increase in $Ti_{<u>}$ towards the bed reduces to zero. This occurs at $y/D_{50} \approx 1$.

This is a significant finding as if a link is to be made between turbulent fluctuations and the mode of entrainment, this break down in linearity in the near-bed region would become important.

The data points with $y/D_{50} < 1$ are all from the logarithmic parts of the profiles taken in the rough bed flume experiments; they are not the parts of the profiles which extend into the inner zone (c.f. Figure 5.1). The interpretation of this with regard to boundary layer structure will be made in Chapter 6.

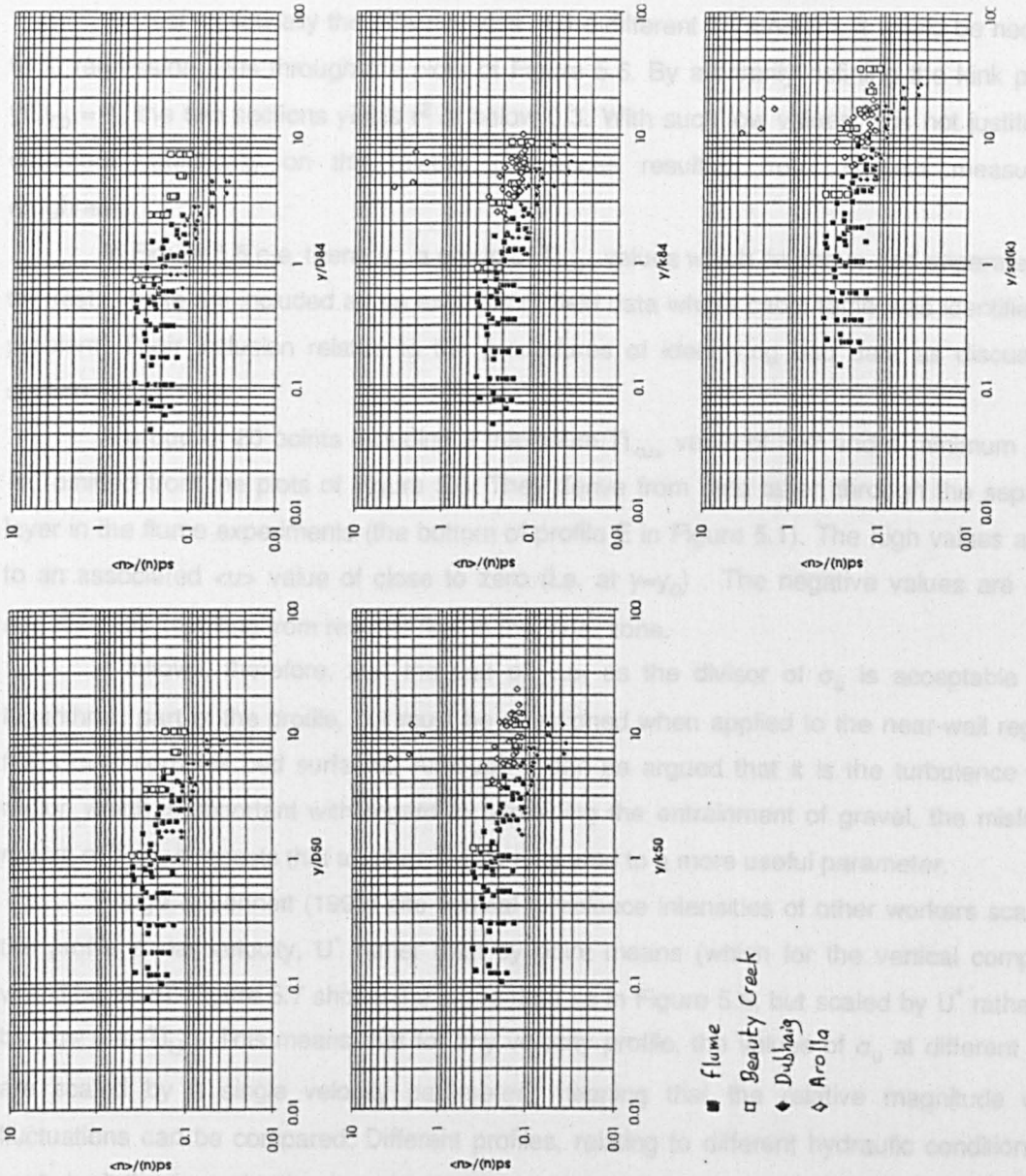

Figure 5.6 $Ti_{<u>}$ plots for Kirkbride's field and flume data against (a) y/D_{50}, (b) y/D_{84}, (c) y/k_{50}, (d) y/k_{84}, (e) y/σ_k. Note: the outlier points relate to rejected data as discussed in Section 3.3.

The two zone structure of the boundary layer revealed in Figure 5.6 a-e raises the important question of whether there is a preferable roughness parameter for collapsing the data in the lower parts of the profile. Sections 3.4 to 3.6 discussed the merits of various parameters in quantitatively describing roughness, and concluded that those derived from in-situ bed morphology measurements are likely to be more appropriate. From the $Ti_{<u>}$ plots, it would appear that there is little difference in the measures of roughness in their ability to collapse the $Ti_{<u>}$ data.

To test statistically the effectiveness of the different parameters, it would be necessary to fit regression lines through the plots of Figure 5.6. By arbitrarily defining the kink point as $y/D_{50} = 1$, the two sections yields r^2 of below 0.3. With such low values, it is not justifiable to comment statistically on the relative differences resulting from different measures of roughness.

In Figure 5.6 c-e, there is a group of $Ti_{<u>}$ values which lie above and separately from the rest. These are included as an example of field data where cable rattle was identified as a problem. Their inclusion relates to the procedures of identifying bad data as discussed in section 3.3.2e.

A group of 20 points including a maximum $Ti_{<u>}$ value of 352 and a minimum of -4.5 is omitted from the plots of Figure 5.6. They derive from data taken through the separation layer in the flume experiments (the bottom of profile E in Figure 5.1). The high values are due to an associated <u> value of close to zero (i.e. at $y \approx y_0$) . The negative values are due to negative <u> resulting from reverse flow in the inner zone.

It follows, therefore, that the use of <u> as the divisor of σ_u is acceptable in the logarithmic part of the profile, but must be questioned when applied to the near-wall region of flows over complex bed surfaces. Although it can be argued that it is the turbulence in this region which is important with regard to explaining the entrainment of gravel, the misleading nature of $Ti_{<u>}$ suggests that another divisor may lead to a more useful parameter.

Bridge & Bennett (1992) cite vertical turbulence intensities of other workers scaled by the profile shear velocity, U^* rather than by point means (which for the vertical component would be zero). Figure 5.7 shows the same data as in Figure 5.6, but scaled by U^* rather than by <u> (i.e. Ti_{U^*}). This means that for any velocity profile, the values of σ_u at different points are scaled by a single velocity parameter, meaning that the relative magnitude of the fluctuations can be compared. Different profiles, relating to different hydraulic conditions, are scaled relative to each other by a parameter relating to the mean hydraulics.

It is quite evident that the use of U^* as the divisor fails completely in collapsing the data of $\sigma(u)$. This is interpreted as meaning that the fluctuations monitored at a point in the profile scale with a mean velocity parameter derived from a similar spatial scale rather than the larger scale of the whole profile. Bed shear stress, as derived from the velocity profile, is too crude a measure of mean hydraulic condition in comparison to the point measure of $\sigma(u)$.

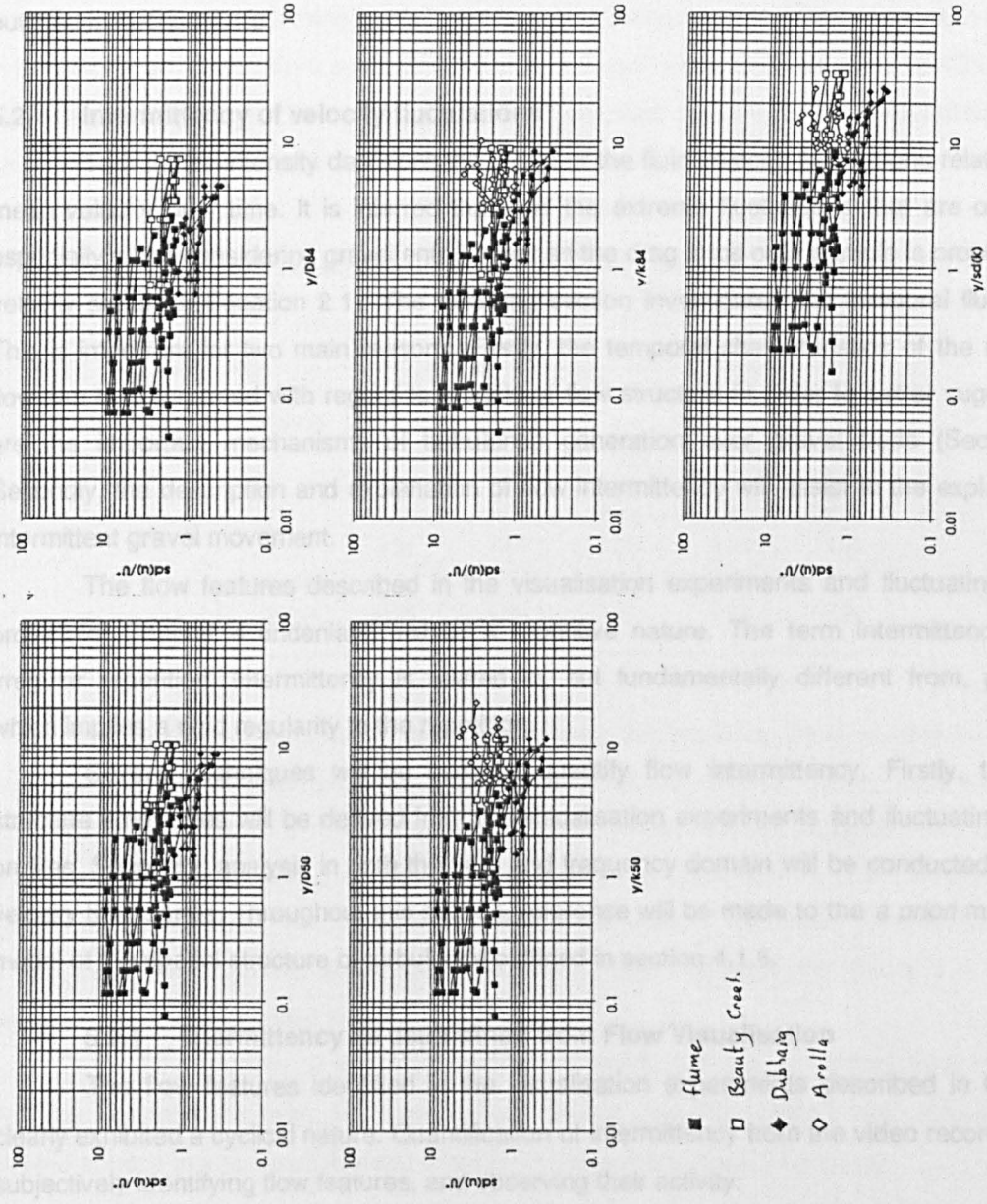

Figure 5.7 Ti_U plots for Kirkbride's field and flume data against (a) y/D_{50}, (b) y/D_{84}, (c) y/k_{50}, (d) y/k_{84}, (e) y/σ_k. Note: the outlier points relate to rejected data as discussed in Section 3.3.

In summary, it has been shown that over water worked mixed gravel beds, the profiles of turbulence intensity are broadly similar to those monitored over smooth beds. The data collapse to a degree when scaled by any roughness parameter, yet the choice of parameter seems to be unimportant in terms of how well the data collapse.

The main finding of this section is that close to the boundary (up to $y \approx D_{50}$), the rate of increase in turbulence intensity decreases to zero. This is interpreted as further evidence for the existence of a boundary layer structure comprising parallel zones above the bed, as outlined in section 4.1.6.

5.2 Intermittency of velocity fluctuations

Turbulence intensity describes the range of the fluid velocity fluctuations relative to the mean velocity over time. It is inferred that it is the extreme fluctuations that are of interest, especially when considering gravel entrainment as the drag force on a particle is proportional to velocity squared (Equation 2.1). The following section investigates the temporal fluctuations. This is important for two main reasons. Firstly, the temporal characteristics of the monitored flow can be interpreted with regard to models of flow structure in order to better suggest what are the important mechanisms of turbulence generation over gravel beds (Section 2.6). Secondly, the description and explanation of flow intermittency will assist in the explanation of intermittent gravel movement.

The flow features described in the visualisation experiments and fluctuating velocity profiles of Chapter 4 undeniably exhibit a repetitive nature. The term intermittency implies irregular repetition. Intermittency is related to, but fundamentally different from, periodicity which implies a rigid regularity to the repetition.

Several techniques will be used to quantify flow intermittency. Firstly, turbulence structure timescales will be derived from the visualisation experiments and fluctuating velocity profiles. Secondly, analysis in both the time and frequency domain will be conducted upon the velocity time series. Throughout this section, reference will be made to the *a priori* mechanistic model of the spatial structure of turbulence outlined in section 4.1.6.

5.2.1 Intermittency as determined from Flow Visualisation

The flow features identified in the visualisation experiments described in Chapter 4 clearly exhibited a cyclical nature. Quantification of intermittency from the video record involved subjectively identifying flow features, and observing their activity.

The procedure for deriving intermittency characteristics involved watching the slowed-down video, identifying an event, and logging the time at which it occurred. A programme was written in BASIC to log the time interval between flow events by the user hitting a key whenever an event occurred.

A problem soon emerged involving identifying events. Eddy shedding from obstacles was by far the clearest intermittent event observed. However, defining the moment of shedding and separating one event from another was virtually impossible. In an attempt to solve this

problem by reducing subjectivity of the observer, the majority of the screen was masked, leaving a window covering 2cm x 2cm positioned over the section of the screen through which most eddies passed. The intention was to log the intermittency of the change in direction of the streamlines rather than of the actual subjectively determined shedding event.

Mean intervals for four replicate loggings downstream of one of the obstacles for five flow settings are given in Table 5.1. It suggests that an increase in flow speed does not affect the eddy shedding period. This is at odds with both the findings of other workers (e.g. Kawanisi *et al*) and with simply watching the video, where the interval between shedding decreased with increasing flow speed. More importantly, it shows that there is an error of up to 40% between replicate loggings of the same sequence. This suggests that the errors associated with the sampling technique are much larger than the differences expected between the different conditions.

Table 5.1 Means of subjectively logged intervals of eddy shedding from an obstacle (seconds; shear stress in Nm^{-2})

τ_0:	3.12	6.38	8.74	9.47	10.34
Replicate:					
1	1.17	0.92	1.05	0.75	0.83
2	0.64	1.11	0.99	0.86	1.32
3	1.13	1.00	1.43	1.38	0.96
4	0.97	0.56	1.21	0.98	1.05
Replicate mean:	0.98	0.90	1.17	0.99	1.04

Although there is a large variation between the replicate loggings, the mean of the replicates suggests a shedding timescale of the order of one second. The intervals were logged from watching the video at 1/4 real speed. A further set of replicate loggings were carried out watching the video at normal speed and slowed down to 1/4, 1/8, 1/16 and 1/24 times normal speed. At each speed, two replicate loggings were made. The mean periods emerged as 1.13s, 0.91s, 0.73s, 0.51s and 0.58s respectively. This suggests that there is a significant subjective error due to video speed.

The two sources of important subjective errors and the amount of time involved in deriving intermittency from the visualisations meant that the method was abandoned and therefore there are no intermittency values from the visualisations.

5.2.2 Intermittency of the Fluctuating Velocity Profile

Chapter 4 contains several sections relating to the analysis of the fluctuating velocity profile as taken in Beauty Creek, Canada. Section 4.2.6 involves deriving most-likely sequences of velocity profile states, but does not consider the likely timescale of such sequences; section 4.2.4 however, considers the duration of the individual profile states.

There is a problem in linking the persistences of specific profile states together in order to derive timescales of intermittency. The concept of coherent structures being superimposed onto a random flow field suggests that there would be two populations of characteristic persistences relating to the random element and the coherent structures.

If we consider that the basic structure being revealed from the fluctuating profiles is that of advecting inverted wedges of high and low momentum fluid, then the two most common constituent half-cycles can be given as 1-2-5-8 and 8-7-4-1 representing the dominant decelerating and accelerating sequences. The full cycle can be given as 1-2-5-8-7-4-1.

Accepting the above proviso concerning the superposition of coherence onto randomness, the timescale of the cycle can be estimated by the sum of the persistences of the elements within the sequence. Mean values for the different components of the different files emerge as uA = 1.76s, uB = 1.85s, vA = 1.02s, vB = 1.01s. As is expected from the persistence histograms (Figure 4.14), the sequence persistence for the u component emerges as longer than those of the v. These are compared to the intermittency timescales from other sources, and are interpreted with respect to calculated bursting periods in Section 6.2.

5.2.3 Intermittency in the Velocity Time Series

Figure 5.8 shows time series of the u and v velocity components for the Beauty Creek AKB2-1 file. It suggests that the fluctuation frequency of the u component is less than for the v, which agrees with the persistence findings of the fluctuating velocity profile analysis. This section aims to quantitatively describe the temporal structure of these sequences.

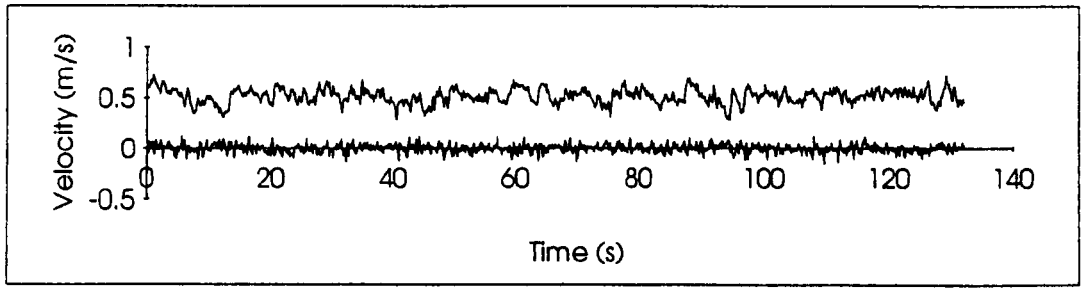

Figure 5.8 u and v velocity time series of one of the Beauty Creek files.

The occurrence of events over time can be analysed in either the time or the frequency domain. In the time domain, the description of the occurrence of 'events' is made with respect to a time origin. Processes can be modelled in the time domain by predicting the value of the process at a time point, t_0, from series and/or error values at one or more preceding time points, t_{-1}, t_{-2} etc.

Analysis in the frequency domain, adopts a fundamentally different approach. Spectral analysis decomposes a series into a superposition of different periodic components. The contribution of these components to the variance of the original series can be derived in order to suggest which frequencies are important in the explanation of the total series variance.

There are two main objectives of these time series analyses. The first is to derive timescales of cyclicity within the velocity signals so that they can be compared to bursting or shedding periods outlined in Chapter 2. The second is to attempt to fit ARMA models to the time series in order to suggest the temporal characteristics of the velocities.

(a) Analysis in the frequency domain: spectral analysis

Spectral analysis deconstructs a fluctuating process into a representation by a combination of sine and cosine waves. The mathematical routine involved in doing this is beyond the scope of this thesis. The spectrum can be considered to be a histogram of the contribution to the total series variance of different wavelengths. A wavelength that is more important is said to have more 'power' in the spectrum. The spectra plotted in this section are power spectra, where the area beneath the spectrum equals the variance.

The shortest wavelength, known as the Nyquist frequency, which can be resolved from a series of data points sampled at an interval of δt is $2\delta t$ (Chatfield, 1975). The longest wavelength that can be fitted to a time series of length T is T/2. When sampling, it is necessary to monitor the series for a time sufficient to accommodate any periodicities which are of importance. The incorporation of part of a low frequency is interpreted in the frequency domain as a trend in the data.

There are several types of spectral analysis. Throughout this work, the SPSS-PC package was used to perform a fast Fourier transform (FFT). This converted the time series, f(t), to a Fourier series of spectral densities S(f) relating to frequencies. The transformation used the Hamming window to smooth the Fourier series.

There are two purposes of deriving the spectra. The first is to determine whether any periods emerge as significant, the inference being that they could be interpreted as turbulent structure. Secondly, if peaks *do* emerge, it is of interest to determine how the associated periods vary with depth, mean hydraulics or roughness. Some general observations on the spectra will be outlined, and then more specific analysis will be carried out.

Completely homogeneous turbulence is defined by $u' \approx N(0,\sigma^2)$, and its spectrum would be represented by a flat line with no significant peaks, at least in the higher period end of the spectrum which is of interest regarding coherent structures. Comparison of spectra of various autoregressive and moving average models is made in section 5.2.3c. The extent of departure from flat and the presence of peaks within a spectrum point towards non-random turbulent flow.

(i) Power spectra

Figures 5.9, 5.10 and 5.11 show spectra for the Dubhaig, Beauty Creek and Arolla field data arranged to represent the positions to which they relate in the profile. Four general points can be made concerning the spectra.

Firstly, power tends to increase with period (c.f. the horizontal line of the white noise spectrum). This consistent trends shows that the turbulence is not homogeneous and lends support to the existence of large scale structure within the turbulent field.

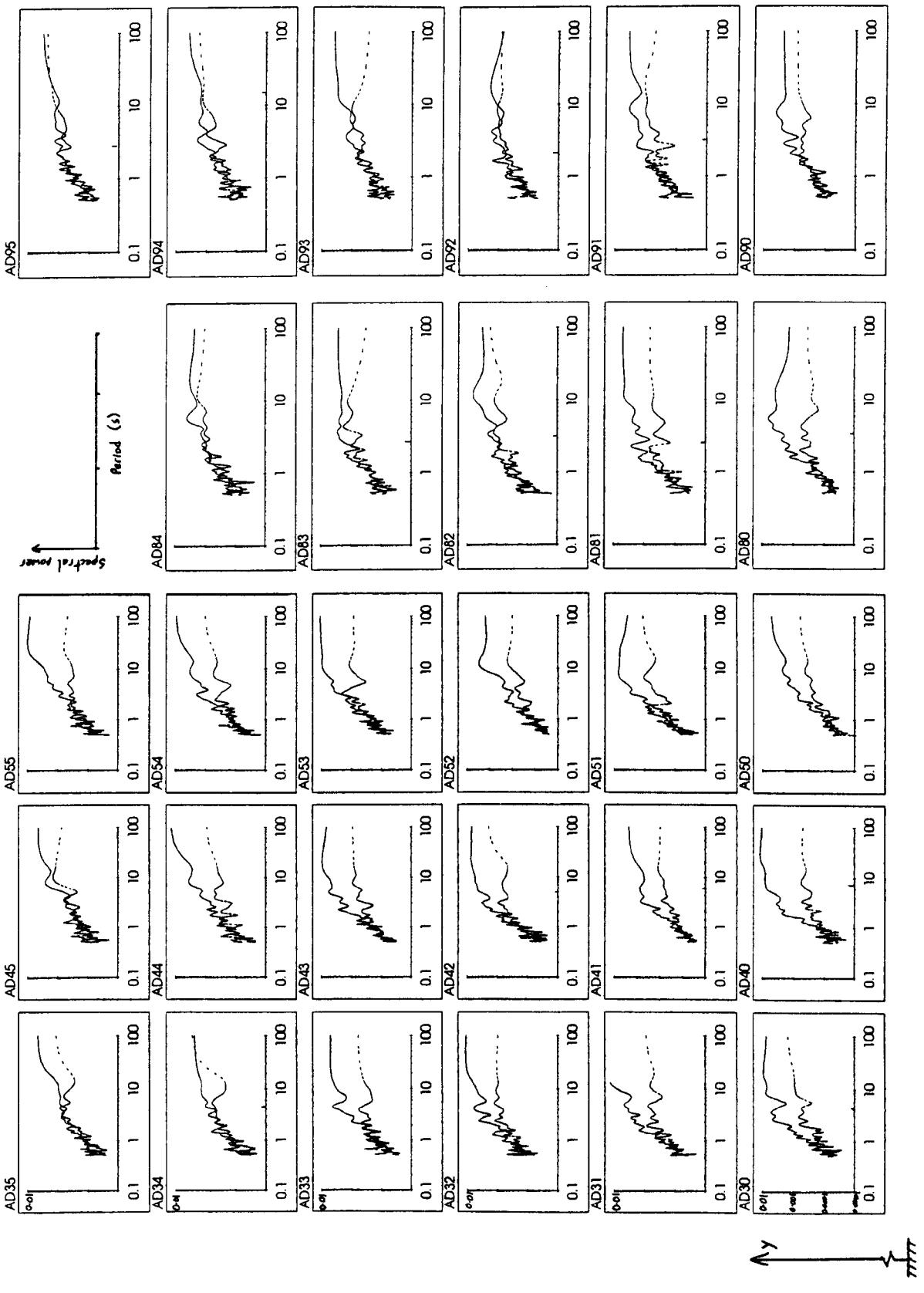

Figure 5.9 Spectra of the u (—) and v (--) velocity components of the Dubhaig data.

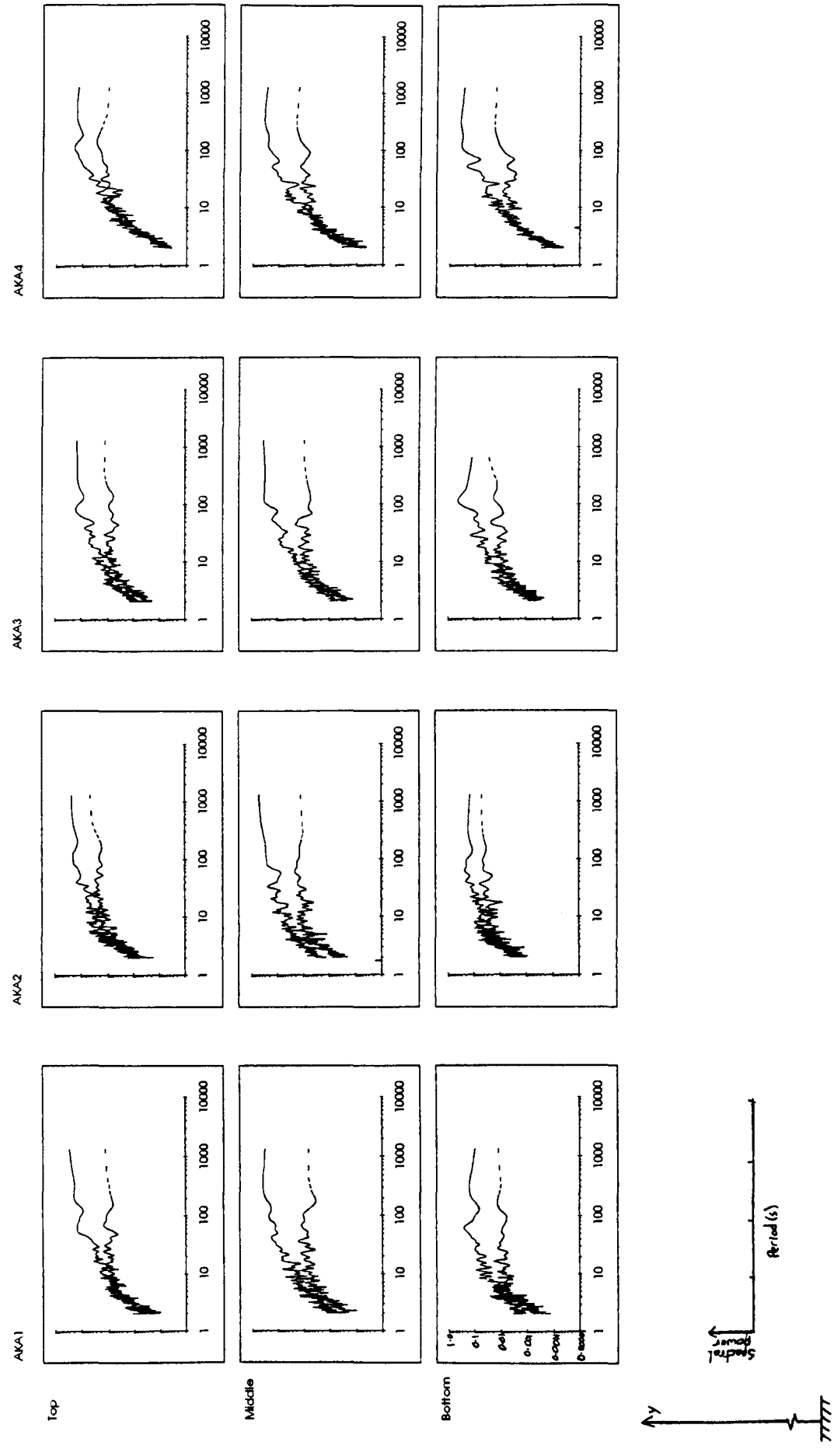

Figure 5.10 Spectra of the u (—) and v (- -) velocity components of the Beauty Creek data (A files).

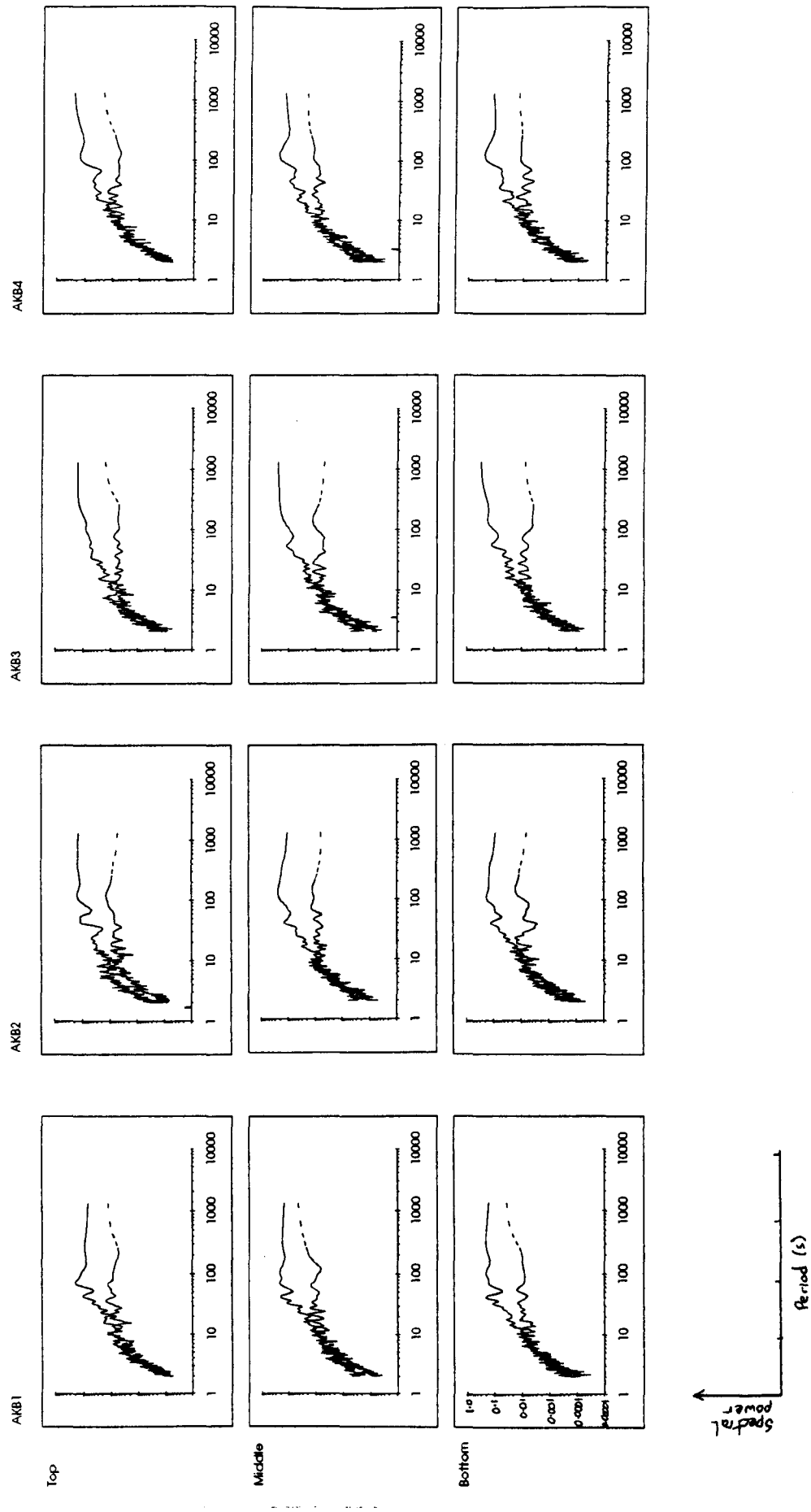

Figure 5.10 Spectra of the u (—) and v (- -) velocity components of the Beauty Creek data (B files).

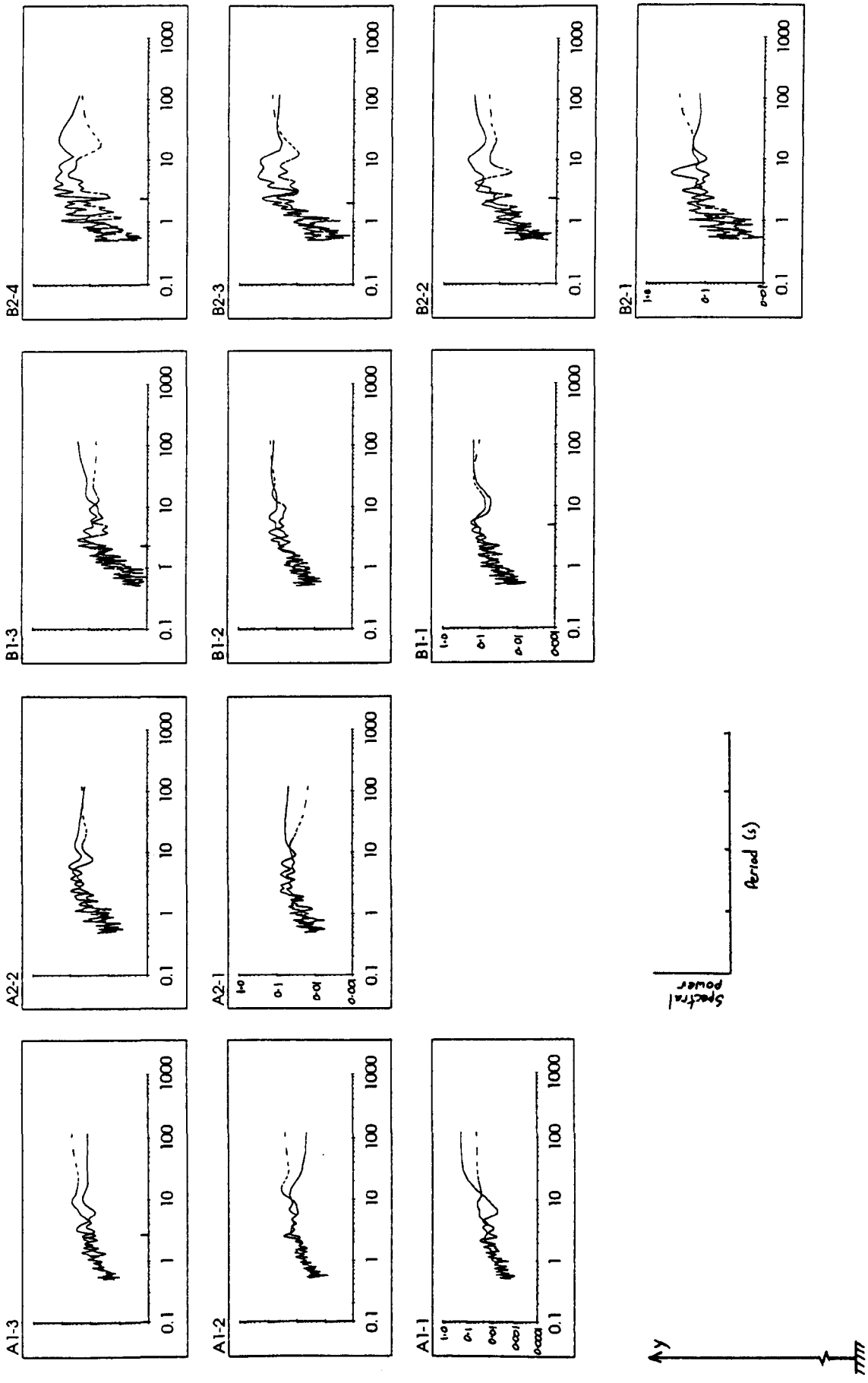

Figure 5.11 Spectra of the u (—) and v (-·-) velocity components of the Arolla data.

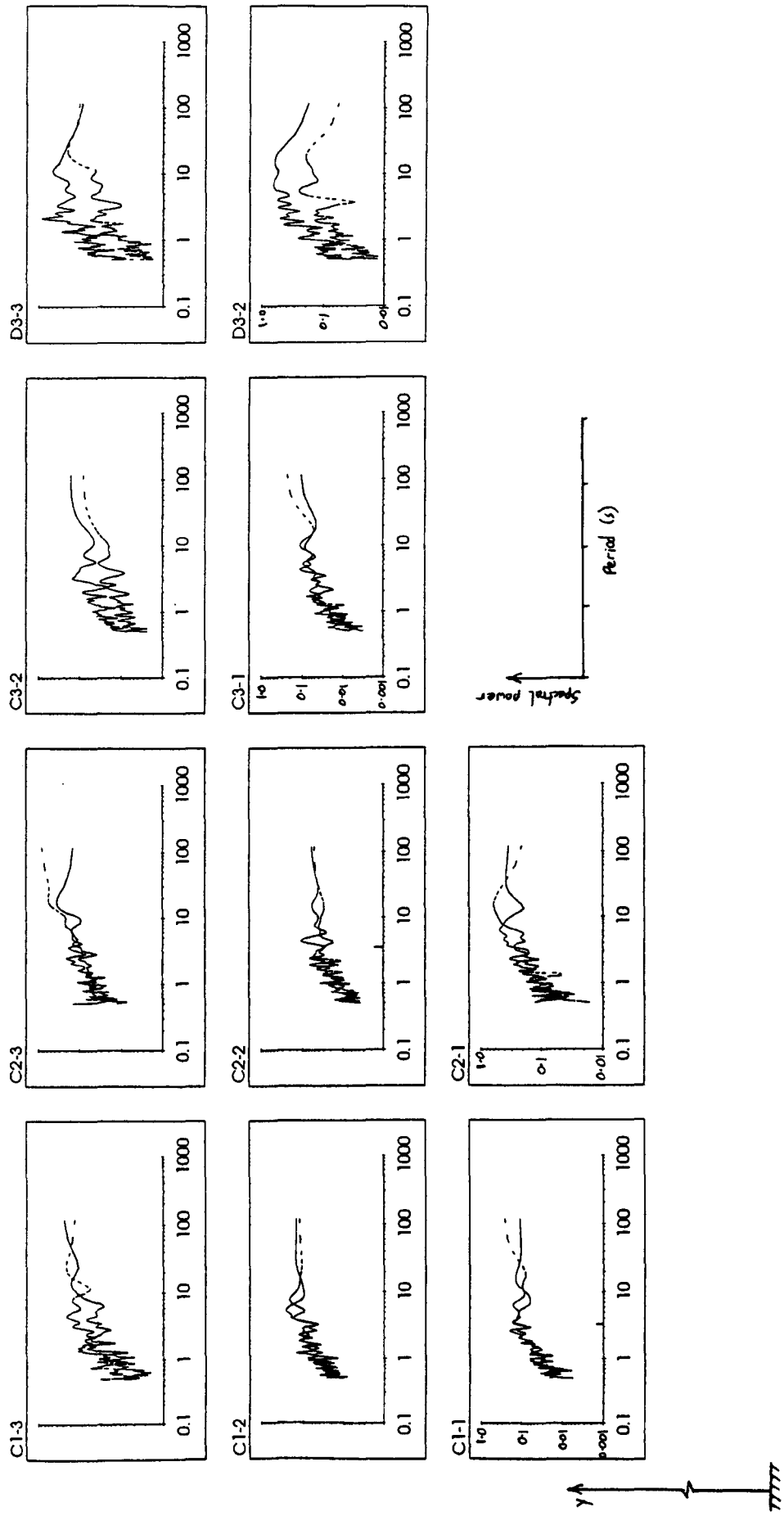

Figure 5.11 Spectra of the u (—) and v (- -) velocity components of the Arolla data (continued)

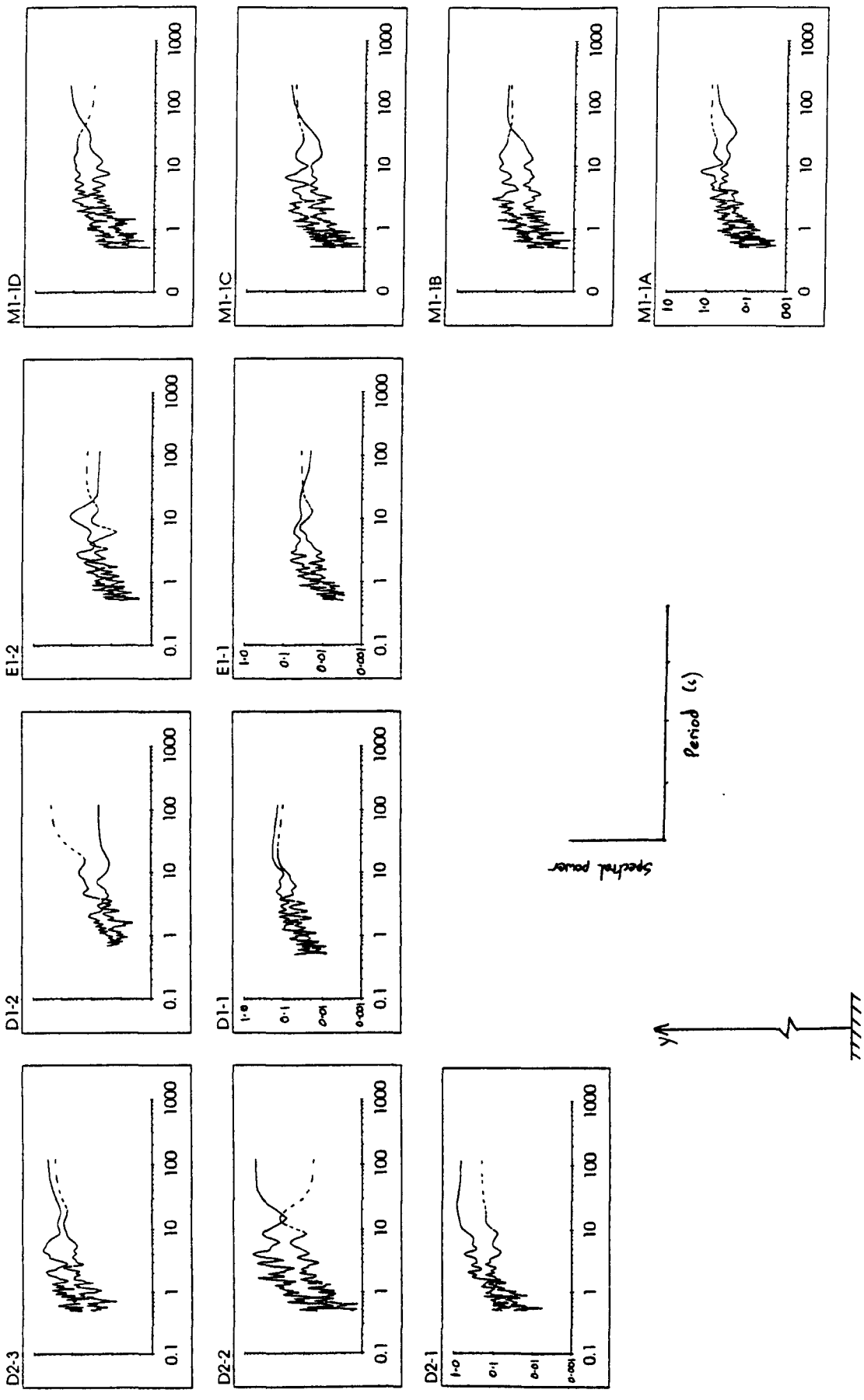

Figure 5.11 Spectra of the u (—) and v (- -) velocity components of the Arolla data (continued)

Another reason for the "roll-off" in the spectra at short periods might be a product of the smoothing of the velocity signal by the ECMs (section 3.1.2; Andre Roy *pers. comm.*). The smoothing effectively spreads the influence of higher frequency fluctuations out over several sampling points. This would have the effect of reducing the power associated with the higher frequencies, and hence cause roll-off in the high frequency (low period) end of the spectrum.

Secondly, the Dubhaig data, which represent lower τ_0 conditions compared to the rest, show a flatter spectrum of the vertical component compared to the streamwise. This suggests that at low τ_0, vortical structures within the flow are expressed more dominantly in the streamwise rather than the vertical velocity component.

Thirdly, some of the spectra show a striking correspondence between spikes and troughs in the u and v components (e.g. AD42, AD33, A2-1). As these tend to be more clear at longer periods (i.e. those of more interest to flow structure), it is encouraging in terms of supporting the idea of the passage of advecting vortices.

Finally, as a general point, there does not immediately appear to be a clear pattern in the position of the peaks in the spectra relative to position in the profile or τ_0. The following section attempts to define these positions in order to look for such patterns.

a. Definition of significant peaks.

The procedure for deriving the confidence limits for any S(f), where S(f) represents the spectral density for the fourier frequencies, f to f+δf, is based on that described by Chatfield (1975, section 7.5). If we propose the null hypothesis, H_o, that the raw series is a stationary white noise process, then the spectrum of this series would be horizontal at I(f) where I(f) equals twice the process variance. Physically, this means that in the original series there are no periodic components, and that it is truly random. Box & Jenkins (1968) show that $2I(f)/S(f)$ is approximately distributed as chi-squared. The number of degrees of freedom, n, for the Fourier series smoothed with a Hamming window with a width of 11 (defining f+δf), is given by 3.87 N/M where N is the number of observations in the time series, M is twice the window width. For any S(f), this gives confidence limits of

$$\frac{n.S(f)}{chi_n^2,\alpha/2} \text{ to } \frac{n.S(f)}{chi_n^2,1-\alpha/2}$$

If, when the α% confidence limits are plotted from a peak, the peak remains isolated from the adjoining fourier series, then it may be stated that the peak is significant at the α% level and H_o is rejected. Conversely, if a trough in the Fourier series occurs within the range of the confidence limits from the peak, then it is not statistically significant. It is this approach that is used to determine which are significant peaks for the calculated spectra.

There are many peaks which are significant at the 5% level. There is a problem in defining what actually constitutes a peak as many have small "blips" on their limbs or two sub-

peaks at the top of a major one. This decision was made subjectively, and each problem case treated individually.

In order to determine whether there is a pattern to the position of the peaks, Figure 5.12 shows the period of the peaks plotted against y. The absence of any systematic pattern in Figure 5.12 suggests that the peaks represent quasi-periodic elements of the flow field specific and peculiar to the individual monitoring points. It also suggests that there is no clear link between the layered structure of the boundary layer and flow periodicity.

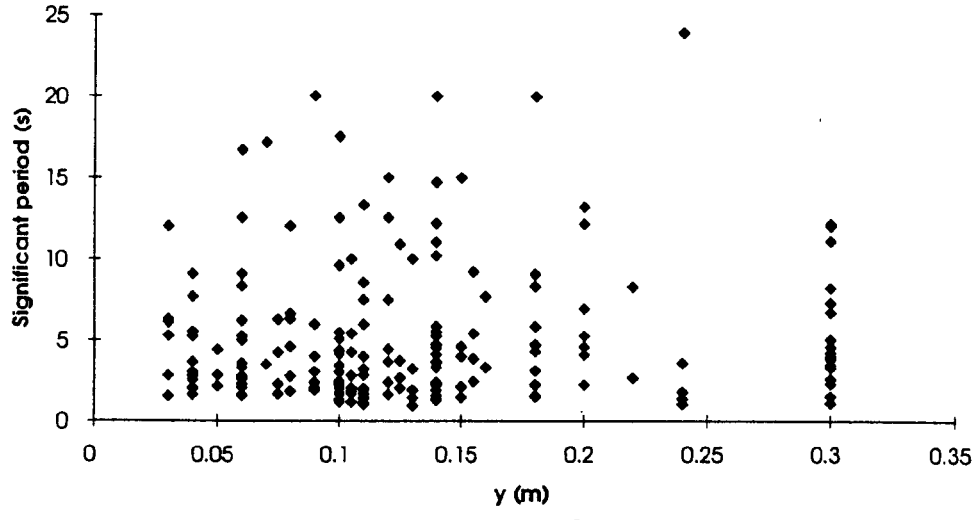

Figure 5.12 The periods of statistically significant peaks in the Beauty Creek velocity spectra against y.

Two of the Arolla files were monitored for 15 minutes at 4Hz during the peak of a muted flood peak resulting from an overcast day. Over the sample, there were no discernible changes in the <u> or σ_u. These files were split into 4 x 400 second sections, and spectra generated individually for each of these replicates.

The spectra from the four replicate series are shown as M1-1A to M1-1D in Figure 5.11. Those from the other show broadly similar patterns. Although there are broad similarities between the spectra (roll-off at <2s, power of v spectra less than equivalent u), the periods of the significant peaks within the spectra are not the same. This casts doubt on any interpretation which may be drawn from the comparison of spectra from different points within the flow.

A general conclusion to be drawn from this is that the flow field over fluvial gravel beds is not composed of any regular periodic component. When considered against the obvious temporal structure observed in the visualisations, it suggests that any cyclical structure of the flow is more intermittent than periodic. In this respect, intermittency is interpreted as meaning that the velocity signals exhibit a repetitive character, but the recurrence of the repetition is irregular.

(ii) Cumulative power spectra

Rather than attempting to define specific periods that contribute significantly to the variance of the series, Lapointe (1993) derived values relating to the frequencies below which a

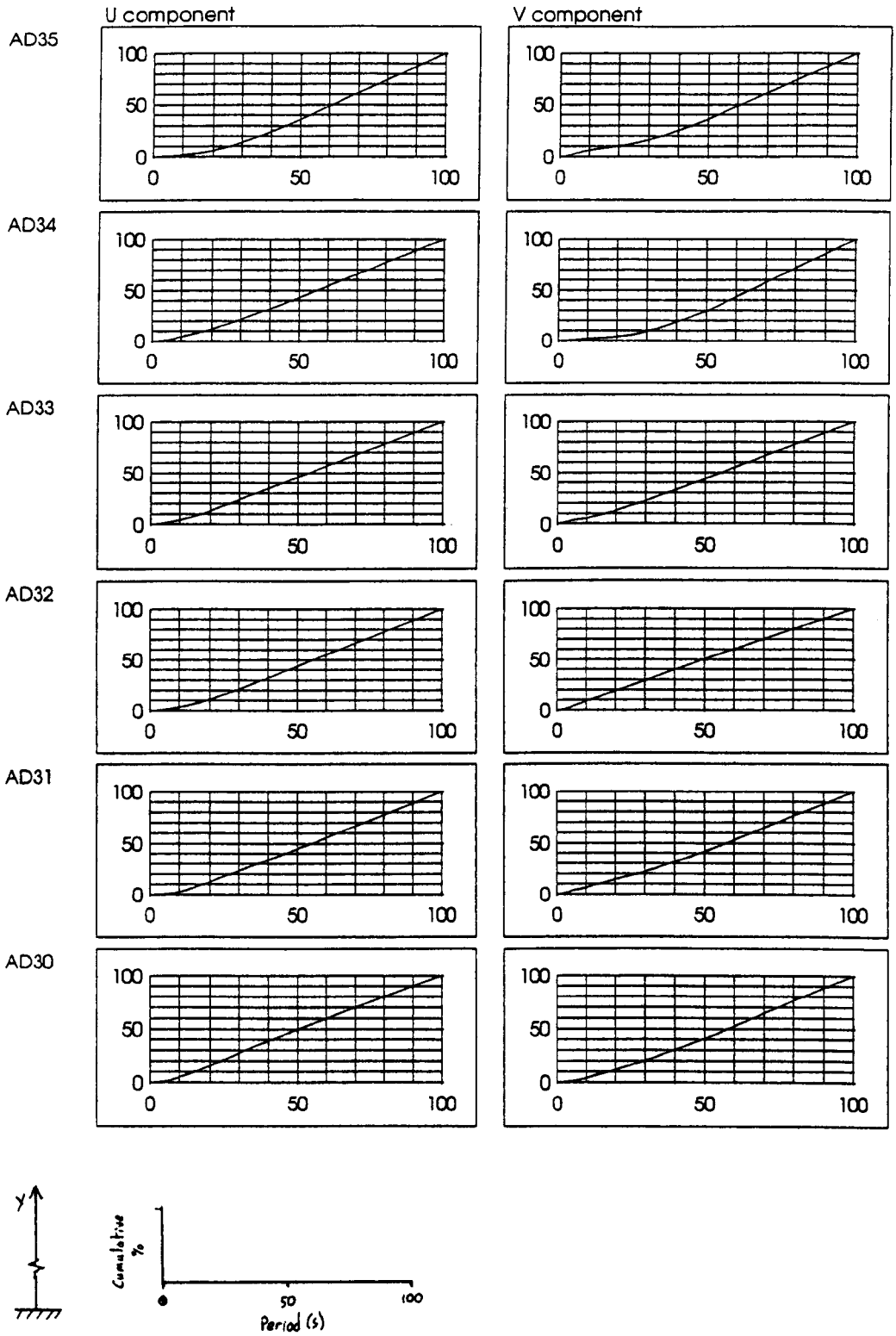

Figure 5.13 Cumulative spectra of one of the Dubhaig profiles.

certain contribution to the total variance was made. This information can be derived from the cumulative power spectrum.

If the power values for the periods are cumulated from the shortest period to the longest, then, within the limit of the length of the series, it can be said that 100% of the variance of that series is contributed by periods of less than the maximum. Percentile values derived from the cumulative spectrum allow statements to be made concerning the period below which a specific percentage of the variance is contributed. The cumulative spectra for the u and v components of the points in the AD30-AD35 profile of the Dubhaig data are shown in Figure 5.13.

The key point that emerges from the cumulative spectra is the amount of power contributed by low frequencies. Typically 90% of the power is contributed by periods of over 15s. Although the power spectra show a lack of distinct periods, the cumulative spectra suggest that the higher period components are important in explaining the total series variance.

Robert *et al* (1993) suggest that the timescale of flow structure (derived from autoregressive modelling) increases with distance from the boundary. Figure 5.14 a & b show the periods below which x% of the variance is generated plotted against depth (where x is the percentile value, 16, 50 or 84). These do not, however, show any systematic variation in any of the percentiles with depth. This suggests either that a shift in flow timescale does not exist, or that spectral analysis does not pick it up.

(b) Analysis in the time domain: ARMA modelling

ARMA modelling is a method of determining whether and how a value in a series is related to past values. The two ways in which values can be serially correlated define whether the process is best represented by an autoregressive (AR) model, a moving average (MA) model, or a mixture of the two. This section will outline the characteristics of these models, explain the derivation of their parameters, compare the best fit models to those suggested by other workers and interpret the models with regard to hydraulic activity.

If the value of a series, v_t can be predicted from previous values , v_{t-1}, v_{t-2} etc., then the process is termed "autoregressive", and can by expressed as

$$v_t = C + \phi_1 v_{t-1} + \phi_2 v_{t-2} + \phi_3 v_{t-3} + \ldots + \phi_{pt-p} + e_t \qquad (5.3)$$

where C is the constant level, v_{t-1}, v_{t-2} etc. are past values and ϕ_1, ϕ_2 etc. are the autoregressive coefficients at lags 1, 2 etc. e_t is a random variable with zero mean and constant variance, the series of which shows no serial correlation. The value of n in ϕ_n which represents the greatest lag at which ϕ_n is significantly different to zero represents the order of the AR model.

A MA model is different to an AR model as the value v_t is predicted by past values of the error term, e_t, e_{t-1} etc., and is given by

$$v_t = e_t - \phi_q e_{t-1} - \phi_2 e_{t-2} - \ldots - \phi_q e_{t-n} \qquad (5.4)$$

Again, the order of the MA model is given by the value of n corresponding to the last significant coefficient, ϕ_q.

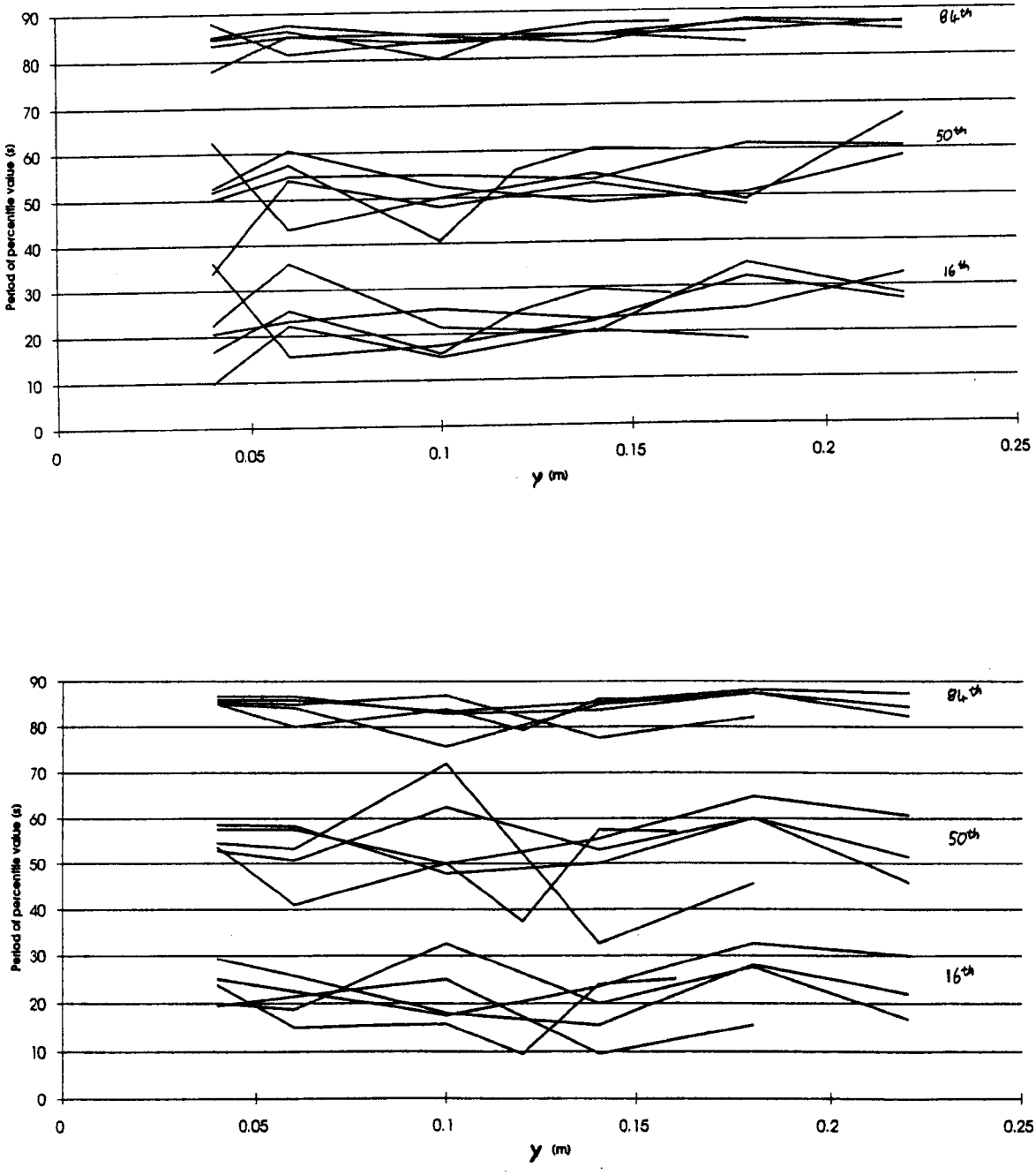

Figure 5.14 Periods of the 16th, 50th and 84th percentiles from the cumulative spectra of the Dubhaig AD30-AD35 profile, (a) u component, (b) v component.

The most appropriate type of model can be estimated in the first instance from plots of the autocorrelation function (ACF) and partial autocorrelation function (PACF) against lags. For white noise, both the ACF and the PACF would not be significantly different from zero at any lag. For processes which exhibit serial correlation, there are distinctive patterns of the ACF and PACF plots relating to different AR or MA models. These will be introduced as appropriate.

Of more use than a descriptive fit of model, which can often be ambiguous, is the derivation of the model parameters, and by statistical testing, the best fit model. MINITAB was used to attempt to fit all combinations of AR and MA models of zero, first and second order to the data series. The best fit model was defined as that which the sum of squares of the residuals was minimised, and all of the model parameters were significantly different from zero. The only *a priori* assumption about the model fitting was that neither the AR or MA part would be above second order.

It has been suggested that velocity time series from gravel bed rivers tend to be best represented by AR2 models (Clifford, 1990; Clifford *et al*, 1992; Robert *et al*, 1993). AR2 models can exhibit pseudo-oscillatory behaviour determined by the inequality

$$\phi_1^2 < -4\phi_2 \qquad (5.5)$$

Clifford *et al* report that 51% of their data satisfied this inequality, whereas Robert & Roy report a value of 100%. The frequency, f, of the pseudo-oscillatory component of these models is calculated from

$$\cos 2\pi f = \phi_1(2\sqrt{-\phi_2})^{-1} \qquad (5.6)$$

Table 5.2 shows the proportions of these data for which the AR2 parameters are significant. It is immediately apparent that not all of the data are AR2. Only the Beauty Creek data have a similar proportion of AR2 files to those reported in the literature. This may be due to the faster sampling rate (10Hz) compared to the other data (4Hz) (Robert *et al*, 1993), and this point is returned to later.

Table 5.2 The proportion of files for which the AR2 parameters are significant.

Data set:	% AR2	% quasi-periodic AR2 (of total):	% quasi-periodic AR2 (of AR2):
Dubhaig:	79	45	56
Arolla:	22	22	100
Beauty Creek:	96	29	30

The proportion of the Arolla files which exhibit AR2 characteristics is considerably lower than the Dubhaig and Beauty Creek data. The major difference from the other data is that the shear stresses tended to be higher, and sediment transport was usually taking place. This

suggests that at active transport conditions, the length of the serial correlation within a velocity series is reduced, suggesting that the timescale of flow structure decreases.

The proportion of the data that represents the quasi-oscillatory form of the AR2 model is generally lower than that reported in the literature. For the Dubhaig data, this proportion is similar to that suggested by Clifford *et al.* Although the Arolla data have the smallest proportion of data to which an AR2 model can be fitted, 100% of these are of the quasi-oscillatory type. The periods of these data, calculated using Equation 5.6 are discussed in section 6.2. An initial observation suggests that the timescales of the v component are less than those of the u. This adds further support to the idea developed in relation to the fluctuating velocity profile that the timescales associated with the u component are greater than the v.

Although the above discussion relates to AR2 model fitting, it was found that this was rarely the most appropriate model. Rather than interpreting the AR2 models in any more depth, the best fit models will be outlined, and more rigorous analysis of the Beauty Creek data will be described.

Table 5.3 shows the best fit models for the Dubhaig, Arolla and Beauty Creek data respectively. The Dubhaig data suggests that although an AR2 model does appear to be the best fit for much of the data, an ARMA 1,1 model appears to give as good a fit. For most of the Arolla data, the best fit model appears to be an AR1. For those files that are AR2, they are, like the Dubhaig data, also ARMA 1,1. Although 96% of the Beauty Creek data can be represented by an AR2 model, most of the data are better represented by a mixed ARMA 1,1.

Table 5.3 Proportion of best fit ARMA models for the Dubhaig and Arolla data defined by the lowest sum-of-squares value and with significant parameters (all values are percentages).

Model:	Dubhaig:	Arolla:	Beauty Creek:
AR1:	17	50	0
AR2:	0	5	0
ARMA 1,1:	0	0	42
AR2 & ARMA 1,1:	79	17	0
ARMA 1,2:	0	0	17
ARMA 1,2 & ARMA 2,1:	0	0	25
Other:	4	17	17

The prevalence of ARMA 1,1 models calls into question the robustness of AR2 as an appropriate model, and necessitates an interpretation of the ARMA 1,1 with respect to what was actually being logged.

Table 5.4 shows various results of model fitting of the Beauty Creek data which has been re-sampled at 5Hz and 2.5Hz. Firstly, the proportion of files for which the AR2 parameters are significant reduce as the sampling rate increases. Robert *et al* (1993) suggest that in some circumstances, model type is dependent on sampling rate. Here, however, the lowest sampling interval is still sufficiently small relative to the apparent timescale given by the quasi-period of the 10Hz model, and hence a similar model should emerge.

Table 5.4 The best fit ARMA models for the Beauty Creek files re-sampled at 5Hz and 2.5Hz.

Model:	10Hz	5Hz	2.5Hz
AR1:	0	17	46
AR2:	0	0	0
ARMA 1,1:	46	4	13
ARMA 1,2:	17	0	0
AR1 & ARMA 2,1:	0	17	13
AR2 & ARMA 1,1:	0	54	17
ARMA 1,2 & ARMA 2,1:	21	0	0
Other:	17	8	11

The velocities sampled here are continuous phenomena which are being sampled discretely. For such a process, as the sampling interval, δt, increases, the independence of consecutively sampled series values would become more plausible. As δt decreases, consecutive series values become less independent due to limitations in the rate of acceleration of the fluid. The velocity would therefore tend to adopt autoregressive characteristics.

In a similar manner, as δt decreases, it is more likely that the random errors, e_t, would be serially correlated. This would introduce characteristics of MA models into the process. It is possible to characterise the MA process that results from this effect (Ferguson, *pers. comm.*).

In addition to these problems, Lane *et al* (1993) discuss the smoothing effects of inbuilt time constants in ECMs. These reduce the independence of consecutive series values as δt decreases, hence introducing higher order autoregressive characteristics. This may explain the reduction in significant AR terms at slower sampling rates. This effect could be removed if the autoregressive nature of the smoothing could be characterised, so that the series could be filtered, and is the subject of ongoing work.

The above discussion suggests that in the majority of cases, the velocity series is best represented by an AR1, a mixed ARMA 1,1 or an AR2 model. It would seem that the high proportion of quasi-periodic AR2 models reported in the literature may be the result of instrument smoothing, and so the apparent periods derived should be treated with caution. In general, the robustness of apparently quasi-periodic AR2 models should be checked before deriving periods from the model parameters.

(c) Relation between spectral analysis and ARMA modelling

Useful interpretation of spectra can only really be made if the process from which they are defined contain quasi-periodic components. The inconclusiveness of the spectral analysis of the velocity data supports the rejection of a quasi-periodic AR2 model as being the most appropriate for velocity data from gravel bed rivers.

The periods as calculated from the model parameters of the u-component series that *do* emerge as the quasi-periodic type are shown as "A" on the axes of the spectra (Figures 5.9, 5.10 and 5.11). Although these occasionally correspond to peaks in the spectra (e.g. B2-3, B2-4), the majority of the AR2 periods bear no relation to spectral peaks. More importantly, large peaks in the spectra never correspond to AR2 derived periods.

In order to determine what the spectra would be like for series which produce AR1, ARMA 1,1 and AR2 models, series were generated using the parameter values of some of the velocity series which yielded such models as the apparent best fit. The spectra of these series were then generated using the same routine as used for the velocity data. The ACF, PACF and spectra of the original and synthetic series are shown in Figure 5.15.

The ACFs and PACFs of the synthetic series compare well to those of the real series, suggesting that the generation technique was reliable. Three points emerge from the spectra. Firstly, the spectra of the AR1 and AR2 series are virtually indistinguishable; the ARMA 1,1 spectra tend to have less power at the low period end. Secondly, all of the spectra except the real ARMA 1,1 yield significant peaks, yet the series were specifically selected for their lack of auto-regressive quasi-periodicity. Finally, the periods of the peaks in the real spectra do not correspond well with those in the synthetic ones.

Time series analysis of the velocity data does not yield any clear patterns regarding the temporal structure of flow over gravel beds. The majority of the data do not show any quasi-periodic characteristics. Any apparent quasi-periodicity emerging from one time series analysis technique (i.e. spectral analysis or ARMA modelling) is not confirmed by the other technique.

Coles (1987) stated that "large coherent structures ... are concealed in a tremendous clatter of noise". Although visual observations of the flow field show that coherent structures *do* exist over gravel beds, the "clatter of noise" seems to have foiled the attempts made here to characterise the periodicities associated with the structures.

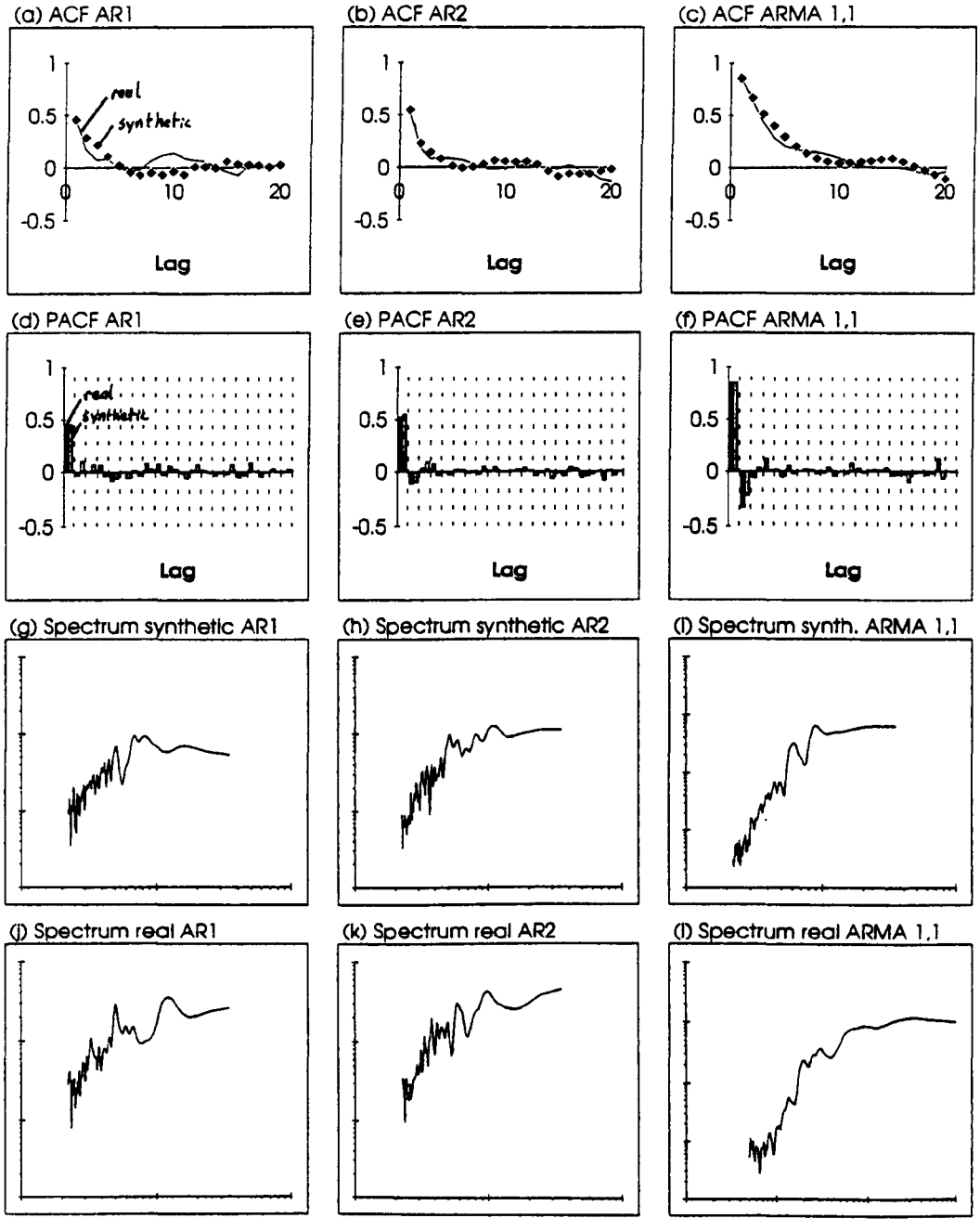

Figure 5.15 ACFs, PACFs and spectra of velocity series with best fit ARMA models of AR1, AR2, ARMA 1,1, and the equivalent ACFs, PACFs and spectra of the synthetic series generated using the same parameters.

Section B: Shear Stress

5.3 Overview of Stress

Stress is a measure of fluid force per unit area (Nm^{-2}). Two stress parameters are of importance here. Bed shear stress, τ_0, is a measure of the mean drag force of the flowing fluid acting on a unit area of the bed. Reynolds stress, τ_R, is a measure of the momentum transfer or the rate of shear within the fluid.

$<\tau_0>$ is commonly derived either from the u velocity profile or from the depth-slope product (Dietrich & Whiting, 1989). For all cases in this work, τ_0 was derived from the velocity profile using the procedure outlined in section 2.2. τ_R is derived from point measurements of two components of velocity, specifically u and v in this work by the relation

$$\tau_R = -\rho_w.u'.v' \qquad (5.2)$$

An instantaneous value of Reynolds stress must be interpreted with respect to not only its magnitude, but also to its direction. This is discussed more fully in relation to the four quadrants defined by the sign combinations of u' and v' in sections 5.4 and 5.5. Mean Reynolds stress, $<\tau_R>$ is the arithmetic mean of the series of τ_R. Comparison of $<\tau_R>$ to other mean measures of stress is made in the next section.

5.3.1 The nature and comparison of mean and fluctuating stresses over gravel beds

$<\tau_0>$ is a commonly measured parameter in field investigations, as it is easily derived from wall normal velocity profiles of <u> usually taken using propeller current meters. Conversely, τ_R is not regularly measured in the field as it requires more sophisticated current metering. τ_0 is averaged over both time and space, and relates to a spatial scale of a similar size to the flow depth, whereas τ_R by definition relates to a point. τ_0 is the most widely used and successful mean flow property for predicting the entrainment of sediment (e.g. Shields, 1936; Andrews & Parker, 1987), and it is of interest here to consider how fluctuating stress can help to improve this explanation.

The two aims of this section are to consider the nature of the frequency distributions of the different measures of stress, and to compare τ_0 and τ_R instantaneously and locally then averaged over both time and space. Firstly, the distributions of the instantaneous stress parameters will be described and quantified using descriptive statistics. Comparison of the corresponding descriptive parameters will then be made for the different measures of stress. Finally, comparison of the time series of the different measures of stress will be made.

The three ECM rig as described in section 4.2.1 provides the opportunity to produce time series of τ_0 over scales of the order of centimetres from the velocities at two adjacent probes. This parameter will be referred to as the "local shear stress", τ_u. The spatial scale of "local" is defined by the probe spacing. The probe configurations used in these experiments (Section 4.2.1) allowed local shear stresses to be calculated over depth ranges of 3-14cm, 10-

20cm, 14-20cm and 20-30cm in a total flow depth of c. 45cm. Time series of τ_u were generated for each configuration, and series of τ_R of the lower probe was used for comparison with τ_u.

Figures 5.16 and 5.17 show typical histograms of τ_u and τ_R respectively. The distribution of τ_u shows a strong positive skew, meaning that the majority of values are relatively low; Figure 5.16b shows that τ_u is actually log-normally distributed, although there is a slight tendency for the majority of the Beauty Creek data to have a slight negative skew to the log-normal distribution of τ_u.

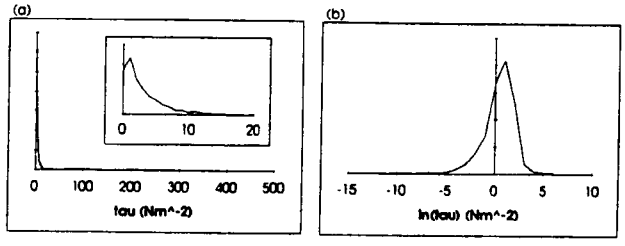

Figure 5.16 Histograms of (a) τ_u and (b) $\ln(\tau_u)$.

τ_R appears to be normally distributed with a low positive mean (Figure 5.17a). Four specific combinations of the product of u'v' are possible determined by the sign of the components, the meaning of which will be discussed in sections 5.4 and 5.5. Figure 5.17b shows that the distribution of $|\tau_R|$ has a strong positive skew, and Figure 5.17c shows that $|\tau_R|$ is log-normally distributed. Generally, there is no systematic difference in the shapes of the distributions of τ_u and τ_R.

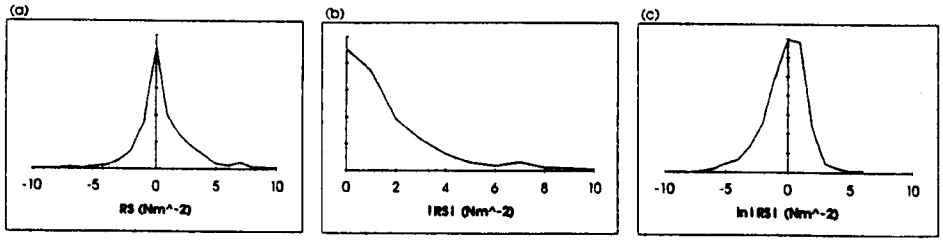

Figure 5.17 Histograms of (a) τ_R, (b) $|\tau_R|$ and (c) $\ln|\tau_R|$.

As τ_u and τ_R are both measures of stress, it is necessary to consider how their magnitudes compare to each other, and which most closely approximates to local τ_0, the shear stress as conventionally derived from the time-averaged velocities at two points.

As τ_u relates solely to shear between one dimensional u vectors, averaging a series is justifiable to obtain a mean value of $<\tau_u>$. Obtaining a mean value of Reynolds stress is, however, less straightforward. An arithmetic mean of a series of τ_R should approximate to $<\tau_u>$ i.e. the positive contributions of u'v' and -u'-v' should be greater than the negative contributions of +u'-v' and -u'+v' products. However, instantaneous values of τ_u may be of large magnitude,

yet the mean stress could still be low. In order to compare this possibility to the other time averaged measures of stress, the mean of the absolute values of τ_u, $|\tau_u|$, is also calculated.

Table 5.5 compares the local $<\tau_0>$ (calculated from the mean velocities at two probes) with both the arithmetic and geometric means of τ_u and $|\tau_R|$. There is a good agreement between τ_0, $<\tau_u>$ and geo$<\tau_u>$, where $<\tau_u>$ overestimates $<\tau_0>$, and geo$<\tau_u>$ underestimates. In contrast, the various mean Reynolds stress values show no relation at all to those of $<\tau_0>$ or $<\tau_u>$. Indeed, some of the $<\tau_R>$ values are negative, for which a physical explanation is difficult to make.

Table 5.5 Comparison of different measures of mean shear stress (all values in Nm^{-2})

File:	y/d:	$<\tau_0>$	$<\tau_u>$	$<\tau_R>$	$\lvert\tau_R\rvert$	G$<\tau_u>$	G$\lvert\tau_R\rvert$
AKA1-1	0.073	2.28	5.16	-1.33	0.09	1.49	0.79
AKA1-2	0.244	4.12	6.85	0.28	2.45	2.98	1.02
AKA1-3	0.732			1.33	1.13		0.88
AKA2-1	0.073	2.39	7.94	-6.46	1.49	2.67	1.56
AKA2-2	0.244	3.59	9.17	-2.41	2.94	2.12	1.63
AKA2-3	0.732			4.31	1.77		1.15
AKA3-1	0.073	3.10	4.64	-0.08	0.19	2.28	1.04
AKA3-2	0.244	3.29	5.38	0.47	0.73	2.23	1.08
AKA3-3	0.732			0.48	0.04		0.80
AKA4-1	0.073	1.66	2.39	1.28	0.77	1.04	0.95
AKA4-2	0.244	2.87	4.11	1.06	6.02	1.73	1.09
AKA4-3	0.732			1.10	0.21		0.77
AKB1-1	0.341	20.13	24.72	0.81	0.73	15.43	1.00
AKB1-2	0.488	1.62	6.27	0.60	3.20	1.21	1.03
AKB1-3	0.732			0.34	1.37		0.73
AKB2-1	0.341	16.84	21.2	0.53	2.57	12.35	0.91
AKB2-2	0.488	0.04	6.63	0.59	14.73	1.14	1.01
AKB2-3	0.732			0.29	6.53		0.72
AKB3-1	0.341	18.32	21.95	0.59	1.79	14.53	0.92
AKB3-2	0.488	0.02	4.96	0.57	1.44	1.16	0.84
AKB3-3	0.732			0.31	0.75		0.59
AKB4-1	0.341	19.28	23.63	0.98	0.74	14.47	0.99
AKB4-2	0.488	0.94	5.83	0.84	3.26	1.34	1.00
AKB4-3	0.732			0.55	4.11		0.67

Before discussing this further, let us consider the correlation of the instantaneous values of the time series of τ_u and τ_R.

Figure 5.18 shows corresponding series of τ_u and τ_R in their raw form and smoothed over a 2s (20 sample) running average. The temporal structure will be discussed further in sections 5.6, 5.7 and Chapter 6. Although there are obvious peaks in each of the series, there does not appear to be an obvious correlation between the two series.

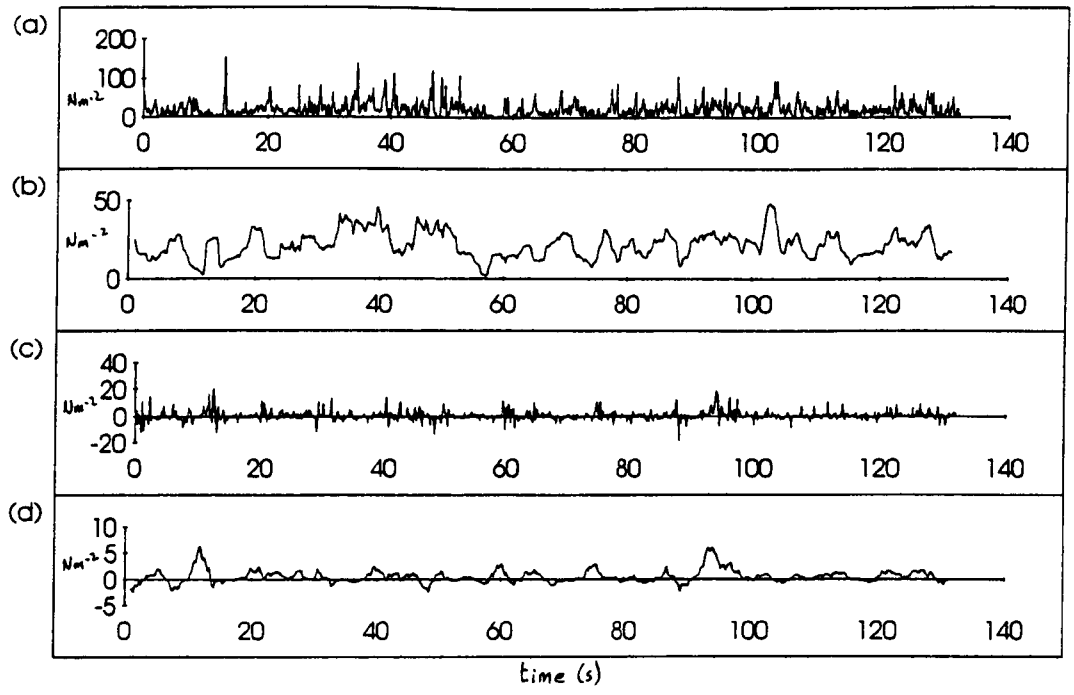

Figure 5.18 Time series of (a) τ_u (c) τ_R, and smoothed time series of (b) τ_u and (d) τ_R using a 2s running average

Table 5.6 Correlation coefficients and r^2 values of τ_u and τ_R for the Beauty Creek data. τ_u is calculated from the velocity gradient between two probes, τ_R is derived from the lower of the two probes.

File:	y(cm):	y/d:	Corr:	r^2(%):
AKA1	3-10	0.067	-0.907	82.2
AKA2	3-10	0.067	-0.903	81.6
AKA3	3-10	0.067	-0.863	74.5
AKA4	3-10	0.067	0.026	0.0
Mean:			**-0.662**	**59.6**
Mean not including AKA4:			**0.891**	**79.4**
AKA1	10-20	0.222	-0.626	39.1
AKA2	10-20	0.222	-0.683	46.6
AKA3	10-20	0.222	-0.748	55.9
AKA4	10-20	0.222	0.233	5.4
Mean:			**-0.456**	**36.8**
Mean not including AKA4:			**-0.686**	**47.2**
AKB1	14-20	0.311	0.084	0.6
AKB2	14-20	0.311	-0.018	0.0
AKB3	14-20	0.311	0.061	0.3
AKB4	14-20	0.311	-0.003	0.0
Mean:			**0.031**	**0.2**
AKB1	20-30	0.444	0.252	6.3
AKB2	20-30	0.444	0.092	0.8
AKB3	20-30	0.444	0.131	1.7
AKB4	20-30	0.444	0.142	2.0
Mean:			**0.154**	**2.7**

Table 5.6 gives the correlation coefficients and r^2 values for the relations between τ_u and τ_R for the Beauty Creek data. Two points are immediately apparent. Firstly, the variation within the replicates at one depth is considerably less than that between different depths. The obvious exception to this is in AKA4, yet there does not appear to be an obvious explanation for this discrepancy.

Secondly, it shows that there is a strong correlation between τ_u and τ_R near to the bed, but this decays up the profile. Indeed, there seems to be a rapid fall off in correlation at y/d > 0.25.

The good correlation between τ_u and τ_R near to the bed suggests that stress generation is dominated by fluctuations in u' rather than in v', whereas higher in the flow, stress is being generated by sizeable fluctuations in v'. As τ_u does not incorporate the v' component except through an implicit correlation between u' and v', this would explain why stress generating fluctuations in v' would not be incorporated into τ_u.

The near-bed correlation of τ_u and τ_R is further evidence for the presence of a different turbulent flow regime near to the bed to that higher in the flow. Such a structure was observed in the visualisations, implied from the fluctuating velocity profile analyses, and suggested by kinks in the wall-normal profiles of turbulence intensity. It is discussed further in Chapter 6.

5.4 The u-v quadrant plot

As both the u' and v' components are incorporated into Reynolds stress, it seems sensible to consider further how they are related, and how together they relate to τ_R. This should then allow a more informed interpretation to be made of what the stress values physically represent. In order to illustrate this, the quadrant plot of u' and v' will be introduced and used.

The quadrant plot is a scatter plot of u'v' couplets plotted in the vertical-streamwise plane relative to <u> and <v> (Figure 5.19). The quadrants will be referred to as Q1, Q2, Q3 and Q4. It has been used in the literature to partition monitored hydraulic activity into the directionally defined quadrants. For instance, "sweep events" are associated with +u' and -v' and are quadrant 4 (Q4) events, whereas bursting is associated with -u' and +v' activity and is a quadrant 2 (Q2) event. Gravel entrainment is associated with Q4 events (Williams *et al*, 1989), and the suspension of fines have been linked to Q2 events (e.g. Lapointe, 1992).

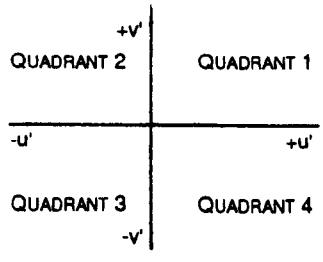

Figure 5.19 Quadrants defined by combinations of u' and v'.

Williams *et al* also found that the positive contribution to total Reynolds stress of the Q2 and Q4 events outweighed the negative contributions of Q1 and Q3 to produce mean positive values of $<\tau_R>$.

This section considers the differences in the stress characteristics *between* the quadrants as this has implications regarding the flow structure in the boundary layer. Variations between the same quadrant for different points in the flow or different boundary conditions will also be investigated.

5.4.1 Visualisation of the fluctuating u-v vector

The disk enclosed in the back cover contains a programme, VECPLOT, which reconstructs the fluctuating u-v vector. It also gives an impression of the absolute Reynolds stress value, $|\tau_R|$, associated with the fluctuations using a fluctuating tone signal. To run the program, insert the disk and type VECPLOT. A typical data file from the Dubhaig data is pre-loaded.

The purpose of visualising the fluctuating vector is merely to give an impression of the characteristics of the fluctuations, and to gain a qualitative insight as to how the high stress events are temporally distributed. This hopefully provides a more informed context against which the discussions and analyses of the following sections can be set.

Observation of the fluctuating vector reveals two main points. Firstly, the high stress events tend to be associated with fluctuations incorporating strong deviations in both the u' and v' components, as would be expected. These events seem to last a finite time before the vector returns to the ambient lower stress condition. Secondly, the vector seems to fluctuate for several sampled points in *either* the +u' or -u' half of the flow field. During these periods, the vector crosses the v' = 0 axis several times. This further supports the idea that the v component fluctuates more than the u as suggested by the lower persistence values of the v profile states of the fluctuating profile analyses.

These descriptive observations generally apply to most of the files used here. When the fluctuating profiles are reconstructed (using the VELPROF programme), it appears that the +u' and -u' transience is associated with the transient high and low momentum profile states.

5.4.2 Distribution of stress between quadrants

If the turbulence was truly structureless over time and u' and v' were uncorrelated, then it would be expected that each quadrant would contain 25% of the total stress. It was shown in section 5.3.1 that the correlation between the series of τ_u and τ_R decays with distance from the bed, the reason suggested being that the v' component becomes increasingly important to the total stress higher in the profile. This is evidence that there *is* variation between the proportion of total stress in each quadrant.

This section investigates how the absolute stress, $|\tau_R|$, is partitioned between the quadrants. Firstly, a general investigation is made into whether some of the quadrants *do* tend

to contain disproportionate amounts of stress. Secondly, the effects of relative depth, roughness and mean hydraulics on the discrepancies will be considered.

Figure 5.20 shows how the distribution of stress between the quadrants changes with distance from the bed. Two points are immediately evident; firstly, the stress is *not* equally distributed between the four quadrants. Indeed, for the AD30 data, less than 9% of the total stress existed in Q1 in contrast to over 40% existing in Q2.

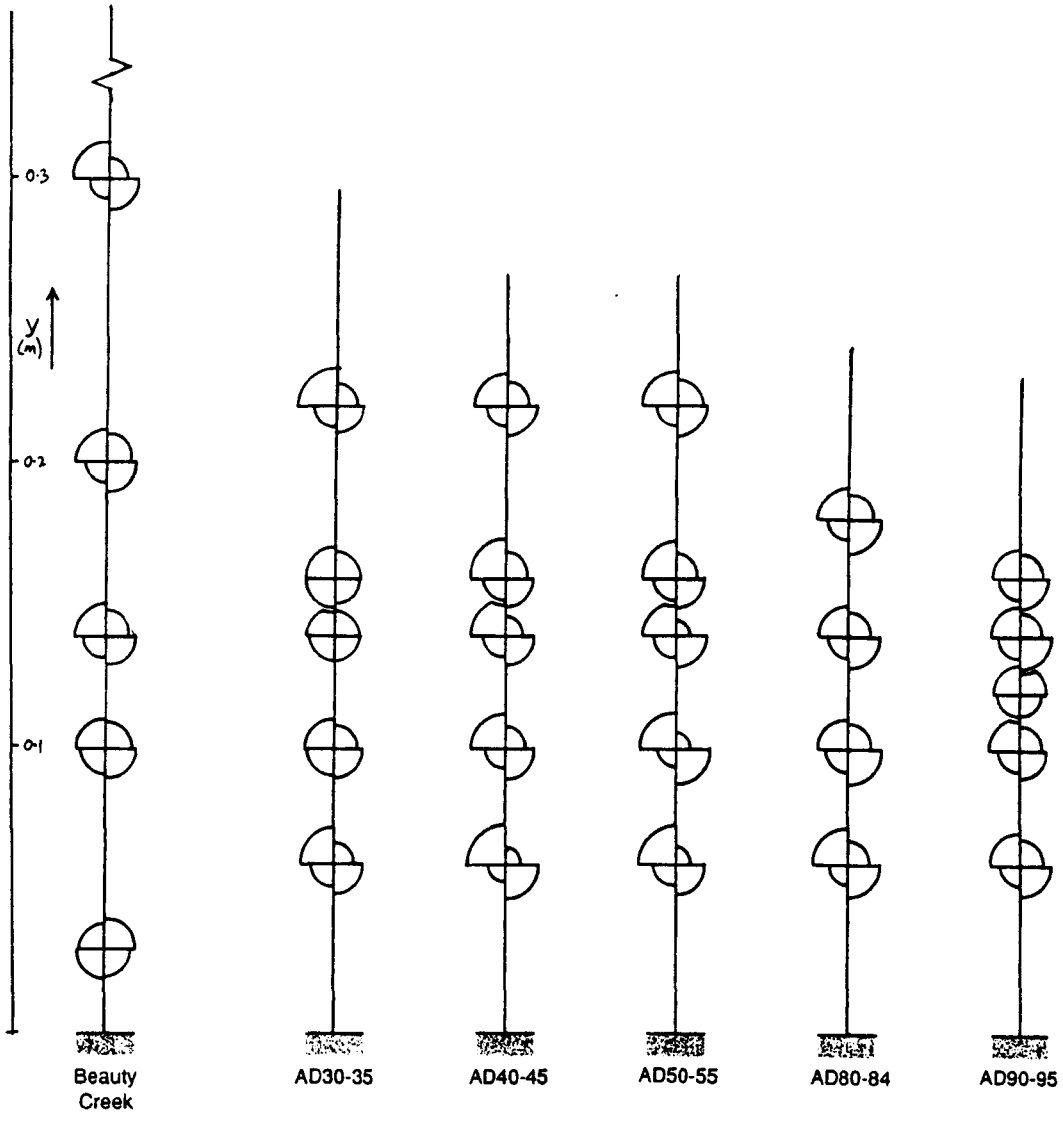

Figure 5.20 Proportion of absolute stress in each quadrant (% ∝ radius^2). Beauty Creek data is averaged from four replicates.

Secondly, there appears to be a systematic shift in the proportion of τ_R between the quadrants at different heights. The Beauty Creek data in Figure 5.20 shows that close to the bed, Q1 and Q3 just dominate the stress field, and this explains the negative $<\tau_R>$ values in Table 5.5. As height increases, Q2 and Q4 become increasingly dominant.

Apart from very close to the bed, Q2 and Q4 are almost always dominant. The proportion of stress in Q2 and Q4 remains dominant at mid depths, but there is a general decrease towards a 4-way split higher in the profile.

Let us now interpret this in terms of dominant hydraulic activity. Q1 represents an "outward interaction" (Williams *et al*, 1989), Q3 an "inwards interaction"; this means that in the near-bed region, the dominant stress-producing hydraulic activity consists of fluid being flung upwards and forwards (Q1) or being decelerated and forced downwards (Q3).

In the near-bed region, this could be interpreted as the monitoring of obstacle derived vortices or vortex ejection. The Q1 events ($u'>0$, $v'<0$) may represent explosions of inner zone fluid into the outer zone as relating to ejections of eddies as observed in the visualisations described in section 4.1. This is significantly different to the classic burst which is associated with a Q2 event. The Q3 events ($u'<0$, $v'<0$) represent downwards, low momentum fluid transfer which, when related to the visualisations may be explained by the lower frontal regions of vortices attached to or rolling off obstacles.

The descriptions of the visualisations implied that the separation between the inner and outer zones approximated to the level of the crests of the larger obstacles. As the lowest probe of the rig used at Beauty Creek is higher than the tops of the larger obstacles yet still picks up a marked difference in the domination of quadrants, it suggests that the influence of the inner zone extends above the level of the crests of the obstacles, and the interface between the two zones is possibly better described as a third zone rather than a layer.

Although the explanation of the near-bed stress field is somewhat speculative, the shift from Q2 and Q4 to Q1 and Q3 nearer to the bed is a significant discovery. It not only supports the inner/outer zone structure of the boundary layer, but suggests that the near-bed region is not dominated by Q2 and Q4 events, but by Q1 and Q3. If the inner zone *is* dominated by eddy shedding from obstacles, it suggests that eddies are shed at velocities greater than $\langle u \rangle$, and are not in themselves Q2 bursting structures.

The shift in dominant stress quadrants from Q1 and Q3 to Q2 and Q4 with increasing distance from the boundary represents a significant shift in the direction of important stress-generating hydraulic activity. Q4 ($u'>0$ $v'<0$) represents sweep-like structures: fluid with high streamwise momentum being directed towards the bed. Events such as these were clearly identified in the visualisations (Section 4.1), and emerged from the analyses of the fluctuating velocity profiles (section 4.2). Their significant contribution to the total stress field shown here is in agreement with results for tidal flows over gravels (Williams *et al*, 1989).

It is clear from these lines of evidence that these sweep-like features are a common feature in the boundary layer over mixed gravel beds, and are important in terms of their contribution to the total stress field.

Of similar dominance to the Q4 events are those of Q2 ($u'<0$ $v'>0$). These represent ejections of lower than average streamwise momentum fluid away from the bed. Again, this type of activity was commonly observed in the visualisation experiments (section 4.1). Unlike

the tidal flow measurements of Williams *et al* where they contributed less to the total stress field than the Q4 events, here they appear to be roughly equal.

It is significant with regard to the entrainment of sediment that the domination of Q2 and Q4 events in the middle and upper parts of the profile does not extend to the bed. This initially suggests that the bed region is protected from the ejections and sweep-like hydraulic events, the latter of which is important for entrainment.

It can be proposed therefore, that a boundary layer over mixed gravel beds is composed of an "inner" zone of obstacle derived vortices as described in section 4.1.2, a transition zone of ejecting vortices and directionally confused vortical activity, and an outer zone of more unidirectional streamwise flow where the stress field is dominated by sweep-like structures and ejections. The details of this structure and a synthesis of all of the evidence for its existence form the basis of Chapter 6.

5.4.3 Distribution of stress within a quadrant

The previous section showed that stress is not evenly distributed between the quadrants, and that the proportion within each changes with depth. This section will consider the discrepancy between the typical magnitudes of the stress between the quadrants, and attempt to assess whether a change in the proportion of stress within a quadrant is explained by a few very important events, or by more smaller ones.

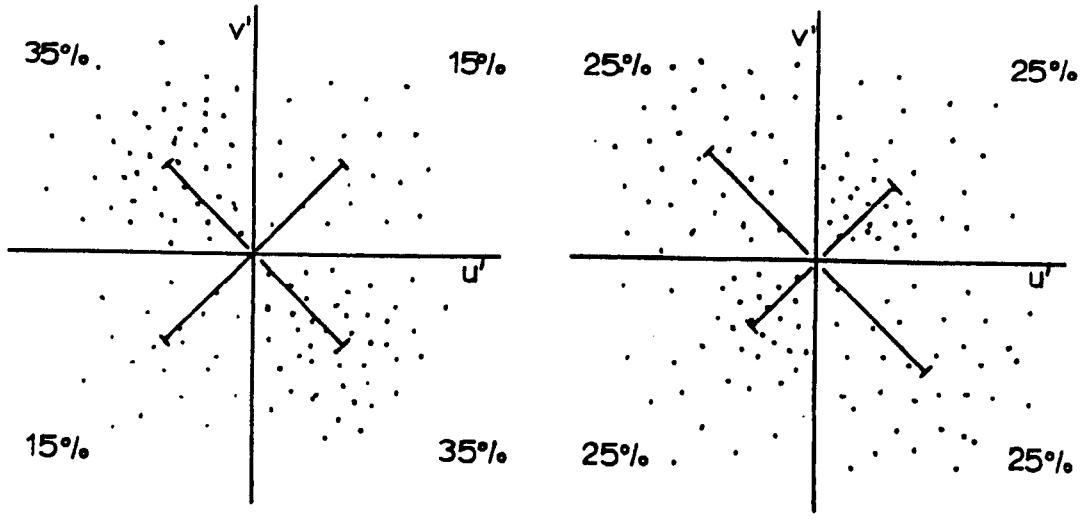

Figure 5.21 Hypothetical quadrant plots. (a) Distribution of total stress between quadrants is unequal but mean absolute stress is the same in each. (b) Stress is equally distributed between quadrants but mean values are different in each.

Figure 5.21 shows two hypothetical quadrant plots. In Figure 5.21a, the proportion of stress within each quadrant is not equal, yet the mean absolute stress within each is the same. Conversely, in Figure 5.21b, the total stress is split exactly evenly between the four quadrants, yet the mean absolute stress in the four is not the same. The following analyses will calculate

the 16th, 50th, 84th, 96th and 99th stress percentile values for each quadrant so that they can be compared both to other quadrants at one point, but also to the same quadrant at different points. The 50th percentile is used as a measure of central tendency, while the higher values should be more revealing regarding flow structure and be of use when interpreting intermittent sediment entrainment in Chapter 7.

Figure 5.22 shows the 84th stress percentiles for the quadrants plotted at the relative depths at which they were taken for the Beauty Creek and Dubhaig data.

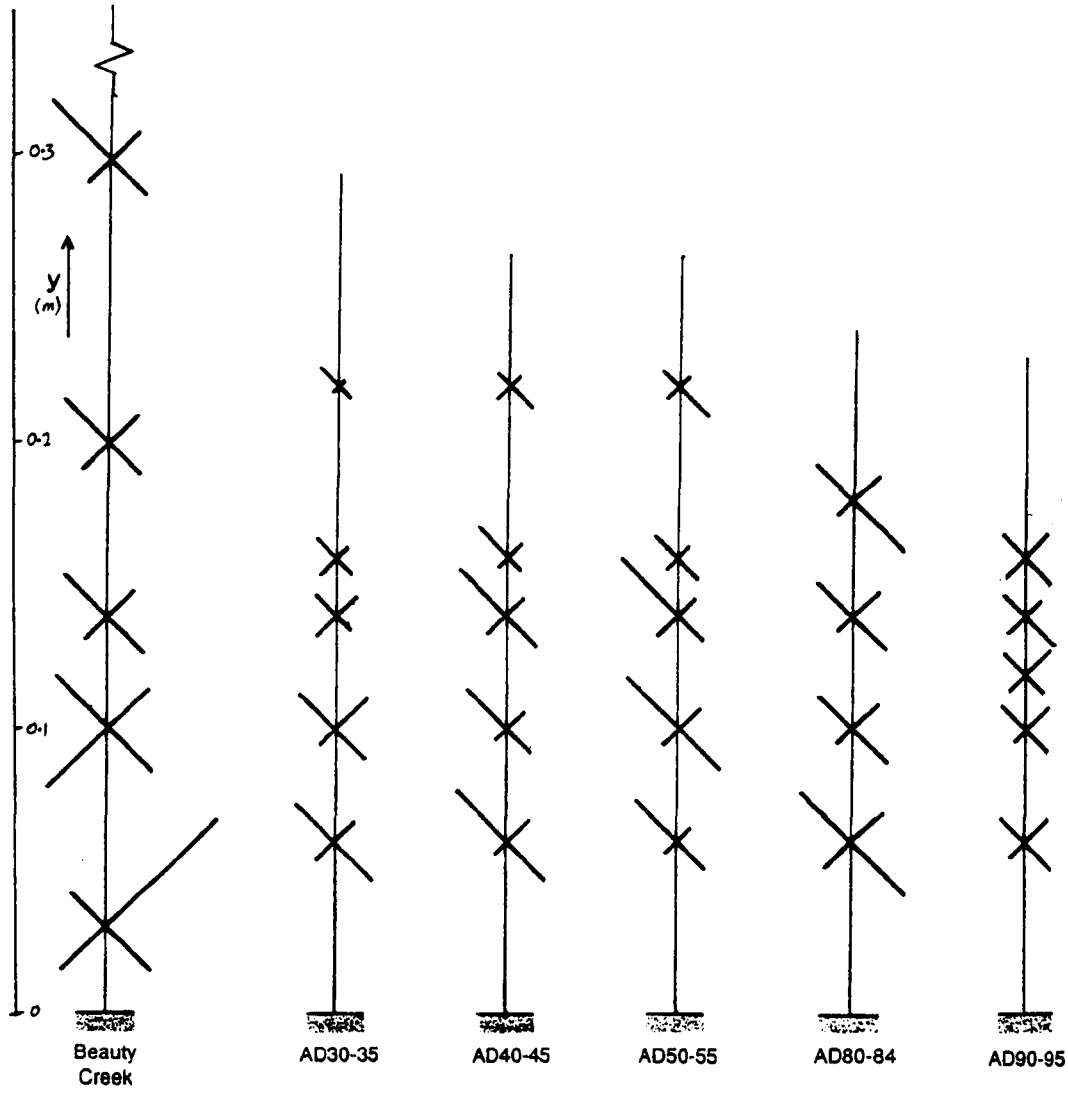

Figure 5.22 Magnitude of the 84th percentile stress value of the absolute stress in each quadrant. Beauty Creek data is averaged from four replicates.

Let us first consider the Dubhaig data. Generally, the 84th stress percentile is higher for Q2 and Q4 than for Q1 and Q3. This means that the ejections and sweep-like events are disproportionately contributing to the total stress field. This agrees with the conclusions drawn from the considerations of the distributions of stress between quadrants of the previous section.

The AD30, AD40 and AD50 profiles suggest that there is a fall-off in absolute stress in all four quadrants higher in the profile. The profiles were taken in conditions of low τ_0 compared to the AD80 and AD90 profiles, and the influence of τ_0 on these patterns is discussed in detail below. Profiles AD30, AD40 and AD50 also suggest that the 84th stress percentile is greater in Q2 and Q4. This suggests that at in conditions of low mean shear stress, stress generated by bursts is greater than that generated by sweeps.

The Beauty Creek data show a significant switch from the stress in Q2 and Q4 being greater than in Q1 and Q3 distant from the bed to the stress in Q1 and Q3 being greater than that of Q2 and Q4 near to the bed. This explains the inequality in total stress between the quadrants in section 5.4.2. Associated with the dominance in Q1 and Q3 near the bed, the actual stress is extremely high.

By attributing the discrepancy in stress between the quadrants to the existence of flow structures, it is implied that the structures produce high stress. If therefore, a structure has expression in, say, Q2, then it would be expected that the difference between the stress percentiles of Q2 and the others would become more marked in the higher percentile values.

Figure 5.23 shows percentile stress values for the quadrants divided by those for the whole series against percentile for the AD30-35 profile. If the preceding paragraph is to be supported, it would be expected that as the percentile values increase, the relative stress of Q2 and Q4 should increase above 1. This does not appear to be the case, and if anything, there is a tendency for all of the lines to converge to 1. This means that the stress associated with flow structures is not exclusively high, but covers a wide range.

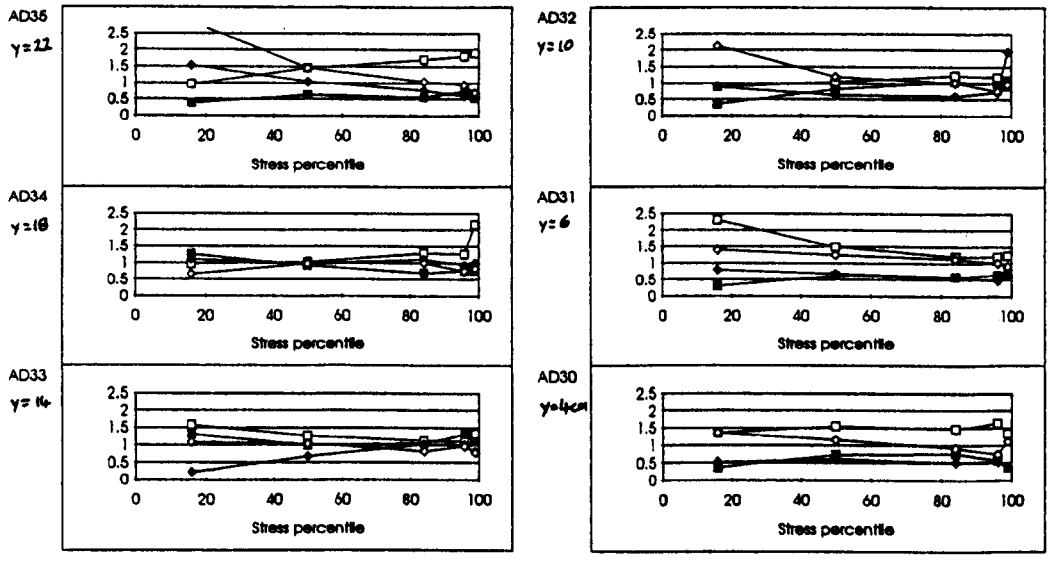

Figure 5.23 The ratio of the nth percentile of stress in each quadrant to the nth percentile of total absolute stress against percentile value, n, for one of the Dubhaig profiles. (Q1 = ■ , Q2 = □ , Q3 = ◆ , Q4 = ◇).

The only systematic trend that can be seen from Figure 5.23 (and from similar plots for other data not shown here) is that as depth increases, Q2 stresses switch from decreasing with

increasing percentile to increasing. This means that at lower depths the Q2 events are associated with low stress, whereas higher in the profile they are associated with high stress.

5.4.4 Influences on the distribution of stress

Let us now consider how the bed roughness and mean flow hydraulics would influence the distribution of stress within and between the quadrants, and hence how they directly and indirectly determine the structure of the boundary layer. The interdependence between roughness and mean hydraulics must not be overlooked. On the timescales relevant here, the roughness will have more of an influence on the mean hydraulics than vice versa i.e. the bed configuration is relatively static. This section will attempt to separate the effects of these two factors on the distributions of stress.

(a) Roughness

Section 4.1 showed that the bed roughness elements have a significant influence on the structure of the boundary layer through their role as hosts for vortices. The roughness height therefore defines the thickness of the inner zone. It also has a strong influence on the thickness and activity within the transition zone, as the spatial scale and shedding frequency of the vortices generated in the inner zone is defined by the scale of the roughness. The comparison of the shedding frequency of obstacle-derived vortices with the intermittency of stress will be addressed in section 6.2.

The visualisations showed that the coarser obstacles are the important ones in defining the spatial scales associated with the inner zone flow structure. In the following analyses, D_{84} and k_{84} will be used as descriptive roughness parameters.

(b) Mean hydraulics

The size and ejection frequency of vortices from the inner zone is not only determined by the roughness, but also by the mean flow hydraulics. If the structures associated with the high absolute stress values in the quadrants are associated with the ejection of inner zone vortices, then their ejection frequencies would be loosely defined by the Strouhal number (Equation 2.11) which incorporates the mean flow field velocity. Similarly, if the events are the product of shear instability between the inner and outer zones, then mean flow hydraulics is again significant, this time in defining the rate of shear through the transition zone.

There is no definite evidence as yet as to how the mean hydraulics affects the thickness of the inner and transition zones. At higher mean velocities, although more energy would be associated with the ejections implying that they would project further from the inner zone, thickening the transition zone, the increased momentum of the outer zone would have the opposing effect of subduing the height of the ejections.

Figure 5.24 attempts to remove the effects of mean τ_0 by plotting the 96th stress percentiles for the four quadrants against y^+. The 96th percentile of absolute stress is arbitrarily chosen as a high stress value. Two main points are immediately apparent. Firstly, these data

do not collapse to colinearity by this method of plotting. Indeed, the three data sets remain broadly distinct, those of higher τ_0 plotting above those of lower τ_0.

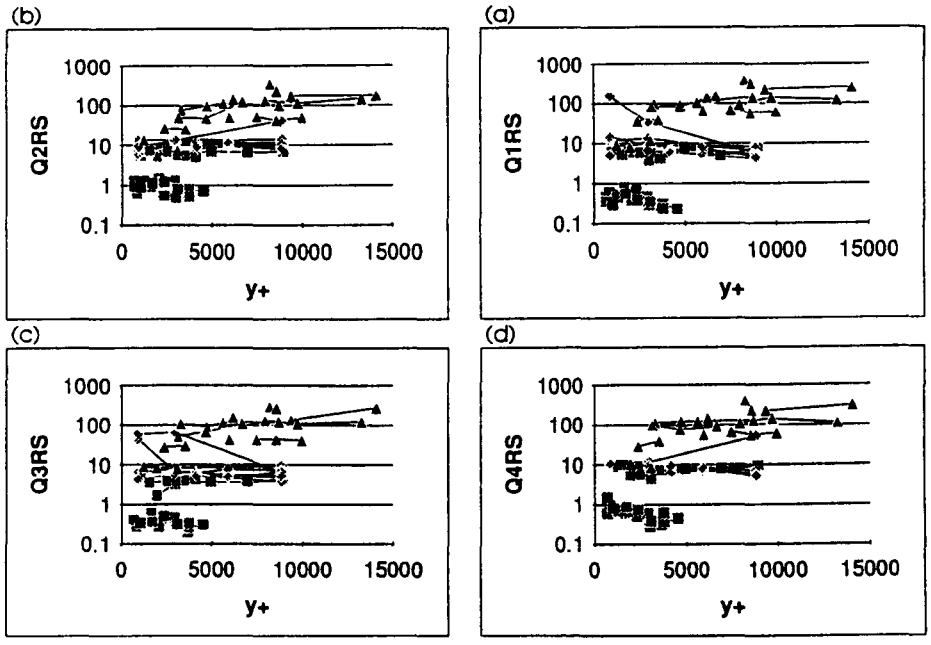

Figure 5.24 The 96th percentile of absolute stress in each quadrant against y^+ for all field data.

Secondly, there appears to be very little variation in $\tau_{R(Qn)}$ (where $\tau_{R(Qn)}$ is the nth percentile stress value) as y^+ increases for any of the quadrants. This means that at the range of τ_0 present here, the magnitude of high τ_R appears to show no dependency on depth.

It is not only the τ_0 values of the Arolla data that are higher than the other data sets; the relative roughness is generally much greater than the other data sets also. Although this could help to explain the difference between the high percentile τ_R for these data, the similarity between the roughnesses of the Beauty Creek and Dubhaig data means that roughness alone cannot explain all of the differences.

In order to account for the effect of both τ_0 and roughness on $\tau_{R(Qn)}$, Figure 5.25 plots $\tau_{R(Qn)}/\tau_0$ against y/k_{84}. The data still do not collapse to co-linearity. It is significant however that the distinction between the Beauty Creek and Arolla data sets is less marked, whereas the Dubhaig data still plot consistently below.

There are two subtle trends within these data. Firstly, there is a suggestion that below $y/k_{84} \approx 2.5$, $\tau_{R(96)}$ increases in Q1 and decreases in Q2, suggesting that in this region, outward interactions are accounting for the high stress at the expense of ejections. This is interpreted as evidence of the extent of the transition zone.

Secondly, as y/k_{84} increases above $y/k_{84} \approx 2.5$ there is a perceptible decrease in $\tau_{R(96)}$ in Q1 and Q4. This means that the high stresses associated with outward interactions and sweeps decrease higher in the profile.

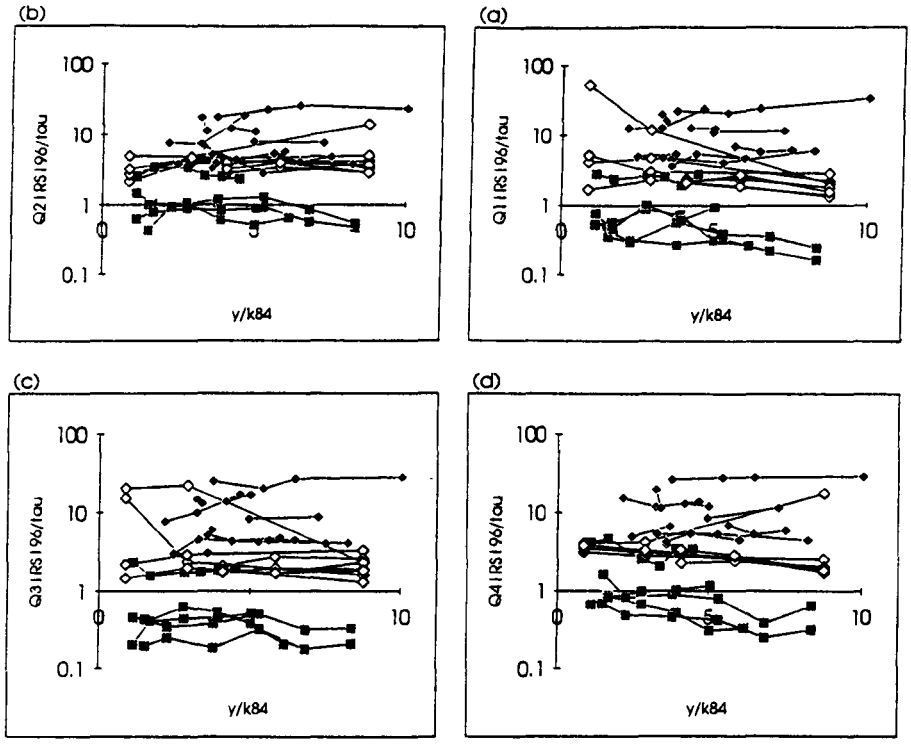

Figure 5.25 The ratio of the 96th percentile of absolute stress in each quadrant to τ_0 against y/k_{84} for all data.

5.5 Movement of the u-v vector in the u-v plane

Chapter 4 showed that the structures within the boundary layer represent organisation within the turbulent flow field which is coherent over centimetres and at least tenths of seconds. The basis of this section (5.6) is to consider the monitoring at a stationary point of the advection or convection of any of the structures as pathways through the u-v quadrant diagram.

This approach will be taken at two levels of resolution. Firstly, the likelihood of transitions between quadrants will be described, then more rigorous analysis of transfer in the u-v plane will be outlined and interpreted. Using a similar type of analysis to that used in section 4.2.6, this will attempt to characterise repeating sequences of vector movement, and interpret these with respect to the proximity to the bed, mean hydraulics and bed roughness.

5.5.1 Transfers between quadrants

Each of the four quadrants are defined by a unique combination of the signs of u' and v'. In a similar manner to that used in section 4.2.6, let us propose that a change in quadrant is most likely to occur with the change in sign of just one of the components. This essentially means that transfer is more likely to take place between adjacent quadrants rather than opposites, i.e. the least likely changes are between Q1 to Q3 and Q2 to Q4.

Derivation of the transition matrices reveals three main points. Firstly, retention within a quadrant is universally more likely than change to another. This is the case in all files regardless of whether they were sampled at 4Hz (Arolla and Dubhaig) or 10 Hz (Beauty Creek). Secondly, and perhaps more importantly, the equi-probability of quadrant transition described in the previous paragraph does not generally apply. Indeed, for all of the Dubhaig

and Beauty Creek data, the most likely transfers occur between v'>0 and v'<0 i.e. Q1→Q4 and Q2→Q3. This is also the case in over 2/3rds of the Arolla data, the other 1/3rd being made up of Q1→Q2 or Q3→Q4 transfers. There were never any transfers between quadrants Q1→Q3 or Q2→Q4. Thirdly, there is a suggestion that the Q1 to Q4 and Q3 to Q2 transitions are more probable than Q4 to Q1 and Q2 to Q3.

Two initial conclusions can be drawn from these findings. Firstly, it suggests that the vectors are quasi-stable in states of either u'>0 or u'<0, moving within these halves of the quadrant field and only occasionally crossing to the other. This supports the finding of sections 4.2.2 and 4.2.4 that the high speed or low speed forms of the velocity profiles are the most stable.

Secondly, the preferential transfer from Q1 to Q4 and Q3 to Q2 (compared to Q4 to Q1 and Q2 to Q3) suggests that rotation is a characteristic of the vector movement. Certainly, the absence of any transfer between opposite quadrants supports this idea. Rotation suggests a more organised mode of quadrant transfer, and would relate to the movement through the sensing field of coherent flow structures.

5.5.2 Sub-sectors of the u-v quadrants

The clear finding that transfers between adjacent quadrants are not equi-probable leads to the question to be addressed in this section which concerns what happens leading up to and directly after a quadrant transfer. In a broader sense, the main objective of this section is to attempt to derive sequences of vector changes in the u-v plane. In doing this, the variations in persistence of the vectors within the different parts of the u-v plane will also be investigated.

The use of only four quadrants to describe the vector position in the u-v plane is rather crude. In order to define these positions in more detail, the plane will be subdivided into several smaller sectors. This should then allow movement within a quadrant to be assessed as well as that between quadrants. Two methods of subdividing the quadrants and defining the sectors will be used, one based on stress, the other on velocity.

(a) Splitting by isostress lines

As stress is essentially a product of u' and v', it is possible to show lines of equal stress on the u-v quadrant plot. These are represented by asymptotic lines, where higher stresses plot further from the <u>,<v> origin. For the purposes of defining sectors in the u-v plane, the 50th and 84th percentile isostresses will be used. By definition, there are more likely to be transitions to or from the <50th percentiles, but these data are grouped together as they are not considered to be important with respect to illustrating structure or being of importance regarding entrainment. These isostresses define 12 sectors which are shown in Figure 5.26a.

The 84th percentile was used rather than the 96th due to problems derived from the limits of the sample length. As much of the data used contained only 400 points, the estimation of the 96th percentile would be rather inaccurate. Also, there are likely to be very few points in the >96th percentile sector.

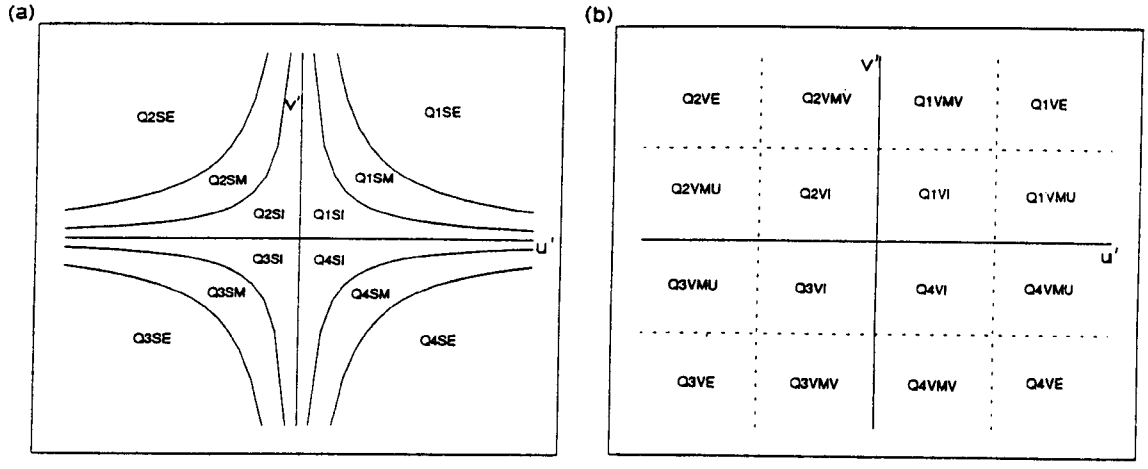

Figure 5.26 (a) 12 quadrant sectors defined using <u>, <v> and the 50th and 84th percentiles of absolute stress in each quadrant. Sector names are derived from the quadrant number, "S" for stress-defined sector, and "E", "M" or "I" for extreme, middle or inner sectors. (b) 16 quadrant sectors defined using <u>, <v>, σ_u and σ_v. Sector name are derived from the quadrant number, "V" for velocity-defined sector, "E" and "I" for extreme or inner, or "MV" or "MU" for middle adjacent to the <v> or <u> axes.

The sectors will be identified by the quadrant number in which they exist, "S" for stress, and either "E" for extreme (>84th percentile), "M" for middle (84th>M>50th) or "I" for inner (<50th percentile).

(b) Splitting by velocity

In order to define sectors using velocity, the standard deviations of u' and v' are used to define the sector boundaries. This produces 16 sectors in a regular grid as shown in Figure 5.26b. Analysis of movement between these sectors will provide better resolution of the spatial movement of the vectors than the stress defined sectors.

The sectors will be identified by their quadrant number, "V" for velocity and one of "E" for extreme, "I" for inner, "MU" for adjacent to the <u> axis but $>\sigma_u$ or $<-\sigma_u$, or "MV" for adjacent to the <v> axis but $>\sigma_v$ or $<-\sigma_v$.

5.5.3 Persistence within the sub-sectors

Consider Figure 5.27. The vertical axis represents the number of single "transfers" involving staying in the same sector as a percentage of the total number of transfers in the series (i.e. n-1). The sectors shown are the "extreme" (>84th stress percentile) sectors of the isostress sector plot.

A probability transition matrix for one of the series of the AD30 data set is shown in Table 5.7. It shows that there is a definite preference for the vector to stay in the same sector, as shown by the high transition probabilities in the top left - bottom right diagonal. High values do not necessarily mean that the vectors remain in the sector for any longer than low values,

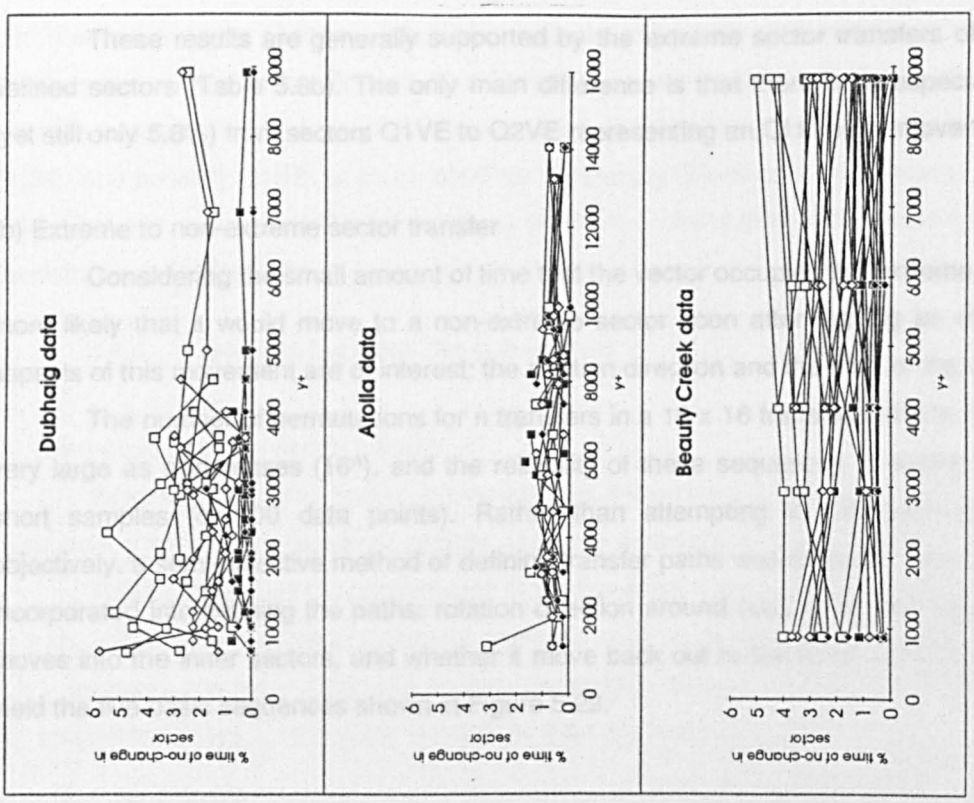

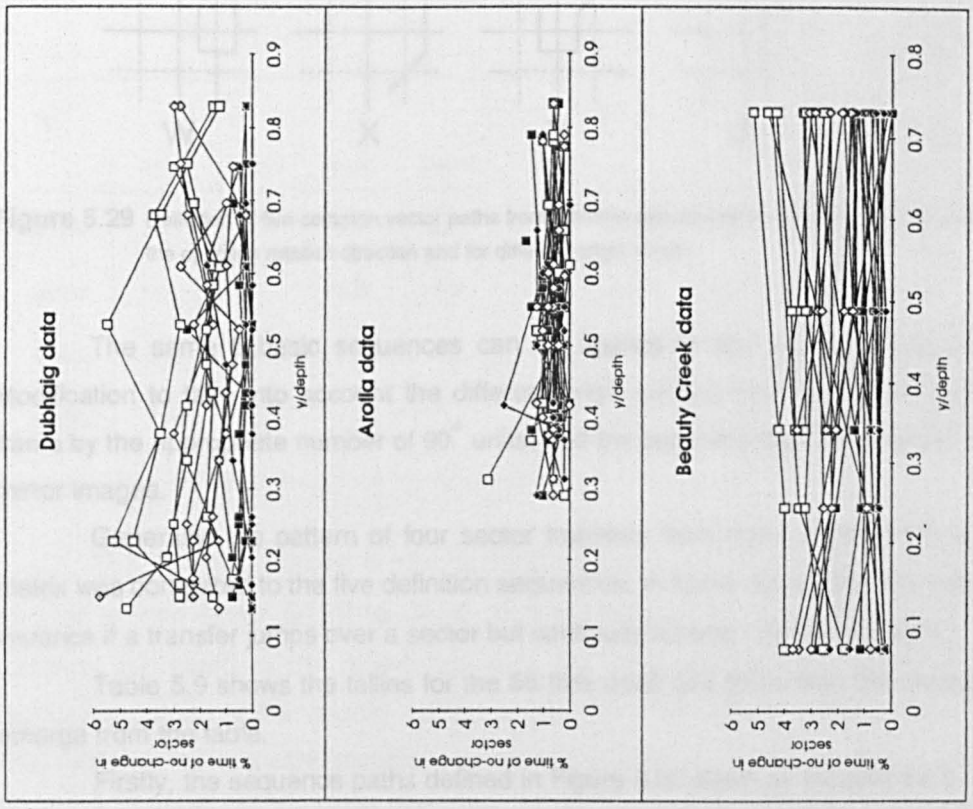

Figure 5.27 The percentage time of no-change from isostress defined extreme sectors against y/depth.

Figure 5.28 The percentage time of no-change from isostress defined extreme sectors against y^+.

but it is inferred that associated with an increase in the number of consecutive sample residence would be an increase in persistence.

Table 5.7 Probability matrix for transitions between sectors of the u-v plane (from rows to columns).

	:	:	:	:	:	:	:	:	:	:	:	:
QIVE:	0	2	1	0	0	0	0	0	0	2	2	1
QIVMV:	1	1	4	0	1	1	0	0	0	1	3	3
QIVMU:	3	4	9	0	0	6	0	0	4	0	9	8
QIVI :	0	1	1	19	7	5	0	1	1	0	0	0
:	0	2	4	6	14	8	0	2	6	0	0	5
:	1	3	3	5	10	6	0	2	9	0	0	3
:	0	0	0	0	1	1	0	1	0	0	0	1
:	0	0	0	4	7	0	0	3	3	0	0	1
:	0	0	3	0	5	9	3	6	12	0	4	7
:	0	1	1	0	0	0	0	0	0	5	3	8
:	2	1	6	0	1	1	0	1	3	7	23	10
:	0	1	11	1	1	6	0	2	11	3	11	18

In Figure 5.27, the Dubhaig and Beauty Creek data occupy more time in the high stress sectors of Q2 and Q4 than the Arolla data. As the Arolla data represent higher values of τ_0, this suggests that high stress Q2 and Q4 events are less persistent than at lower τ_0 (Dubhaig and Beauty Creek).

The high stress events of Q2 and Q4 represent sweeps or ejections , those events associated with gravel entrainment and sediment suspension respectively. If intermittent entrainment at marginal transport conditions is influenced by such events (as suggested by coastal workers, e.g. Williams *et al*, 1989), it suggests that it is either very high stress events of low persistence which provide enough of a "shock" to move sediment, or that the sediment reacts to the lower stress but (presumably) more persistent events. This is discussed in further detail in section 6.4.

If it can be proposed that associated with the lower τ_0 conditions of the Dubhaig and Beauty Creek data would be lower mean advection velocities of flow structures, then it would be expected that the monitored structures would persist for longer. The implication of this is that the low persistence of the high stress events in Q1 and Q3 at any τ_0 suggests that structures in these quadrants exhibit little coherence in comparison to those of Q2 and Q4.

The purpose of plotting these data against y/d is to determine whether the persistence of the high stress events within the sectors shows any relation to the position relative to the

bed. For the majority of these data, there appears to be very little systematic variation with depth in any of the sectors. Figure 5.28 a-c show the same data as 5.27, but plotted against y^+. There is a suggestion that as y^+ decreases, there is a slight increase in percentage in sector Q4SE (and possibly Q1SE) at $y^+ <= 3000$ for the Beauty Creek data and some of the Dubhaig data. This would suggest that at lower τ_0 conditions, the sweep-like events become more persistent near to the bed.

5.5.4 Transfers between the subsectors

(a) Extreme to extreme sector transfer

Extreme to extreme sector movement was determined by allowing the transfer to take place over 5 links for the isostress sectors, and over 4 sectors for the velocity defined sectors.

Table 5.8a shows the percentages of the transfers which took place from each extreme to every other potential extreme for the isostress sectors. It supports two findings of section 5.5.1: transfers are more likely with an associated sign change in v' and transfers from Q1 to Q4 and Q3 to Q2 are considerably more likely than the reverse.

Table 5.8 Percentages of transfers taking place between extreme sectors defined by (a) isostress lines (b) mean and standard deviation of u and v (from rows to columns).

(a)

	Q1SE	Q2SE	Q3SE	Q4SE
Q1SE	-	2.1	2.1	23.2
Q2SE	1.1	-	5.3	6.3
Q3SE	1.1	32.6	-	4.2
Q4SE	11.6	10.5	0	-

(b)

	Q1VE	Q2VE	Q3VE	Q4VE
Q1VE	-	5.8	0.0	17.4
Q2VE	2.3	-	1.2	2.3
Q3VE	0.0	25.6	-	0.0
Q4VE	11.6	0.0	0.0	-

The strongest transfer is from sector Q3SE to Q2SE, an II (inward interaction) to ejection. The other strong transfer is from sector Q1SE to Q4SE representing an OI (outward interaction) to sweep. The strength of these transfers compared to the others suggests that they represent a significant tendency for clockwise rotation of the velocity vector in either the high speed or slow speed states rather than between fast and slow speeds.

It is worthy of note that there was never a sector Q2SE - Q4SE transfer, although a weak transfer exists from sector Q4SE to Q2SE. These would relate to the coupling of sweeps-bursts-sweeps, and the absence of strong transfers suggests that the sequence of a burst-sweep cycle is more complex than simply movement between Q2 and Q4.

These results are generally supported by the extreme sector transfers of the velocity defined sectors (Table 5.8b). The only main difference is that there is a respectable transfer (yet still only 5.8%) from sectors Q1VE to Q2VE representing an OI to burst movement.

(b) Extreme to non-extreme sector transfer

Considering the small amount of time that the vector occupies the extreme sectors, it is more likely that it would move to a non-extreme sector soon after leaving an extreme. Two aspects of this movement are of interest: the rotation direction and the path of the vector.

The number of permutations for n transfers in a 16 x 16 transition matrix soon become very large as n increases (16^n), and the reliability of these sequences is limited by relatively short samples (c. 400 data points). Rather than attempting to characterise sequences objectively, a semi-objective method of defining transfer paths was devised. Three criteria were incorporated into defining the paths: rotation direction around (<u>,<v>), how soon the vector moves into the inner sectors, and whether it move back out to the outer sectors again. These yield the five basic sequences shown in Figure 5.29.

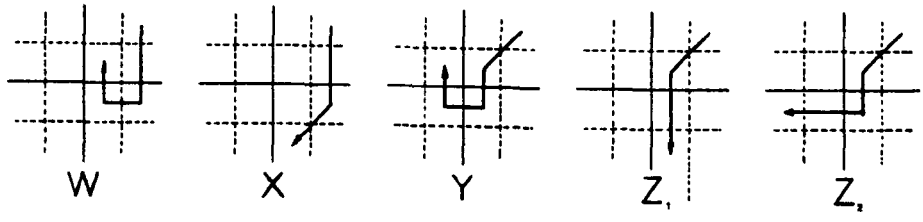

Figure 5.29 Definition of five common vector paths from extreme velocity-defined sectors. They can be modified for the opposite rotation direction and for different origin sectors.

The same 5 basic sequences can be applied to any of the 4 extreme quadrants. Modification to take into account the different origin sectors can be made by rotation of the frame by the appropriate number of 90° units, and the opposing rotation direction by using their mirror images.

Generally, the pattern of four sector transfers from each extreme for each transition matrix was compared to the five definition sequences. In some occasions this was modified, for instance if a transfer jumps over a sector but continues around one of the paths.

Table 5.9 shows the tallies for the 86 files used (the three field data sets). Four points emerge from the table.

Firstly, the sequence paths defined in Figure 5.29 seem to account for c. 60% of those leaving from extreme sectors. Of those which do not, they are random, confused sequences showing no systematic patterns.

Secondly, preferential transfer across the v'=0 axis again emerges. This is shown by the higher values in the clockwise cells compared to the anti-clockwise for sectors Q1VE and

Q3VE and vice-versa for sectors Q2VE and Q4VE. This is universal for all of the extreme sectors and paths except for those of Z_2.

Table 5.9 Percentages of sector transfer sequences from extreme sectors following the five common routes defined in Figure 5.29.

Sequence:	Direction:	Q1VE	Q2VE	Q3VE	Q4VE	Totals
W	Clockwise:	3.5	1.2	3.5	4.7	24.5
	Anti-clockwise:	0.0	5.8	0.0	5.8	
X	Clockwise:	30.2	11.6	37.2	3.5	133.7
	Anti-clockwise:	3.5	20.9	3.5	23.3	
Y	Clockwise:	8.1	1.2	9.3	2.3	44.1
	Anti-clockwise:	3.5	5.8	2.3	11.6	
Z_1	Clockwise:	11.6	1.2	5.8	1.2	38.5
	Anti-clockwise:	1.2	7.0	0.0	10.5	
Z_2	Clockwise:	2.3	2.3	1.2	7.0	19.8
	Anti-clockwise:	0.0	2.3	1.2	3.5	
None		36.0	40.7	36.0	26.7	139.4

Thirdly, some of the paths emerge as more popular than others. Path X is undoubtedly the most popular regardless of the start sector. This represents at least two transfers in the outer sectors before moving into the inner ones. As these movements remain on the same side of the <u> axis as the origin sector, it suggests that it is associated with periods of transient high or low momentum streamwise flow in agreement with the findings of the fluctuating velocity profiles of sections 4.2.2 and 4.2.4.

Path Y is the second most common sequence. It involves movement into the inner sectors and rotation around (<u>,<v>). Transfer into the inner sectors suggests the end of a high stress event, intuitively interpreted as the departure of a structure and reversion to the ambient lower momentum conditions. As the investigation of the movement around the inner sectors comprises the following sub-section, it shall not be discussed here, but is the subject of the next section.

Path Z involves the same number of crossings and re-crossings of the <u> and <v> axes as X, but takes place in the inner sectors. The common rotational direction with the equivalent X origins suggest that these represent similar structures, but the lower % occurrence values mean that they are less likely to occur.

Path W involves the crossing and re-crossing of the same axis without the crossing of the other. This implies that it represents fluctuations on one of the velocity components while the other maintains its value relativeto the mean. This path is not very common and sometimes rather confused.

The structuring of the boundary layer into an inner zone comprising ejecting vortices, an outer zone of advecting vortical structures, and a transition zone, leads to the proposition that these may be discernible by differing u-v vector paths. As the actual composition of these zones is not definitely known, it is not possible to say what these will be.

Figures 5.30a-c show plots of vector path identifiers against y/depth, y/k_{84} and y^+. The remarkable randomness of the plots means that there are no systematic shifts in the preferred paths taken from the extreme sectors as determined by distance from the bed relative to depth, roughness or τ_0. This does not necessarily mean that there is no variation in the composition of the turbulence structure with distance from the bed, but that this method of characterising the nature of the structure is not sensitive enough to differentiate it.

(c) Movement within the inner sectors

The previous two subsections showed that in the outer sectors, movement tends to head towards and across the axis of v' = 0. This section will investigate firstly the direction of rotation within the inner sectors, and then the paths that originate within the inner sectors but move into the outer ones. The general approach taken involves considering an increasing number of transfers.

Table 5.10 Percentages of clockwise or anticlockwise rotation of the u-v vector from the inner (velocity defined) sectors.

Origin sector:	Q1VI	Q2VI	Q3VI	Q4VI
% clockwise:	73	15	59	19
% anticlockwise:	27	78	16	74

Table 5.10 shows the percentages of the rotation directions taken within the inner sectors involving one transfer. It clearly supports the preference to cross the v' = 0 axis rather than u' = 0 axis. Movement from sector Q3VI is six times more likely to be anti-clockwise than clockwise, and the lowest differential of preferred direction (sector Q1VI) is still $2^1/_2$ more likely to go clockwise than anti-clockwise. However, the tendency for clockwise rotation is markedly muted in comparison to transfers from the extreme sectors.

Once the v'=0 axis has been crossed, the likelihood of the vector continuing in the same corridor parallel to one of the axes is similar to crossing the axis. There is also a relatively small but consistently finite chance of crossing through the (<u>,<v>) origin, but any other transfers are very insignificant.

Of the vectors that go the "wrong" way, they are twice as likely to stay within the inner sectors than move to an outer one. Figure 5.31 depicts the common path shapes which involve one or two transfers from an inner sector origin. Figure 5.32 shows the likelihood of a path originating from an inner sector against the three measures of depth i.e. y/depth, y/k_{84}, y^+. Unlike the equivalent plot for extreme to inner sector paths of Figure 5.30, Figure 5.32 shows

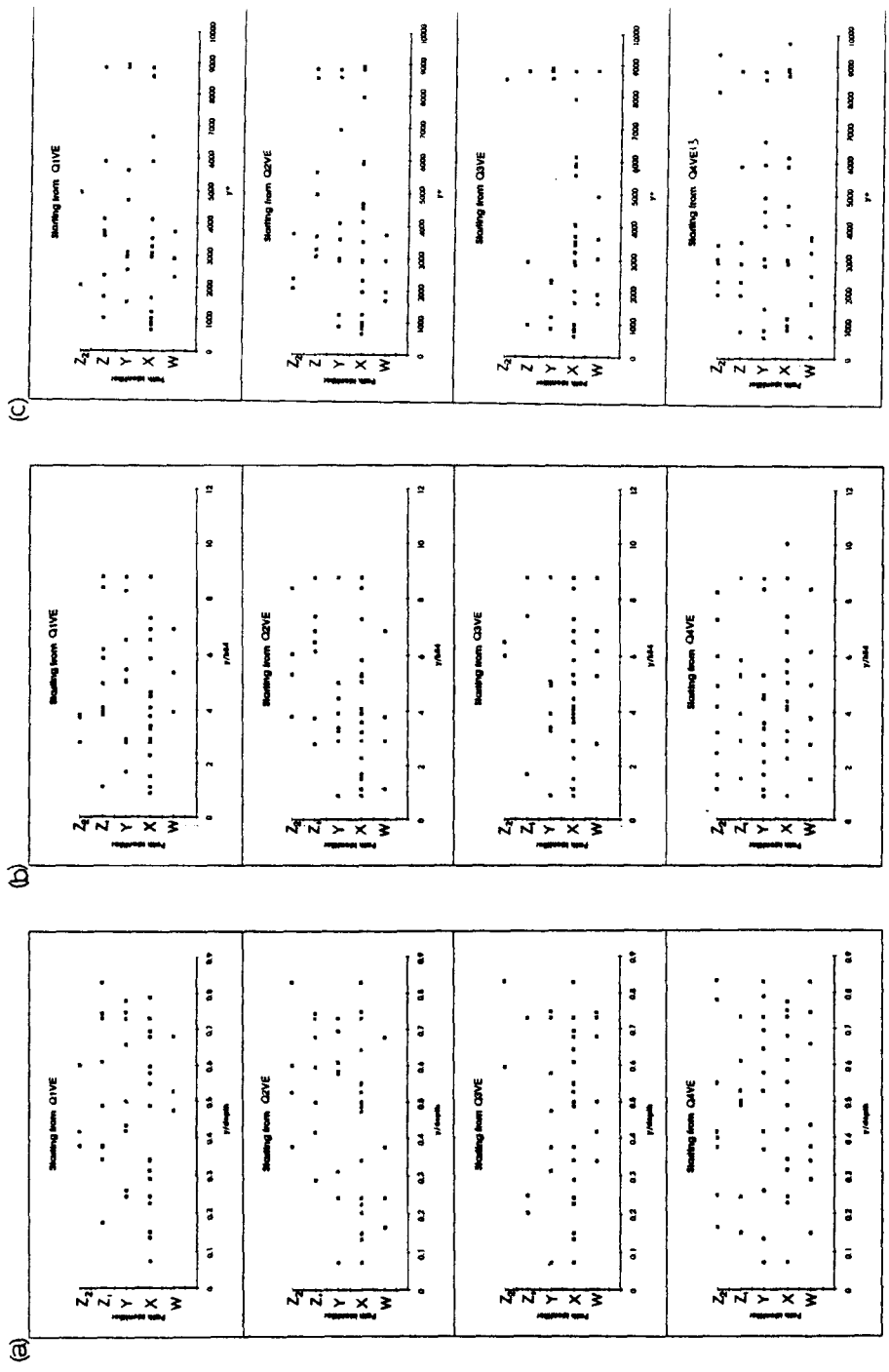

Figure 5.30 The path taken from extreme sectors against (a) y/depth, (b) y/k_{84} and (c) y^+.

that the chance of heading the "wrong" way from an inner sector tends to be greater at higher values of y/depth, y/k_{84} or y^+. In all cases, the tendency to rotate the "right" way is still greater than the opposite.

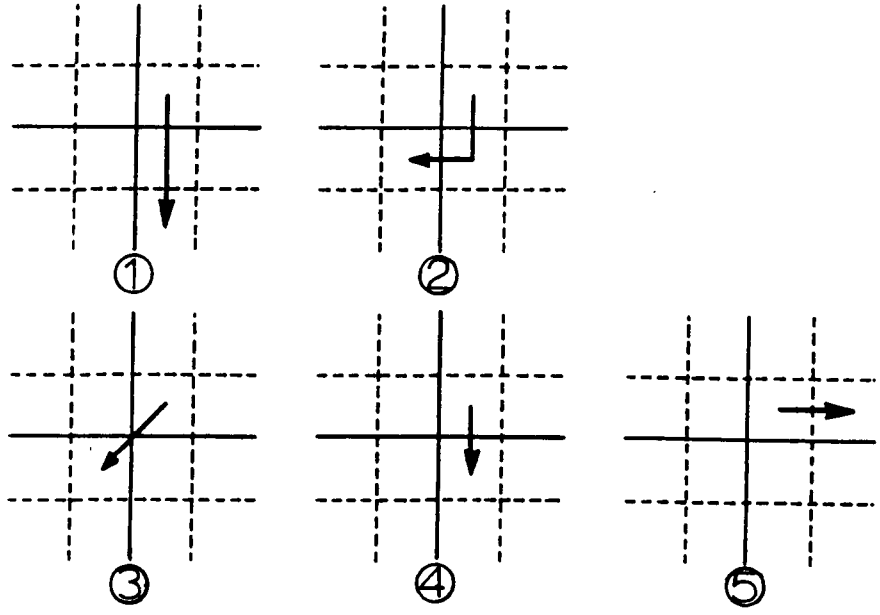

Figure 5.31 Definition of the five common vector paths from inner velocity-defined sectors. They can be modified for the opposite rotation direction and for different origin sectors.

In summary, two main points have emerged in relation to the movement of the velocity vector in the u-v plane. Firstly, the vector is more likely to cross the v' = 0 axis than the u' = 0. This supports the findings of the fluctuating velocity profile analysis that the flow exists in quasi-stable high-speed or low-speed states with other fluctuations superimposed upon them. The wider range of boundary conditions incorporated into this analysis suggests, however, that this phenomena is more widespread in boundary layer flows over fluvial gravel beds beyond the specific conditions of the Beauty Creek site.

Secondly, there is no substantial evidence that distance from the bed or roughness have any influence on the movement characteristics of the velocity vector in the u-v plane. There is a suggestion that at conditions of higher τ_0 the preference to cross the v' = 0 axis weakens with distance from the bed, but it is not possible to support further this assertion.

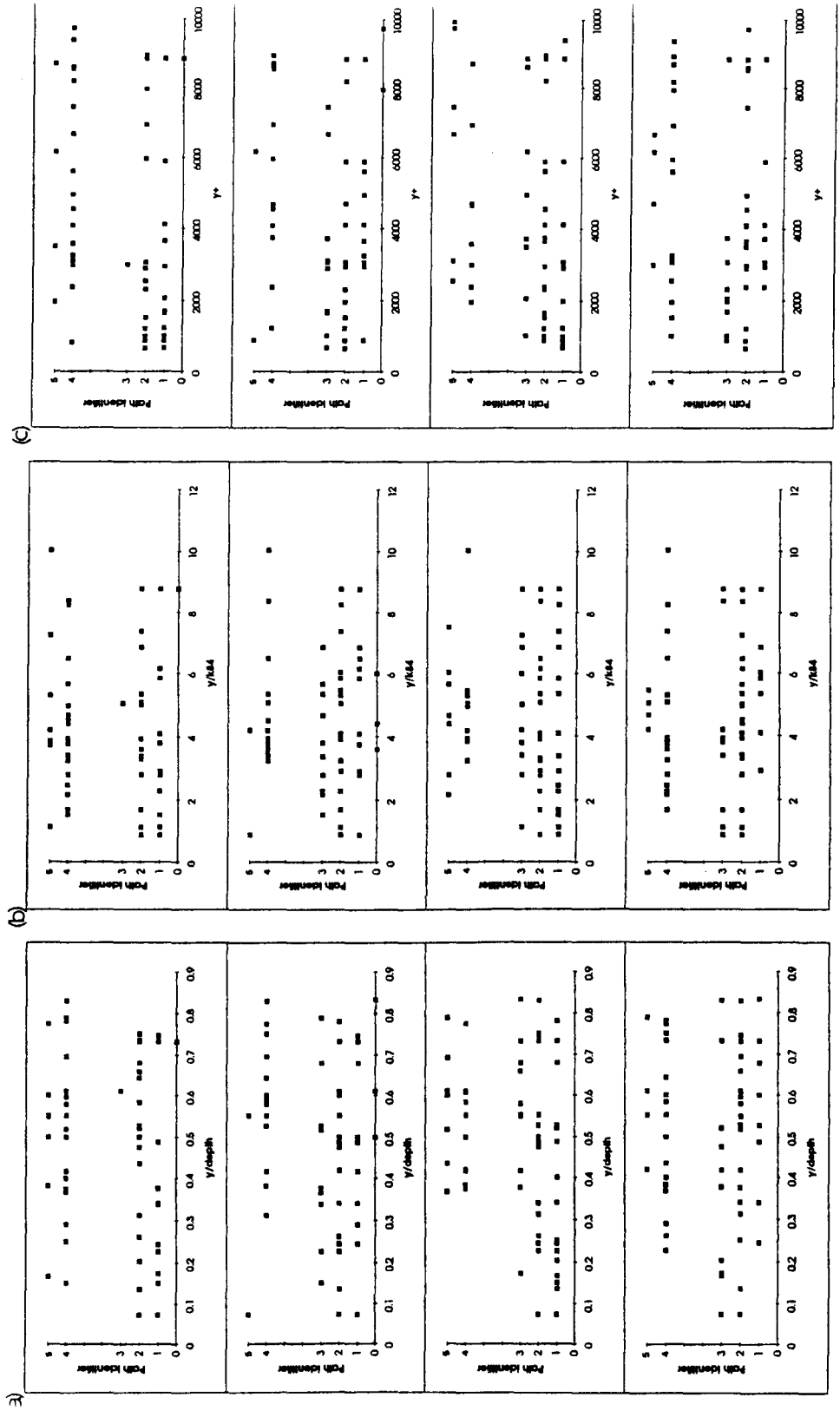

Figure 5.32 The path taken from inner sectors against (a) y/depth, (b) y/k_{84} and (c) y^+.

5.6 Stress intermittency

Figure 5.33 shows the same corresponding time series of u and v as shown in Figure 5.8 and the time series of τ_R. The time series of τ_R suggests that significant fairly discrete fluctuations from the mean τ_R exist, yet these do not necessarily correspond to obvious fluctuations in the velocity components. This implies that the temporal characteristics of τ_R may be different from those of the velocity time series.

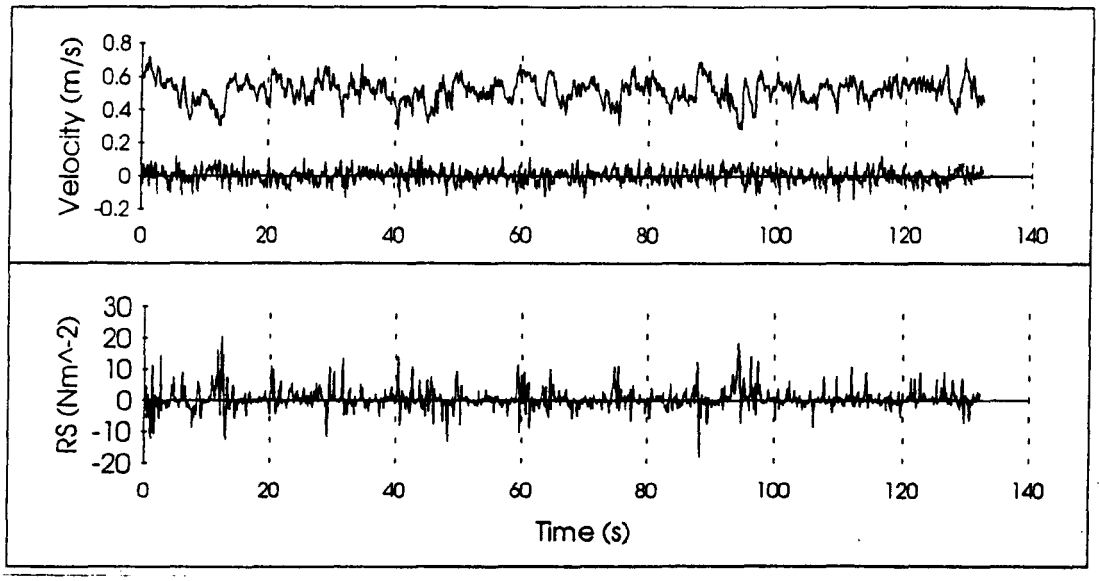

Figure 5.33 Time series of u, v and τ_R for one of the Beauty Creek files.

These observations raise two sets of questions; the first relate to the temporal characteristics of the structures, and how they relate to mean hydraulics, roughness and position in the profile. These will be addressed in sections 5.7 and 5.8. The second ask why such obvious fluctuation events emerge from the stress series and not from the velocity series. This is addressed in the next section.

5.7 Spectral analysis of Reynolds stress time series

Power spectra of the τ_R series were generated using the same routines as used for the velocity series (section 5.2.3). The spectra were plotted against period and are shown in Figures 5.34, 5.35 and 5.36 for the field data sets. They are arranged in the relative position to that which they were taken in the profiles.

The difference between these spectra and those of velocity is the presence of clearly defined peaks. The fact that these emerge in the spectra of τ_R yet not in the individual spectra of u or v suggests that the temporal structure of the flow is expressed jointly in both components of velocity together. The absence of one of the components removes too much information to allow the resolution of the temporal structure through the other component alone, rather like attempting to identify a melodic tune by listening only to the bass line.

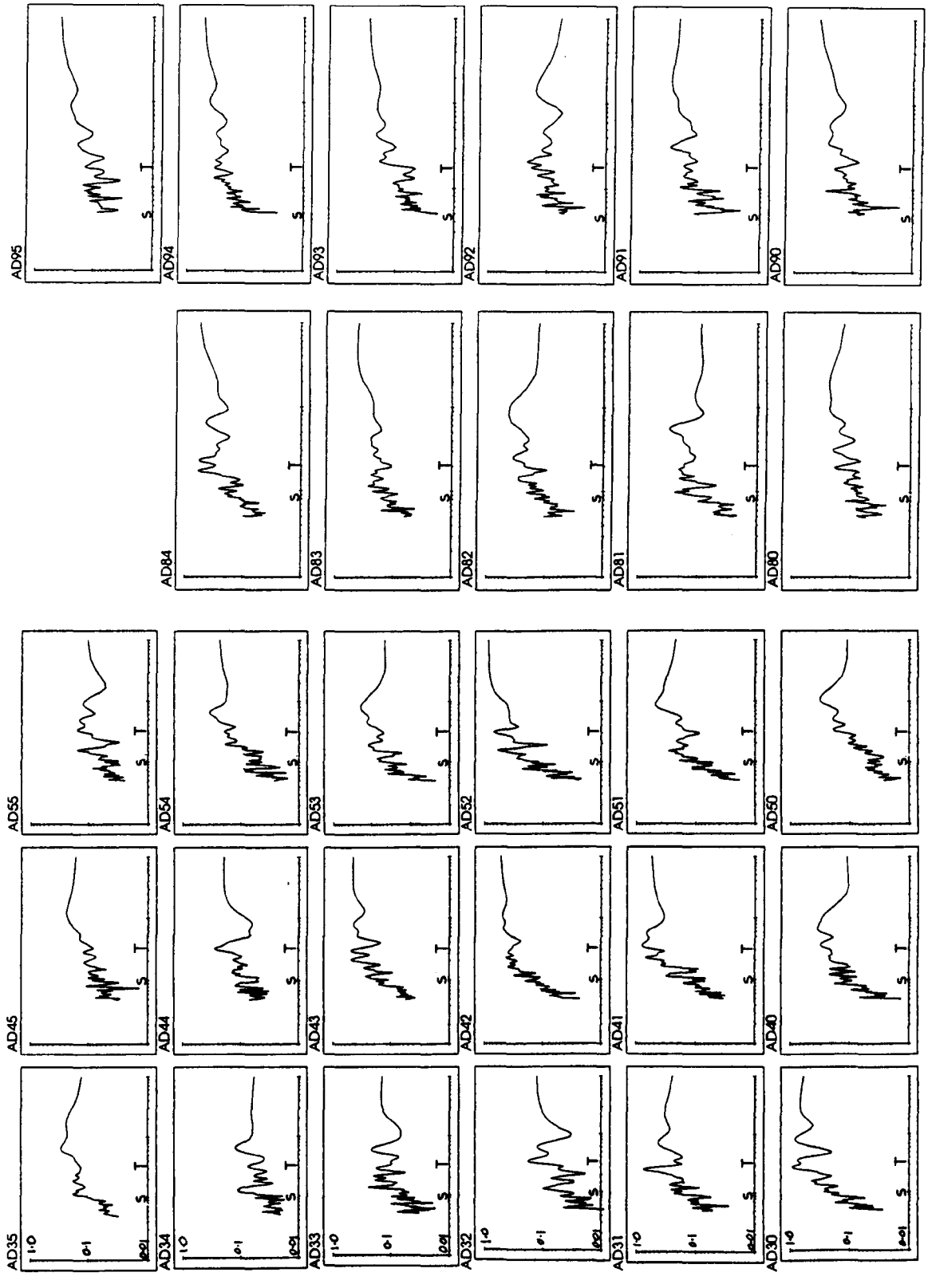

Figure 5.34 Spectra of τ_R for the Dubhaig data. Symbols are referred to in discussion in Chapter 6.

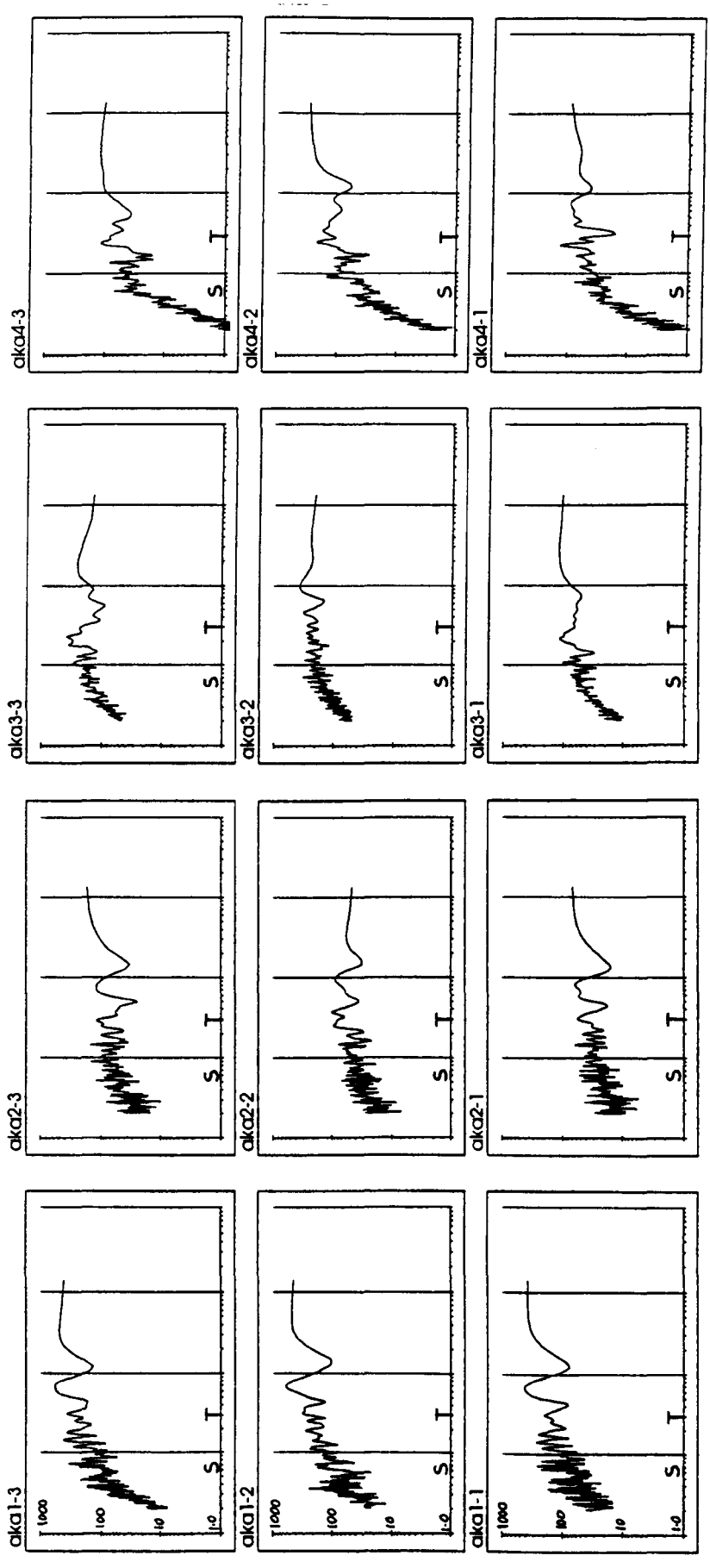

Figure 5.35 Spectra of τ_R for the Beauty Creek data, A files. Symbols are referred to in discussion in Chapter 6.

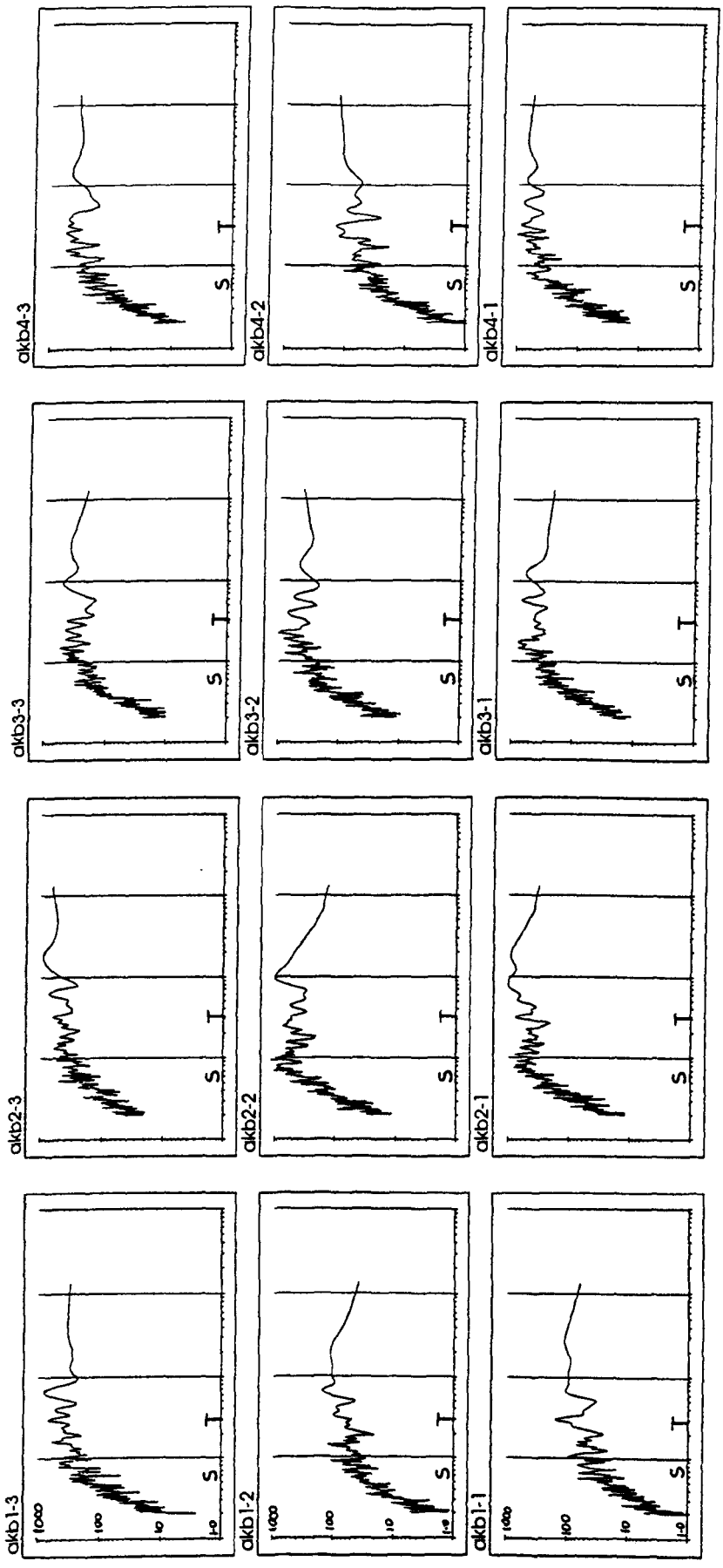

Figure 5.35 Spectra of τ_R for the Beauty Creek data, B files. Symbols are referred to in Chapter 6.

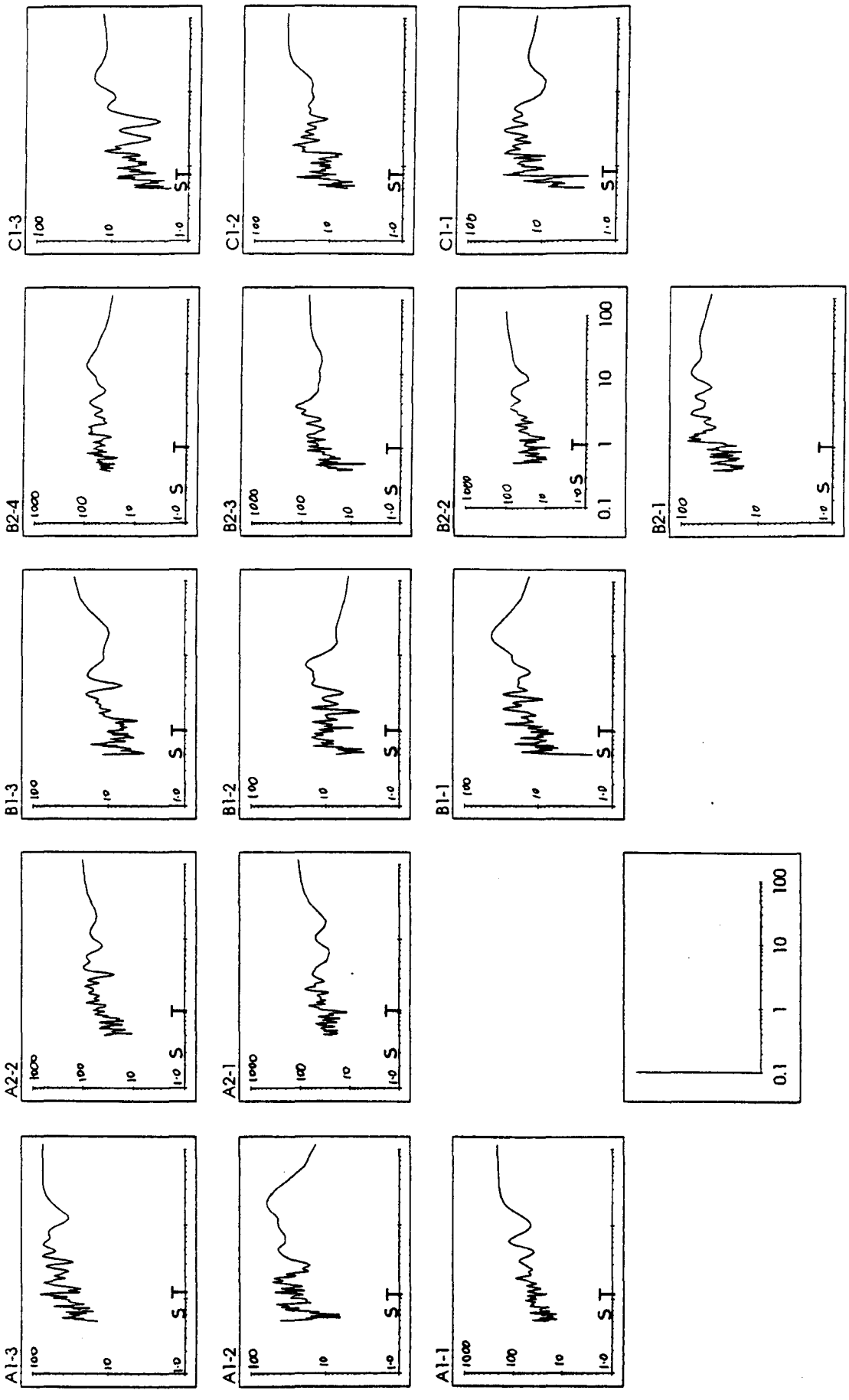

Figure 5.36 Spectra of τ_R for the Arolla data. Symbols referred to in Chapter 6.

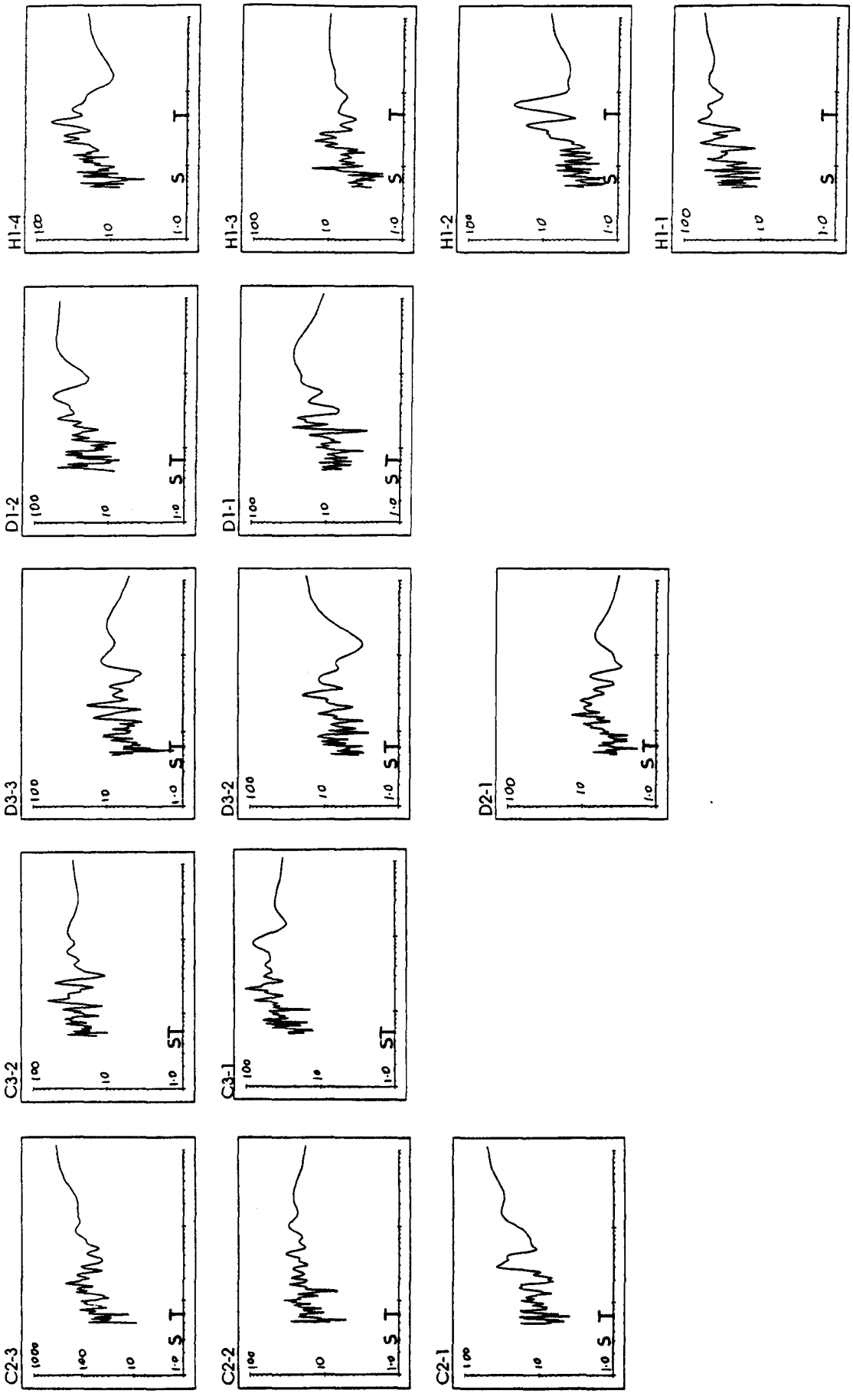

Figure 5.36 Spectra of τ_R for the Arolla data (continued).

Generally, there are far fewer peaks in these spectra compared to those of velocity, and the peaks tend to be more clearly independent of the surrounding spectrum. Although many of the spectra show single dominant peaks, many have multiple yet still significantly independent peaks (e.g. AD30). This suggests that several regimes of macro-turbulence co-exist to produce flow structures with differing temporal signatures.

(a) Beauty Creek data

Figure 5.35 a & b show the τ_R spectra for the Beauty Creek A and B files. The four profiles in each of the figures were taken as replicates of each other.

For each profile, the spectra at the different points are remarkably similar in the position of the dominant peaks and the height of the peaks relative to the lower period part of the spectra. For instance, the different points in the AKA1 profile yield a dominant peak at c. 6.8-7.2s, the power being c. 150% that of the lower period peaks; the AKB3 profile seems to have two sets of peaks at c. 1-3s. and 5-12s.

The presence of such obvious dominant peaks and the similarity of their period within each profile is strong evidence for the presence of coherent flow structure with a consistent temporal signature.

There appears to be no systematic variation in the period of the dominant peak within each profile. This suggests that the timescale of the flow structure is independent of the distance from the bed.

The conversion of temporal scale of the stress intermittency to a spatial scale of the apparent structure producing the signature can be made by multiplying the timescale by the mean velocity for the point. As all of the velocity profiles of these data approximate to logarithmic in form and that period is roughly constant with depth, this means that the spatial scale of turbulence also increases with the logarithm of distance from the bed.

Let us consider the dominant peak in the AKB2-2 spectrum in Figure 5.35b. The period of the peak is 10s, and the mean velocity of the u component at this point is $0.63ms^{-1}$. If we are proposing that this peak relates to a flow structure, its size would be 10x0.63 = 6.3m. It is clear that structures of this size cannot exist within the boundaries of the flow depth. This means that the periods emerging from the spectral analysis are not related to a single physical flow structure, but to a cyclical change in condition. Intermittent ejections of a vortex from an obstacle separated by periods of relative inactivity would, in the absence of any other structure, be resolved through spectral analysis as the period from ejection to ejection rather than of the advection of the vortex itself. In this respect, the periods being resolved in the Beauty Creek data are more likely to be an artificial spatial scale representing the distance over which the structure generating the important variance in stress would be advected.

A general interpretation of the above arguments suggests that the stress-producing events exist as quasi-periodic transient occurrences which occupy a significant part of the boundary layer.

The variation in spectra between profiles is considerably greater than that between points within a profile. The A and B files were taken as two sets of four replicates, yet the spectra are not replicated. This draws into question the interpretation of the intermittency or quasi-periodicity of any non-replicated file taken over coarse gravels.

It suggests that the specific location of the monitoring rig relative to individual roughness elements is very important in determining the monitored signature of the flow. Robert *et al* (1992) show that the turbulence profile is significantly affected by a roughness transition. The site at Beauty Creek was chosen for its homogeneously rough bed, and so the changes in the turbulence revealed here must be a product of local variation in roughness. This means that the precise location of the rig relative to the local roughness features is essential in order to explain the monitored signals. It also points to the necessity for further research into the effect of individual roughness elements on the downstream turbulence structure.

It is significant that although the spectra of stress are significantly different for the replicate files, the mean velocity profiles are indistinguishable. This suggests that the flow events responsible for the quasi-periodicity are not important in defining the mean velocity profile, and is evidence for the presence of an organised but intermittent structure superimposed on a less structured.

(b) Dubhaig data

The spectra of τ_R for the Dubhaig files (Figure 5.34) again show very clear significant peaks of dominant periodicity. Indeed, the independence of the peaks from the rest of the spectra tends to be even more marked than for the Beauty Creek data. There is also a more marked fall-off in high frequency power of the Dubhaig τ_R spectra compared to those of the Beauty Creek data, which is evidence of smoothing by the of the 0.2s time constant of the ECM used at the Dubhaig.

Unlike the Beauty Creek data, there is not as clear a similarity in the period of the peaks within each profile, and there is more variation in the number of independent peaks within the profiles. There are two possible reasons for this: non-simultaneous sampling and movement of the wading rod between samples.

Section 5.2.3 showed that different spectra can result from different sections of the same velocity series. The τ_R spectra of the four 200s sections of the long (15 minute) Arolla sample (M1-1) are shown in Figure 5.37. There are some similarities between the spectra; all except M1-1d show a significant peak at $\underline{c}$.0.3-0.6s, and the general pattern of the peaks in the 1-10s section is similar. Such similarities draw into question interpretations made of temporal structure from individual peaks. It is clear that the four spectra *are* "similar", but the details of the timescales involved differ. The similarity of the spectrum forms *does* support the presence of turbulence structure at a point, but that the specifics of the structure vary over time, perhaps at another frequency too long to be revealed by the relatively short sample lengths used here.

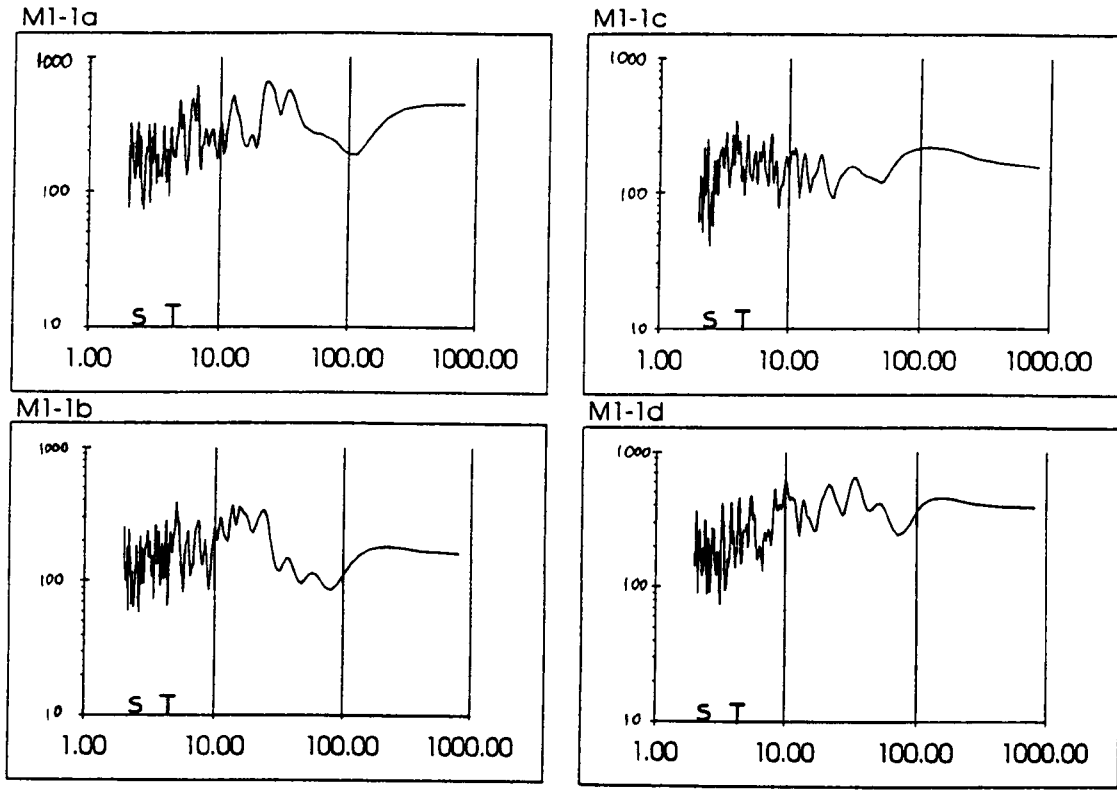

Figure 5.37 Spectra of τ_R for the four sections of the long M1-1 Arolla data file.

Secondly, in between sampling each point in a profile, the wading rod was removed to adjust the height of the probe. Although it was replaced to the same point as precisely as possible (the bed was visible), it is possible that the repositioning was not exact. As was shown with the Beauty Creek data, location of the monitoring rig relative to individual roughness elements appears to be very important in affecting the turbulence signature.

Subjectively, some of the profiles appear to show a degree of continuity in the position of the peaks th rough depth (e.g. profiles AD30-AD35 and AD50-AD55 in Figure 5.34). Most, however, do not, and the multiple peaks fog the patterns. This means that it is impossible to plot the periods of the dominant peaks against depths, although percentiles of the cumulative spectra are plotted in this way in section 5.8.

(c) Arolla data

The τ_R spectra for the Arolla data (Figure 5.36) are considerably more confused than those of the Beauty Creek or Dubhaig data. This is probably due to the considerably higher Reynolds numbers of the flow, higher relative roughness and fewer points in the profiles which makes trends between the points less easy to discern.

The peaks in the τ_R spectra are again more significantly independent than those in the velocity spectra. The absence of continuity of a dominant period through the depths may be

attributable for these data to the same reasons as given for the Dubhaig data, although there are some differences between the two sets of files.

Firstly, the problem of non-simultaneity of sampling of the different points in the profiles is further compounded by bedload transport causing changes in the local bed configuration. This alone probably accounts for the non-similarity of the spectra at the different points.

Secondly, the effect of moving the probe in between samples was minimised as it was attached to a fixed iron bar which had been driven into the river bed. Although there was a degree of movement of this bar, it can be considered as static.

5.8 Cumulative power spectra of τ_R

The periods of the 16th, 50th and 84th percentiles were derived from the cumulative power spectra of τ_R. These are shown plotted against y^+, y/depth and y/k_{84} in Figure 5.38. It should be noted that the differences in the lengths of the data files of the three data sets means that the percentile values are not directly comparable between data sets, but are between files of the same data set.

There is a suggestion that the 84th percentile values show a decrease with increasing y/depth or y/k_{84}. This would mean that as distance from the bed increases, the variance is increasingly not being explained by the longer periods. This suggests that the timescale associated with the turbulence is decreasing with distance from the bed.

The translation of this to the spatial scale can again be made by multiplication of the periods by the corresponding point mean velocity, and again emerge typically as several metres. This can be interpreted as meaning that the longer period contributions to the variance are not associated with a connected succession of single vortical structures which are coherent over space.

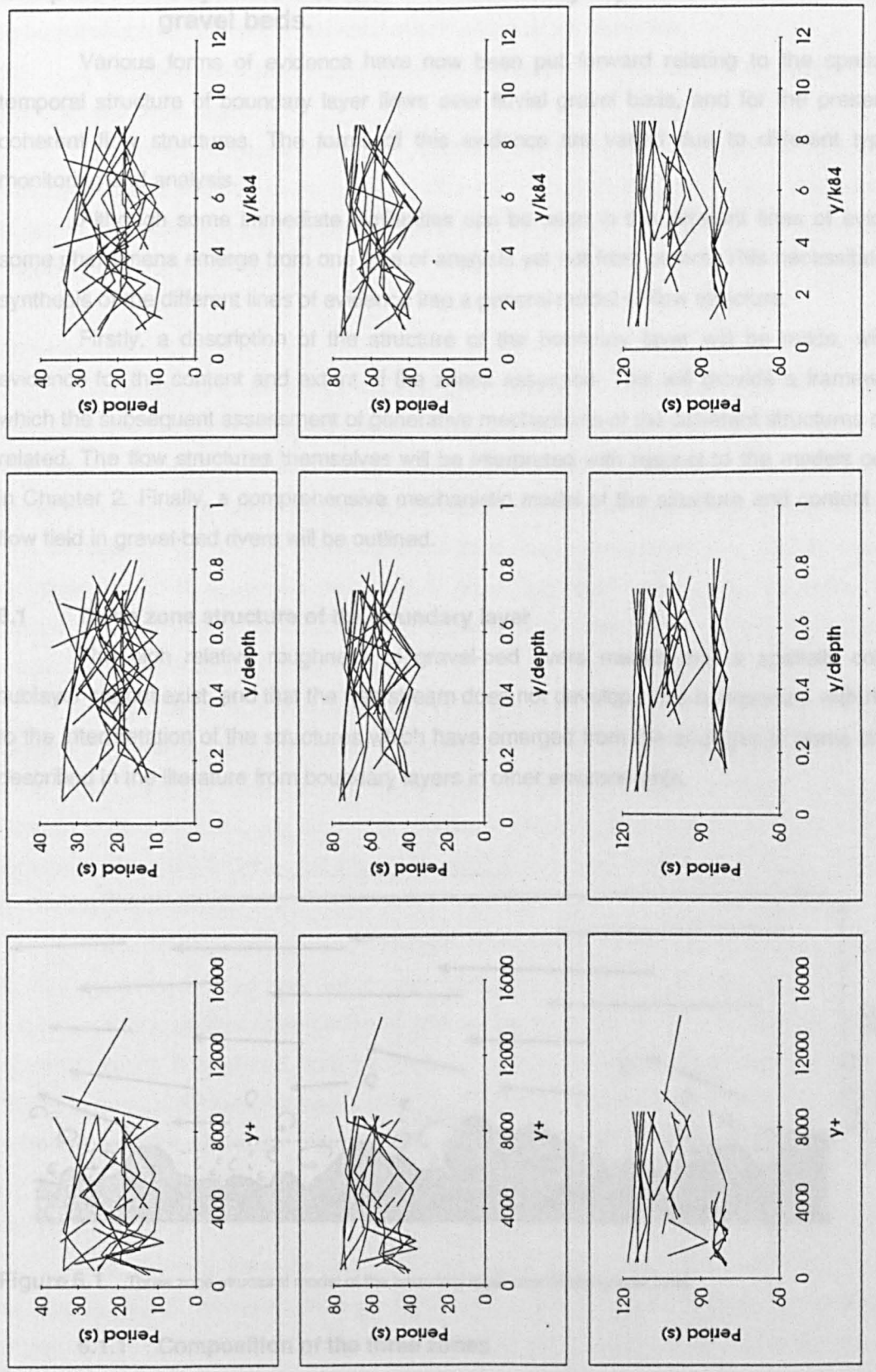

Figure 5.38 Period of the 16th, 50th and 84th percentiles of the cumulative power spectra of τ_R against y^+, y/depth and y/k_{84}.

Chapter 6 A synthesised model of boundary layer structure over fluvial gravel beds.

Various forms of evidence have now been put forward relating to the spatial and temporal structure of boundary layer flows over fluvial gravel beds, and for the presence of coherent flow structures. The forms of this evidence are varied due to different types of monitoring and analysis.

Although some immediate similarities can be seen in the different lines of evidence, some phenomena emerge from one type of analysis yet not from others. This necessitates the synthesis of the different lines of evidence into a general model of flow structure.

Firstly, a description of the structure of the boundary layer will be made, with the evidence for the content and extent of the zones assessed. This will provide a framework to which the subsequent assessment of generative mechanisms of the coherent structures can be related. The flow structures themselves will be interpreted with respect to the models outlined in Chapter 2. Finally, a comprehensive mechanistic model of the structure and content of the flow field in gravel-bed rivers will be outlined.

6.1 Three zone structure of the boundary layer

The high relative roughness of gravel-bed rivers means that a spatially coherent sublayer cannot exist, and that the free stream does not develop. This is important with respect to the interpretation of the structures which have emerged from the analyses in terms of those described in the literature from boundary layers in other environments.

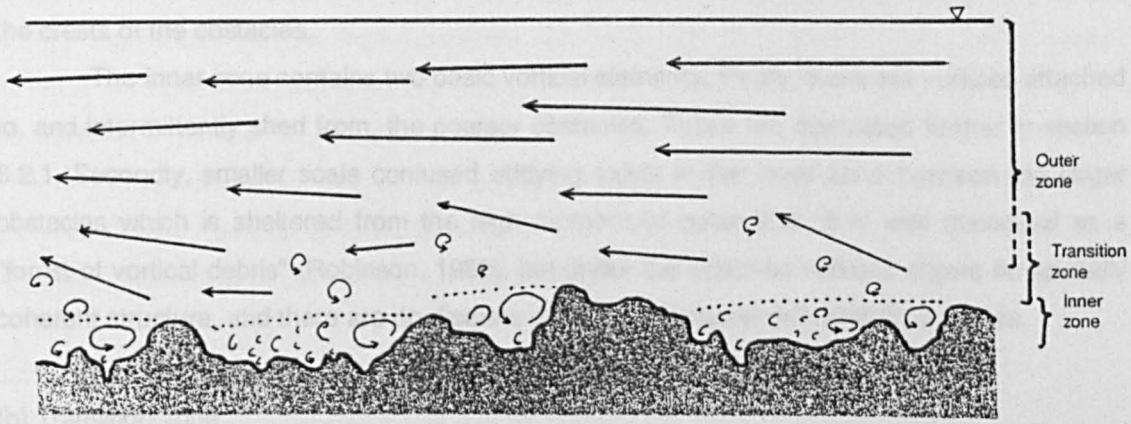

Figure 6.1 Three zone structural model of the boundary layer over fluvial gravel beds

6.1.1 Composition of the three zones

Figure 6.1 shows the basic structure of the boundary layer based on the visualisations. It comprises three zones:

(a) an inner zone of vortices attached to and shedding from the larger obstacles, and more confused eddying around the finer particles,

(b) an outer zone of more unidirectional streamwise flow containing larger coherent turbulent structures which are advected over the tops of the obstacles,

(c) a transition zone which represents the interaction and momentum exchange between the inner and outer zones.

The model proposed in section 4.1.6 did not explicitly include the transition zone, although various lines of evidence from Chapter 5 support this as a more representative structure. Retrospective viewing of the visualisation video sheds new light on the dynamics and importance of the transition zone.

(a) Inner zone

The inner zone represents the flow field between the roughness elements. Its lower limit is the dead water in the interstices between the constituent bed particles. The upper limit is less clearly defined. Qualitatively, the visualisations would suggest that in a time averaged sense, it is defined as below an imaginary plane pinned to the crests of the "larger" obstacles. The definition of "large" is in reference to the local roughness assemblage, and so cannot be definitely related to a specific percentile of either the roughness series distribution or the particle size distribution. Mechanistically, the crests define the position of the shear layer that separates the inner and outer zones.

Consideration of the limited velocity profile data that extends into the inner zone (section 5.1.1) suggests that the inner zone exists below the point at which the velocity goes to zero. This is generally lower than the crests of the coarser obstacles. The profiles of turbulence intensity show a kink at $\leq k_{84}$ above the bed below which Ti_u is constant. Although the precise location of this relative to the obstacle field is difficult to determine, it suggests that it lies above the crests of the obstacles.

The inner zone contains two basic vortical elements. Firstly, there are vortices attached to, and intermittently shed from, the coarser obstacles. These are discussed further in section 6.2.1. Secondly, smaller scale confused eddying exists in the inner zone between the larger obstacles which is sheltered from the high momentum outer flow. It is well described as a "forest of vortical debris" (Robinson, 1989), but unlike the attached vortices shows no spatially coherent structure, and there are no discrete vortices associated with specific particles.

(b) Transition zone

The interface between the inner and outer zones was initially referred to as the separation "layer". However, although it is picked out very clearly by high Ti_u values in the region close to the crests of the obstacles (section 5.1.3), as distance increases away from the obstacles, the definition is less clearly that of a layer, but more of a zone.

It can be considered as a layer in the time-average sense, across which vortical structures pass between the inner and outer zones. Hence, at any instant, it is unlikely to be in its time-average position.

Apart from the visualisations, the main line of evidence regarding the characteristics of this zone emerges from the quadrant analysis (Sections 5.4 & 5.5). There is a shift in the important contribution to total Reynolds stress from Q1 and Q3 in the near-bed region to Q2 and Q4 higher in the profile. This is in agreement with the flow visualisations; the Q1 stresses can be explained by the individual ejections of vortices from obstacles away from the inner zone. Observations from the visualisations suggest that such ejections would be characterised by high streamwise fluctuations and upwards vertical transient fluctuations from the mean. It is significant that these are *not* Q2 events which are usually associated with bursting, which means that bursting and eddy shedding are different flow structures.

Although Q1 and Q3 tend to contain disproportionately more of the sampled points than Q2 and Q4 in the transition zone, the discrepancies in the proportion of total absolute stress in the four quadrants can be attributed to higher absolute stress values (Section 5.4.3, Figure 5.22). It is suggested that below $y/k_{84} \approx 2.5$, as y decreases, the magnitude of the stress values increase in Q1 at the expense of Q2. $y/k_{84} \approx 2.5$ can therefore be taken as a guide to the extent of the influence of the ejecting vortices on the stress field of the boundary layer, and is another marker of the upper extent of the transition zone.

(c) Outer zone

The outer zone is characterised as a flow field with a mean streamwise flow direction; u increases approximately as ln(y), and Ti_u decreases roughly linearly as ln(y) increases.

Superimposed on the mean streamwise flow field are distinct coherent structures. Morphologically, there appear to be two types. Firstly, the visualisations reveal large vortices being advected at greater than mean flow velocity, although their vortical coherence is less distinct than those ejecting from obstacles. Secondly, the fluctuating velocity profile yielded inverted "wedges" being advected in the flow field. In the light of this, wedge-like structures *can* be identified in the flow visualisation video.

In the outer zone, Q2 and Q4 contribute disproportionately to the total stress. Q2 is associated with ejections of low momentum fluid through the boundary layer. Q4 represents high momentum fluid fluxes towards the boundary.

6.2 Coherent structures in the boundary layer

Although vortex generation in the inner zone is a product of the roughness, it is the coupling of the inner and outer zones which defines the nature of the vortical activity and its temporal structure. This section will consider how the coupling takes place firstly by comparing the observed structures to those which would be generated either by eddy shedding or layer interaction, and then considers alternative generative mechanisms and eddy interaction.

6.2.1 Evidence for eddy shedding

It is clear from the visualisations that eddies *are* intermittently shed from obstacles, but are not the same as the larger vortical structures in the outer zone. This means that it is not

appropriate to attempt to describe the temporal characteristics of the larger outer zone eddies using the Strouhal relation (e.g. Clifford & French, 1993).

The mean period that would be produced from eddy shedding from obstacles can be estimated using the Strouhal equation by re-arranging Equation 2.11 to give 1/f. As the visualisation experiments suggest that eddies are shed predominantly from the larger obstacles, k_{84} will be used as the obstacle size.

The boundary layer in gravel-bed rivers does not develop into the free stream, and so U_∞ is not known. U_{max} would be a good approximation to U_∞, but the uncertainty regarding the velocity profile over gravel beds (Kuhnle, 1992; section 2.2), estimating U_{max} from the velocity profile would be open to error. <U> is therefore taken as the velocity parameter, calculated at y = 0.4d using the regression of u on ln(y).

The mean shedding periods calculated for all of the field data range from 0.24s to 0.70s, although these are probably overestimates as $<U> < U_\infty$. The periods are shown as "s" on the horizontal axis of the τ_R spectra.

There is no systematic correspondence between the calculated eddy shedding periods and peaks in the spectra, and they tend to exist in the low period part of spectrum where there is a relatively small amount of power. If eddy shedding *was* going to express itself in the spectra, it would be expected that it would emerge in those of the lower probe of the Beauty Creek files, as these files were the ones that produced disproportionately high amounts of absolute stress in Q1 and Q3. There is not, however, any suggestion whatsoever that the calculated periods correspond to a peak. This suggests that the structure which is a direct product of eddy shedding does not contribute significantly to the total variance of τ_R. This does not mean, however, that eddy shedding is an insignificant process with respect to explaining flow structure; section 6.3 discusses how the eddies interact with other structures.

A paradox has emerged regarding eddy shedding: although it has been observed in the visualisations, there is no quantitative evidence from the field data that eddy shedding produces any quasi-periodic flow component. Consideration of Acarlar & Smith's plot of eddy shedding period against Re (Figure 2.6) suggests that in the highly turbulent environment of gravel-bed the shedding from obstacles would be intermittent and highly irregular. As well as this, the assemblage of obstacle sizes and shapes mean that eddies of different sizes will be shed at different rates, and the chance of monitoring eddies from a single obstacle would be small.

In section 2.3.2, a model was proposed which predicts the size of the "dominant" eddy from the assemblage shed from an array of different sized obstacles. The model cannot be tested here as the bed profiles were not of sufficient length to produce a large enough sample of obstacle sizes.

6.2.2 Evidence for layer roll-up

Section 2.3.1 speculated that roll-up between the inner and outer zones may be a mechanism for vortex generation, by suggesting that the sublayer vorticity is replaced by the

attached vortices in the inner zone. This effectively is an interpretation of the mechanism of the "coupling" of vortical activity of the inner and outer zones.

As one way of testing whether zone coupling is similar to layer roll-up, the burst frequency, T_b given by Equation 2.9 can be compared to the timescales of the outer zone intermittency. The calculated burst periods are shown on the corresponding τ_R spectra as a "T" on the horizontal axes (Figures 5.34 to 5.37). Visual comparison suggests there is a degree of correspondence between the calculated burst periods and peaks in the spectra. This degree of correspondence can be classified into three categories: T_b corresponds with the dominant spectral peak, T_b corresponds to a significant peak but not the dominant one or T_b does not correspond to a peak at all. The correspondence is taken to be approximate, as there are errors in the estimation of both T_b and the spectra.

Table 6.1 shows the percentages of files within each correspondence category for the three data sets. It suggests that the burst period, Tb, compares favourably to the peaks in the τ_R of the Dubhaig and Beauty Creek data. This is strong support for a mechanism of bursting being the dominant mechanism for coherent structure generation in gravel bed rivers, and the scaling of the process with outer zone variables.

Table 6.1 Percentages of correspondence of T_b with peaks in the τ_R spectra.

Data set:	Dubhaig	B Creek	Arolla
T_b = dominant peak:	46%	34%	14%
T_b = another peak:	46%	45%	25%
No correspondence:	8%	21%	61%

T_b bears little relation to the peaks in the τ_R spectra of the Arolla data. The difference between the Arolla data and the rest is that sediment transport was taking place. If spectral peaks are interpreted as evidence for bursting, this would suggest that the conditions which produce sediment transport also prevent bursting from taking place, or sediment transport itself stops fluid bursting.

6.3 Proposal of a mechanistic model of coherent structure generation

Two issues have emerged concerning coherent structures in the outer zone which need to be rationalised. Firstly, there is convincing qualitative evidence that eddies are shed from obstacles, although there is no quantitative support for this from monitored flow intermittency. Secondly, a form of advecting high and low speed fluid wedges exist over gravel beds, yet the temporal scale of the coherent structures is very similar to that expected for inner-outer zone fluid bursting. The issues to address here are whether the wedges and fluid bursting represent the same phenomena, and how eddy shedding interacts with the outer zone structures.

Let us interpret this with respect to the sublayer-outer layer roll-up model; if we replace the sublayer streaks with shedding eddies, and sublayer-outer zone roll up by instabilities along the high-low momentum interface of the wedges, then a coupled eddy-shedding/inverted wedge model can be proposed.

This model crudely satisfies the mechanistic similarity to the sublayer-outer layer roll-up model in order for it to exhibit a similar temporal structure. The significance of the coupling of the inner and outer zone relates to the interaction of their own temporal properties. Eddy shedding would take place in the absence of the advecting wedges and would exhibit a characteristic quasi-periodic structure (e.g. Kawanisi *et al*, 1993). Likewise, wedge advection would take place without the rough boundary, again producing a characteristic intermittency (e.g. Nakagawa & Nezu, 1983), although this is less well understood. The coupling of the two systems would mean that the temporal structures would interact, and this appears to produce the characteristic burst period, T_b.

There is still the problem of explaining the initial presence of the advecting wedges. The burst/sweep model of sublayer/buffer zone roll-up over smooth beds does not involve an initial perturbation to "trip" the system into action; the intermittency is an inherent quality of the flow condition and is self-perpetuating. Likewise, we can consider the succession of advecting high and low speed wedges over gravel beds as self-perpetuating.

Figure 6.2 proposes how the wedges and eddy shedding interact. Due to the incipient cyclicity, there is no starting point.

Eddies shedding from obstacles will have two effects on the wedges: they will affect the morphological coherence of the wedges, and extract energy from them. All models of wedges in the literature mention shear-induced eddies along the high speed front (Figures 2.8, 2.9 & 2.10). The difference in gravel-bed rivers is that eddy shedding provides a ready source of crudely transverse vortices, and so the effect of these would be to exacerbate the morphological destruction of the wedges.

The transverse vortices extract energy from the high momentum side of the front and re-distribute it to the low momentum side. The suggestion made by Yalin (1992) that transverse vortices grow to the size of the flow depth does not seem credible in gravel-bed rivers. A more likely scenario is one of high speed fronts becoming progressively diffuse as the transverse eddies produced by the eddy shedding disperse the front's energy.

The diffusion of a high momentum region would produce a low momentum fluid mass. The visualisations showed that eddies are preferentially shed into the outer flow during "lulls" in the outer zone velocity. The ejection of low momentum fluid associated with the eddies would tend to further block the outer zone flow. In order to satisfy continuity, this would produce the next high momentum zone.

The proposal of high and low speed wedges being associated with surface waves made by Levi (1983b) gains some support from the visualisations made at high discharge. The implication of this is that the waves define the presence and spacing of the wedges, and hence

it is necessary to understand the generation of surface waves if we are to explain the presence of wedges.

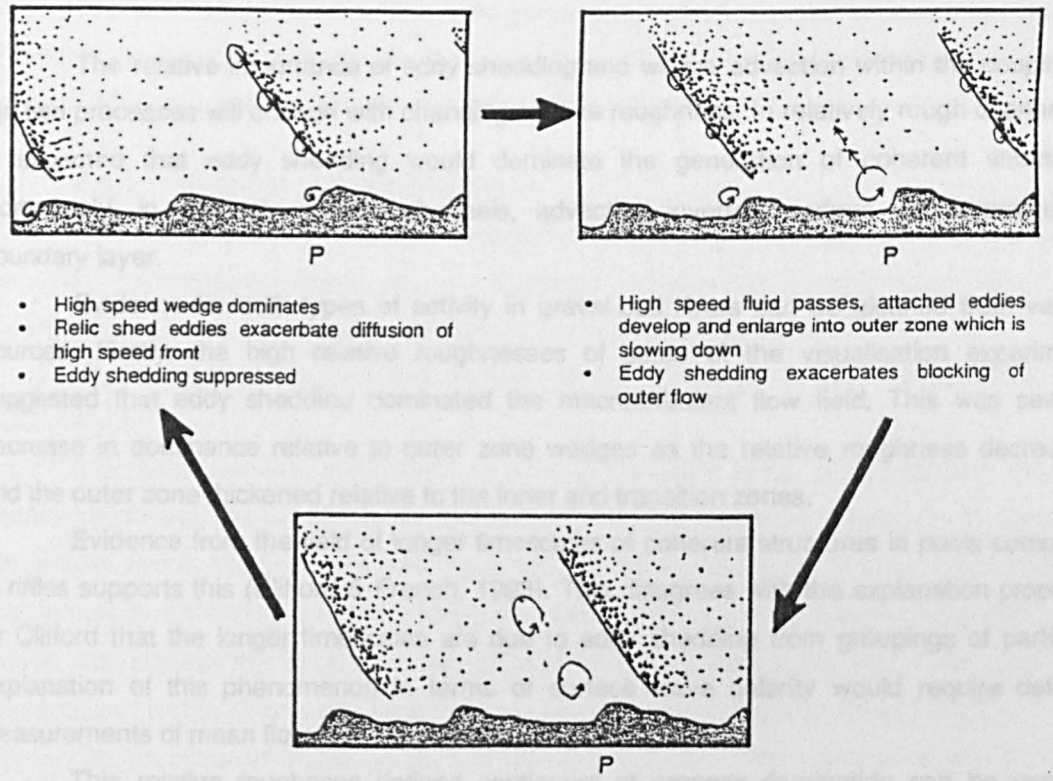

Figure 6.2 The mutual interference of advecting wedges and eddy shedding. Descriptions relate to activity at point "P".

The properties of surface waves are determined by fluid viscosity and flow depth. The explanation of surface waves and the interaction with the flowing fluid can be made with reference to the Froude number, $Fr = U/\sqrt{(g.d)}$. If $Fr<1$, flow is said to be subcritical, and the surface waves travel faster than the mean flow velocity; if $Fr>1$, flow is supercritical and the surface waves travel more slowly than the fluid mass. Flow in gravel-bed rivers rarely becomes supercritical (Leopold & Wolman, 1960), so it can be assumed that surface waves travel faster than the mean flow. This is supported by the visualisation sequence shown in Figure 4.9.

Associated with the front of a wave is a high water surface slope which produces a positive pressure head and hence streamwise acceleration. This would appear to conveniently explain the advection of high momentum zones.

The length of the surface waves in the visualisation experiments is similar to the flow depth, and hence the use of the waves to explain the presence of the wedges may be

reasonable. However, in Beauty Creek, although surface waves existed, their wavelengths were considerably smaller than the flow depth. It is therefore difficult to link them to the wedges which emerged from the analysis of the fluctuating velocity profile. Specific observation of the surface waves was never made during data collection. An objective assessment cannot therefore be made of the importance of surface waves on flow structure.

The relative importance of eddy shedding and wedge advection within the coupling of the two processes will change with changing relative roughness. In relatively rough channels, it is expected that eddy shedding would dominate the generation of coherent structures. Conversely, in relatively smooth channels, advecting inverted wedges will dominate the boundary layer.

Evidence for both types of activity in gravel-bed rivers can be gleaned from various sources. Firstly, the high relative roughnesses of some of the visualisation experiments suggested that eddy shedding dominated the macroturbulent flow field. This was seen to decrease in dominance relative to outer zone wedges as the relative roughness decreased, and the outer zone thickened relative to the inner and transition zones.

Evidence from the field of longer timescales of coherent structures in pools compared to riffles supports this (Clifford & French, 1993). This disagrees with the explanation proposed by Clifford that the longer timescales are due to eddy shedding from groupings of particles. Explanation of this phenomenon in terms of surface wave celerity would require detailed measurements of mean flow and depth which are not available.

This relative roughness defined continuum of process domination can be used to interpret how gravel-bed rivers relate, in a hydraulic sense, to other types of rivers. It has been shown several times that the timescales of coherent structure in sand bed rivers scale solely with flow depth (e.g. Jackson, 1976; Lapointe, 1992). As these are of low relative roughness, they can be seen as defining one end of the spectrum. This is possibly complicated by a further process of eddies shed from sand bedforms.

The structures monitored over coastal gravels represent flows over a gravel bed but at low relative roughness. Although eddies will be shed from particles, the turbulent field would be dominated by outer zone flow structures. It is likely that this is influenced by structures generated in the free stream, a section of the flow which does not generally develop in the depth-limited conditions of gravel bed rivers.

At the other end of the relative roughness scale, flows in boulder bed channels represent high relative roughness conditions. In such conditions, an outer layer would not have the opportunity to develop, and eddy shedding would dominate the flow field.

The range of relative roughnesses of gravel-bed rivers cannot be defined; a gravel-bed river at low flow can have a relative roughness comparable to boulder bed rivers. In spite of this, from the evidence outlined here the two processes of coherent structure generation both make an important contribution to the turbulent flow field.

6.4 Implications for gravel entrainment

Velocity fluctuations in the boundary layer flow result in intermittent entrainment of gravel (Drake *et al*, 1988; Williams *et al*, 1989). Before considering the mechanisms of this any further, it is necessary to outline more precisely what aspect of the flow-sediment interaction is of interest here.

The emphasis will concern the discussion of the mechanisms of sediment entrainment. The failure of the SGN system described in section 3.7.4 mean that quantitative relationships between flow intermittency and gravel entrainment will not be made.

6.4.1 Modes of gravel entrainment

At the end of the visualisation experiments, discharge was increased until sediment transport commenced. There are no hydraulic measurements associated with these observations, so only a qualitative assessment of the effects can be made.

At the scale of the individual particle, several modes of sediment entrainment were observed.

The finer particles, which tend to exist in the inner zone, protected from the high momentum flow by the larger obstacles, react dominantly to upwards forces ($v' > 0$) which are themselves due to the confused eddying within this zone. The upwards force responsible for entrainment is not included in the widely used force balance model outlined in section 2.1.1. Indeed, the relatively low streamwise velocities which the particles in the inner zone experience would mean that the streamwise force balance would rarely lead to entrainment at all.

On the increase of discharge, two factors affect the entrainment of coarse particles. Firstly, the momentum of the outer zone increases, hence increasing the drag force on the obstacles. Secondly, the vibrations of the vortices attached to the lee of the obstacles are transmitted to the obstacle causing it to rattle within its pocket. A similar phenomenon is referred to as the "added mass" of the vortex to the particle (Hardisty, *pers.comm.*). The actual entrainment of the obstacle clasts was usually associated with the sweep-like motions of the advecting high momentum fronts ($u' > 0$) which correspond to the overpassing of a sloping front of a surface wave, and is clearly seen in the photo sequence of Figure 4.9. The timescale of coarse particle entrainment is significantly greater than the period of the advection of wedges. The significance of this is that the entrainment of a single particle cannot be attributed solely to a single discrete flow fluctuation. The inertia of a large particle requires several high flow fluctuations to cause it to move out of its pocket.

In terms of the significance of these different entrainment modes for the total flux of sediment transport, the entrainment of the finer particles by the upwards forces was minimal. The removal of a large particle had a further effect of causing intense local scour and associated local entrainment in a "flurry" of transport activity. These events would appear to be similar to the "sweep transport events" described by Drake *et al* (1988).

This confirms the proposition made by various workers that the sweeping of high momentum fluid towards the bed is the dominant process responsible for coarse sediment

entrainment (e.g. Grass, 1982; Drake *et al*, 1988; Williams *et al*, 1989). What has been suggested here is the mechanism by which the high momentum fluid exists and is brought close to the bed.

An increase in flow discharge in the visualisation experiments produced a sharp increase in transport rates. Over time, the rates reduced with no further change in discharge. This phenomenon has been studied in detail in the literature under the area of bed armouring (e.g. Sutherland, 1987; Parker & Sutherland, 1990), but none of the studies have specifically considered the changes in the juxtaposition of bed surface particles in relation to flow structure.

Observations of the interaction of flow and bed sediment suggest that (at marginal transport conditions) for a given flow field, there is a quasi-stable arrangement of the constituent bed obstacles as determined by the dimensions of their wakes (Figure 6.3). It has been found that flow resistance in maximised at critical spacings of roughness elements, where these can consist of cross-stream batons (Johnson & Le Roux, 1946), artificially fixed dunes (Davies, 1980) and artificial and self-formed gravel clusters (Brayshaw, 1984; Hassan & Reid, 1990).

The reason proposed for the maximisation of resistance concerns the interaction of near-bed flow with the roughness surface (Morris, 1955; Nowell & Church, 1979. Closely spaced roughness elements produce 'skimming flow' over their upper surface, and the flow is effectively blind to the resistance of the surface. As the spacing increases, 'wake interference' takes place whereby flow separation occurs in the lee of the obstacles, and energy is dissipated by the formation and decay of the vortex. Widely spaced roughness elements act as isolated obstacles.

The phenomenon of bed texture adjusting to produce wake interference requires the scale of investigation of entrainment to be re-examined. If an armoured bed resists entrainment and maximises energy dissipation for the hydraulic conditions at which it was formed, then entrainment can be considered to be the result of the bed texture re-adjusting to a changed set of hydraulic conditions. This means that although the movement of individual particles *is* in response to flow fluctuations, the fluctuations are themselves a product of the dis-equilibrium between the bed texture and the mean flow energetics. A more appropriate way of considering the problem of explaining gravel entrainment, therefore, would be to investigate more closely the relationships between mean flow energetics and bed texture.

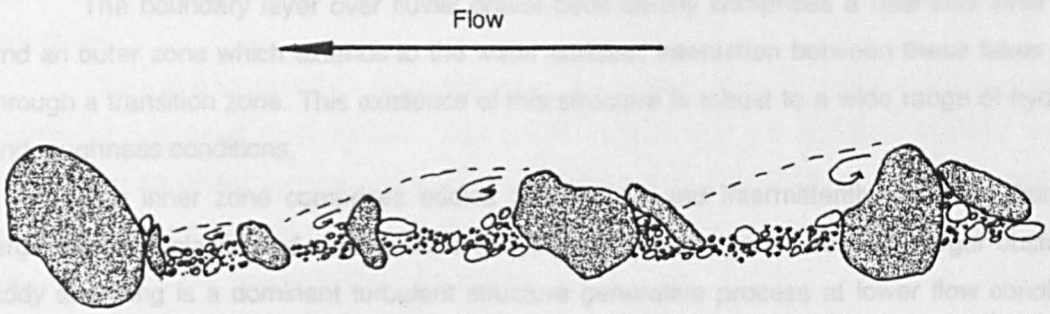

Larger obstacle clasts - responsible for providing protection for finer material in their wake zones. Entrained by high speed streamwise flow events after gradual winnowing of supportive fines.

Finer particles - react mostly to vertical forces of inner zone eddying, but majority entrained in association with removal of an obstacle clast.

Figure 6.3 Two storey bed structure.

Chapter 7 Conclusions

7.1 The structure of the boundary layer in gravel bed rivers

The boundary layer over fluvial gravel beds clearly comprises a near-bed inner zone and an outer zone which extends to the water surface. Interaction between these takes place through a transition zone. This existence of this structure is robust to a wide range of hydraulic and roughness conditions.

The inner zone comprises eddies attached to and intermittently shedding from the larger obstacle clasts, and smaller scale eddying in the wake zones between larger obstacles. Eddy shedding is a dominant turbulent structure generative process at lower flow conditions, but at higher flow conditions up to and including the entrainment of the host obstacles, it becomes very erratic.

The interface between the inner and outer zones is characterised by high negative Reynolds stress. It is suggested that this corresponds to the ejection of eddies from the inner zone. At $y \approx k_{84}$, there is a kink in the turbulence intensity profile which is interpreted as the average upper extent of the influence of eddy shedding on the boundary layer.

In the outer flow zone at low flow conditions, there is a mixture of larger vortices and confused wedges of high and low speed fluid. It is not clear what the origins of the structures are, although there is some evidence for coalescence of shedding eddies. At higher flow conditions, including those resulting in sediment entrainment, inverted wedges of high speed fluid are advected downstream. These are tentatively linked to the passage of water surface waves, but there is insufficient evidence to elaborate on this.

After an outer zone high speed front has passed, low speed fluid bursts from the near-bed region. This tends to block the outer flow, the result being a release of high speed fluid as the next high-speed front.

It is not possible to state which element drives the system of flow structures. Eddy shedding from obstacles appears to dominate flows with relatively low mean velocity, whereas advecting wedges seem to dominate faster flows. If the wedges can be linked to water surface waves, then it is possible that the explanation of flow structures in gravel-bed rivers may be made with respect to the Froude number.

The magnitude of the streamwise velocity fluctuations are partly explained by the mean velocity and the boundary roughness. The point where the velocity is monitored relative to the local obstacle field is very important in determining the size of the fluctuations. A better explanation of this would require closely spaced measurements of the velocity field within the inner and transition zones. This would be possible using an LDA, and would be a valuable contribution to the understanding of near-bed flow.

7.2 Timescales of flow structure

Flow visualisations suggest that all of the flow structures mentioned above are crudely intermittent with timescales of up to seconds. However, very little temporal structure emerges from the velocity time series, and that which apparently exists is not robust to testing by other techniques.

There is a tendency for Reynolds stress to produce spectral peaks at the approximate position of calculated burst periods. This would suggest that the apparent bursting process observed in the outer zone is similar to that mentioned in the literature. As the timescale of bursting is different to that of eddy shedding, the implication is that the period of eddy shedding would be tied to the activity in the outer zone.

7.3 Implications for gravel entrainment

Two aspects of the flow structure are important in determining gravel entrainment. Firstly, vertical velocity fluctuations in the wake zones of larger obstacle clasts entrain fine material. Secondly, the high speed "sweep-like" structures are responsible for entraining the larger clasts. Although the timescale of entrainment is greater than that of an individual flow structure, the larger particles are often given the final push by high speed fluid associated with a wedge, often corresponding to the overpassing of a water surface wave front.

7.4 Similarities with other environments

This work began by applying models of turbulent structures from smooth bed laboratory experiments, sand-bed rivers and tidal flows to the relatively rougher gravel-bed river environment. The process of eddy shedding from gravel beds appears to be identical to that from single obstacles, but the more turbulent flows of gravel-bed rivers means that the structures and periodicities are by no means as clear.

The characteristics of the advecting inverted wedges correspond well to those reported from other environments. Questions still remain regarding what actually generates them and whether they are related to the classic burst/sweep model involving layer roll-up.

The majority of field based work reported in the literature makes use of a single probe to monitor velocity, whereas most of the laboratory work uses flow visualisation. This work has shown that interpretations of the same flow field from different techniques can be quite different.

In this work, the visualisations and fluctuating velocity profiles were invaluable in providing a broader picture of the flow field against which the point monitoring of velocity could be interpreted. Monitoring or observing flow simultaneously at several points gives an extra dimension to the description of the flow field. Multiple probes and flow visualisation are the key to understanding and explaining the mechanisms and structures operating within the flow field of the highly turbulent, highly irregular environment of gravel-bed rivers.

References

Acarlar, M.S. & Smith, C.R. 1987 'A study of hairpin vortices in a laminar boundary layer. Part 1. Hairpin vortices generated by a hemisphere protuberance' *J. Fluid Mech.* 175, 1-41.

Aguirre-Pe, J. & Fuentes, R. 1990 'Resistance to flow in steep rough streams' *Journal of Hydraulic Engineering* 116 (11), 1374-1386.

Andrews, E.D. & Smith, J.D. 1992 'A theoretical model for calculating marginal bedload transport rates' in Dynamics of Gravel-bed Rivers, Billi, P., Hey, R.D., Thorne, C.R. & Tacconi, P (eds.), Wiley, Chichester, pp 41-54.

Andrews, E.D. & Parker, G. 1987 'Formation of a coarse surface layer as the response to gravel mobility' in Sediment Transport in Gravel-bed Rivers, Thorne, C.R., Bathurst, J.C. & Hey, R.D. (eds.), Wiley, Chichester, pp 243-267.

Andrle, R. & Abrahams, A.D. 1989 'Fractal techniques and the surface roughness of talus slopes', *Earth Surface Processes and Landforms*, **14**, 197-209.

Arnell, R.D., Davies, P.B., Halling, J & Whomes, T.L. 1991 Tribology: Principles and Design Applications, Macmillan.

Ashworth, P.J. 1987 'Bedload transport and channel change in gravel-bed rivers' PhD thesis, 35200., Univ. of Stirling, Scotland.

Ashworth, P.J. & Ferguson, R.I. 1989 'Size selective entrainment of bedload in gravel bed streams' *Water Resources Research* 25, 627-634.

Ashworth, P.J., Ferguson, R.I. & Powell, M. 1992 'Bedload transport and sorting in braided channels' in Dynamics of Gravel-bed Rivers, Billi, P., Hey, R.D., Thorne, C.R. & Tacconi, P (eds.), Wiley, Chichester, pp 497-518.

Aubrey, D.G. & Trowbridge, J.H. 1985 'Kinematic and dynamic estimates from electromagnetic current meter data' *Journal of Geophysical Research*, 90 (C5), 9137-9146.

Barrage, A. & Dracos, T. 1976 'Turbulence measurements in rivers' in Hydraulic Problems Solved by Stochastic Methods, Hjorth, P., Jonson, L. & Larsen, P. (eds.), pp 107-127.

Bathurst, J.C. 1978 'Flow resistance of large-scale roughness' *ASCE J. Hydr. Div.* 104, 1587-1603.

Bathurst, J.C. 1982 'Theoretical aspects of flow resistance' in Hey, R.D., Bathurst, J.C. & Thorne, C.R. (eds.) Gravel-bed Rivers, John Wiley & Sons.

Bathurst, J.C. 1985 'Flow resistance estimation in mountain rivers' *ASCE J. Hydr. Div.* 111, 625-643.

Bedeus, K. & Invicsics, L 1963 'Observations of the noise of bedload' *Proc. Int. Ass. Soc. Hydrol.*, 65, 384-390.

Berger, E. & Wille, R. 1972 'Periodic flow phenomena', *Ann. Rev. Fluid Mech.* 4, 313-340.

Best, J. 1992 'On the entrainment of sediment and the initiation of bed defects: insights from recent developments within turbulent boundary layer research' *Sedimentology* **39**, 797-811.

Best, J. 1993 'On the interactions between turbulent flow structure, sediment transport and bedform development: some considerations from recent experimental research' in Turbulence: Perspectives on Flow and Sediment Transport, Clifford, N.J., French, J.R. & Hardisty, J. (eds.), Wiley, Chichester.

Blackwelder, R.F. & Eckelmann, H. 1979 'Streamwise vortices associated with the bursting phenomenon' *Journal of Fluid Mechanics*, 94(3).

Bowden, K.F. & Fairburn, L.A. 1952 'Further observations of the turbulent fluctuations in a tidal current' *Phil. Trans. Roy. Soc.* Series A, 24, 335-356.

Bowden, K.F. & Fairburn, L.A. 1956 'Measurements of turbulent fluctuations and Reynolds stresses in a tidal current. *Proc. Roy. Soc. Lond.*, 237 Ser. A, 422-438.

Box, G.E.P. & Jenkins, G.M. 1968 'Some recent advances in forecasting and control. Part 1' *Applied Statistics*, 17, 91-109.

Bray, D.I. 1979 'Estimating average velocity in gravel-bed rivers' *Journal of the Hydraulics Division*, ASCE 105, 1103-1122.

Bray, D.I 1982 'Flow resistance in gravel-bed rivers' in Gravel- bed Rivers, Hey, R.D., Bathurst, J.C. & Thorne, C.R. (eds.), Wiley, Chichester.

Brayshaw, A.C. 1984 'Characteristics and origin of cluster bedforms in coarse grained alluvial channels', *Memoir Canadian Society Petroleum Geologists*, **10**, 77-85.

Brayshaw, A.C., Frostick, L.E., Reid, I. 1983 'The hydrodynamics of particle clusters and sediment entrainment in course alluvial channels' *Sedimentology* 30, 137-143.

Bridge, J.S. & Bennett, S.J. 1992 'A model for the entrainment of sediment grains of mixed shapes, sizes and densities' *Water Resources Research* **28** (2), 337-363.

Brown, G.L. & Thomas, A.S.W. 1977 'Large structure in a turbulent boundary layer' *Physics of Fluids Supplement*, 20, pp 243.

Burkham, D.E. & Dawdy, D.R. 1976 'Resistance equation for alluvial channel flow' *Journal of the Hydraulics division*, ASCE, 102, pp 1479-1489.

Carling. P.A., Kelsey, A. & Glaister, M.S. 1992 'Effect of bed roughness, particle shape and orientation on initial motion criteria' in Dynamics of Gravel-bed Rivers, Billi, P., Hey, R.D., Thorne, C.R. & Tacconi, P (eds.), Wiley, Chichester, pp 23-39.

Chadwick, A & Morfett, J. 1986 Hydraulics in Civil Engineering, Allen & Unwin, London.

Chatfield, C. 1975 The Analysis of Time Series: Theory and Practice, Chapman & Hall.

Chang, H.H. 1988 Fluvial Processes in River Engineering, Wiley, New York, 432pp.

Chang, C.C. & Chern, R.L. 1991 'Vortex shedding from an impulsively started rotating and translating circular cylinder' *Journal of Fluid Mechanics* 233, 265-298.

Chezy, A. de 1775 'Memoire sur la vitesse de l'eau conduite dans une regole' reprinted in *Annals de Ponts et Chaussees*, 60, pp1921.

Church, M., McLean, D.G. & Wolcott, J.F. 1987 'River bed gravels: sampling and analysis' in Sediment Transport in Gravel-bed Rivers, Thorne, C.R., Hey, R.D. & Bathurst, J.C. (eds.), Wiley, Chichester, pp 291-338.

Cimbala, J.M., Nagib, H.M. & Roshko, A. 1981 'Wake instability leading to new large scale structures downstream of bluff bodies' *Bull. Am. Phys. Soc.* 26, 1256.

Cimbala, J.M., Nagib, H.M. & Roshko, A. 1988 'Large structure in the far wakes of two-dimensional bluff bodies' *Journal of Fluid Mechanics,* 190, 265-298.

Clifford, N.J. 1990 'The formation, nature and maintenance of riffle-pool sequences in gravel-bed rivers' PhD thesis, University of Cambridge. 365pp.

Clifford, N.J., McClatchey, J. & French, J.R. 1991 'Discussion - Measurements of turbulence in the benthic boundary layer over a gravel bed and Comparison between acoustic measurements and predictions of bedload transport of marine gravels.' *Sedimentology* 38, 161-171.

Clifford, N.J., Robert, A. & Richards, K.S. 1992 'Estimation of flow resistance in gravel-bed rivers: A physical explanation of the multiplier of roughness length' *Earth Surface Processes and Landforms*, **17**, 111-126.

Clifford, N.J. & French, J.R. 1992 'Monitoring and analysis of turbulence in geophysical boundaries - some practical and analytical issues' paper presented at 'Turbulence: Perspectives on Sediment Transport' Symposium, Department of Geography, University of Hull, April 1992.

Coleman, N.L. 1981 'Velocity profiles with suspended sediment' *Journal of Hydraulics Research*, 19, 211-229.

Coles, D. 1987 'Coherent structures in turbulent boundary layers' Perspectives in Turbulent Studies, Int. Symposium DFVLR Res. Centre, Gottingen, May, 1987.

Davies, T.R. 1980 'Bedform spacing and flow resistance' *Journal Hydraulics Division, ASCE*, **106**, 423-433.

Dietrich, W.E. & Whiting, P. 1989 'Boundary shear stress and sediment transport in river meanders of sand and gravel' in River Meandering, Ikeda, S. & Parker, G. (eds.), Am. Geophys. Union Water Resources Monograph, 12, pp 1-50.

Drake, T.G., Shreve, R.L., Dietrich, W.E., Whiting, P.J. & Leopold, L. 1988 'Bedload transport of fine gravel observed by motion picture photography' *Journal of Fluid Mechanics* 19, 2193-2217.

Falco, R.E. 1977 'Coherent motions in the outer regions of turbulent boundary layers' *Physics of Fluids*, 20(10), S124-132 (Suppl.)

Ferguson R.I. & Ashworth, P.J. 1992 'Spatial patterns of bedload transport and channel change in braided and near-braided rivers' in Dynamics of Gravel-bed Rivers, Billi, P., Hey, R.D., Thorne, C.R. & Tacconi, P (eds.), Wiley, Chichester, pp 478-496.

Ferguson, R.I. & Werritty, A. 1983 'Bar development and channel change in the gravely River Feshie, Scotland' International Association of Sedimentology, Special Publication 6, pp 181-193.

Ferro, V. & Giordano, G. 1991 'Experimental study of flow resistance in gravel bed rivers' *Journal of Hydraulic Engineering*, 117(10), 1239-1246.

Fiedler, H. & Head, M.R. 1966 'Intermittency measurements in the turbulent boundary layer' *J. Fluid Mech.* **25** (4), 719-735.

Furbish, D.J. 1987 'Conditions for geometric similarity of coarse stream-bed roughness' *Mathematical Geology*, 19(4), 291-307.

Gerrard, H. 1966 'The three dimensional structure of the wake of a circular cylinder' *J. Fluid Mech.* 25, 143-164.

Gordon, C.M. 1975 'Period between bursts at high Reynolds number' *The Physics of Fluids* 18(2), 141-143.

Grant, H.L. 1958 'The large eddies of turbulent motion' *J. Fluid Mech.* 4, 149-198.

Grass, A.J. 1971 'Structural features of turbulent flow over smooth and rough boundaries' *Journal of Fluid Mechanics* 50, 233-255.

Grass, A.J. 1982 'The influence of boundary layer turbulence on the mechanics of sediment transport' Euromech, 156: Mechanics of Sediment Transport, pp 3-17.

Grass, A.J., Stuart, R.J. & Mansour-Tehrani, M. 1991 'Vortical structures and coherent motion in turbulent flow over smooth and rough boundaries' *Phil. Trans. R. Soc. Lond.* A, 336, 35-65.

Guza, R.T., Clifton, M.C. & Rezvani, F. 1987 'Field intercomparison of electromagnetic current meters' *Journal of Geophysical Research*, 93, pp 9302-14.

Hardisty, J. 1990 'Bedload processes in turbulent flow. Part 1: Data acquisition systems' Working paper 11, School of Geography, University of Hull, UK.

Hassan, M.A. & Reid, I. 1990 'The influence of microform bed roughness elements on flow and sediment transport in gravel-bed rivers' *Earth Surface Processes and Landforms*, **15**, 739-750.

Heathershaw, A.D. & Thorne, P.D. 1985 'sea-bed noises reveal the role of bursting in sediment transport by tidal currents' *Nature*, 316, 339-342.

Head, M.R. & Bandyopadhyay, P. 1981 'New aspects of turbulent boundary layer structure' *J. Fluid Mèch.* 107, 297-338.

Hey, R.D. 1979 'Flow resistance in gravel-bed rivers' *ASCE Journal of the Hydraulics Division HY4*, 365-379.

Hinze, J.O. 1975 Turbulence, 2nd ed., McGraw-Hill, New York.

Hussain, A.K.M.F. 1983 'Coherent structures - reality and myth' *Physics of Fluids*, 26(10), 2816.

Hutchings, J.M. 1991 Tribology: Friction and Wear of Engineering Materials, Edward Arnold.

Jackson, R.G. 1976 'Sedimentological and fluid-dynamic implications of the turbulent bursting phenomenon in geophysical flows', Journal of Fluid Mechanics, 77(3), 531-560.

Johnson, J.W. & LeRoux, E.A. 1946 'Discussion of "Flow in a channel of definite roughness"', *Trans. ASCE*, **111**, 555-559.

Johnson, P. & Muir, T.C. 1969 'Acoustic detection of sediment movement' *Journal of Hydraulics Research* 75, 519-540.

Kawanisi, K., Maghrebi, M.F. & Yokosi, S. 1993 'An instantaneous 3-D analysis of turbulent flow in the wake of a hemisphere' *Boundary-Layer Meteorology* **64**, 1-14.

Keulegan, G.H. 1938 'Laws of turbulent flows in open channels', *Journal of Research, National Bureau of Standards*, 21, 707-741.

Kim, H.T., Kline, S.J. & Reynolds, W.C. 1971 'The production of turbulence near a smooth wall in a turbulent boundary layer', *Journal of Fluid Mechanics*, 50(1), pp 133.

Kim, J. & Moin, P. 1986 'The structure of the vorticity field in turbulent channel flow. Part 2: Study of ensemble-averaged fields' *Journal of Fluid Mechanics*, 162, pp 339.

Kim, H.J. & Durbin, P.A. 1988 'Investigation of the flow between a pair of circular cylinders in the flopping regime' *J. Fluid Mech.* 196, 431-448.

Kirchner, J.W., Dietrich, W.E., Iseya, F. & Ikeda, H. 1990 'The variability of critical shear stress, friction angle, and grain protrusion in water-worked sediments' *Sedimentology* 37, 647-672.

Kline, S.J., Reynolds, W.C., Schraub, F.A. & Runstadler, P.W. 1967 'The structure of turbulent boundary layers' *Journal of Fluid Mechanics* 30, 741-773.

Kline, S.J. & Robinson, S.K. 1990 'Turbulent boundary layer structure: Progress, status and challenges' In Gyr, A. (ed.) Structure of Turbulence and Drag Reduction, Springer-Verlag, Berlin.

Kuhnle, R.A. 1992 Discussion of Ferguson *et al* in Dynamics of Gravel-bed Rivers, Billi, P., Hey, R.D., Thorne, C.R. & Tacconi, P (eds.), Wiley, Chichester, pp 493.

Lam, K. & Cheung, W.C. 1988 'Phenomena of vortex shedding and flow interference of three cylinders in different equilateral arrangements' *J. Fluid Mech.* 196, 1-27.

Lane, S.N., Richards, K.S. & Warburton, J. 1993 'Comparison between high frequency velocity records obtained with spherical and discoidal electromagnetic current meters' in Clifford, N.J., French, J.R. & Hardisty, J. Turbulence: Perspectives on Flow and Sediment Transport, John Wiley & Sons Ltd, Chichester.

Lapointe, M. 1992 'Burst-like sediment suspension events in a sand-bed river' *Earth Surf. Proc. & Landforms* **17**, 253-270.

Lapointe, M. 1993 'Monitoring alluvial sand suspension by eddy correlation' *Earth Surf. Proc. & Landforms* **18**, 157-175.

Laufer, J. 1975 'New trends in experimental turbulence research' *Ann. Rev. Fluid Mech.* 7, 307-326.

Leopold, L.B., Wolman, M.G. & Miller, J.P. 1964 Fluvial Processes in Geomorphology, W.H. Freeman, San Francisco.

Leopold, L.B. & Wolman, M.G. 1960 'River meanders' *Bulletin of the Geological Society of America*, 71, 769-94.

Levi, E. 1983a 'A universal Strouhal law' *Journal of Engineering Mechanics*, **109** (3), 718-727.

Levi, E. 1983b 'Oscillatory motion for wall-bounded turbulence' *Journal of Engineering Mechanics*, **109** (3), 728-740.

Levi, E. 1991 'Vortices in Hydraulics' *Journal of Hydraulic Engineering*, **117** (4), 399-413.

Lighthill, M.J. 1963 'Laminar boundary layers' in Rosenhead, L. (ed.), Clarendon Press, Oxford.

Limerinos, J.T. 1970 'Determination of the Manning coefficient from measured bed roughness in natural channels' U.S.G.S. Water Supply Paper 1898b, 47pp.

Lyles, L. & Woodruff, N.P. 1972 'Boundary layer flow structure: effects on detachment of non-cohesive particles' in Sedimentation, Shen, H.W. (ed.), Fort Collins, Colorado.

McQuivey, R.S. 1973a 'Principles and measuring techniques of turbulence characteristics in open channel flows' *USGS Professional Paper* 802a.

McQuivey, R.S. 1973b 'Summary of turbulence data from rivers, conveyance channels and laboratory flumes' *USGS Professional Paper* 802b.

Mandelbrot, B.B. 1983 The Fractal Geometry of Nature, Freeman, New York.

Manning, R. 1891 'On the flow of water in open channels and pipes' *Transactions of the Institute of Civil Engineers of Ireland*, 20, 161-207.

Massey, B.S. 1979 Mechanics of Fluids, Van Nostrand Reinhold Company, London.

Matsui, T & Okude, M. 1981 'Vortex pairing in a Karman vortex street' In *Proc. Seventh Biennial Symposium on Turbulence*, Rolla, Missouri.

Moller, W. 1938 'Experimentelle Untersunchung zur Hydromechanik der Kugel' *Z. Phys.*, 39, 57-80.

Morris, H.M. 1955 'Flow in rough conditions', *Trans ASCE*, **120**, 373-398.

Muller, A. & Gyr, A. 1986 'On the vortex formation in the mixing layer behind dunes' *Journal of Hydraulics Research*, 24(5), 359-375.

Naden, P. 1987 'An erosion criterion for gravel-bed rivers' *Earth Surface Processes & Landforms*. 12, 83-93.

Nagel, E. 1961 The Structure of Science, Harcourt, Brace & World Inc., New York.

Nagib, H. & Desruelle, D. 1982 'Controlled excitation of the far wake instability' *Bull. Am. Phys. Soc.* 27, 1193.

Nakagawa, H & Nezu, I. 1981 'Structure of space-time correlations of bursting phenomena in open channel flow' *J. Fluid Mech.*, 104, 1-43.

Nikuradse, J. 1933 'Stromungsgesetze in rauhen Rohrne (Laws of flow in rough pipes)' Ver. deutscher Ingenieure, Forschungsheft, no. 361, Berlin.

Nowell, A.R.M. & Church, M. 1979 'Turbulent flow in a depth limited boundary layer' *Journal of Geophysical Research* 84, 4816-4824.

Nychas, S.G., Hershey, H.C. & Brodkey, R.S. 1973 'A visual study of turbulent shear flow' *J. Fluid Mech.* 61(3), 513-540.

Offen, G.R. & Kline, S.J. 1975 'A proposed model of the bursting process in turbulent boundary layers' *J. Fluid Mech.* 70(2), 209-228.

Paintal, A.S. 1971. 'Concept of critical shear stress in loose boundary open channels' *Journal of Hydraulic Research* 9, 91-113.

Parker, G. & Sutherland, A.J. 1990 'Fluvial armour' *Journal of Hydraulics Research*, 28, 529-44.

Perry, A.E. & Chong, M.S. 1982 'On the mechanism of wall turbulence' *J. Fluid Mech.* **119**, 173-217.

Perry, A.E., Lim, K.L. & Henbest, S.M. 1987 'An experimental study of the turbulence structure in smooth- and rough-wall boundary layers' *J. Fluid Mech.* **177**, 437-466.

Rao, N.K., Narasimha, R. & Badri Narayanan, M.A. 1971 'The 'bursting' phenomenon in a turbulent boundary layer' *J. Fluid Mech.* 48(2), 339-352.

Richards, K.S. 1976 'The morphology of riffle-pool sequences', *Earth Surface Processes and Landforms*, **1**, 71-88.

Richards, K.S. 1982 Rivers: Form and Process in Alluvial Channels, Methuen, London.

Richards, K.S. & Milne, 1979 'Problems in the calibration of an acoustic device for the observation of bedload transport' *Earth Surface Processes and Landforms*, 4, 335-346.

Richards, K. & Clifford, N.J. 1991 'Fluvial geomorphology: structured beds in gravely rivers' *Progress in Physical Geography*, 15(4), 407-422.

Robert, A. 1988 'Statistical properties of sediment bed profiles in alluvial channels' *Mathematical Geology*, 20(3), 205-225.

Robert, A. 1990 'Boundary roughness in coarse grained channels' *Progress in Physical Geography* 14(1), 42-70.

Robert, A. & Richards, K.S. 1988 'On the modelling of sand bedforms using the semivariogram' *Earth Surface Processes & Landforms* 13, 459-473.

Robert, A., Roy, A.G.. & De Serres, B. 1992 'Changes in velocity profiles at roughness transitions in coarse grained channels' *Sedimentology*, **39**, 725-735.

Robert, A., Roy, A.G. & De Serres, B. 1993 'Space-time correlations of velocity measurements at a roughness transition in a gravel-bed river' in Turbulence: Perspectives on Flow and Sediment Transport, Clifford, N.J., French, J.R. & Hardisty, J. (eds.), Wiley, Chichester.

Robinson, S.K. 1990 'Coherent motions in the turbulent boundary layer', *Ann. Rev. Fluid Mech.*, 104, 387-405.

Schlichting, H. 1979 Boundary Layer Theory, McGraw-Hill, 7th edition.

Shields, A. 1936 'Anwendung der Aenlichkeitsmechanik und der turbulenzforschrung auf die geschiebebewegung' *Mitteilung der Preussischen versuchsanstalt fuer Wasserbau und Schiffbau*, Heft 26, Berlin.

Smith, C.R. 1978 'Visualisation of turbulent boundary layer structure using a moving hydrogen bubble wire probe' *Coherent Structure of Turbulent Boundary Layers*, AFOSR/Lehigh University Workshop, pp48.

Smith, C.R. & Metzler, S.P. 1983 'The characteristics of low-speed streaks in the near-wall region of a turbulent boundary layer', *J. Fluid Mech.*, 129, 27-54.

Smith, C.R., Walker, J.D.A., Haidari, A.H. & Sobrun, U. 1991 'On the dynamics of near-wall turbulence' *Phil. Trans. R. Soc. Lond.* 336, 131-175.

Spivack, H.M. 1946 'Vortex frequencies and flow patterns in the wake of two parallel cylinders at varied spacing normal to an air stream' *Journal of Aeronautical Science*, 13, 289-301.

Strouhal, V. 1878 'Uber eine besondere Art der Tonerregung' *Annalen de Physik Und Chemie*, 5, 216-251.

Strykowski, P.J. & Sreenivasan, K.R. 1990 'On the formation and suppression of vortex 'shedding' at low Reynolds numbers' *J. Fluid Mech.* 218, 71-107.

Sutherland, A.J. 1987 'Static armour layers by selective erosion' in Thorne, C.R., Bathurst, J.C. & Hey, R.D. (eds.), Sediment Transport in Gravel-bed Rivers, 243-267, John Wiley & Sons.

Taneda, S. 1959 'Downstream development of wakes behind cylinders' *J. Phys. Soc. Japan* 14, 843-848.

Theodorsen, T. 1952 'Mechanism of Turbulence', In *Proc. 2nd Midwest Conf. Fluid Mech. Columbus, Ohio*, pp 1-18.

Thomas, D.G. & Kraus, K.A. 1964 'Interaction of vortex streets' *J. Appl. Phys.* 35(12), 3458-3459.

Thorne, P.D., Williams, J.J. & Heathershaw, A.D. 1989 'In situ measurements of marine gravel threshold and transport' *Sedimentology* 36, 61-74.

Townsend, A.A. 1976 The Structure of Turbulent Shear Flow, Cambridge University Press, 429pp.

Townsend, A.A. 1979 'Flow patterns of large eddies in a wake and in a boundary layer' *Journal of Fluid Mechanics*, 95, 515-537.

Tritton D.J. 1977 Physical Fluid Dynamics, Wokingham, Van Nostrand.

Tywoniuk, N & Warnock, R.G. 1973 'Acoustic detections of bedload fluvial processes and sedimentation' *Proceedings of the 9th Canadian Hydrology Symposium*, Ottowa. pp 728-749.

Walker, J.D.A. 1990 'Wall layer eruptions in turbulent flows' in Structure of Turbulence & Drag Reduction, Gyr, A (ed.), Springer-Verlag.

Walker, J.D.A. & Herzog, S. 1988 'Eruption mechanisms for turbulent flows near walls' In Hirata, M. & Kasagi, V. (eds.) 2nd Symposium on transport phenomena in turbulent flows, Hemisphere, New York.

Wallace, J.M., Eckelmann, H. & Brodkey, R.S. 1972 'The wall region in turbulent shear flow' *J. Fluid Mech.* **54**, 39-48.

White, C.M. 1940 'The equilibrium of grains on the bed of a stream' *Proceedings of the Royal Society*, 174A, 322-38.

Wiberg, P.L. & Smith, J.D. 1987a 'Calculations of the critical shear stress for motion of uniform and heterogeneous sediments' *Water Resources Research* 23, 1471-1480.

Wiberg, P.L. & Smith, J.D. 1987b 'Initial motion of sediment in streams of high gradient' *IAHSP* 165, 299-308.

Wiberg, P.L. & Smith, J.D. 1991 'Velocity distribution and bed roughness in high-gradient streams' *Water Resources Research* 27(5), 825-838.

Wilkinson, R.H. 1984 'A method for evaluating statistical errors associated with logarithmic velocity profiles' *Geo-Marine Letters*, 3, 49-52.

Williams, J.J., Thorne, P.D. & Heathershaw, A.D. 1989 'Measurements of turbulence in the benthic boundary layer over a gravel bed' *Sedimentology* 36, 959-971.

Williamson, C.H. 1985 'Evolution of a single wake behind a pair of bluff bodies' *J. Fluid Mech.* 159, 1-18.

Willmarth, W.W. 1975 'Structure of turbulence in boundary layers' *Adv. in Appl. Mech.*, 15, 159-254.

Winant, C.D. & Browand, F.K. 1974 'Vortex pairing: the mechanism of turbulent mixing-layer growth at moderate Reynolds number' *J. Fluid Mech.* **63**, 237-255.

Yalin, M.S. 1992 River Mechanics, Pergamon Press, Oxford, 220pp.

Zdravkovich, M.M. 1968 'Smoke observations of the wake of a group of three cylinders at low Reynolds number' *J. Fluid Mech.* 32, 339-351.

Appendix 1 Summary of flow and bed details for the field data

File	Sampling	Sample	y	Depth	<u>	tau	D50	D84	k50	k84	sd(k)	d/sd(k)	y/depth	y/D50	y/sd(k)
	freq (Hz)	length (s)	(cm)	(cm)	(m/s)	N(m)^-2	(cm)	(cm)	(cm)	(cm)	(cm)				
Dubhaig data:															
ad30	4	100	4	29.5	0.2383	0.895	2.52	5.06	2.74	3.57	0.83	35.41	0.1356	1.5873	4.8019
ad31	4	100	6	29.5	0.265	0.895	2.52	5.06	2.74	3.57	0.83	35.41	0.2034	2.381	7.2029
ad32	4	100	10	29.5	0.3066	0.895	2.52	5.06	2.74	3.57	0.83	35.41	0.339	3.9683	12.005
ad33	4	100	14	29.5	0.3315	0.895	2.52	5.06	2.74	3.57	0.83	35.41	0.4746	5.5556	16.807
ad34	4	100	18	29.5	0.3491	0.895	2.52	5.06	2.74	3.57	0.83	35.41	0.6102	7.1429	21.609
ad35	4	100	22	29.5	0.3542	0.895	2.52	5.06	2.74	3.57	0.83	35.41	0.7458	8.7302	26.411
ad40	4	100	4	26.5	0.1981	1.387	2.52	5.06	1.91	2.63	0.89	29.78	0.1509	1.5873	4.4944
ad41	4	100	6	26.5	0.2349	1.387	2.52	5.06	1.91	2.63	0.89	29.78	0.2264	2.381	6.7416
ad42	4	100	10	26.5	0.2825	1.387	2.52	5.06	1.91	2.63	0.89	29.78	0.3774	3.9683	11.236
ad43	4	100	14	26.5	0.3066	1.387	2.52	5.06	1.91	2.63	0.89	29.78	0.5283	5.5556	15.73
ad44	4	100	18	26.5	0.3355	1.387	2.52	5.06	1.91	2.63	0.89	29.78	0.6792	7.1429	20.225
ad45	4	100	22	26.5	0.3612	1.387	2.52	5.06	1.91	2.63	0.89	29.78	0.8302	8.7302	24.719
ad50	4	100	4	26.5	0.1937	0.936	2.52	5.06	1.91	2.63	0.89	29.78	0.1509	1.5873	4.4944
ad51	4	100	6	26.5	0.2384	0.936	2.52	5.06	1.91	2.63	0.89	29.78	0.2264	2.381	6.7416
ad52	4	100	10	26.5	0.254	0.936	2.52	5.06	1.91	2.63	0.89	29.78	0.3774	3.9683	11.236
ad53	4	100	14	26.5	0.2853	0.936	2.52	5.06	1.91	2.63	0.89	29.78	0.5283	5.5556	15.73
ad54	4	100	18	26.5	0.3112	0.936	2.52	5.06	1.91	2.63	0.89	29.78	0.6792	7.1429	20.225
ad55	4	100	22	26.5	0.3336	0.936	2.52	5.06	1.91	2.63	0.89	29.78	0.8302	8.7302	24.719
ad80	4	100	4	24	0.3201	7.96	4.23	6.56	2.5	3.56	1.03	23.26	0.1667	0.9456	3.876
ad81	4	100	6	24	0.3573	7.96	4.23	6.56	2.5	3.56	1.03	23.26	0.25	1.4184	5.814
ad82	4	100	10	24	0.4785	7.96	4.23	6.56	2.5	3.56	1.03	23.26	0.4167	2.3641	9.6899
ad83	4	100	14	24	0.5729	7.96	4.23	6.56	2.5	3.56	1.03	23.26	0.5833	3.3097	13.566
ad84	4	100	18	24	0.6469	7.96	4.23	6.56	2.5	3.56	1.03	23.26	0.75	4.2553	17.442
ad90	4	100	4	23	0.4867	2.12	4.23	6.56	2.5	3.56	1.03	22.29	0.1739	0.9456	3.876
ad91	4	100	6	23	0.5296	2.12	4.23	6.56	2.5	3.56	1.03	22.29	0.2609	1.4184	5.814
ad92	4	100	10	23	0.5924	2.12	4.23	6.56	2.5	3.56	1.03	22.29	0.4348	2.3641	9.6899
ad93	4	100	12	23	0.5868	2.12	4.23	6.56	2.5	3.56	1.03	22.29	0.5217	2.8369	11.628
ad94	4	100	14	23	0.6193	2.12	4.23	6.56	2.5	3.56	1.03	22.29	0.6087	3.3097	13.566
ad95	4	100	16	23	0.6519	2.12	4.23	6.56	2.5	3.56	1.03	22.29	0.6957	3.7825	15.504
Arolla data:															
ara1	4	120	5	16	0.4688				0.88	1.51	0.73	21.98	0.3125		6.8681
	4	120	8	16	0.5505				0.88	1.51	0.73	21.98	0.5		10.989
	4	120	13	16	0.633				0.88	1.51	0.73	21.98	0.7812		17.17
ara2	4	120	7.5	20	0.7829	0.416			0.88	1.51	0.73	27.47	0.375		10.302
	4	120	11	20	0.8888	0.416			0.88	1.51	0.73	27.47	0.55		15.11
arb1	4	120	13	26	1.1158				1.08	2.39	0.92	28.17	0.5192		14.626
	4	120	15	26	1.2044				1.08	2.39	0.92	28.17	0.5962		16.793
	4	120	18	26	1.2324				1.08	2.39	0.92	28.17	0.6923		19.502
arb2	4	120	9	31	1.1213	1.54			1.08	2.39	0.92	33.59	0.2903		9.7508
	4	120	13	31	1.24958	1.54			1.08	2.39	0.92	33.59	0.4194		14.085
	4	120	15	31	1.3998	1.54			1.08	2.39	0.92	33.59	0.5		16.793
	4	120	24	31	1.4413	1.54			1.08	2.39	0.92	33.59	0.7742		26.002
arb3	4	120	13	33	1.4477	1.156			1.08	2.39	0.92	35.75	0.3939		14.085
	4	120	15	33	1.7127	1.156			1.08	2.39	0.92	35.75	0.4545		16.251
arc1	4	120	7	19	0.871	4.68			2	3.23	1.18	16.14	0.3684		5.9473
	4	120	11	19	1.0542	4.68			2	3.23	1.18	16.14	0.5526		8.921
	4	120	15	19	1.116	4.68			2	3.23	1.18	16.14	0.7895		12.744

File	Sampling freq (Hz)	Sample length (s)	y (cm)	Depth (cm)	<u> (m/s)	tau N(m)^-2	D50 (cm)	D84 (cm)	k50 (cm)	k84 (cm)	sd(k) (cm)		d/sd(k)	y/depth	y/D50	y/sd(k)
arc2	4	120	8	20	1.077	11.15			2	3.23	1.18		16.99	0.4		6.7969
	4	120	12	20	1.4062	11.15			2	3.23	1.18		16.99	0.6		10.195
arc3	4	120	11	19	1.207	3.55			2	3.23	1.18		16.14	0.5526		8.921
	4	120	11	19	1.4966	3.55			2	3.23	1.18		16.14	0.5789		9.3458
ard1	4	120	9	14	0.9985	3.05			1.63	2.5	1.01		13.85	0.6429		8.9021
ard2	4	120	9	18	1.323	4.68			1.63	2.5	1.01		17.80	0.5		8.9021
	4	120	11	18	1.3649	4.68			1.63	2.5	1.01		17.80	0.6111		10.88
	4	120	15	18	1.3848	4.68			1.63	2.5	1.01		17.80	0.8333		14.837
ard3	4	120	11	19	1.3208				1.63	2.5	1.01		18.79	0.5526		10.386
	4	120	13	19	1.3835				1.63	2.5	1.01		18.79	0.6579		12.364
arh1	4	120	12	30	0.1915	2.88			1.9	2.98	1.09		27.40	0.3833		10.502
	4	120	13	30	0.1992	2.88			1.9	2.98	1.09		27.40	0.4167		11.416
	4	120	18	30	0.3057	2.88			1.9	2.98	1.09		27.40	0.6		16.438
	4	120	22	30	0.2117	2.88			1.9	2.98	1.09		27.40	0.7333		20.091
arm1	4	120	13	18	1.454	100.62			1.08	2	0.8		22.61	0.7222		16.332
arm2	4	120	12	18.5	1.403	100.62			1.08	2	0.8		23.24	0.6486		15.075
akarn	4	120	8	15	0.962				2.2	3.3	1.4		10.71	0.5333		5.7143
Beauty Creek data:																
aka1	10	120	3	41	0.346	3.09	2.91	4.18	2.61	3.42	0.87		47.07	0.0732	1.0309	3.4443
	10	120	10	41	0.49	3.09	2.91	4.18	2.61	3.42	0.87		47.07	0.2439	3.4364	11.481
	10	120	30	41	0.667	3.09	2.91	4.18	2.61	3.42	0.87		47.07	0.7317	10.309	34.443
aka2	10	120	3	41	0.365	2.92	2.91	4.18	2.61	3.42	0.87		47.07	0.0732	1.0309	3.4443
	10	120	10	41	0.512	2.92	2.91	4.18	2.61	3.42	0.87		47.07	0.2439	3.4364	11.481
	10	120	30	41	0.677	2.92	2.91	4.18	2.61	3.42	0.87		47.07	0.7317	10.309	34.443
aka3	10	120	3	41	0.348	3.18	2.91	4.18	2.61	3.42	0.87		47.07	0.0732	1.0309	3.4443
	10	120	10	41	0.515	3.18	2.91	4.18	2.61	3.42	0.87		47.07	0.2439	3.4364	11.481
	10	120	30	41	0.673	3.18	2.91	4.18	2.61	3.42	0.87		47.07	0.7317	10.309	34.443
aka4	10	120	3	41	0.402	2.19	2.91	4.18	2.61	3.42	0.87		47.07	0.0732	1.0309	3.4443
	10	120	10	41	0.524	2.19	2.91	4.18	2.61	3.42	0.87		47.07	0.2439	3.4364	11.481
	10	120	30	41	0.672	2.19	2.91	4.18	2.61	3.42	0.87		47.07	0.7317	10.309	34.443
akb1	10	120	14	41	0.499	3.09	2.91	4.18	2.61	3.42	0.87		47.07	0.3415	4.811	16.073
	10	120	20	41	0.626	3.09	2.91	4.18	2.61	3.42	0.87		47.07	0.4878	6.8729	22.962
	10	120	30	41	0.667	3.09	2.91	4.18	2.61	3.42	0.87		47.07	0.7317	10.309	34.443
akb2	10	120	14	41	0.517	2.92	2.91	4.18	2.61	3.42	0.87		47.07	0.3415	4.811	16.073
	10	120	20	41	0.634	2.92	2.91	4.18	2.61	3.42	0.87		47.07	0.4878	6.8729	22.962
	10	120	30	41	0.639	2.92	2.91	4.18	2.61	3.42	0.87		47.07	0.7317	10.309	34.443
akb3	10	120	14	41	0.496	3.18	2.91	4.18	2.61	3.42	0.87		47.07	0.3415	4.811	16.073
	10	120	20	41	0.615	3.18	2.91	4.18	2.61	3.42	0.87		47.07	0.4878	6.8729	22.962
	10	120	30	41	0.611	3.18	2.91	4.18	2.61	3.42	0.87		47.07	0.7317	10.309	34.443
akb4	10	120	14	41	0.488	2.19	2.91	4.18	2.61	3.42	0.87		47.07	0.3415	4.811	16.073
	10	120	20	41	0.612	2.19	2.91	4.18	2.61	3.42	0.87		47.07	0.4878	6.8729	22.962
	10	120	30	41	0.643	2.19	2.91	4.18	2.61	3.42	0.87		47.07	0.7317	10.309	34.443

Appendix 2 VELPROF programme listing

```
'VELPROF Instantaneous velocity profile programme.
CLS
DIM a(2000), b(2000), c(2000), d(2000), e(2000),
f(2000), g(2000), h(2000)

PRINT
"*************************************************************
******************
PRINT "  This programme displays fluctuating
velocity profiles using "
PRINT : PRINT "  simultaneous 3-point u and v
component velocity data."
PRINT : PRINT "  The data was logged at 10Hz, and
this is the default rate."
PRINT
"*************************************************************
******************

'Next bit reads in file, heights etc...
PRINT : INPUT "Enter the DRIVE: of the data file: ",
drv$
tint = .1
OPEN drv$ + "veldata.csv" FOR INPUT AS #1
'... and scale the heights to fit on the screen..

y1 = (14 / 45) * 200
y2 = (20 / 45) * 200
y3 = (30 / 45) * 200


'Next bit totally cosmetic

PRINT : PRINT "  When running....": PRINT
PRINT "      P = pause"
PRINT "      R = review"
PRINT "      I = changes speed (lies about sampling
rate...)"
PRINT "      S = step through series"
PRINT "      B = backwards run"
PRINT "      F = forwards run"
PRINT "      X = Exit"
PRINT : PRINT "  Reading the raw data..."

'Next bit opens file, strips header, reads in values,
assigns x-values
'to arrays a-d, and y's to e-h.

i = 0
suma = 0: sumb = 0: sumc = 0
DO
    i = i + 1
    INPUT #1, a, b, c, d, e, f
    a(i) = a * 100: b(i) = c * 100: c(i) = e * 100
    e(i) = b * 100: f(i) = d * 100: g(i) = f * 100
    suma = suma + a: sumb = sumb + c: sumc =
sumc + e
LOOP WHILE NOT EOF(1)
ava = suma / i: avb = sumb / i: avc = sumc / i

'....cosmetic...

BEEP
PRINT : PRINT : PRINT "          Press any key to
start..."
WHILE INKEY$ = "": WEND


SCREEN 2
CLS
10          'marker to return to in case of re-run
t0 = TIMER
stp = 1     'stp = 1 for forwards run, -1 for reverse
j = 0

'Locate statements are all cosmetic..

LOCATE 1, 1: PRINT "File: "; filin$
LOCATE 5, 1: PRINT "Commands:"
LOCATE 7, 3: PRINT "P = pause"
LOCATE 8, 3: PRINT "R = review"
LOCATE 9, 3: PRINT "I = change speed"
LOCATE 10, 3: PRINT "B = backwards"
LOCATE 11, 3: PRINT "F = forwards"
LOCATE 12, 3: PRINT "S = step"
LOCATE 13, 3: PRINT "X = exit"
LOCATE 11, 1: PRINT """
LOCATE 16, 1: PRINT "Default sampling "
LOCATE 17, 1: PRINT "interval = 0.1s."


'The next bit increments through the arrays and plots
the profile.
'It includes the test loops to stop, reverse etc...

DO UNTIL j = i              'sets up loop for plotting
    j = j + stp
    IF j = 0 THEN GOTO 13 ELSE    'prevents
crashing at zero in reverse

    st$ = INKEY$            'st$ is general flag for
keyboard input
    IF st$ = "r" OR st$ = "R" THEN
        INPUT "  Enter re-start point number: ", num
        j = num
        IF j = 0 THEN GOTO 12
        LOCATE 3, 16: PRINT "    "
    ELSEIF st$ = "p" OR st$ = "P" THEN
11      PRINT "  Press any key to continue..."
        WHILE INKEY$ = "": WEND
    ELSEIF st$ = "x" OR st$ = "X" THEN GOTO 40
    ELSEIF st$ = "i" OR st$ = "I" THEN
        INPUT "Enter new sampling interval (default
= 0.1s): ", tint
    ELSEIF st$ = "s" OR st$ = "S" THEN
12   LOCATE 2, 1: PRINT
    LOCATE 3, 1
    PRINT "Point number: "; j
    LOCATE 1, 30

'Next bit is all the graphics bit.
    LINE (201, 200)-(640, 0), 0, BF      'clears the
profiles without
    LINE (0, 200)-(199, 110), 0, BF      'clearing
screen

'Draws the velocity profile....
    LINE (200, 200)-((200 + ava), (200 - (y1)))
    LINE ((200 + ava), (200 - y1))-((200 + avb), (200
- y2))
    LINE ((200 + avb), (200 - y2))-((200 + avc), (200
- y3))


    LINE (200, 200)-(200, 0)
```

```
      LINE (200, 200)-((200 + a(j)), (200 - (y1)))
      LINE ((200 + a(j)), (200 - y1))-((200 + b(j)), (200 -
y2))
      LINE ((200 + b(j)), (200 - y2))-((200 + c(j)), (200 -
y3))

'Draws the vectors....
      IF fil$ = "2" THEN GOTO 20 ELSE
      LINE (300, (200 - y1))-((300 + a(j)), (200 - (y1 +
e(j))))
      LINE (300, (200 - y2))-((300 + b(j)), (200 - (y2 +
f(j))))
      LINE (300, (200 - y3))-((300 + c(j)), (200 - (y3 +
g(j))))

PRINT "Press RETURN to get out, F or B + RETURN
to step.."
INPUT out$

IF out$ = "F" OR out$ = "f" THEN
j = j + 1
GOTO 12
ELSEIF out$ = "B" OR out$ = "b" THEN
j = j - 1
GOTO 12
END IF

      ELSEIF st$ = "b" OR st$ = "B" THEN
            stp = -1
            LOCATE 10, 1: PRINT "*"
            LOCATE 11, 1: PRINT " "
      ELSEIF st$ = "f" OR st$ = "F" THEN
13          stp = 1
            LOCATE 10, 1: PRINT " "
            LOCATE 11, 1: PRINT "*"
      END IF

      LOCATE 3, 1
      PRINT "Point number: "; j
      LOCATE 1, 30

      WHILE TIMER < (t0 + tint): WEND        'keeps
execution speed
      t0 = TIMER                             'constant

'Next bit is all the graphics bit.
      LINE (201, 200)-(640, 0), 0, BF        'clears the
profiles without
      LINE (0, 200)-(199, 110), 0, BF        'clearing
screen

'Draws the velocity profile....
      LINE (200, 200)-((200 + ava), (200 - (y1)))
      LINE ((200 + ava), (200 - y1))-((200 + avb), (200
- y2))
      LINE ((200 + avb), (200 - y2))-((200 + avc), (200
- y3))

      LINE (200, 200)-(200, 0)
      LINE (200, 200)-((200 + a(j)), (200 - (y1)))
      LINE ((200 + a(j)), (200 - y1))-((200 + b(j)), (200 -
y2))
      LINE ((200 + b(j)), (200 - y2))-((200 + c(j)), (200 -
y3))

'Draws the vectors....
IF fil$ = "2" THEN GOTO 20 ELSE
      LINE (300, (200 - y1))-((300 + a(j)), (200 - (y1 +
e(j))))
      LINE (300, (200 - y2))-((300 + b(j)), (200 - (y2 +
f(j))))
      LINE (300, (200 - y3))-((300 + c(j)), (200 - (y3 +
g(j))))
20 LOOP

LOCATE 1, 40
40 PRINT : PRINT : PRINT : PRINT : PRINT : PRINT
: PRINT : PRINT
PRINT : PRINT : PRINT : PRINT : PRINT : INPUT
"Another run (Y/N)? ", run$
IF run$ = "y" OR run$ = "Y" THEN
      CLS
      GOTO 10
      ELSE
      END IF
CLOSE #1

SUB sstep


END SUB
```

Appendix 2 VECPLOT programme listing

```
'VECPLOT.BAS
DIM a(1000), b(1000)
CLS
PRINT : PRINT "This program graphically shows the changing u-v vector magnitude "
PRINT "and direction, and acoustically reproduces the associated kinematic stress."
PRINT : PRINT : PRINT "The screen will show the vector plotted as u' v' coordinates from the "
PRINT "centre of the screen."
PRINT : PRINT "It's probably a good idea to close the door!"
PRINT : PRINT : PRINT "Press any key to begin...."
WHILE INKEY$ = "": WEND

PRINT : PRINT "When running:"
PRINT : PRINT "  P will pause the program, any other key will then restart it"
PRINT "  R allows you to review part of the sequence"
PRINT "  X will exit."

PRINT : PRINT "Reading data....."
OPEN "vecdata.dat" FOR INPUT AS #1
i = 0
totu = 0: totw = 0
DO
    i = i + 1
    INPUT #1, w, u
    a(i) = u: b(i) = w
    totu = totu + u: totw = totw + w
LOOP UNTIL EOF(1)
avu = totu / i: avw = totw / i
BEEP: PRINT : PRINT "Press any key to continue...."
WHILE INKEY$ = "": WEND
10
SCREEN 2
CLS
t0 = TIMER
min = 100: max = -100
FOR j = 1 TO i
    CLS
    PRINT j
    'WHILE TIMER < t0 + .25: WEND
    't0 = TIMER
    LINE (300, 100)-(300 + ((a(j) - avu) * 600), 100 + ((b(j) - avw) * 600))
    v = ABS((a(j) - avu) * (b(j) - avw) * 500000)
    IF v > 32500 THEN v = 32500 ELSE
    IF v < 40 THEN v = 40 ELSE
    'PRINT v
    SOUND v, 4

    st$ = INKEY$              'st$ is general flag for keyboard input
    IF st$ = "p" OR st$ = "P" THEN
        PRINT "  Press any key to continue..."
        WHILE INKEY$ = "": WEND
    ELSEIF st$ = "r" OR st$ = "R" THEN
        INPUT "Enter the point number at which you would like to re-start: ", n
        j = n
    ELSEIF st$ = "x" OR st$ = "X" THEN GOTO 20
    ELSE
    END IF

NEXT j

20
INPUT "Do you want to start again (Y/N)? ", restart$
IF restart$ = "y" OR restart$ = "Y" THEN GOTO 10 ELSE END
```